CONTROLLED DELIVERY SYSTEMS FOR NEURONAL TISSUE ENGINEERING

by

Lauren Elizabeth Kokai

Bachelor of Science, University of Pittsburgh, 2004

Submitted to the Graduate Faculty of

Swanson School of Engineering in partial fulfillment

of the requirements for the degree of

Doctor of Philosophy

University of Pittsburgh

2009

UNIVERSITY OF PITTSBURGH

SWANSON SCHOOL OF ENGINEERING

This dissertation was presented

by

Lauren E. Kokai

It was defended on

October 15, 2009

and approved by

Xinyan Tracy Cui, PhD, Assistant Professor, Department of Bioengineering

Steven R. Little, PhD, Assistant Professor, Departments of Chemical Engineering, Bioengineering, and Immunology

Douglas J. Weber, PhD, Assistant Professor, Departments of Physical Medicine and Rehabilitation and Bioengineering

Dissertation Director: Kacey G Marra, PhD, Assistant Professor, Departments of Surgery and Bioengineering

CONTROLLED DELIVERY SYSTEMS FOR NEURONAL TISSUE ENGINEERING

Lauren Elizabeth Kokai, PhD

University of Pittsburgh, 2009

Complete transection of peripheral nerves can result from trauma, tumor removal, infection, or as adverse consequences of various surgeries. Current commercially available nerve guides cannot repair large nerve defects because these guides are engineered to provide mechanical support for the developing axon and do not actively promote axonal growth. For large nerve gaps, targeting axonal growth is particularly important because the length of the nerve that must be regrown is the distance from the lesion to the innervated muscle. Therefore, there is enormous clinical potential for a nerve guide capable of improving axonal outgrowth across large nerve defects. Our underlying hypothesis is that delivery of Glial Cell Line-Derived Neurotrophic Factor (GDNF) from a nerve guide will improve peripheral nerve regeneration across large defects.

To test this hypothesis, biodegradable poly(caprolactone) (PCL) nerve guides were prepared with manufacturing parameters optimized for protein delivery and retention at the injury site. Quantitative changes in the diffusion of small molecular weight proteins and glucose through PCL conduit walls were measured to determine the independent and combinatorial effects of three fabrication variables: wall thickness, pore size and porosity percentage. Double-walled microspheres were then fabricated as a method of sustained protein delivery, and were incorporated within the luminal wall of PCL nerve guides using a novel solvent specific embedding technique.

The overall efficacy of our nerve guide design was confirmed by encapsulating and delivering GDNF in the rat sciatic nerve injury model. Evaluation of sensory reinnervation

following a long gap, 1.5cm nerve injury at 16 weeks showed a significant increase in animal response time to stimuli from animals treated with GDNF as opposed to negative control PCL guides. Furthermore, the measured gastrocnemius contraction force in animals treated with GDNF was significantly higher than negative controls and was not significantly different from the isograft positive control group. Histological assessment of explanted conduits after 16 weeks showed improved tissue integration within GDNF releasing nerve guides compared to negative controls. Nerve fibers were present across the entire length of GDNF releasing guides, while nerve fibers were not detectable beyond the middle region of negative control guides. Therefore, the results reported within this dissertation support our original hypothesis that; the long-term delivery of a neurotrophic factor from nerve guides results in improved functional recovery above negative controls following large axonal defects in the peripheral nervous system.

TABLE OF CONTENTS

LIST OF TABLES

LIST OF FIGURES

ACKNOWLEDGEMENTS

I gratefully acknowledge my mentor, Kacey G. Marra, PhD for her contribution to this project, for without her, this dissertation could not have been prepared. From the very beginning of my participation in the Plastic Surgery Research Lab as an undergraduate, I have been allowed innumerable opportunities for both personal and professional growth. Dr. Marra has provided me with guidance when designing experiments, when preparing manuscripts, presentations, and grant or fellowship applications, and most importantly, when serving as a mentor for junior scientists myself. In addition to Dr. Marra's academic guidance, I know that I would not be the scientist I am today had she not provided me with so many opportunities to think independently, to make mistakes, and to constantly grow as a team leader within the lab. For these acts, I am forever grateful and hope to become the caring and passionate mentor that she has always been for me.

I also wish to acknowledge the department of Bioengineering for providing me with the opportunity to study at the University of Pittsburgh. In particular, I would like to thank Dr. Borovetz and Lynette Spataro for the incredible amount of work they put into the graduate program. I am also very grateful for the assistance and project guidance I have received from my committee members (and co-authors), Dr. Tracy Cui, Dr. Doug Weber and Dr. Steve Little.

I would also like to acknowledge all of the project assistance I have received from members of the Plastic Surgery Research Lab, particularly from Daniel O'Donnell, Natasa

Miljkovic, MD, PhD, Han Li, MD, Jed McAtee and Nick Oyster. I am particularly indebted to Julio Clavijo-Alvarez, MD, PhD for the many years he has acted as my mentor and friend. I cannot thank Julio enough for the guidance he has provided me with experimental design, statistical analysis, presentation preparation and career development. Additionally, I have been offered an incredible amount of guidance and materials from the Center for Biologic Imaging and am particularly grateful to Donna Stolz, PhD for all of her assistance. I also thank the McGowan Institute of Regenerative Medicine for providing me with a fantastic fellowship opportunity under the NIH Cellular Approaches to Tissue Engineering and Regeneration (CATER) training grant.

On a personal note, I would like to thank my family and friends for the constant support and love I have received over the past 27 years. My parents have supported me with open minds and encouraging words and I could never have accomplished this degree without them. I also cannot thank my two wonderful sisters enough for being the very best friends I could ever have. From as early as I can remember, Jen (PhD) has been a playmate, a competitor, and a role model. I have never hesitated to look to her for guidance, support, and love and know that she will never turn her ear from me no matter how obnoxious or stubborn I may be. I also thank Lindsay for the amazing amount of love and friendship she has provided for 25 years. She always supports me with words of encouragement and is never afraid of using humor to bring me back from the stresses of life. Additionally, I thank Eric Means, M.E and Oliver Grey Kokai-Means for their love and support. Finally, I thank my grandmother, Marian Wakeling. She is without doubt, the strongest, most amazing woman I have ever met.

During my 9 years in Pittsburgh, I have also been very fortunate to make a number of close friends with whom I have celebrated the good times and shared the bad. Candace

Brayfield, PhD, Dr. Kurt and Alexandra Beschorner, Katie Bieryla, PhD, Katie O'Callaghan, and Alicia DeFail Baumberger, PhD have all served as incredible sources of balance and perspective during my graduate career. Whenever I have found myself in a moment of doubt, I have been able to reach out to this support group and have found instant love and assistance. No matter where my life path takes me, I will always be honored to have them as such great friends.

1.0 INTRODUCTION

1.1 INCIDENCE AND IMPACT OF PERIPHERAL NERVE INJURIES

Because of the intimate nature of nerve development within tissue structures, including superficial or subcutaneous tissues, nerves are often considerably vulnerable to injury during trauma or surgical procedures. For example, nerves which are in direct contact with bone may be severed as a consequence of bone fracture or damage. Additionally, nerves traverse joints with little or no intervening soft tissue which renders them exposed during joint dislocation, stretch or compression. For example, the peroneal nerve is frequently and seriously injured in association with knee injuries with or without fracture. Nerves are also damaged as a side effect of various surgical procedures. The ilioinguinal and iliohypogastric nerves are typically injured as a result of surgical procedures in the lower abdominal wall and cause disabling pain in the groin. The ilioinguinal nerve can be entrapped by scar, sutures or staples or stretched or contused as a result of herniorrhaphy, appendectamy or other gynecological procedures such as child birth [1]. Additionally, the cavernosal nerve within the neurovascular bundle on the rectolateral aspect of the prostate is often severed during prostatectomy, leading to end organ morbidity with significant impairments in the quality of life for a large group of patients [2].

Nerve injuries which result in partial or total loss of motor or sensory functions can cause personal tragedy and great suffering for patients as well as substantial socioeconomic burden.

Nerve-related upper extremity outpatient visits and procedures in the United States have been estimated at ~ 2.7 million per year, which accounts for 13% of total outpatient visits. Of these 2.7 million, upper extremity nerve lesions resulting in possible paralysis and sensory defects in the affected extremity corresponded to 8% of the patient procedures [3]. For example, the usual arm level injury would likely involve (among others) the radial nerve. Types of trauma affecting this nerve include humeral fracture, glass, knife and gunshot wound and contrusive soft tissue injuries. Because the human hand is such a delicate sensory organ and working tool, studies point out that transection injuries of nerve trunks in hand injuries are highly costly as the patient loses work production (sick leave), may have to change work or even retire [4, 5]. In a 2005 Swedish study, it was estimated that the median cost for society of an employed person with a median nerve injury is ~51K euros [6].

When nerve damage occurs, direct anastamosis of the severed nerve ends is the most surgically preferred method of repair. However, when nerves cannot be aligned due to tension at the site of coaptation, a non-essential sensory nerve is often harvested during a second surgical procedure and grafted autologously [7]. There are several negative aspects to the use of nerve autografts including; semi-permanent sensory loss from the target organ of the harvested nerve, potential development of neuromas at the donor site, and the necessity of harvesting a large length of nerve which may not always be available, such as in combat casualty care. Because of these drawbacks with nerve autografts, nerve guides have emerged as a potential mode of bridging small nerve gaps for repairing peripheral nerve defects.

There are currently five nerve guide implants approved by the U.S Food and Drug Administration for human application that provide an alternative to using precious autologous nerve tissue. A 2006 evaluation of the efficacy of nerve guides reported that regeneration

success obtained with resorbable synthetic nerve guides is within the range of 0 to 69% which is equivalent to repair achieved with autologous nerve grafts [8]. Therefore, there is strong evidence that nerve guides can be used in treating nerve lesions instead of autologous nerve. However, currently nerve guides cannot repair large (greater than 3 cm of lost nerve tissue) defects because guides are only engineered to provide an initial mechanical support for the developing axon. Therefore, nerve guides meet a basic function for gross guidance for nerve fascicles between the proximal and distal stumps. The guides rely on self-regulatory biological mechanisms by containing growth factors secreted by the surviving nerve stumps and existing Schwann cells to the injured area. However, by exploiting the natural regenerative capacity of the peripheral nerves by developing conduits which promote and direct axonal outgrowth, it may be possible to overcome the current length barriers for synthetic nerve grafts.

1.2 PERIPHERAL NERVE ANATOMY

The peripheral nervous system (PNS) resides outside the central nervous system and functions to receive input from the environment and innervate muscle tissue for motor control. To accomplish this task, the PNS consists of cranial nerves arising from the brain, spinal nerves originating from the spinal cord, and the sensory nerve cell bodies (Figure 1a) [9]. Sensory information is transmitted to the central nervous system through afferent fibers in the dorsal spinal roots while outgoing efferent motor fibers originating within the ventral horns of the spinal cord serves the limbs and organs in terms coordinating body movement (Figure 1b) [10].

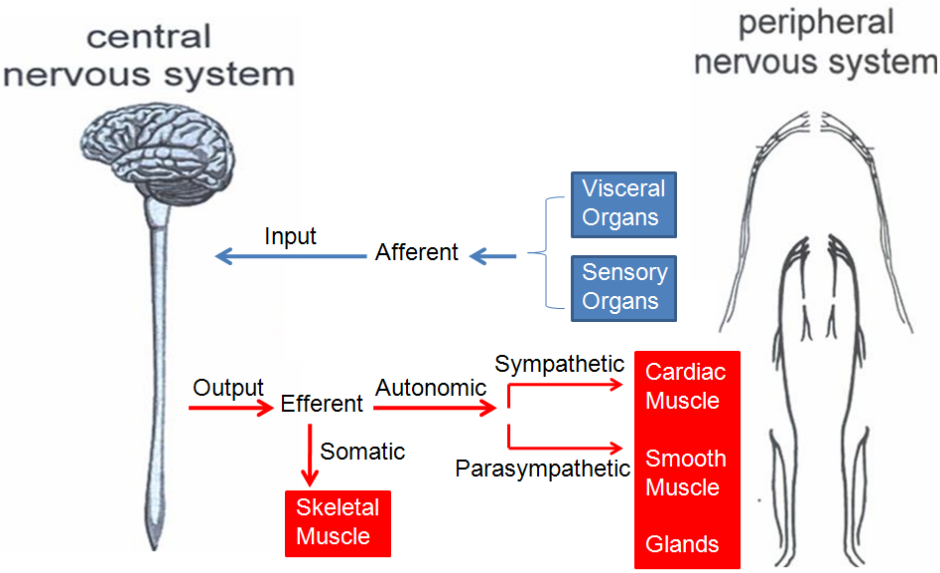

Figure 1. The Organization of the Peripheral Nervous System (Modified from [11, 12]).

1.2.1 Nerve architecture

The functional element of the peripheral nervous system is the neuron, which consists of a cell body and axonal and dendritic extensions. The cell bodies of neurons originate in the spinal cord, dorsal root ganglion and autonomic ganglion. The axons of peripheral nerves extend from the centrally located cell bodies and terminate in neuromuscular endings (motor neurons), end-organs, or receptors (sensory or sympathetic fibers). Histologically, peripheral nerves can be divided amongst two classifications, those nerve fibers which are myelinated or those that are unmyelinated. This distinction in nerve type describes the presence or absence of an accompanying layer of Schwann cells which concentrically encircle an axon with a lipoprotein covering, termed myelin (discussed in Section 1.2.2). Nerve fibers are further organized by

distinct layers of connective tissue which provides a framework for nerve fibers and the accompanying blood vessels [13].

Beginning with the most basic layer of nerve trunk organization, individual nerve fibers composed of an axon surrounded by Schwann cells are supported by an organized layer of connective tissue termed the endoneurium. The endoneurium is mostly collagen and divides nerve fibers into small undulating groupings which allows nerves to resist elongation under tension [14]. Additionally, fibroblasts, mast cells and macrophages reside within the endoneurium [10]. Groups of nerve fibers are further surrounded by an additional layer of connective tissue termed the perineurium, which condenses many layers of flattened fibroblasts and organized elastin and collagen fibrils into bundles of nerve fibers called fascicles. The function of the perineurium is to provide further protection for nerve fibers and to maintain an intra-fascicle pressure necessary for promoting a proximal-distal flow within the cytoplasm of axons. Additionally, the perineurium is the primary source of tensile strength of the peripheral nerve [10].

Finally, fascicles are further protected by the epineurium, a sheath of loose fibro-collagenous tissue that provides motility for the nerve trunk from surrounding structures. The epineurium is composed of longitudinally aligned collagen and elastin fibers and a small volume of adipose tissue which cushions the nerve against deforming forces. Cellular populations within this connective tissue layer include fibroblasts and mast cells. Additionally, the epineurium is highly vascularized and contains lymphatics which provide drainage for the arterial and venous supply [10]. Together, the nerve fibers, endoneurium, perineurium, and epineurium constitute motor, sensory or sympathetic peripheral nerve trunks (Figure 2).

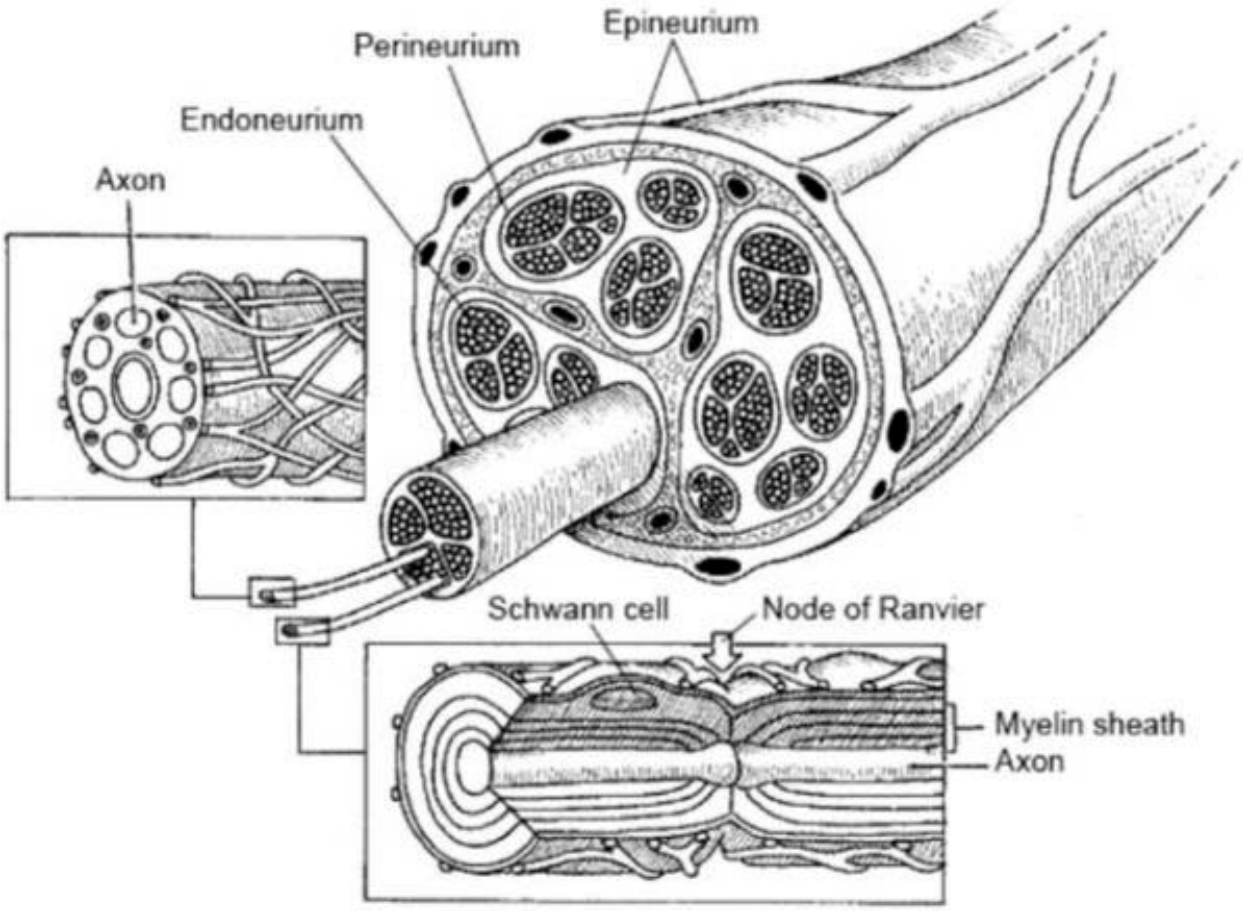

Figure 2. Organization of Peripheral Nerve Trunks. (Image from [15])

Depending on axon diameter and nerve conduction velocity, peripheral nerve fibers can be classified amongst three groups described in Table 1 [10].

Table 1. Classification of Peripheral Nerve Fibers

Group	*Diameter (µm)*	*Conduction Velocity (M/sec)*	*Function*
A	2.5 – 22	15 -100	Myelinated somatic afferent and efferent
B	3	3 – 15	Myelinated preganglionic autonomic (visceral)
C	0.2 – 1.5	0.3 – 1.6	Unmyelinated somatic afferent and autonomic postganglionic efferent (pain, pilomotor, sudomotor and vasomotor)

1.2.2 Schwann cells

In the PNS, Schwann cells are located around the axons (myelinated axons) or are related to several axons (nonmyelinated axons) and aid in axon function. Sensory and motor nerves contain both unmyelinated and myelinated axons in a ratio of 4 to 1 [16]. In myelinated axons, Schwann cells align longitudinally along the length of an axon and concentrically envelope the axons with tightly compressed lipid membranes. As the nerve fiber matures, the number of wrappings of Schwann cells around axons increases and as such, an increase in myelination around an axon indicates increased nerve fiber development [14].

During embryonic development, Schwann cells and neurons of the peripheral nervous system are generated together in the neural crest and migrate ventrally into the peripheral body tissues. As the number of nerve fibers increase, neuronal signaling correspondingly promotes an increase in Schwann cell populations [17]. Studies performed *in vitro* suggest that direct cell contact between axons and Schwann cells promotes Schwann cell proliferation [18]. In addition, direct neuronal contact promotes a large increase in the amount of secreted levels of major basal lamina components such as types I, III, IV and V collagen and laminin by Schwann cells [17, 19]. Furthermore, Schwann cells also maintain neuronal development through paracrine signaling by secreting factors such as Glial Cell Line-Derived Neurotrophic Factor (GDNF), Neuturin, Ciliary Neurotrophic Factor (CNTF), and Leukemia Inhibiting Factor (LIF).

In addition to neuronal maintenance, another vital function of Schwann cells is to insulate the axon and improve the efficiency of action potential propagation within the transmitting axon. Gaps in the connectivity of myelin are called Nodes of Ranvier and are important for the propagation of action potentials along the length of nerve fibers. While unmyelinated axons propagate electrical impulses at 2 to 2.5 m/s, myelinated fibers can conduct electrical impulses at 3 to 150 m/s [16].

1.2.3 Supporting vasculature

Peripheral nerves are abundantly vascularized by an intraneural plexus of successively dividing vessels which provides a rich supply of oxygen and nutrients to all elements of the nerve trunks [14]. From either the main vessel of a limb or their named branches, arteriae nervorum enter a nerve and travel predominantly in the epineurium and interfascicular epineurium, though the perineurium is also traversed by blood vessels [13]. These large outer blood vessels divide and

supply the perineurium and intrafascicular space as a fine mesh of obliquely running capillaries. The importance of nerve vasculature is evident from literature reporting impaired nerve regeneration when the blood supply is restricted from entering an area of injured nerve by nonporous tubes [20, 21].

1.3 NATIVE REPONSE TO NERVE INJURY

Severe nerve injuries are most commonly caused by trauma, which may include glass, knife and gunshot wounds [1]. In addition, motorcycle and car accidents often result in traction injuries that are particularly damaging to the brachial plexus and result in limited upper limb range of motion [22]. Furthermore, peripheral nerves may be injured during bone fractures or joint dislocations. Depending on the severity of nerve damage, the potential for nerve regeneration ranges between high for mild injuries that do not disrupt the connective tissue macrostructure to extremely poor when large segments of nerve trunks are lost.

1.3.1 Classification of nerve injuries

The degree of damage to a nerve fiber depends on the nature, site and severity of the injury [14]. By distinguishing injuries according to the harm placed upon the endoneurial tube, nerve injuries may be classified into three fundamental categories: neurapraxia, axonotmesis, and neurotmesis [13, 14].

Neurapraxia describes the mildest form of nerve injury and involves a temporary interruption of nerve fiber conduction without a loss of axonal continuity between the neuron and

end organ. This type of injury can result from compression of the nerve fiber or from relatively mild, blunt blows that occur close to the nerve [23]. Following direct compression and ischemia, paralysis and sensory impairment occur within 15 to 45 minutes of injury [14]. However, because the overall organization of the connective tissue is maintained along with the microscopic anatomy of the axon, recovery occurs easily and requires a recovery period that ranges between several minutes to up to 5-6 weeks [13]. Because the axon is contained within the endoneurial tube and the regenerative process is ensured, this type of injury is not addressed further within the context of the described work within this dissertation.

Axonotmesis is a more severe injury than neurapraxia and involves the loss of continuity of both the axon and the corresponding sheath of associated myelin, however with this injury the general framework of connective tissue is maintained. This type of injury commonly results from cuts and lacerations, bone fractures, traction, and prolonged compression [23]. Because the axonal innervations of target organs are interrupted, end-target regions of both motor and sensory functions are lost and recovery can require a significant amount of time. The final classification of nerve injury, neurotmesis, reflects severe forms of injury such as cuts, stretch or laceration of tissue which results in an interruption of not only the nerve fiber, but also the perineurial and endoneurial connective tissue structure.

A similar classification system developed by Sunderland scales nerve injuries according to damage done to fascicular structure. A simple grade-I or first-degree injury describes neurapraxia. Grade-II injuries are used to describe a loss of axon continuity with a preservation of endoneurial organization (axonotmesis). Grade-III injuries require that the axon and endoneurial continuity are lost with the preservation of perineurium, also described as a mixed axonotmesis-neurotmesis injury. With grade IV injuries, there is a loss of fascicle structure

which includes the axons, endoneurium and perineurium. This is the predominant type of nerve injury [13]. The final level of nerve injuries according to the Sunderland scale is grade V or complete neurotmesis. Figure 3 illustrates the relationship between the two common descriptive scales for peripheral nerve injury.

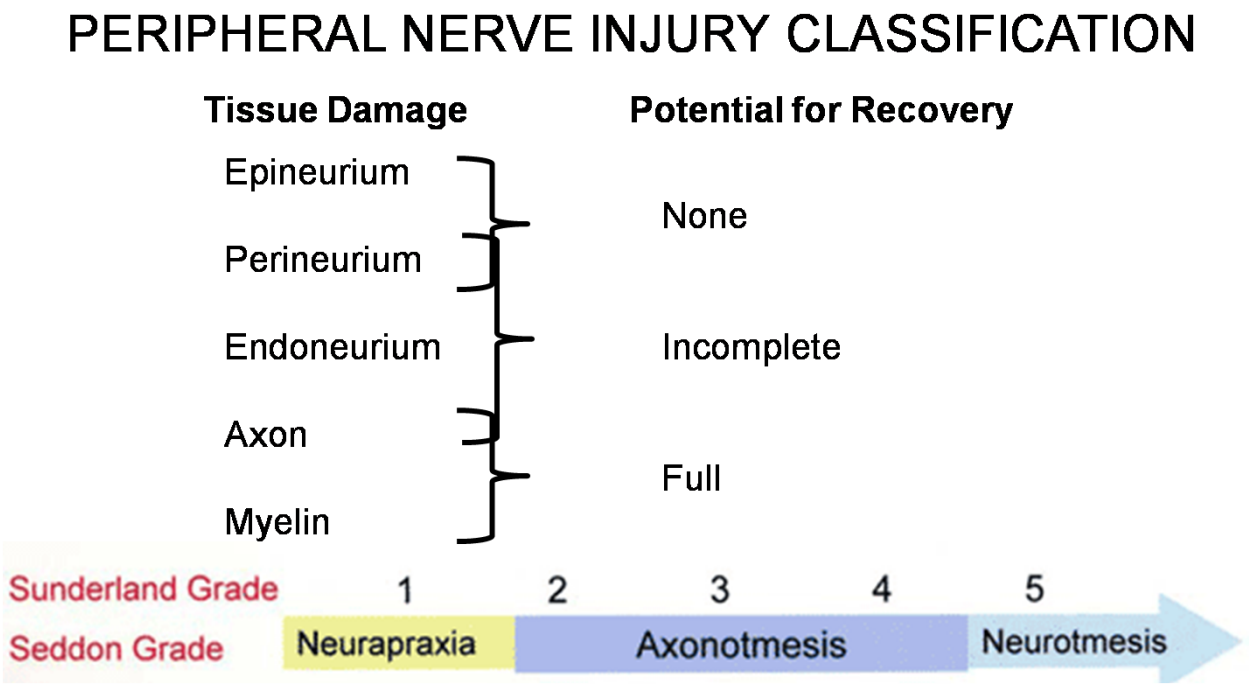

Figure 3. Classification of Peripheral Nerve Injuries (Image modified from [24]).

Each degree of nerve injury results in a unique mechanism for nerve regeneration. Assuming the offending agent ceases to operate, injuries resulting with neurapraxia are temporary and do not result in a discontinuity of nerve fibers, and therefore the regenerative process is straight forward and will not be discussed further. However, axonotmesis and neurotmesis related injuries result in a disorganization of the remaining nerve fiber or trunk

which requires a more complex regenerative process that proceeds in two stages. The first stage involves the disintegration of the axon and myelin sheath along the entire length of the nerve, known as Wallerian degeneration. Following degeneration, the entire axon pathway has perished and regeneration of the axon proceeds as described below.

1.3.2 Wallerian degeneration and nerve regeneration

The degenerative response to injury within the mammalian PNS is a highly conserved process [25]. Upon axotomy, nerve fibers are severed and the connective tissue of the endoneurial tube becomes so disorganized that the normal architecture is completely destroyed. Within the first hours after injury, neurotubules and neurofilaments fragment, resulting with the axoplasms filling with granular material [26]. Protease activity and separation from metabolic resources of the nerve cell body cause the distal axon cytoskeleton to break down and the cell membrane collapses. The dissolution of cell components within the endoneurial tubes in the distal end results in debris which is further compacted by Schwann cells shedding their myelin lipids. From 2 to 3 days after injury, Schwann cells inside the basal lamina proliferate and cooperate with infiltrating macrophages and monocytes to remove and recycle both axonal and myelin-derived materials. These cells also prepare the environment into which regenerating axons grow by releasing neurotrophins which lead axons toward their synaptic targets, resulting in restored neuronal function.

Proximal to axonal disruption, the nerve stump immediately swells after injury as the gap in nerve continuity is filled with a blood clot [23]. Following the typical tissue response to damage (*e.g.* edema and non-specific cellular responses) the neuron undergoes central chromatolysis as the function of the neuron shifts from maintenance of nerve conduction to

regenerating structural proteins [10]. In addition to the dissolution of Nissl bodies, the neuron also experiences nuclear eccentricity, nuclear and nucleolar enlargement, cell swelling and a retraction of the dendrites [27]. Synthesis of glycolytic and respiratory enzymes and neuronal lipoproteins necessary for axonal membrane synthesis all increase [10]. After Wallerian degeneration has occurred, the distal injury site has been cleared and the regenerating nerve fibers grow from the proximal stump across the gap and toward the distal endoneurial tubes to reinnervate the target organs. Schwann cells differentiate from a replicating satellite cell population and accompany the proximal sprouts across the area of injury.

1.3.3 Surgical strategies for nerve repair

The surgical management of peripheral nerve injuries depends upon meticulous microsurgical techniques and aims to enable the maximum number of axons to regenerate [28, 29]. Depending on the severity of tissue damage, common surgical techniques for nerve repair include nerve stump realignment through primary nerve repair or when a gap exists, auto- or allografts may be employed.

1.3.3.1 Anastamosis of proximal and distal nerve stumps

Primary nerve repair is defined as the placement of a nerve suture immediately after or within the first several days following injury such that the injured nerve is still in the inflammatory phase and has not yet begun to scar [3]. Primary nerve repair, also known as end-to-end anastamosis, can be performed when a nerve can be realigned such that the elongation required to reapproximate the nerves is no more than 10% of the nerve length [30]. Beyond 10% in nerve

strain, the microcirculation is reduced and the potential for tearing of the nerve and a break-down of the repair is high.

The three most commonly used techniques for primary nerve repair include: utilizing a few well placed sutures in the epineurium to maintain alignment of the major fascicles within the nerve, group fascicular suturing, and the epineurial splint technique in which the external epineurium is peeled back and rejoined on the deep surface relieving tension from fascicles which are later coapted internally [3]. Regardless of the technique selected, primary nerve repair must be performed without excessive tension and requires that sutures are not placed in the endoneurium or perineurium. When tension is excessive, the nerve gap must be bridged with either a nerve graft or nerve conduit.

1.3.3.2 Nerve grafting

The standard approach for repairing segmental defects in nerve continuity involves grafting autologous donor nerve, typically the sural nerve, as a bridge across the nerve gap. Common surgical techniques for nerve grafting include free nerve grafting ("cable grafting"), and interfascicular nerve grafting. Cable nerve grafting was developed by Seddon to allow for a defect in a single, thick nerve to be repaired using small cutaneous nerves that can be harvested without a loss of function. In this technique, several thin skin nerves are assembled using stitches or glue and fashioned between the interstump gap with two sites of anastamosis. With this technique, some segments of the graft often survive better than others causing partial fibrosis of the graft. Additionally, failure of the sprouting axons to cross the distal anastamosis has been shown to occur in 14% of grafts longer than 3 cm [3].

The disadvantages experienced by surgeons when performing cable grafting led to the development of the interfascicular grafting technique in which cutaneous segments of the graft

are not sutured or glued together but instead, minor units of the graft are dissected and connected individually across a nerve defect. Inherent challenges with this technique include the potential of neuroma formation at donor nerve harvesting sites. To avoid this, surgeons often remove the entire length of nerves at higher levels such that the proximal stump disappears into the depth of the subfascial space and thus causing large longitudinal skin incisions which result in visible scar formation. Additionally, donor nerves have changing fascicular patterns along the longitudinal axis which the requires surgical skill and time for dissection into usable segments for grafting [3].

Though autologous graft placed into a defect results in a better outcome than primary nerve sutures performed under tension, there is a very large disadvantage in this type of therapy, mainly the requirement of a second surgery to harvest the nerve. Sensory deficits and painful neuroma formation can occur at the donor site. Unfortunately, motor and sensory recovery following nerve grafting (as measured by the Medical Research Council Grading System for Nerve Recovery) is often below standards as indicated by a 2000 study in which only 50% of patients demonstrated useful recovery following ulnar nerve repair [31]. For these reasons, the development of synthetic nerve guidance channels is of enormous utility for surgeons attempting to manage neurotmesis related problems. The disappointing functional outcome of peripheral nerve trauma urges researchers to optimize therapeutic interventions.

1.4 CONDUITS FOR BRIDGING NERVE GAPS

Although nerve grafts serve as the standard of care for bridging nerve defects, the major disadvantages associated with their use has led to the development of engineered conduits

through which nerves with a defect distance of 3 cm or less can regenerate through [32]. Nerve guides (also referenced as guidance channels) are cylindrical conduits of either biologic-based or synthetic materials that have been used beginning in the late 1970's to bridge nerve defects [5]. The use of such nerve guides has many advantages, including providing an enclosure for the accumulation of secreted neurotrophic factors from endogenous cells within the site of injury, supporting fibrin clot formation between the injured nerve stumps, preventing neuroma and fibrous tissue formation and decreasing tension across a nerve gap [5, 33, 34].

Within the enormous breadth of nerve guide literature, many of the mechanical requirements of implantable nerve guides have been defined. For example, the guide must be of the proper dimensions: the length must be long enough to bridge the gap without tension and the width must house the nerve stumps without compression. Furthermore, the material must be mechanically sound to resist tearing from sutures yet soft enough to avoid tissue inflammation from mechanical irritation [1]. Finally, it must be possible to produce a porous guide wall yet the nerve guide must be slowly degrading so as to provide support for the entire regeneration period and have a low degree of swelling to avoid compression of the nerve injury. With these parameters in mind, nerve guides have been constructed from a variety of both biologic and synthetic based materials [35] and with a variety of design additives such as luminal fillers [36] or delivered growth factors [37].

1.4.1 Biomaterials for nerve guide synthesis

Both natural and synthetic materials have been used to fabricate nerve guides. The essential parameters of a nerve guide material is that the selected material must be easily formed into a conduit that accommodates the nerve being repaired, it should require little effort from surgeons

to implant, it must be sterilizable and biocompatible [38]. The term biocompatible indicates that the implanted material not cause inflammation, irritation, or scarring [1]. Ideally, an implanted nerve guide should also be biodegradable so as to avoid a secondary procedure for device removal [8].

1.4.1.1 Natural materials

Collagen types I and III constitute 49% of the total protein in nerves [39]. Because of this, collagen has been widely assessed as a biomaterial for nerve guide fabrication [40-42]. When compared to silicone conduits, work by Kemp et al., suggest that collagen guides enhance axonal regeneration, myelination and vascularization in a 10 mm rat sciatic nerve defect [43]. The increase in nerve area and dramatic increase in myelinated nerve fiber numbers were attributed to previous work demonstrating that collagen rapidly revascularizes and integrates into the host tissue following implantation [44]. Though collagen guides have demonstrated useful functional sensory and motor recovery in animal models of peripheral nerve injury, the rapid degradation rate of the material requires that the collagen be cross-linked so as to provide mechanical stability for the regenerative period required for critical size defects [45, 46].

In addition to collagen, purified natural extracellular matrix (ECM) components such as laminin and fibronectin have shown a significant role in axonal development [9]. Laminin is the first ECM protein expressed during embryogenesis and has been shown to both promote axonal outgrowth and guide developing neurites [35]. Other naturally derived molecules that have demonstrated utility in nerve guide fabrication as either the main component for nerve guide fabrication or as a copolymer or nerve guide coating include hyaluronic acid [47, 48], fibrinogen [49], alginate [50], chitin [51, 52], and chitosan [53].

Disadvantages of manufacturing these materials include high cost and potential xenograft problems that exist because the materials are typically extracted from animal sources. In addition, natural polymers tend to collapse following implantation or have early resorption periods that prevent mechanical support of regenerating nerves across long gaps [21]. Despite this, two nerve guide implants that are currently commercially available are composed of type I collagen, the NeuroMatrix/NeuroFlex by Stryker, and the NeuraGen by Integra Neurosciences. Both of these guides are limited to two centimeters in length and are therefore designed for relatively short gaps.

1.4.1.2 Synthetic materials

Biodegradable, well characterized, FDA established polymers such as poly(lactic acid) (PLA), poly(glycolic acid) (PGA), poly(caprolactone) (PCL), and copolymers thereof, have also been used to manufacture nerve guides [20, 54-56]. Two guides composed of biodegradable polymers are sold commercially. The Neurotube by Synovis Micro Companies is comprised of PGA, degrades within three months of implantation and is therefore optimal for very small defects (shorter than 1 cm). The Neurolac by Polyganics which is composed of poly-DL-lactide-co-caprolactone, degrades within 16 months. Both of these implants are packaged in lengths no greater than 4 centimeters [57].

Non-degradable polymers such as silicone [58, 59], polyethylene [60], polyurethanes [61], Teflon [62] and polysulfone [63] have also been examined in human implant studies. While one commercially available guide is made of a non-degradable poly(vinyl alcohol) hydrogel, the Salubridge by SaluMedica LLC, most surgeons prefer fully resorbable scaffolds. This is because permanent materials pose a higher risk for infection, are more likely to result in chronic inflammation and may cause late adverse effects due to nerve compression [64]. In general,

synthetic materials are often attractive candidates for nerve tissue engineering because their chemical and physical properties (for example stiffness, degradation rate and porosity) can in theory be optimized to the specific needs of the application.

1.4.2 Fabrication techniques

Successful synthetic nerve guides are optimized for not only the essential mechanics and geometry of the nerve that is being replaced as discussed in Section 1.4, but nerve guides should also allow for the attachment and migration of the endogenous Schwann cell population and provide adequate mass transfer of nutrients and metabolites. To accomplish this, nerve guides have been fabricated using a variety of conventional techniques which include particulate leaching, electrospinning and super-critical fluid technology. While each processing methodology has inherent attributes and drawbacks, the following sections describe effective methods of processing biodegradable materials into cylindrical conduits with high porosity and surface area.

1.4.2.1 Particulate leaching

Particulate leaching requires the dispersal of a porogen within a polymeric or biologically monomeric solution, followed by particle leaching. Because the particulate employed temporarily holds volume within the scaffold wall, pores remain following particle removal. Typically porogens include sodium chloride, sucrose or lipid microparticles such as those made of Softisan 154 and Witepsol H42 [65]. Benefits of using this fabrication technique include the capability of producing scaffolds with locally porous internal structures, the low cost of the fabrication process and the production of highly interconnected porous microstructures [66].

Synthesis of porous nerve guides using the method of particulate leaching has been performed with poly(caprolactone) [67], poly-D,L-lactide [68-71], poly(lactic-co-glycolic acid) [71-73], and copolymers such as trimethyl carbonate and ε- caprolactone [74], poly(L-lactide-co-ε-caprolactone) [75, 76], and poly(3-hydroxybutyrate-co-3-hydroxyhexanoate) [77]. Important conclusions drawn from this body of work include: solvent casting with porogens is an easily adaptable method for producing highly porous nerve guides with interconnected pores, the pore morphology of resulting nerve guides is defined by the size of the salt crystals and the salt weight fraction of the polymer solution [71] and it is possible to create both uniform (homogenously) porous guides as well as asymmetric conduits with directed solute permeability [73]. However, it has also been reported that dip-coating often results in guides that range in wall thickness along the length, with as much as 45% variability in nerve guide wall thickness within a single guide [77]. Histological evaluation of regenerated nerve using solvent cast nerve guides showed that nerve guides with small pore diameters of 10 μm or less result in smaller and less myelinated nerve fibers than those produced of 30 – 50 μm [77].

1.4.2.2 Electrospinning

Electrospinning is performed using either a polymeric or natural solutions that is pumped into a highly charged spinneret adjacent to a collector. When a significantly large voltage is applied to a solution of choice, surface tension is created in the spinneret (typically a small orifice or flat-tipped needle) and droplets of solution stretch and elongate until a continuous jet is ejected onto a dynamic collecting surface [66]. Solvent evaporation or cooling of the polymer melt solution once the jet stream reaches the collector results in electrospun fibers with diameters ranging between 200 nm and 5 mm. Electrospinning can be used with relatively small expense

and can be used to create scaffolds of high porosity and surface area. Furthermore, though it can be challenging to accurately control deposition of electrospun fibers, literature suggests that pore sizes can be controlled through defined fiber diameter and spacing.

Several studies have been conducted to measure neurite outgrowth within electrospun nerve guides of varying biomaterial, fiber size, and fiber orientation [78-81]. *In vitro* studies using dorsal root ganglion explants have demonstrated that neurites follow highly aligned poly(L-lactide) fibers upon contact and are longer in length than those cultured on randomly aligned substrates [82]. Furthermore, Patel et al., demonstrated that aligned nanofiber matrices reduced neurite branching and encouraged neurite outgrowth, a highly desirable feature of nerve guides [83].

In addition to processing and aligning polymer fibers, electrospinning techniques can also be utilized for incorporating cells and growth factors within the nerve guide wall [66]. In a 2007 study by Chew et al., highly aligned fibers of caprolactone copolymerized with ethyl ethylene phosphate were electrospun with glial cell line-derived neurotrophic factor (GDNF) such that ~5 ng/mg GDNF was cumulatively released over 80 days (measured *in vitro*) [84]. The authors demonstrated that fiber alignment in the longitudinal direction resulted in improved nerve regeneration as measured with electrophysiology when compared to circumferentially aligned fibers. Furthermore, longitudinally aligned fibers used in combination with GDNF delivery resulted in increased number of myelinated axons, nerve cross sectional area and myelin thickness [84]. The percentage of rats with functional recovery as measured with electrophysiology was also improved with GDNF treatment when compared to aligned conduits that did not deliver GDNF. While the addition of growth factor delivery from electrospun nerve guides presented an improvement in nerve guide fabrication, the technique used to incorporate

GDNF was suboptimal and resulted with a burst release of GDNF within the first day, a drawback common with single walled microsphere delivery systems that is likely a result of the protein aggregates near the surface of the polymer matrix.

1.4.2.3 Gas foaming and supercritical fluid technology

Gas foaming of biodegradable polymers allows for a solvent-free formation of porous materials by saturating molded polymer solutions with pressurized gas, typically carbon dioxide (CO_2). By slowly releasing the pressure within the system, air bubbles within the material nucleate, potentially reaching 100 μm in size. Disadvantages of this fabrication technique include the possibility of pores resulting which are not interconnected and are variable in size. Through addition of effervescent salts, the effectiveness of creating highly porous structures can be improved [66].

Alternatively, porous nerve guides have been generated using both biological and synthetic materials by lyophilizing the solvent at supercritical temperatures. Using this technique, nerve guides have been constructed of collagen-glycosaminoglycans [85], chitosan [86], chitin/chitosan [87], poly(D, L-Lactide) [54], and poly(lactic-co-glycolic acid) [88]. To create nerve guides, polymers were first dissolved in an appropriate solvent, typically acetic acid, water, or acetone. The polymer solution was then injected into a cylindrical mold that was cooled by liquid nitrogen to temperatures of at least -40°C. Frozen conduits were then lyophilized to sublimate and remove the solid solvent, creating pores from the displaced liquid volume. Through this process, highly porous (< 90%) polymer guides can be generated [54].

Advantages of this fabrication technique include the batch-to-batch consistency in nerve guide geometry because of the employment of molds. Depending on the complexity of the mold design, guides have been fabricated with longitudinally aligned channels [88] or microtubules

[86], or with radially aligned pores [85]. Drawbacks of using this fabrication technique include the requirement of a more sophisticated apparatus for guide fabrication, the potential for the resulting pore morphology to be oriented instead of interconnected, and the small diameter of generated pores (often less than 10 μm) [54].

1.4.3 Chemotrophic factors

Neurotropism is a concept describing events in nerve regeneration in which axonal growth is directed by a chemotactic diffusible substance along a concentration gradient towards the source [89]. The growth cone of the regenerating axon actively samples the environment for both permissive and inhibitory soluble factors through different tyrosine kinase cell surface receptors [90]. This concept was first demonstrated in the 1980's when it was shown that a distal nerve stump can attract axons from a neighboring proximal stump over distances of about 0.5 cm even when the stumps were placed out of alignment [91]. In a study by Politis et al., proximal stumps of transected rat sciatic nerve were inserted into the single inlet end of a hollow, Y-shaped Silastic tube. Regenerating axons were provided with a vacant arm as an alternative target to the distal sciatic nerve graft arm. In addition, 0.2 micron pore size filters were placed between the distal nerve segment and the proximal segment. These results strongly supported the hypothesis that rat sciatic nerve fibers migrate exclusively toward the distal nerve stump because of a chemical gradient of soluble tropic molecules secreted by cells within the distal nerve stump [25]. Furthermore, these chemical attractants are not exclusively neurotropic as both the migration of Schwann cells and endoneurial fibroblasts are also promoted [89].

1.4.3.1 Nerve Growth Factor and other Neurotrophic Factors

Neurotrophic factors investigated to promote peripheral nerve regeneration include nerve growth factor (NGF), brain-derived neurotrophic factor (BDNF), neurotrophin-3 (NT-3), neurotrophin-4/5 (NT-4/5), ciliary neurotrophic factor (CNTF), and glial cell line-derived growth factor (GDNF) (Table 2) [9].

Table 2. Neurotrophic Factors Investigated to Promote Nerve Regeneration

Substance	*Abb.*	*Function*
Nerve Growth Factor	NGF	Survival and maintenance of sympathetic and sensory neurons
Brain-Derived Neurotrophic Factor	BDNF	Supports motor neuron survival and promotes axonal growth of motor and sensory neurons
Neurotrophin-3	NT-3	Promotes motor neuron survival and motor and sensory growth
Neurotrophin-4	NT-4	Supports axonal outgrowth of motor neurons
Glial Cell Line-Derived Neurotrophic Factor	GDNF	Upregulated by Schwann cells after injury. Promotes survival of motor, sensory and autonomic neurons
Ciliary Neurotrophic Factor	CNTF	Produced by Schwann cells. Promotes motor neuron survival, outgrowth and sprouting

Because NGF is a known promoter of sensory neuron survival, outgrowth and branching, extensive research has been invested in the delivery of NGF into nerve lesions [92, 93]. NGF is continuously expressed at low levels in uninjured peripheral nerve and is upregulated in the distal nerve stump upon nerve injury or transection [94]. In addition, NGF has been shown to promote sensory neuron survival, outgrowth and branching [95]. When used in solution inside a nonporous silicone tube, NGF treatment has been shown to yield significantly more myelinated

fibers, thicker myelin sheaths, and higher recordings of nerve conduction velocity than those values seen in the negative controls [96]. Because of the short half-life of NGF, delivery methods have been investigated for the sustained delivery of the neurotrophic factor over the duration of nerve regeneration. NGF has been encapsulated within biodegradable microspheres [97, 98] or lipid microtubules [99], adsorbed onto the polymer surface of the nerve guide or coated on the inside of the nerve guides with centrifugal casting [100]. When used in a critical size defect in the rat animal model (13 mm), high doses of NGF (20 to 50 ng/mL) have resulted in a total fiber number and fiber width that was comparable to autograft controls within transverse sections from the midpoint of the implanted guide [101]. However, NGF treatment groups were inferior to autografts in the distal regions of the conduits, suggesting that NGF was not supplied to the injured nerve for enough time or at sufficient concentration. In addition, when compared directly, alternative neurotrophic factors such as BDNF, NT-3, and GDNF have proven more successful than NGF for promoting nerve regeneration in terms of myelinated axon diameter [102] and total number of myelinated axons [103]. Finally, work by Doubleday and Robinson suggest that tropic molecules secreted from the distal nerve stump that direct axonal outgrowth are unlikely to include NGF as rats immunized to NGF produced the same directed growth [89].

BDNF has been reported in the literature to support motor neuron survival [104], as well as promote both motor neuron [105] and sensory neuron axonal outgrowth [106]. The effects of BDNF on peripheral nerve regeneration have been assessed following delivery by osmotic mini-pumps [107, 108], calcium alginate spheres [109] or through direct cross-linking to a collagen nerve guide matrix [110]. In studies performed comparing BDNF treatment to lactated Ringer solution for repair of a primary cut and repair injury in the rat sciatic nerve, BDNF did not result

in an improvement in either fiber count or mean axon diameter above the negative control [108]. Additionally, 6 mm sciatic nerve defects repaired with BDNF covalently linked to collagen nerve guides did not result in an improved nerve conduction velocity but did show improvement in the mean axon count [111]. In addition to BDNF, CNTF has also been shown to promote motor neuron survival, outgrowth and sprouting [112-114]. When used in combination with BDNF, CNTF has been shown to promote axonal sprouting into the distal segment of a 6 mm defect in the sciatic nerve as well as increasing the average axonal diameter [111]. However, CNTF has also been demonstrated to participate in glial scarring resulting in nonpermissive growth as an inducer of reactive gliosis [115, 116].

Following peripheral nerve lesion, GDNF has also been correlated with improved regeneration in several *in vivo* models [103, 117-125]. GDNF has been reported to promote not only axonal outgrowth and maturation [119, 123, 126], but also Schwann cell proliferation and myelination of normally unmyelinated small axons [127]. Therefore, this trophic factor holds great potential as a therapeutic for the treatment of neurodegenerative diseases [128]. Further documentation of GDNF use in *in vivo* studies can be found in Section 5.1.

1.4.4 Additional factors for enhanced nerve regeneration

Acidic and basic Fibroblast Growth Factors, (aFGF and bFGF) are strong promoters of angiogenesis, are mitogenic for endothelial cells, fibroblasts, and Schwann cells and have therefore been hypothesized to enhance peripheral nerve regeneration following injury [129-132]. When bFGF was adsorbed onto nitrocellulose paper that was implanted within the lumen of a silicone nerve conduit in a rat sciatic nerve, histological transverse sections of the proximal half of the excised conduits revealed that bFGF improved tissue integration of perineurial-like

cells, vasculature, and Schwann cells when compared to silicone controls which resulted in fibrin matrix and erythrocytes [131]. Furthermore, aFGF used in combination with a collagen matrix to repair a 1 cm rat sciatic nerve defect demonstrated regeneration comparable to autografts and were superior to collagen used with NT-3 or BDNF [133].

Similar to aFGF and bFGF, Vascular Endothelial Growth Factor (VEGF) has been shown as an angiogenic factor through high specificity of endothelial cell migration and has been hypothesized to aid in nerve regeneration. Silicone conduits filled with matrigel and VEGF were fabricated to quantify the morphological effect on Schwann cell and axonal regeneration. Results indicated that very high doses of VEGF (500 ng/mL) were required to produce significantly improved increase in total fiber counts and axon diameter as compared to matrigel controls without VEGF. However, the fascicular area and myelin thickness of the regenerated nerve was not improved, nor was the resulting gastrocnemius muscle mass higher than negative controls [134].

Other trophic factors such as Endothelial Growth Factor (EGF) and Insulin-like Growth Factor (IGF) have also been employed in *in vivo* models of nerve repair with limited results. The effects of EGF on axonal regeneration were evaluated within collagen tubes across a 7 mm gap in the sciatic nerve in the rat animal model. Although EGF was used at a very high dose of 3 mg/mL, no significant improvements were observed in electrophysiological recordings or axonal regeneration [135]. The IGFs (IGF-I and IGF-II) have neurotrophic effects *in vivo* [136, 137] and are upregulated in distal regains of peripheral nerve following crush injuries and then decrease with the progression of nerve regeneration [138]. Results from a study comparing IGF therapy within nerve guides made from acellular muscle grafts with cultured Schwann cells across a 2 cm rat sciatic nerve defect showed a decrease in nerve regeneration when compared to

grafts used without IGF. However, autografts used in combination with IGF delivered via osmotic pump had a significantly increased axon count and an improved g-ratio compared to autografts without IGF-I [139]. These contrasting results may indicate a negative response of the IGF dosage used in combination with Schwann cell populations seeded within the muscle grafts. These studies underline the need for further development of controlled release systems to progress the current understanding of the dose dependent effects of nerve regeneration following growth factor administration.

1.4.5 Tissue engineered nerve guides

Tissue engineered nerve guides have been fabricated to investigate the regenerative capacity of complex scaffolds that integrate multiple cell adherence and axonal guidance cues for nerve repair. In addition to soluble factors, nerve regeneration can also be improved by supplementing nerve guides with supportive extracellular matrix components such as small intestinal submucosa (SIS) or with cell adhesion molecules. Furthermore, genetically engineered cells that are capable of overexpressing active growth factors in a controllable, sustained manner for the entire duration of nerve regeneration have been incorporated into nerve guides.

1.4.5.1 Nonautologous / acellular grafts

Because the internal structure and extracellular matrix of grafted nerve segments have proven highly effective for promoting nerve repair in terms of guiding cell migration and promoting axon elongation, several types of acellular tissue grafts have been investigated as potential nerve guides [140]. Studies using decellularized sciatic nerve allograft show that the manner in which the grafts are decellularized significantly affects the capacity to support nerve

regeneration. While freeze-thaw cycles and chemical treatments with Triton-X produce acellular grafts with greatly reduced axonal regeneration when compared to fresh isograft controls, the use of sophisticated and lengthy processing protocols of harvested allografts have achieved nerve regeneration comparable to the gold standard of nerve repair, the autograft in a 1 cm rat sciatic nerve defect [140].

Acellular nerve grafts have also been prepared from venous and muscle grafts [141]. The first uses of acellular muscle grafts involved digital nerve repair; a lack of viable Schwann cell populations were seen in grafts of increased length [141]. Therefore, nerve regeneration in venous and muscle grafts seeded with cultivated Schwann cell populations were compared to isograft controls. In terms of both regenerated axon counts and nerve conduction velocity, both muscle and vein grafts failed to equal the regenerative capacity of positive control treatments [141, 142].

As an alternative to grafting whole tissue, small intestinal submucosa (SIS) has also been processed into conduits for nerve repair. SIS is a minimally immunological xenograft transplant processed from the extracellular matrix of porcine small intestine. The material has been reported to contain a large number of inherent tissue growth stimulating factors. In addition, depending on the processing technique used, SIS is readily reorganized and absorbed by the host, providing great potential to replace the lesioned nerve segment with native tissue [143]. However, when SIS nerve guides were implanted across a 1 cm defect and allowed to regenerate for 90 days, a period adequate for measureable nerve regeneration across this established defect length, no functional recovery could be measured and sciatic nerve growth into the guide was restricted to the proximal portions of the conduit. These results may have occurred as a result of the rapid resorption rate of SIS, which is between 4 and 16 weeks [144]. It is therefore possible

that implanted guides comprised of SIS were not mechanically adequate to support axonal outgrowth over the entire regeneration period.

1.4.5.2 Schwann cell seeded nerve guides

The importance of Schwann cells for peripheral nerve regeneration has been well documented [145, 146]. Schwann cells produce extracellular matrix, cell adhesion molecules, integrins and neurotrophins, and have therefore been intensely studied as additives in nerve guide implants. Therefore, it has been hypothesized that the use of artificial conduits containing viable Schwann cell populations would be a promising strategy to repair peripheral nerve injuries [147-149]. Nerve guides investigated with seeded Schwann cell populations and matrigel have shown that functional recovery following nerve regeneration was similar between autograft controls and only those conduits seeded with autologous Schwann cells populations [150]. Implantation of conduits with Schwann cells isolated from mice of the same strain or mice of the same litter resulted in inferior functional recovery following repair of a 6 mm sciatic nerve defect [150]. These results are disappointing for the potential therapeutic use of nerve guides with human Schwann cells as it is not clinically feasible to isolate and expand the required number of Schwann cells for implantation (due to donor site morbidity and time required for Schwann cell culture and expansion). However, new culture protocols that improve Schwann cell proliferation and expansion may allow Schwann cell seeded nerve guide to be more clinically useful someday.

1.4.5.3 Gene therapy

The success of neurotrophin delivery from nerve guides toward improved nerve regeneration has often been cited as suboptimal due to low dosages and short delivery periods [151]. In addition, the stability of such growth factors is generally poor, causing the bioactivity

of delivered proteins to be uncertain [37]. Therefore, the transplantation of genetically modified cells which overexpress specified neuroregenerative proteins have been investigated with great interest [9]. In particular, genetically modified fibroblasts have been studied for the sustained delivery of bFGF [152], CNTF [153], NGF, BDNF, and NT-3 [154]. While these cells have not been utilized toward peripheral nerve repair, genetically modified fibroblasts hold promise for both supporting axonal outgrowth and delivering neurotrophic factors directly within the site of nerve injury.

Schwann cells have also been modified to overexpress factors such as bFGF and GDNF and have been used in peripheral nerve studies. When implanted in a critical size, 1.5 cm, sciatic nerve defect, silicone tubes filled with matrigel and Schwann cells overexpressing bFGF improved both the number and length of regenerated myelinated axons when compared to controls [132]. Schwann cells have also been genetically modified to overexpress GDNF [155]. In the rat animal model, 1 cm sciatic nerve defects were bridged with silicone tubes filled with saline, Schwann cells, or Schwann cells overexpressing GDNF. Histological analysis of regenerated nerves showed an increase in myelinated fiber number and density, myelin sheath thickness, and the overall nerve area as highest in animals with GDNF expressing Schwann cells. Additionally, nerve conduction velocity and compound muscle action potential were greater with the experimental GDNF group. It was not noted in this study if transfected cells migrated from the implanted nerve conduit or if any adverse consequences of using genetically modified cells were observed.

While results with genetically engineered cells have shown great potential for delivering a continual supply of active growth factors which promote nerve regeneration, challenges with gene therapy use in humans remain. It would be beneficial if modified cells implanted within

nerve guide could respond to environmental cues to cease protein overexpression. In this manner, neurotrophin expression could be used to lead regenerating axons into the a graft and then expression could be stopped once it is no longer necessary [9].

1.5 SUMMARY AND LIMITATIONS OF PREVIOUS RESEARCH

A difficulty in human nerve regeneration is that the axon length that must be regrown is not just the length of the gap, but is the length from the lesion to the innervated muscle. Consequently, end organs (such as muscle) may become atrophied before the axon can reinnervate them. Therefore, it is insignificant if the axon reaches the correct location in the periphery or not as the resulting nerve remains nonfunctional. While nerve guides serve as a barrier to infiltrating fibroblasts and inflammatory cells for scar minimization, guides are not successful for gaps greater than 3 cm because nothing within commercially available nerve guides actively promotes axonal growth. And so, any manipulation that speeds axonal growth would have an enormous impact on large gap PNS repair as it would improve the likelihood of serviceable motor and sensory control, which is the end goal of surgeons and patients.

The methods for improving nerve guides for repairing long nerve defects described within this chapter have included: 1) optimization of nerve guide materials and fabrication techniques for obtaining high porosity, low immunogenicity and slow degradation rates, 2) delivery of chemotrophic factors for promoting axon and Schwann cell survival and 3) supplementing nerve guides with extracellular matrix components or genetically engineered cells in tissue engineered nerve guides. In terms of commercial success, it is highly desirable that a nerve guide be manufactured such that it is an off-the-shelf product that does not require seeding

of cell populations at the time of implantation. For this reason, nerve guides that serve as a drug delivery vehicle for neurotrophic factors to enhance nerve regeneration may be more clinically relevant. However, the nerve guide delivery systems described herein are plagued by short release periods and low concentrations of delivered growth factors. Therefore, a current limitation within nerve guide design is the ability of nerve guides to deliver a physiologically relevant concentration of neurotrophic factors over the entire regeneration period required for repairing long nerve defects.

1.6 HYPOTHESIS AND SPECIFIC AIMS

Our underlying hypothesis is that delivery of Glial Cell Line-Derived Neurotrophic Factor (GDNF) from nerve guides using microsphere technology will result in functional recovery in the *in vivo* environment following large axonal defects in the peripheral nervous system. This hypothesis is based on the following observations. First, GDNF is expressed by Schwann cells, and injury results in rapid up-regulation in distal segments of lesioned sciatic nerve [156]. However, with increasing gap length, the GDNF levels at the site of the injury are not sufficient to compensate for the lack of target derived neurotrophic factors to maintain cell survival [157]. Second, GDNF has been shown to prevent avulsion-induced motorneuron death following complete nerve transection whereas NGF, BDNF, and IGF have all failed to enhance cell survival or cell size [126]. Third, GDNF treatment with guidance channels following spinal cord injury resulted in a reduction of reactive astrocytosis and macrophage accumulation [120]. Finally, histological comparison of nerve guides implanted with and without added GDNF showed that nerve guides releasing GDNF increased nerve fiber number, fiber diameter, and

additionally myelin thickness was improved, an indication of improved nerve regeneration [103, 158].

The specific aims presented here were designed to systematically evaluate key design parameters of a polymer nerve guide prototype and assess GDNF therapies in regards to functional recovery following large lesions in peripheral nerve trunks.

Specific Aim 1: To quantify the *in vitro* effect of nerve guide wall porosity percentage and wall thickness on growth factor and nutrient diffusion through PCL nerve guide walls. The work performed towards this aim is described within chapter 2.

Specific Aim 2: To develop a nerve guide that can deliver encapsulated proteins for the duration required for the regenerating peripheral nerve axon to reach the distal nerve stump following transection. The performed towards this aim is presented within chapters 3 and 4.

Specific Aim 3: To quantify the *in vivo* effect of GDNF delivery from a PCL nerve guide in terms of histological and functional regeneration of the sciatic nerve across a critical size (1.5 cm) defect. The work performed towards this aim is presented within chapter 5.

2.0 DIFFUSION OF SOLUBLE FACTORS THROUGH DEGRADABLE POLYMER NERVE GUIDES: CONTROLLING MANUFACTURING PARAMETERS

2.1 INTRODUCTION

2.1.1 Structural requirements

While some of the mechanical requirements of implantable nerve guides are obvious, for example the guide must be of the proper dimensions (the length must be long enough to bridge the gap without tension and the width must house the nerve stumps without compression) and the material must be strong enough to resist tearing from sutures yet soft enough to avoid tissue inflammation, other design aspects are less clear. As shown as early as 1985, a critical facet in nerve regeneration is the delivery of oxygen and nutrients to the surviving nerve tissue [159]. Presumably, the nerve guide should maximize the influx of oxygen and nutrients through pores in the guide wall. However, there is a limit in wall porosity because of opposing needs to allow interstitial fluids into the guide, prevent inflammatory cells from migrating into the lumen, and minimize the diffusion of growth factors out of the guide lumen.

2.1.2 Optimization of nerve guide wall porosity parameters: previous studies

It was initially presumed beneficial to place transected nerve stumps in nonporous silicon tubes because the guide would contain the fluid and cells that come from the regenerating nerve stumps to the injury site. However, a 1985 study by Jenq and Coggeshall showed that by allowing the extracellular fluid and its cells into the lumen of the guide through macroscopic holes in the guide wall, the number of both myelinated and unmyelinated axons was significantly increased [159]. In a subsequent study, the authors further specified that pore size was an important factor in determining nerve repair. Using two pore diameters, 1.2 micron and 5 microns, the authors saw 8/8 rats had full recovery using the 5 micron pore size while only 4/9 rats recovered using the 1.2 micron pore size in an 8 mm gap. It is important to note here that the authors defined successful regeneration as producing nerve cables with at least 1000 axons uniting the proximal and distal nerve stumps [160]. The most dramatic change that occurred in the nerve tissue was the extensive development of the perineurium, the layer of fibroblasts and collagen that surrounds axons and forms fascicles. The authors hypothesized that the significant increase in both myelinated and unmyelinated axon counts that were seen in silicone tubes with macroscopic holes in the walls was a result of an increase in the number of support cells lining each fascicle and supporting the axon. Though the authors do not speculate how this would impact the functional outcome of the nerve regeneration (the authors did not indicate if the animal regained use of the muscle), it was left to determine if the increased number of axons were beneficial, or if they merely indicated greater axonal branching. Finally, in 1989 the effect of two pore sizes that varied in molecular weight cut off were examined in 4 or 8 mm gaps in LVG hamsters [161]. The authors concluded that molecular weight cut off of the guide wall made a significant difference and lower numbers of myelinated axons were seen in pores

permeable to proteins with a molecular weight of 10^6 Da versus 10^5 Da. This was presumably because the type of growth factor that could escape the lumen of the tubes was restricted. Unfortunately, functional recovery of the animals was not addressed.

A 2002 study by Rutkowski and Heath used computer models of diffusion to predict maximum axonal growth from experimental data on diffusivities, uptake rates, and nerve growth factor production rates [162]. This publication demonstrated the impact of certain variables, one of which was the supply of oxygen and nutrients, on axonal and Schwann cell growth. The effects of both porosity and wall thickness were examined to determine their impact on the luminal concentrations of a secreted growth factor and oxygen. Pore size was controlled by using a salt leaching technique using salt crystals $\leq$ 106 microns in diameter. Porosity percentage was altered by the salt content in the polymer solution which was then poured into molds. The final porosity percentage was therefore an estimate. As expected, it was determined that lower porosity better retains secreted growth factors but at the expense of oxygen, a critical factor in the survival of Schwann cells and other support cells. Conclusions obtained from the computer model were that larger porosity allows for more oxygen diffusion and an increasing wall thickness reduces the diffusion of soluble factors out of the guide.

Nerve guide porosity and wall thickness have been evaluated in an *in vitro* system in which parameters were evaluated for their ability to influence nerve growth in excised dorsal root ganglia [163]. Conduits were made with varying porosity, (0, 55%, 65%, 75% and 85%) and wall thicknesses (0.56 mm, 0.81 mm, 1.10 mm, 1.28 mm, and 1.44 mm). From this *in vitro* work it was shown that axon growth was slightly increased with increasing porosity and was significantly reduced in conduits with wall thicknesses greater than 0.8 mm. When these conduits were seeded with Schwann cells, nonporous conduits had much lower growth compared

to the porous ones. Such *in vitro* findings correlate well with results obtained from diffusion models described above.

2.1.3 Chapter aims

The purpose of Specific Aim 1 was to optimize nerve guide fabrication parameters such that lysozyme diffusion through poly(caprolactone) (PCL) conduit walls was minimized while nutrient (glucose) permeability was maximized. To achieve this, the effect of three fabrication variables (wall thickness, pore size and porosity percentage) on both glucose and protein diffusion was tested. While it is unlikely that protein loss from a porous scaffold will be entirely eliminated, it was determined that a 10% loss of protein payload would be acceptable. However, because Schwann cell survival has been indicated as being limited by blood nutrient diffusion, we also aimed to determine the maximum nerve guide permeability to soluble glucose. Though glucose is a small, hydrophilic molecule and as such cannot be used to model the inward diffusion of large biomolecules such as polysaccharides or triglycerides, it was hypothesized that modeling glucose permeability was an adequate method of approximating critical blood nutrient diffusion for molecules such as oxygen and blood glucose.

2.2 METHODS

2.2.1 Reagents

All chemicals were analytical grade or purer and were purchased from commercial suppliers. Poly(caprolactone) (average Mw ~65,000, average Mn ~42,500, pellets), ethyl acetate, ninhydrin, sodium chloride (crystalline, fine), poly(vinyl alcohol) (average Mw 9,000-10,000, 80% hydrolyzed), poly(DL-lactide-co-glycolide) (lactide:glycolide (50:50), mol wt 40,000-75,000 units), lysozyme from chicken egg white, glucose assay kit (GAGO-20), tetrahydrofuran, 1,6-hexanediamine, and D-(+)-Glucose were all purchased from Sigma-Aldrich (St. Louis, MO). Glass capillary tubes, premium glass microscope slides, and Tissue-Tek Cryo-OCT Compound were purchased from Thermo Fisher Scientific (Waltham, MA). The Micro Bicinchoninic Acid (BCA) Protein Assay Kit (23235) was purchased from Pierce (Rockford, IL). 26G Needles were purchased from Becton Dickinson (Franklin lakes, NJ). Poly(L-lactide) was purchased from Durect Corporation (Pelham, AL).

2.2.2 Polymer nerve guide fabrication

Permeable nerve guides were created by dissolving PCL in ethyl acetate. To the dissolved polymer solution, sodium chloride impregnation was accomplished by adding NaCl in a specified v/v% (NaCl:PCL) amount. Large crystals of NaCl were first ground into a fine powder with a mortar and pestle and then sifted through sieves of known mesh diameter. Glass capillary mandrels 1.5 mm in diameter were coated with a 17% w/v% aqueous solution of poly(vinyl alcohol) (PVA), air dried and then immersed into the polymer slurry creating NaCl/PCL mandrel

coatings. The ethyl acetate was allowed to evaporate for a minimum of ten minutes between successive mandrel immersions into the polymer slurry. After the completion of the dip-coating process, the resulting polymer conduits were submerged in distilled water to allow for salt and PVA dissolution, and the glass mandrels were removed. Porosity percentage was varied through altering volume percentages of sodium chloride in the polymer-solvent slurry. The nerve guide wall thickness was varied by the number of immersions performed in the dip-coating technique used to create the guides.

2.2.3 Nerve guide porosity measurement

Wall porosity percentage was determined after scanning electron microscopy (SEM) image analysis. PCL nerve guides were dried, cut into thin sections with a razor blade and mounted on metal stubs covered in copper double sided tape. The guides were then gold-coated to 3.5 nm thick using a Cressington 108 auto sputter-coater (Cressington, Watford UK), and viewed with a JEM-6330f (Jeol, Peabody, Ma) scanning electron microscope operated at 5kv acceleration. Low magnification images were used for image analysis as previous literature has shown better agreement of image analysis of material porosity with actual porosity values (Figure 4A) [164]. To determine the guide porosity, the proportion of pixels dedicated to ‘wall area’ versus ‘pore area’ was determined with ImageJ software [165]. Because of the subjective nature of thresholding grey-scale images, Otsu’s method of thresholding was employed to decipher grayscale levels within the image that were considered polymer or empty space, creating a binary image from which pixel areas could be calculated (Figure 4B) [164]. For bi-level thresholding, Otsu’s method optimizes the threshold such that the variance between light and dark pixels is

maximized [166] and as a result, the variance in pixels associated with the pores and walls is minimized.

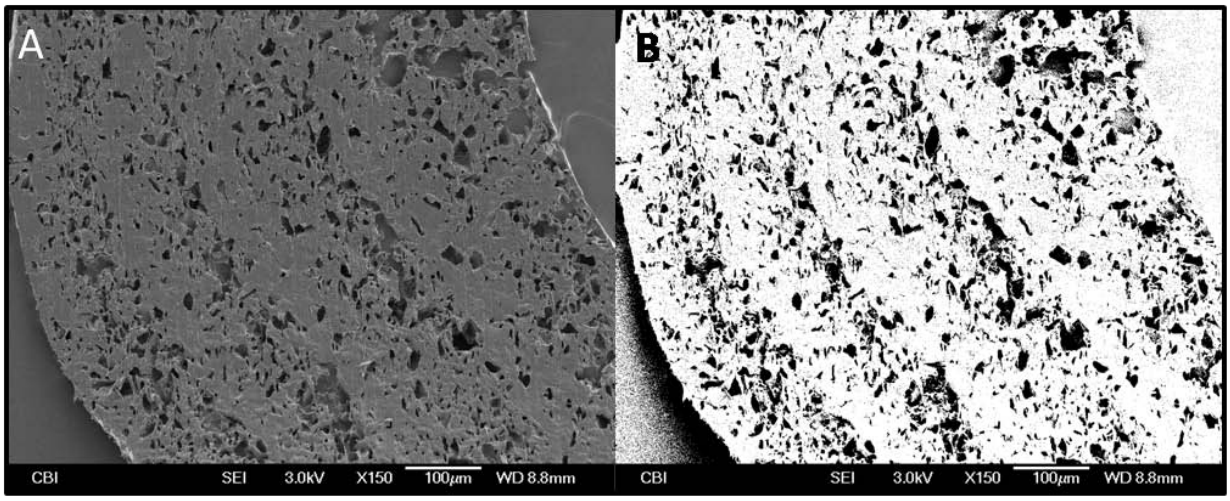

Figure 4. Scanning electron image of 50% porous PCL nerve guide in original format (A) and as processed with Otsu thresholding by ImageJ (B).

2.2.4 Nerve guide wall thickness measurements

To determine the wall thickness of PCL nerve guides, 5 lots of six nerve guides were fabricated using the dip-coating manufacturing technique described above. Within each batch of nerve guides, the number of immersions of the glass mandrel into the polymer slurry varied between a single immersion and seven consecutive immersions. After the nerve guides were detached from the mandrel and dried, each guide (2 cm in length) was cut into six sections of similar length and

submerged in Optimal Cutting Temperature (O.C.T.) compound and frozen for sectioning with a cryostat. The nerve guides were then sectioned (15 µm) and mounted onto glass slides. Optical microscopy and a stage micrometer were then used to determine the wall thickness of PCL nerve guides. For each image of a nerve guide cross section, over 15 radial measurements were taken, perpendicular to the tangent of the inner wall, (at approximately 24 degrees apart) and were averaged to obtain the mean wall thickness for each nerve guide (Figure 5A - B). Averages were used to assess the influence of the number of mandrel immersions on the wall thickness of the final nerve guide as well as to ensure reproducibility of our fabrication methods over a number of nerve guide batches.

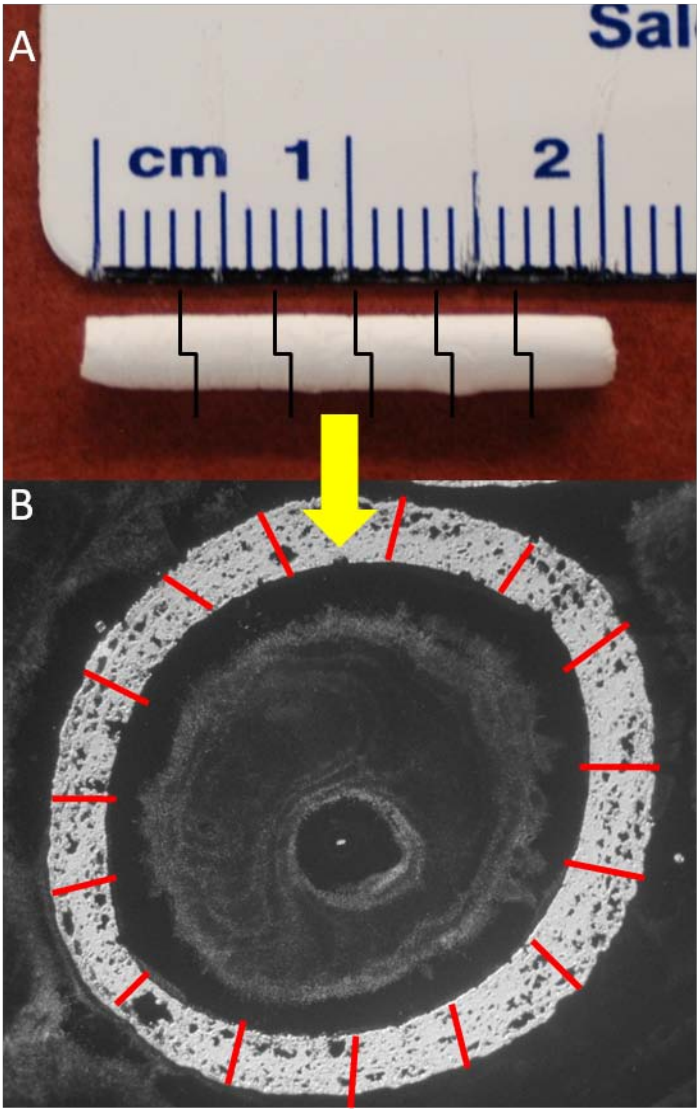

Figure 5. Image of a PCL nerve guide divided longitudinally into six lengths (A). Each length of nerve guide was placed vertically into a square mold, sectioned (15 µm) using a cryostat, mounted onto a glass slide and viewed with a light microscope (B). From each cross section, 15 radial wall measurements (tangential to the circumference) were averaged to determine the mean and standard deviation of nerve guide wall thicknesses.

2.2.5 Optimization of nerve guide porosity and wall thickness

PCL nerve guides were fabricated as described above and the effect of each variable (wall thickness, pore size and porosity percentage) on glucose and protein diffusion was tested using factorial analysis (Table 3). To measure the diffusion of glucose or protein through the guide wall, both ends of the guide were sealed with a water-proof sealant E-6000 craft adhesive. Nerve guides were discarded if the sealant extended more than 1 mm onto the surface of the nerve guide wall, thus eliminating any guides from the study which might have a significantly reduced porosity due to the experimental design. After the sealant was allowed to dry, 50 µl of solution with dissolved glucose (10 mg/mL) (to mimic blood nutrient diffusion) or lysozyme (8 mg/mL) was injected through a 26G needle into the PCL nerve guide lumen through a sealed end. Any opening that was created with the needle was securely closed and the guide was submerged in 5.0 mL of phosphate buffered saline. After 4 hours, the extraluminal solution was aspirated and the concentration of diffused solution was measured with an appropriate assay (glucose: Glucose Assay Kit; lysozyme: bicinchoninic acid protein assay). Preliminary experiments for comparing nerve guide permeability over time indicated that a 24 hour period of solute diffusion through nerve guide walls allowed all experimental groups with transluminal flow to reach system equilibrium and thus all external solutions contained an identical concentration of measured solute. 4 hours was therefore chosen as a time point for measuring initial significant differences in nerve guide permeability. Considering the physiological concentration of blood glucose is ~0.9 mg/mL [167] and our anticipated neurotrophic factor dosage is 100 ng/mL [103, 125], the initial glucose or lysozyme solutions are not physiologically relevant. The injected solution concentrations were adjusted to match the minimum working range of the glucose assay (20

μg/mL) and the Micro BCA protein assay (0.5 μg/mL) with consideration to the dilution of solutes caused by submerging the fluid-filled nerve guide in saline solution.

Table 3. Fabrication Parameters Used to Create Nerve Guide Standards.

Standard Number	*Wall Thickness (mm)*	*Porosity (%)*	*Pore Size (μm)*
1	0.2	50%	10 – 38
2	0.6	50%	10 – 38
3	0.2	50%	75 – 150
4	0.6	50%	75 – 150
5	0.2	80%	10 – 38
6	0.6	80%	10 – 38
7	0.2	80%	75 – 150
8	0.6	80%	75 – 150

The numerical response resulting from each experimental group was the percentage of material that diffused from the PBS solution inside the guide through the guide wall and into extra-luminal solution. The solute was considered to have 100% permeability if the concentration of the solute inside the lumen of the nerve guide and the aqueous external PBS solution were equal (the system was in equilibrium). While the initial diffusion studies were useful for evaluating key fabrication parameters that limit growth factor loss from the guide lumen, this preliminary study was an estimate for the behavior of such solutes through the guide after implantation. For example, protein fouling would be expected to occur immediately following guide implantation *in vivo* and could have an effect on the guide wall permeability.

Therefore, the diffusion of lysozyme and glucose were subsequently modeled after the nerve guides were incubated in a 10% FBS saline solution for 24 hours prior to performing similar diffusion studies as described above.

2.2.6 Ninhydrin assay

A ninhydrin assay was used to verify the presence of amine groups on the surface of poly(caprolactone) nerve guides. Ninhydrin (triketohydrindene hydrate) is a chemical that reacts with free amine groups creating a solution colored Ruhemann's purple that can be compared to samples of known protein concentration [168]. Following protein fouling diffusion experiments, each nerve guide was immersed in a 1.0 M ninhydrin solution for 1 minute and then transferred to a glass vial that was heated at 75°C for 15 minutes. The treated guide was then dissolved in 4 mL of tetrahydrofuran (THF). The absorbance of the final solution was measured at 560 nm using a SpectraFluor Plus plate reader (Tecan, Switzerland). A standard curve was prepared using known concentrations of 1,6-hexanediamine.

2.2.7 Statistical analysis

Multiple nerve guide batches were created for each measurement with a minimum repetition of five. Results are expressed as the mean ± standard deviation or standard error where indicated. Analysis of variance (ANOVA) was used to determine statistical significance between experimental groups. The least significant difference method was used for multiple comparisons with $p < 0.05$.

2.3 RESULTS

2.3.1 Scanning electron microscopic analysis of PCL nerve guides

Porous poly(caprolactone) nerve guides were created using a dip-coating, salt-leaching technique. The resulting nerve guides were 2-3 cm in length and flexible (Figure 6 A - B). SEM analysis revealed that nerve guides of low porosity (50% porous) displayed smooth inner walls and several blind-ended (pores that are exposed only at a surface) or closed pores (pores that are isolated within the polymer matrix). In contrast, highly porous nerve guides (80% porous) consisted of walls that were less smooth with highly interconnected pores for transluminal flow and solute diffusion (Figure 7).

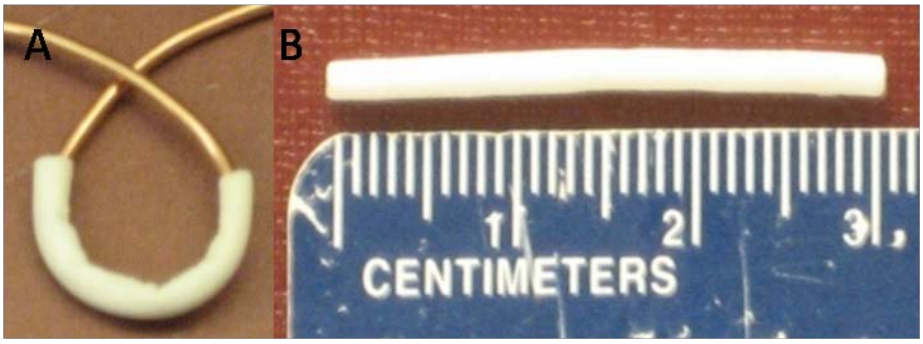

Figure 6. Photo of a flexible PCL nerve guide (A). Image of nerve guide after fabrication (B).

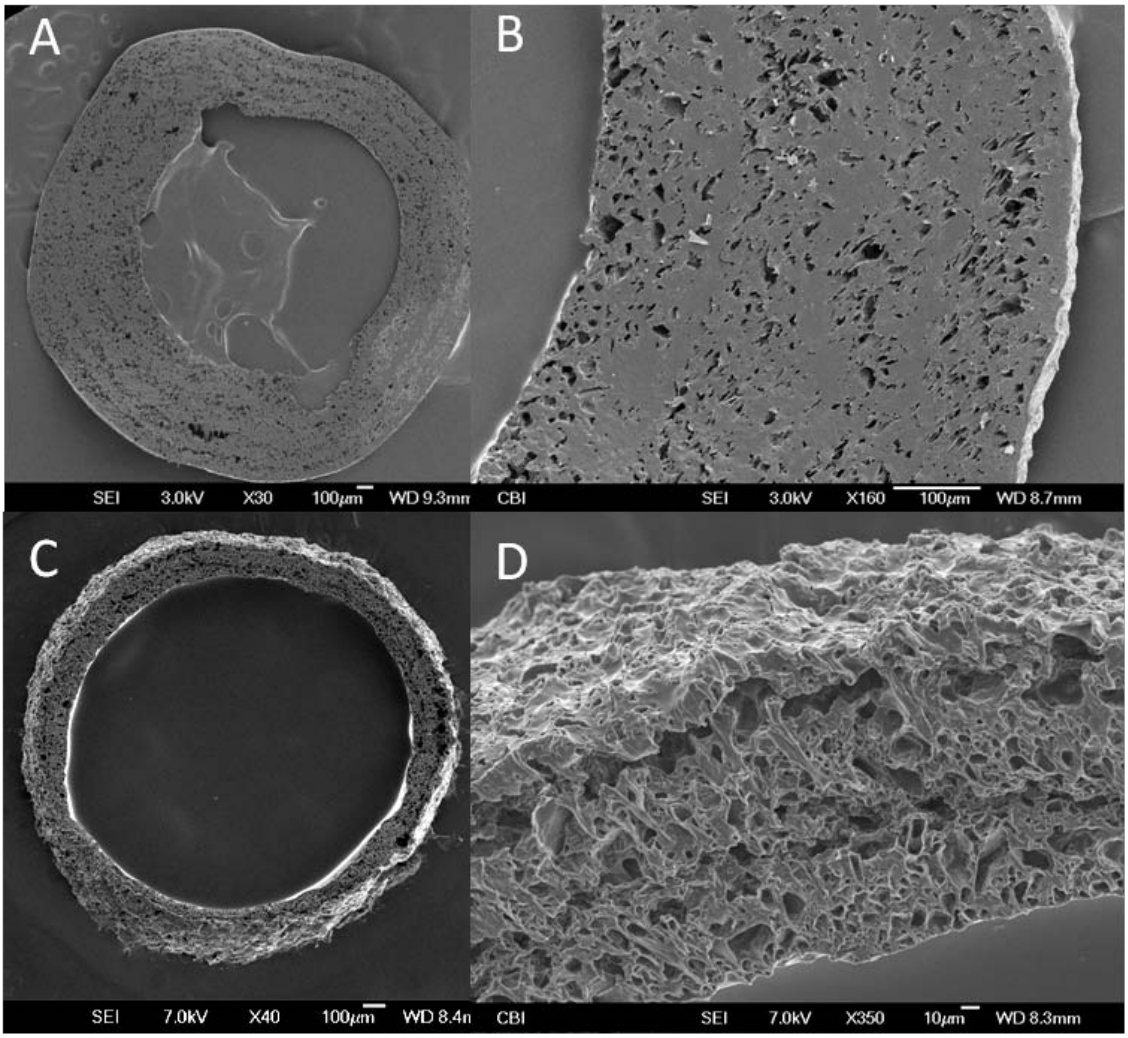

Figure 7. Scanning electron images of low porosity (50%) nerve guides revealed guides with smooth luminal surfaces (A) and blind-ended and closed pores (B). In contrast, highly porous nerve guides (80% porous) had walls that were less smooth (C) with highly interconnected through-pores (D).

2.3.2 Validation of nerve guide porosity

Photographs of SEM images of nerve guide cross-sections were used with ImageJ software to determine the porosity percentage of the nerve guide walls. The theoretical porosity was determined by the addition of a known volume of NaCl (density: 2.16 g/cm3) to a known volume of PCL (density: 1.145 g/cm3). NaCl crystal diameter ranged between 10 – 38 μm. Results obtained from binary image analysis of the percentage of open space compared to guide wall are shown in Figure 8. Nerve guide porosity was measured for guides of 50% NaCl/PCL composition to 70% NaCl/PCL in 5% increments. For all nerve guides, the measured average porosity was within 3% of the theoretical porosity, with the greatest variation seen in the 60% porous nerve guides where 57.2% was measured. Standard deviation in guide porosity averages ranged between 6% and 11%, indicating an acceptable rate of consistency between nerve guide batches.

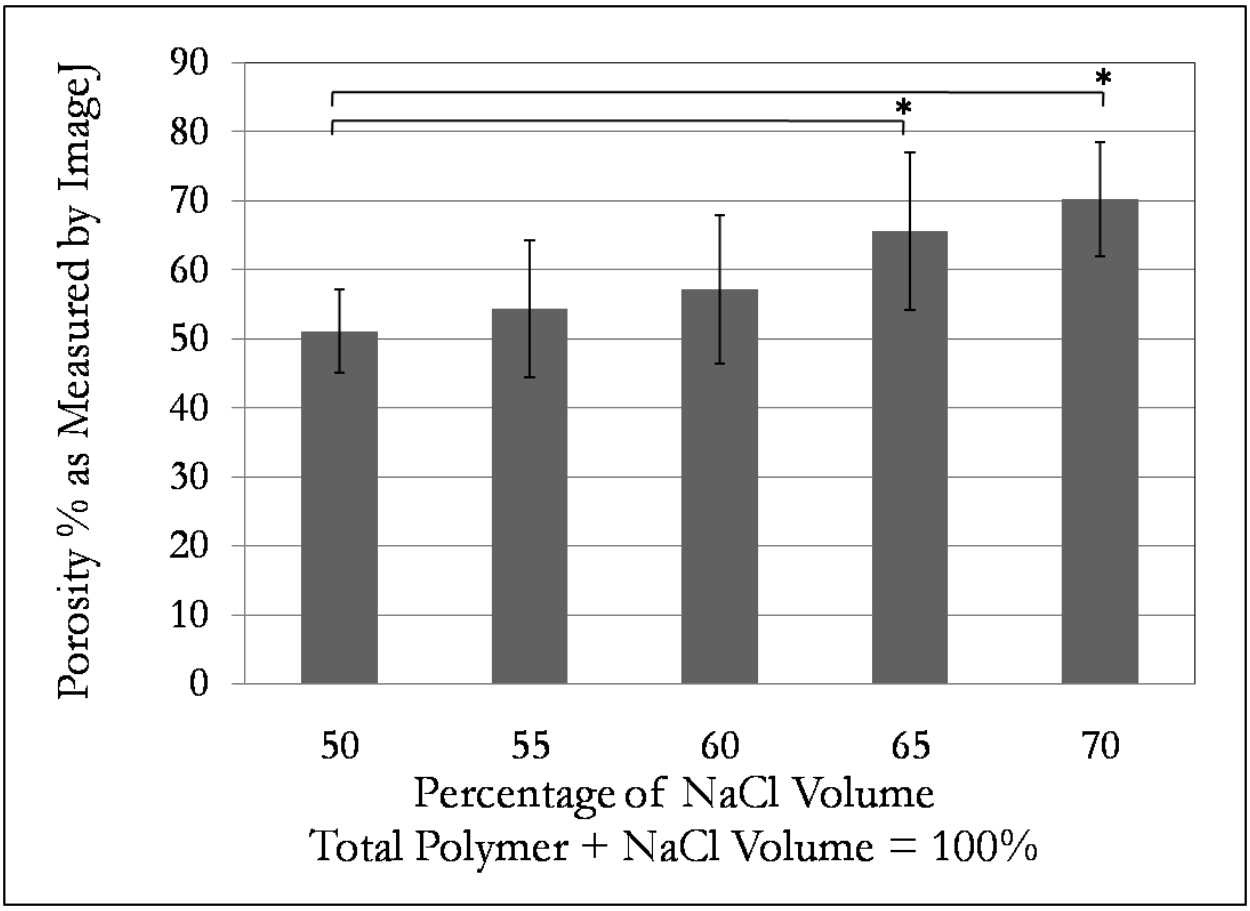

Figure 8. Porosity of the PCL conduits as determined by the percentage of open space in nerve guide walls. Error bars represent mean ± standard deviation for n=5. Significance between groups is indicated by asterisks ($p<.05$).

2.3.3 Validation of nerve guide wall thickness

Wall thickness varied depending on the number of immersions used to create each nerve guide. PCL nerve guides were fabricated with two wall porosities (50% and 80%) and a variable number of immersions of the mandrel into the polymer slurry. At least 6 cross sections of each guide from all batches were analyzed to obtain mean wall thickness (Figure 9). Results indicated that the nerve guide wall thickness was proportional to the number of mandrel immersions into the polymer slurry. Furthermore, the 80% porous nerve guides required more mandrel immersions into the polymer slurry to create a nerve guide of similar thickness to the 50% porous guides. This difference in thickness was caused by the change in viscosity of the polymer solution required to create the original PCL/NaCl slurry. When guides of 50% porosity were fabricated, a polymer solution of 20% (w/v) PCL was originally prepared. To this solution, 5.659 g of sodium chloride was added. However, in order to create an 80% porous nerve guide of the same original polymer solution concentration, 22.638 g of NaCl would have been required. Because porosity percentage was due to a volume ratio of NaCl to PCL, a more reasonable weight of NaCl (7.92 g) was instead added to a 7% polymer solution to manufacture 80% porous nerve guides. However, these two polymer/NaCl slurries had slightly different viscosities which contributed to the difference in nerve guide wall thickness due to the number of mandrel immersions.

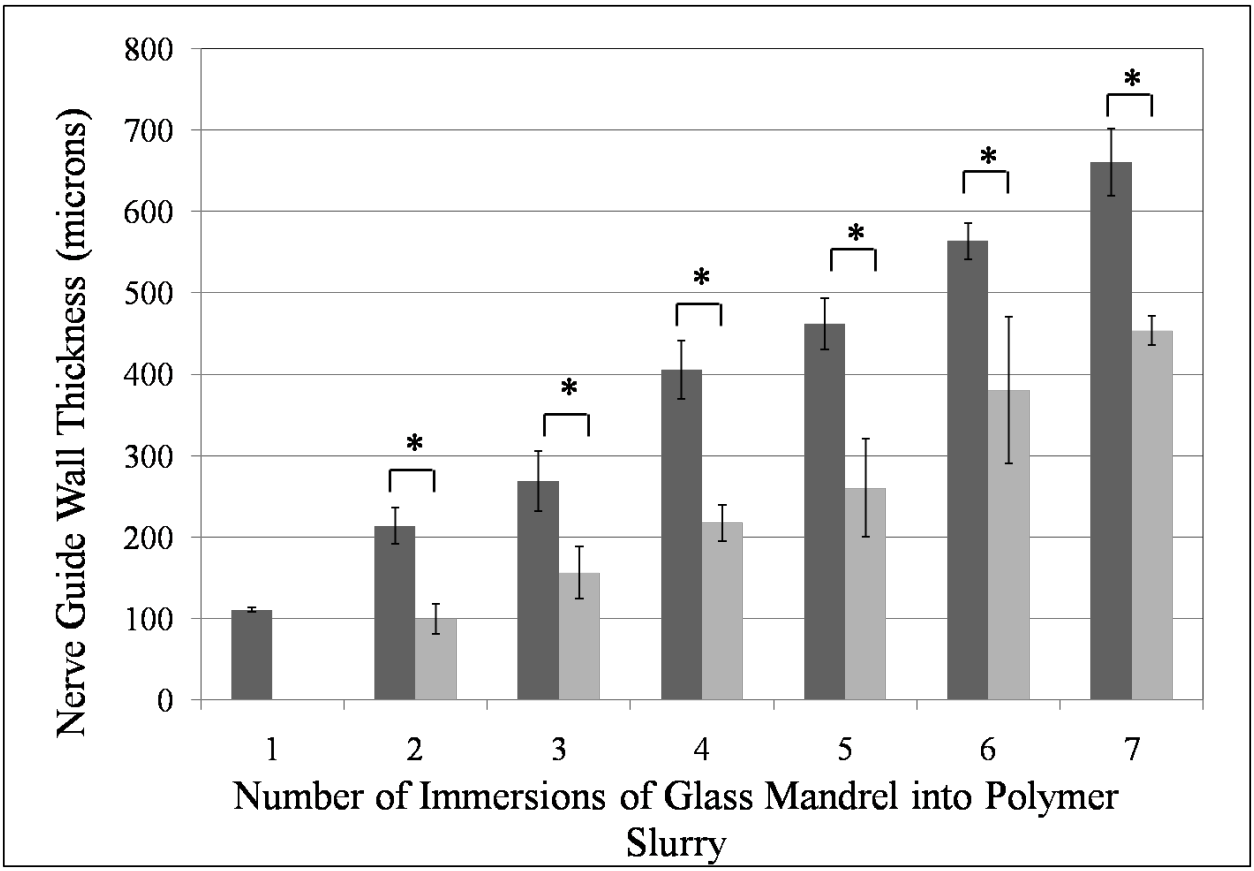

Figure 9. Wall thickness of PCL nerve guides as measured with light microscopy and a stage micrometer from 5 batches of samples. ■ 50% porosity, ■ 80% porosity. Statistical significance between porosity percentage groups and between successive immersions was achieved (asterisks represent $p<.0001$). Results are expressed as mean ± SE for n=5 guide lots.

2.3.4 Optimization of nerve guide wall parameters

Parameters of a nerve guide that affect diffusion include wall thickness, pore size (creating pore tortuosity), and pore percentage. The effect of each variable on glucose and protein diffusion through PCL nerve guides was tested using factorial analysis. This type of analysis allows all three parameters to be tested simultaneously instead of modifying each factor at discrete values one at a time [169]. Each parameter was tested at a low and high value to provide a contrast of averages. The effect of each possible value between the selected ranges on lysozyme or glucose diffusion for all three parameters was then estimated. Additionally, simple effects, potential parameter interactions, and main effects are revealed through this type of analysis.

The low and high porosity percentages were chosen specifically because 50% porous guides are the lowest porosity percentage with interconnected pores when using the lowest pore diameter and thus transluminal flow, while porosities greater than 80% produced mechanically unstable guides. Wall thicknesses were chosen as 200 μm for the low variable range because this thickness is considered sufficient for nutrient diffusion [170], and 600 μm was considered the high endpoint for the wall thickness range because this is a wall thickness that minimizes diffusion [162]. Finally, pore sizes were selected because 10-38 μm is the minimum salt crystal diameter that can be successfully sieved and 75-150 μm is the largest crystal range that can be impregnated into PCL that would not disrupt the wall continuity upon leaching in the 0.2 mm thick guide. These three parameters were varied to determine which combination most successfully contained lysozyme within the lumen of the guide while simultaneously permitting glucose to diffuse freely through the guide walls.

2.3.4.1 Nerve guide porosity percentage

The results indicate that porosity percentage is the main parameter affecting lysozyme and glucose diffusion through PCL nerve guides (Figure 10A). For the period during which solute diffusion was measured for nerve guides made of 10-38 μm pores and wall thicknesses of 0.6 mm, nerve guides which are 50% porous appeared to be almost impermeable for both glucose and lysozyme. However, when the porosity was increased to 80%, nearly 50% of the concentration of glucose was able to diffuse through the nerve guide wall and into the surrounding aqueous environment. Under similar conditions, approximately 44% of the lysozyme concentration was lost. When the pore diameter was increased, it was observed that lysozyme diffusion increased to a small extent while glucose diffusion was not affected (Figures 10B and 10C). At low porosity percentages, such as 50%, a pore size increase from 10-38 μm to 75-150 μm produced no effect on the diffusion of solutes through the guide wall. This was most likely caused by the large number of closed pores seen in the 50% porous nerve guide SEM images. However, for more highly porous guides, the pores are interconnected and protein diffusion is slightly increased. The diffusion of the small molecule, glucose, does not appear to be affected by the diameter of the pores and thus subsequent experiments involved a smaller diameter pore size so as to minimize lysozyme loss (Figure 10B).

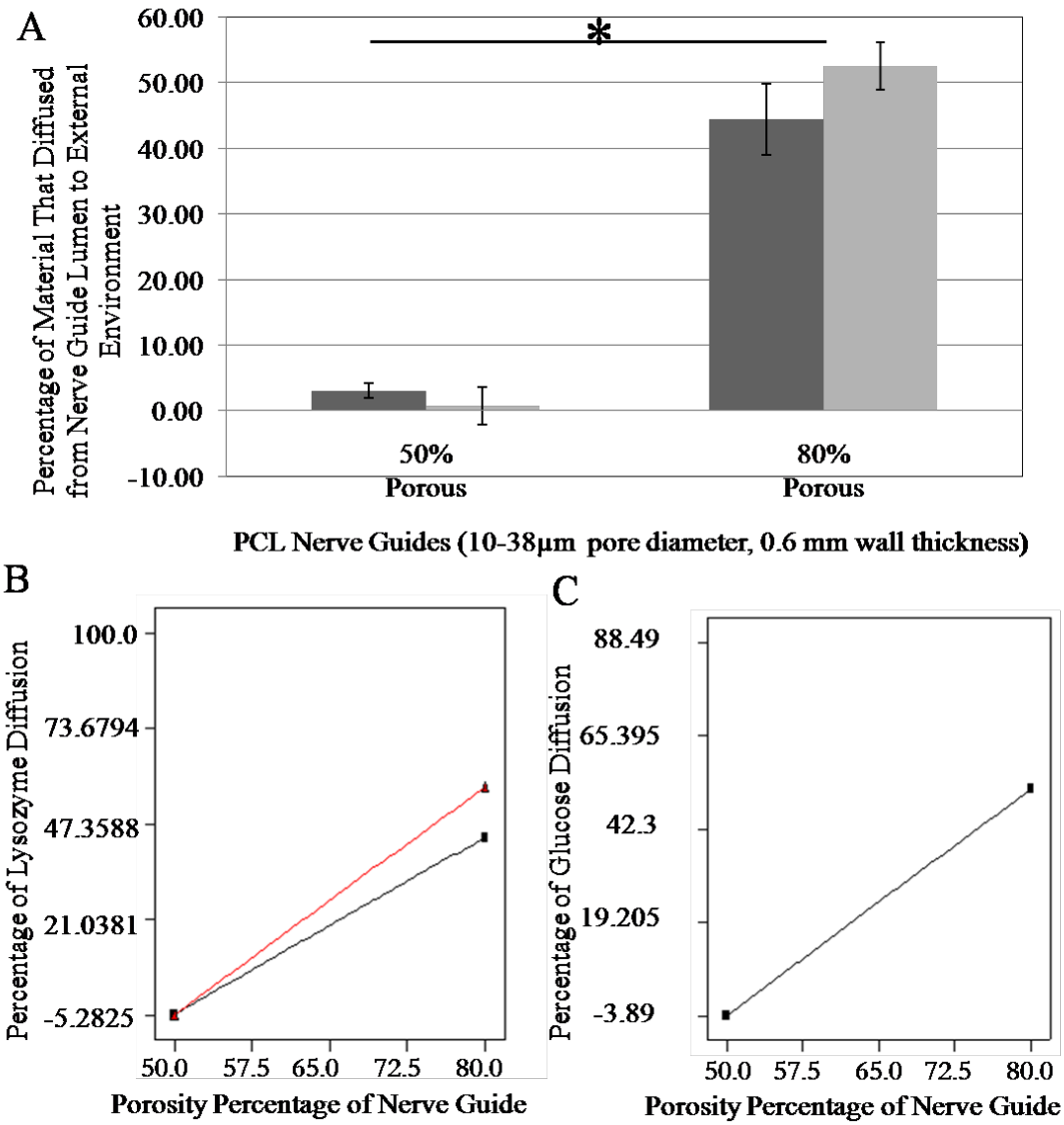

Figure 10. A) Percentage of material that diffused through PCL nerve guides as determined by glucose assay kit and bicinchoninic acid protein assay. Guide wall was 100% permeable to solute if the concentration of the solute inside the lumen of the nerve guide and the aqueous external PBS solution were equal. ■ lysozyme, ■ glucose. B) Porosity percentage and pore size interact to increase lysozyme diffusion when both parameters are simultaneously increased. The red line indicates 75-150 µm pore diameter while the black line is 10 – 38 µm pore diameter. C) Diffusion of glucose increased with porosity percentage regardless of an increase in pore size. Differences between solute permeability due to wall porosity percentage are significant ($p<.0001$). Results are expressed as mean ± standard deviation for n=5.

2.3.4.2 Nerve guide wall thickness

Increasing nerve guide wall thickness is an additional manufacturing parameter that limits the diffusivity of both lysozyme and glucose. As expected, when the wall thickness of the nerve guide was increased, the permeability of both lysozyme and glucose was decreased through the nerve guide walls (Figure 11A). The impact of wall thickness was most significant on the diffusion of glucose, which decreased from ~82% permeable with a 0.2 mm thick nerve guide wall to ~53% permeable in a nerve guide of 0.6 mm thickness (Figure 11B). This is a significant decrease of 29% ($p < .0001$). The results indicated that there was a smaller decrease in lysozyme wall permeability with a 25% reduction of solute diffusion (Figure 11C, $p < .05$).

Because nutrient diffusion is critical to nerve regeneration and glucose diffusion was significantly increased by maximizing the wall porosity percentage, nerve guide wall porosity percentages were not considered adequate below 80%. Furthermore, pore diameter was a useful parameter for minimizing lysozyme diffusion in highly porous guides (80% porous) while glucose diffusion was not affected. Therefore, further studies were performed using guides of 10 – 38 μm pore diameter. Optimization experiments indicated that the thickness of the nerve guide wall needed to be analyzed using discrete parameter values in increments between the initial minimum and maximum ranges of 0.2 and 0.6 mm. Therefore, analysis in protein diffusion using nerve guides of variable wall thickness were performed to determine the wall thickness parameter that would best restrict lysozyme permeability while simultaneously allowing for adequate glucose diffusion (Figure 12A).

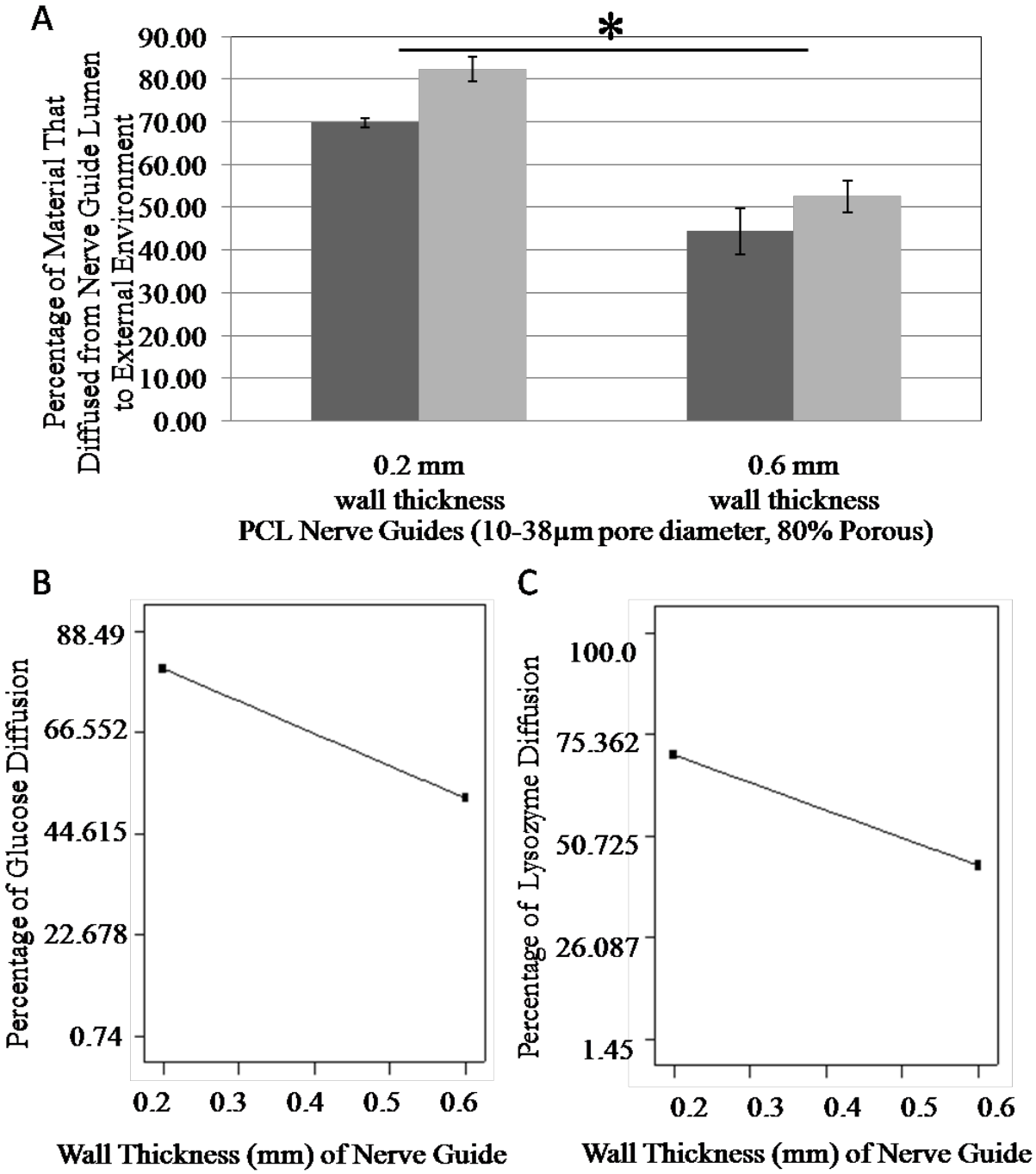

Figure 11. A) Percentage of material that diffused through PCL nerve guides as determined by glucose assay kit and bicinchoninic acid protein assay. ■ lysozyme, ■ glucose. B) The permeability of PCL nerve guides to lysozyme as affected by nerve guide wall thickness. C) The permeability of PCL nerve guides to glucose as affected by nerve guide wall thickness. Results are expressed as mean ± standard deviation for n=5. (* $p < 0.05$)

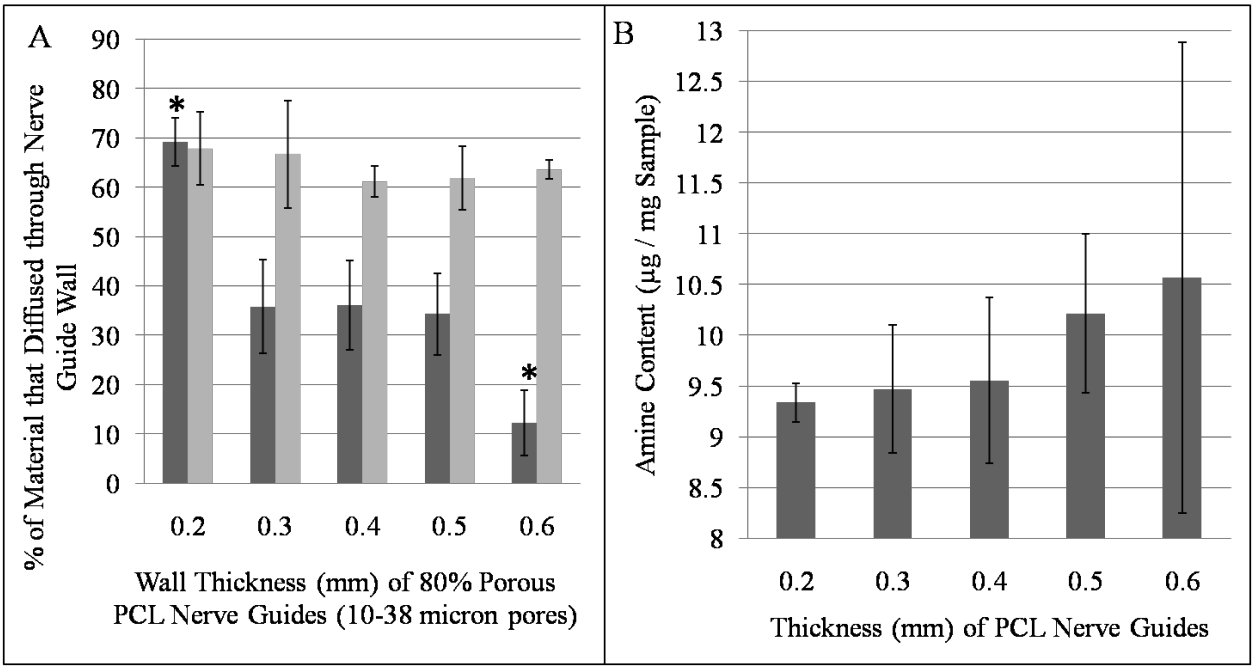

Figure 12. A) Percentage of material that diffused through PCL nerve guides as determined by glucose assay kit and bicinchoninic acid protein assay. ■ lysozyme, ■ glucose. Results are expressed as mean ± standard deviation. Asterisks indicate significant differences at 0.2 and 0.6 mm wall thicknesses for lysozyme diffusion ($p<.0001$). There was no significance between any of the glucose measurements ($p > 0.05$). B) Ninhydrin analysis of PCL nerve guides of 5 wall thicknesses following protein adsorbtion. Results are expressed as mean ± standard error for n=3. There was no significant difference between groups ($p > .05$).

2.3.5 Effects of protein fouling on PCL nerve guide permeability

To determine the effect of protein fouling on solute diffusion through the nerve guide wall, nerve guides were incubated in 10% FBS in phosphate buffered saline solution for 24 hours prior to performing a diffusion study as described above. Protein fouling caused a decrease in lysozyme

diffusion from within the nerve guide (Figure 12B). Initial diffusion studies indicated that nerve guides of 10 – 38 μm pore diameter and 80% porosity that were not coated with protein allowed approximately 45% of the lysozyme concentration originally contained within the lumen of the nerve guide to diffuse through the polymer wall. After the PCL surface was treated with a protein rich solution, the percentage of lysozyme that diffused from the internal, luminal environment of the nerve guide significantly decreased to approximately 10% ($p<.0001$). A ninhydrin anaylsis of protein deposition on the nerve guide surface suggested that proteins adhered not only to the external surfaces of the nerve guides but also throughout the internal pore surface of the polymer conduit, though experimental values were not statistically significantly different between groups ($p > .05$).

2.4 DISCUSSION

Polycaprolactone was initially chosen for use in nerve guides because it is a slowly degrading polymer that can provide sound mechanical support for the regenerating nerve for over one year. In addition, the degradation products, succinic acid, butyric acid, valeric acid, and caproic acid, are nontoxic and do not cause inflammation [171]. Furthermore, though PCL is typically a very rigid polymer (elastic modulus of 206 – 345 MPa), high porosity has been shown to decrease rigidity and allows for the creation of soft, flexible nerve guides [172]. While it is highly desirable for the implanted nerve guide to move fluidly within an animal as the animal regains mobility, previous studies performed with our PCL nerve guides shows that the PCL guides are also easily sutured across a sciatic nerve gap and maintain mechanical stability for the duration of 16 week *in vivo*. Finally, the hydrophobic properties of PCL would enhance the capacity of

the nerve guide to contain both delivered and secreted neurotrophic factors within the area of the nerve injury due to the low diffusivity of hydrophilic proteins through the material [173].

It is well known that the peripheral nervous system is abundantly vascularized throughout axonal trunk lengths by vasa nervorum. Nerve trunks are supplied by blood vessels along their course by arteriae nervorum, which are intimately related to the nerve, and supply not only the supporting tissues of nerve trunks with oxygen and nutrients, but also contribute to the nutrition of the nerve fiber itself [14]. The importance of nerve vasculature is evident from literature reporting improved regeneration by nerve gap bridging devices that are porous when compared to identical but nonporous guides [21, 174]. Creating a porous nerve guide that permits adequate metabolic exchange across the tube wall while retaining growth factors to the internal lumen of the guide is a substantial challenge. The goal of Specific Aim 1 was to optimize nerve guide fabrication parameters such that lysozyme diffusion through poly(caprolactone) (PCL) conduit walls was minimized while nutrient (glucose) permeability was maximized.

Nerve guide porosity was increased through increasing porosity percentage and pore diameter, which created tortuosity, and by decreasing nerve guide wall thickness. The results indicate that in a hydrophobic material, such as PCL, porosity percentage is the main effect determining both hydrophilic protein diffusion as well as the permeability of small molecules such as glucose. When PCL nerve guides were increased in porosity from 50% to 80%, with other parameters held constant, the permeability of the nerve guides to lysozyme increased from 3% to 45% ($p < .05$), an increase of 42%. Glucose diffusion was also improved with an increase in wall porosity percentage, with permeability increases of nearly 9% for every 10% increase in wall porosity percentage.

Because lysozyme must diffuse through the PCL nerve guide walls through water-filled interconnected channels, an increase in pore size would be expected to decrease the pore tortuosity (the ratio of the length of a curved path to the direct distance between the ends of the path) when porosity percentage is held constant. Previous literature has shown that as the tortuosity of porous PCL is decreased, the diffusion of lysozyme that permeates through PCL membranes increases [173]. Therefore, the diffusion of lysozyme in this system was expected to decrease with a decrease in pore diameter. Our results confirm this hypothesis; however, the effects of pore diameter were seen as an interaction effect with porosity percentage. As pore diameter and porosity percentage were simultaneously increased, the permeability of PCL to lysozyme also increased. The permeability of PCL to glucose, a smaller molecule, was not affected by pore diameter. This parameter interaction is especially helpful for our optimization purposes as high porosity percentage nerve guides allow for more glucose diffusion, while protein loss can be minimized by reducing the nerve guide pore diameter. Wall thickness studies indicated that by increasing the guide wall thickness, both glucose and lysozyme diffusion would be reduced.

In the early stages of nerve regeneration, prior to the fibrous encapsulation of the nerve guide that occurs due to the foreign body response, proteins from biological fluids such as blood plasma would be expected to adsorb onto the PCL guide surface. It was initially hypothesized that protein adsorption would limit the diffusion of lysozyme through the nerve guide wall because small pores would limit solute diffusion through the guide walls. As indicated by Figure 8, protein fouling greatly decreased the diffusion of lysozyme through the guide wall while glucose diffusion was not significantly affected. The dramatic decrease in lysozyme permeability was most likely caused by protein adsorption that occurred throughout the entire

surface area of the internal pore channels, decreasing the available pore diameter. Furthermore, proteins have a large number of both negative and positive charges and an adsorbed protein monolayer would present a modified surface to the diffusing lysozyme. Because lysozyme has a high surface activity on negatively charged surfaces [175], large amounts of lysozyme may adhere to the internal luminal surfaces, effectively limiting channel passageways from further protein diffusion. Glucose (Mw 180 Da), a molecule roughly 81 times smaller than lysozyme (Mw 14,600 Da), does not appear to be significantly affected by protein fouling [73].

In addition to protein fouling, a fibrous capsule surrounding the nerve guide would also be expected to form after *in vivo* implantation thus further reducing the capacity of growth factors to diffuse outward. At longer time points, it would be expected that the majority of released protein would be retained in the injury site within the lumen of the nerve guide.

2.4.1 Limitations

In this study, PCL nerve guides were fabricated according to specifications for wall thickness, pore size and porosity percentage. However, there are some considerable limitations within the manufacturing procedure that limit the precision of the final measured nerve guide parameters. First, the nerve guides are prepared using a dip coating technique, which does not result in a constant wall thickness along the entire length of the final guide. The analysis performed on the effect of wall thickness as a result of the number of immersions of the glass mandrel into the polymer solution resulted in an average thickness value for the range of potential measurements distributed along the length of the guide. The information obtained from the wall thickness evaluation provides a guide for an end user to approximate the number of immersions required for a nerve guide to be of a specified wall thickness range, however it is suggested that a nerve

guide be measured using calipers to ensure that the final nerve guide has been produced with the final desired wall thickness.

A second limitation within the manufacturing protocol for PCL nerve guides is inherent in the method used to obtain the range of salt crystals for creation of pores. While sodium chloride was first ground to a fine powder and then separated into particle size ranges using sieves, this process does not distinguish between individual pieces of NaCl and agglomerates [164]. Analysis of this type of preparation and measurement of NaCl by Grant et al., has shown that NaCl separated through sieving results in a distribution in the equivalent volume diameter of salt samples with fractions containing a significant proportion of small diameter particles due to the passage of agglomerates through the salt sieve [164]. Alternative porogens include lipid microparticles such as Softispan 154 or Witepsol H42 as discussed in Section 1.4.2.1.

An additional limitation within studies performed toward nerve guide optimization concerns the use of nonphysiologically relevant concentrations of solutes required for the diffusion analysis of glucose and lysozyme from the interior of the PCL nerve guides. While normal blood levels of glucose are ~0.9 mg/mL [167] and our anticipated neurotrophic factor dosage is 100 ng/mL [103, 125], the assays used to measure each solute required that much more concentrations of each be used. The use of highly concentrated solutions of both glucose and lysozyme may cause the effects of nerve guide manufacturing on solute diffusion to be over estimated. Furthermore, the diffusion studies performed within this study aim do not assess the diffusion of protein released from a delivery device incorporated within the polymer nerve guide scaffold. The goal of Specific Aim 1 was to conduct optimization studies on nerve guide manufacturing parameters to maximize the percentage of a potential neurotrophic factor retained within the lumen of the nerve guides. However, such studies do not account for proteins

delivered over several weeks. It is anticipated that because the external surface of the nerve guide will have been exposed to blood for a sufficient period for the development of a fibrous capsule surrounding the material, the flux of proteins from the nerve guide lumen will be severely limited.

2.5 CONCLUSIONS

PCL nerve guides were reproducibly manufactured with tailored porosity percentage, wall thickness, and pore diameter through a dip-coating salt leaching technique. For factorial analysis, these three parameters were varied across ranges to measure the response of glucose and lysozyme diffusion through the guide wall. Initial optimization experiments resulted in the highest glucose diffusion from guides of 80% porosity. Because initial nutrient and oxygen delivery is so critical to axon and Schwann cell survival at the site of nerve injury, nerve guide porosity was not considered adequate below 80%. Additionally, it was determined that at high porosity percentages, decreasing the pore diameter was a measurable method of decreasing the lysozyme permeability of PCL nerve guides while not creating a loss of glucose permeability. PCL fouling studies were used to fine tune the desirable nerve guide wall thickness. Results indicated that nerve guides of 0.6 mm thickness decreased the loss of lysozyme to ~10% without significantly diminishing glucose permeability. Based on the results of this study, nerve guides of 80% porosity percentage with 10 – 38 μm pore diameter and 0.6 mm wall thickness will be used for *in vivo* studies.

3.0 DEVELOPMENT OF A DOUBLE WALLED MICROSPHERE DELIVERY SYSTEM FOR GLIAL CELL LINE-DERIVED NEUROTROPHIC FACTOR

3.1 INTRODUCTION

Conventional methods of drug administration include oral formulations or bolus application via injection (e.g. intravenous, intramuscular, subcutaneous, or intrathecal) [176]. The benefits of using simple administration routes such as oral formulations include the ease of use, patient comfort and low expense, all factors which lead to high patient compliance. However, there are limitations in the use of these traditional delivery methods for therapeutics targeting peripheral nerve repair. Oral administration of proteins such as Glial Cell Line-Derived Neurotrophic Factor (GDNF) is not a suitable mechanism for investigating potential benefits of the drug due to the potential for drug degradation in the intestinal tract and low epithelial permeability to large proteins [177]. Furthermore, oral or injected administration of GDNF allows for the possibility of unwanted side effects from systemic administration of high dosages necessary for therapeutic efficacy at the site of nerve ligation [178].

As an alternative to systemic administration, early investigations of neurotrophic factors in peripheral nerve defects applied a direct application of protein growth factor at the site of nerve injury immediately following surgical repair [179, 180]. However, because of the short half life (*e.g.* minutes) of proteins such as GDNF, this method of delivery is not optimal for

treatment of a large nerve defects considering the slow growth rate of axons across critical size nerve gaps which can take several weeks. Therefore, when evaluating the efficacy of neurotrophic factors toward improving nerve regeneration, it may be beneficial to use a controlled release system that is capable of delivering neurotrophins to Schwann cells and nerve stumps at the site of ligation in the sciatic nerve over a sustained period. With such a delivery system, GDNF could be administered in a localized manner, allowing for higher concentrations of the growth factor to be administered and potentially avoiding systemic side effects.

Encapsulation of proteins within polymeric microspheres is a well documented method of controlled drug delivery [181-185]. Benefits of microsphere delivery systems include non-invasive placement and localized release of large amounts of therapeutic agents, circumventing deleterious side effects from systemic administration [186]. Because of this, larger, more effective dosages can be administered. Furthermore, microspheres can be administered through injection and thus avoiding surgical procedures or microspheres can be embedded within gels or constructs for combined tissue engineered therapies [184, 187, 188]. Finally, microspheres can be manufactured with biodegradable materials which eliminate the need for device recovery [182].

3.1.1 Single walled microsphere delivery systems

Single walled microspheres are produced from a single polymer or copolymer phase and can be produced in a wide range of sizes (1 – 100 nm for nanospheres and 1 – 100 μm for microspheres) [187]. Single walled biodegradable microspheres are most often fabricated using polymers or copolymers of lactic and glycolic acids due to their proven safety and biocompatibility [5]. Microspheres have been used to successfully encapsulate a variety of growth factors including

Transforming Growth Factor – β (TGF-β) [184, 189], CNTF [190], FGF-1 [185], NGF [97, 100, 191], and GDNF [192, 193].

There are several advantages to using single walled microspheres for the delivery of either hydrophobic or hydrophilic drugs *in vivo*. Single polymer microspheres are easy to fabricate and can be manufactured with materials that are well characterized and relatively inexpensive. In addition, it is possible to encapsulate a wide range of protein macromolecular sizes including high molecular weight globular proteins such as BSA as well as small molecular weight proteins such as lysozyme. Furthermore, when biodegradable polymers are utilized for microsphere production, removal of the drug delivery device is not necessary. Finally, polymer microspheres can be made with a mean diameter range below 10 μm, a size that allows for *in situ* injection, and thus allows for an easy method of localized drug delivery.

3.1.1.1 Materials and fabrication techniques

Fabrication techniques for single walled microspheres include emulsification-solvent evaporation, polymer phase separation (coacervation), spray drying, or techniques employing supercritical fluids (e.g. rapid expansion of supercritical solutions) [194]. Emulsification – solvent evaporation processes have been used frequently for microencapsulation processes because of the ease in fabrication and therefore the technique is discussed in detail in the following paragraphs. Fabrication of microspheres through coacervation requires a change in polymer phase from one of soluble to insoluble. This can be accomplished by altering the temperature of the solvent in which the polymer of choice is dissolved or by adding a third component which interacts with the organic solvent but not with the polymer. This method requires large quantities of organic components which can prove difficult to remove completely from the final microspheres. Spray drying has been used to create microspheres through

atomization of a solution using compressed air through a dessicating chamber. This method is typically used to create porous microspheres and is most successful when the polymer and drug are dispersed in the same solution. The use of fluids such as carbon dioxide at supercritical pressures or temperatures are an alternative microencapsulation technique that avoid large amounts of residual solvents and have thus been recently explored as an alternative to solvent evaporation techniques. However, the nucleation of particles occurs during expansion, which typically occurs at a rate of 10^{-7} seconds, producing high shear stress which can denature dissolved molecules such as proteins [194].

Production of microspheres through the solvent evaporation method has been studied extensively and can be used to encapsulate apolar, hydrophobic molecules as well as hydrophilic molecules such as proteins. Initially, polymers are dissolved in a poorly water soluble, volatile solvent such as dichloromethane or chloroform. This mixture is then emulsified in a large volume of aqueous solution containing a surfactant such as poly(vinyl alcohol). For apolar molecules, the drug to be encapsulated is dispersed within the organic solvent in which the polymer is dissolved. Therefore, when the polymer/drug mixture is emulsified within the aqueous solution, the solvent evaporates allowing the polymer to harden while entrapping some portion of the dissolved drug within the polymer matrix.

Encapsulation of hydrophilic proteins such as GDNF requires an additional emulsion step resulting in a water-oil-water (W/O/W) double emulsion system. In this process, the protein to be delivered is dissolved in an aqueous solution and emulsified within the polymer/organic solvent solution. This emulsion is then added to a large quantity of poly(vinyl alcohol) (PVA) in water and the resulting solution is stirred until the solvent evaporates and the polymer droplets solidify.

Materials with which microspheres have been produced include a variety of polyesters and polyanhydrides. The encapsulation of highly water soluble proteins within aliphatic polyesters based on lactic and glycolic acids have received considerable attention due to the proven biocompatibility, predictability of degradation kinetics, ease of fabrication, and past regulatory approval in suture applications [195]. Generally, PLA, PGA and copolymers thereof are hydrophilic and thus undergo bulk degradation of the polymer backbone through hydrolytic cleavage of ester linkages (Figure 13, from [187]). Unlike large PLA or PGA implants, microspheres that are 300 μms or less in diameter undergo a homogenous degradation in terms of core and surface degradation rates [182].

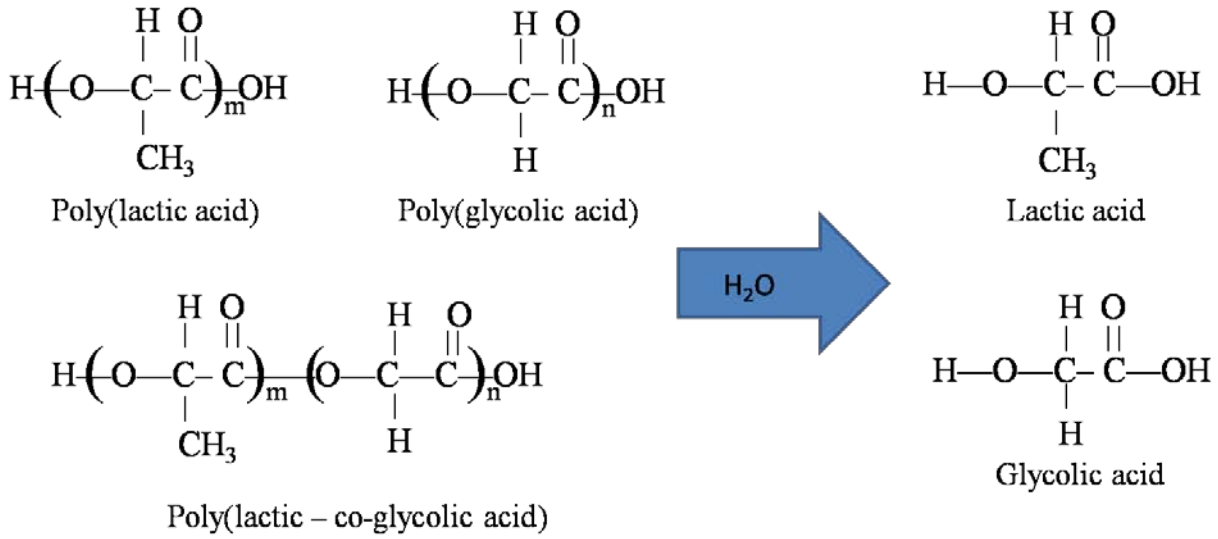

Figure 13. Common polyesters for microsphere fabrication with predicted degradation products. (Image modified from [187])

Poly(lactide) (PLA) exists as both D- or L- stereoisomers, allowing for considerable versatility in the performance characteristics (*e.g.* glass transition temperature, melting point, degradation rate) of PLA/PGA copolymers. DL-PLA is more sterically hindered and therefore less crystalline than either D-PLA or L-PLA. In addition, lactic acid has a side methyl group which causes lactide monomers to have more hydrophobicity than glycolide monomers. Finally, the copolymers of PGA and PLA are less crystalline than either of the homopolymers. Factors which affect rate of polymer hydration and thus biodegradation include: monomer stereochemistry, co-monomer ratio, polymer chain linearity, and polymer molecular weight. Table 4 lists the approximate biodegradation times for PLA, PGA and commonly used PLGA polymers. Biodegradation time varies depending on microsphere surface area and porosity, and has a large impact on encapsulate release kinetics from microspheres in solution.

Table 4. Biodegradation of lactide/glycolide polymers. Reproduced from [195].

Polymer	***Biodegradation Time Months (approx.)***
Poly(L-lactide)	18 – 24
Poly(DL-lactide)	12 – 16
Poly(glycolide)	2 – 4
50:50 (DL-lactide-co-glycolide)	2
85:15 (DL-lactide-co-glycolide)	5
90:10 (DL-lactide-co-glycolide)	2

3.1.1.2 Limitations of single walled microsphere encapsulation

While there are many advantages to microsphere delivery methods, there are also several disadvantages inherent to the encapsulation process. Large hydrophilic proteins are difficult to encapsulate within hydrophobic polymers. Therefore, high energy mixing is used to entrap the protein within nearly spherical occlusions of aqueous solution inside the hardened polymer microspheres (Figure 14A) [181]. These discrete occlusions remain following polymer hardening and water removal during the lyophilization process, which results in macropores in the microsphere structure [196]. This results in microsphere release kinetics of an initial burst of protein within the first 24 hours of placement in aqueous solution either *in vitro* or *in vivo* (Figure 14C) [197, 198]. Depending on the size of the microspheres and the type of polymer, the liberated protein within the first 24 hours can be over 50% of the total encapsulated material [181].

Additionally, the solvent evaporation method results in a considerable loss of hydrophilic protein material to the aqueous solution and therefore manufacturing procedures result in low encapsulation efficiency and a considerable loss of expensive growth factors during fabrication [9]. Finally, there are several mechanisms through which encapsulated proteins may become denatured during the encapsulation process as discussed in Section 3.1.3.

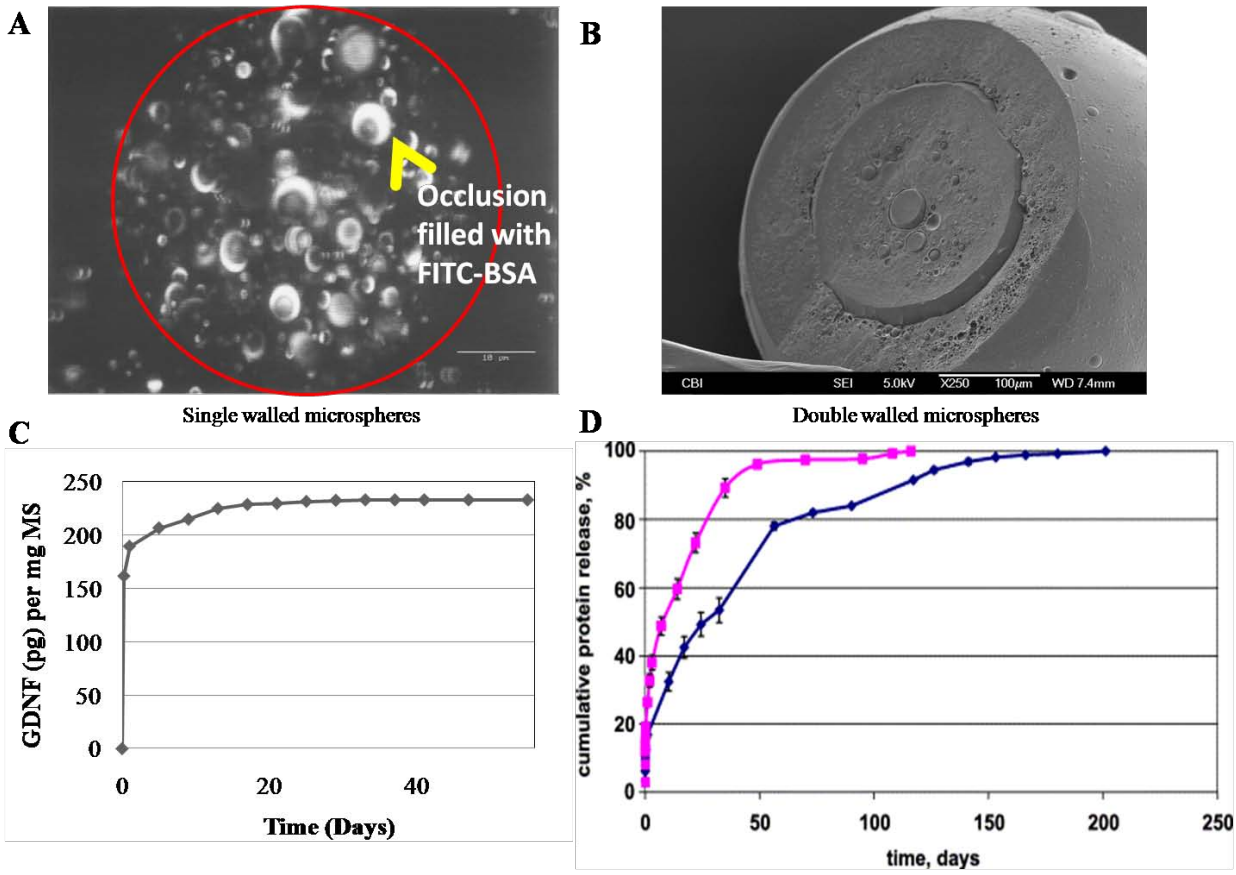

Figure 14. Comparison of single walled and double walled microspheres. A) Three dimensional confocal micrograph depicting the spherical occlusions of fluorescently labeled protein within a single PLGA microsphere (edge is marked with red circle) (Image modified from [196]). B) Scanning electron micrograph of a double walled PLGA/PLLA microsphere. C) Cumulative release profile of GDNF from a single walled PLGA microsphere *in vitro*. D) Cumulative release profile of BSA from double walled PLGA/PLLA microspheres (Image from [199]).

3.1.2 Double-walled microsphere delivery system

The technique for preparing double-walled (DW) microspheres was first patented by Edith Mathiowitz and Robert Langer in 1989 as a novel method of creating a controlled delivery

system [200]. In this type of delivery system, a substance to be delivered is encapsulated within a polymeric sphere and a second, unique polymer forms a capsule around that inner sphere. By localizing the growth factor to the core of double-walled microspheres, the amount of material through which the drug must diffuse is increased thus slowing the drug release rate (Figure 14B). DW microspheres have been used to encapsulate bovine serum albumin (BSA) [199], doxorubicin [201], piroxicam [202] and etanidazole [203]. With these double-walled microsphere systems, *in vitro* release profiles ranged between 60 days for etanidazole and ~240 days for BSA (Figure 14D).

3.1.2.1 Materials and fabrication techniques

Double-walled microspheres are primarily fabricated through a single step manufacturing process in which two polymers form a core and shell morphology through phase separation. The fabrication process requires the addition of a non-solvent or a second polymer that is incompatible with the first polymer to a two-polymer continuous phase solution, which is mixed briefly and then added to a nonsolvent aqueous solution. As the solvent slowly evaporates, the homogenous mixture separates resulting in one polymer precipitating around a core [204]. Alternatively, double walled microspheres have been produced by coating single walled microspheres following microsphere formation and hardening with a second unique polymer [199], employing multiple concentric nozzles which create dual polymer jets of the microsphere core polymer surrounded by an annular stream of the shell polymer [205], and through solvent removal with a non-solvent solution [206].

3.1.2.2 Limitations for double-walled microsphere encapsulation

Despite the improved release kinetics that DW microspheres present as compared to standard, single-walled double emulsion microspheres, some of the drawbacks of encapsulating proteins with a solvent evaporation method continue to exist. During the DW microsphere fabrication process, the protein to be encapsulated is added directly to PLGA dissolved in an organic solvent, potentially denaturing the protein. Furthermore, high energy mixing and addition of the dissolved protein and polymer solution to a large aqueous volume is still required. Therefore, the encapsulation procedure results in a substantial loss of expensive drug or protein materials.

3.1.3 Instability of proteins during the microencapsulation process

Proteins are particularly sensitive to destabilization during fabrication of both single and double walled microspheres because of the globular structure, the complex internal architecture which may dictate the activity of ligand binding sites, the numerous chemically active side chain moieties, as well as the structural dependence on numerous labile bonds [207]. Protein stability in relationship to proteins is defined as the retention of the tertiary structure of the protein conformation such that an enzyme, for example, retains the active site for natural substrate binding and is therefore functionally stable [207].

There are a variety of mechanisms through which encapsulated proteins may denature during the microsphere fabrication process (Figure 15). In the manufacturing process of microsphere formation, proteins may be denatured due to the use of organic solvents for polymer dissolution, the employment of high energy mixing necessary to encapsulate the protein and create the oil in water emulsions [181], exposure of the protein at the organic/aqueous interface

[208], as well as by lyophilization of the microspheres (and therefore, the encapsulated protein) to remove moisture. Additionally, proteins may denature due to hydration and erosion of the polymer during protein liberation. Microspheres are typically stored under desiccation and then rewetted in a manner that reconstitutes the protein in aqueous solution much more slowly then would occur in direct solubilization. This process, termed moisture induced aggregation, is known to cause denaturation of encapsulated proteins [209]. Other potential sources for protein denaturation during release periods include the acidic microenvironment that results from polymer degradation and the accumulation of free carboxylic acid end groups and the presence of hydrophobic polymer surfaces [207]. Finally, depending on the intrinsic stability of the protein, the functional protein structure may be lost due to natural degradation occurring during storage and release.

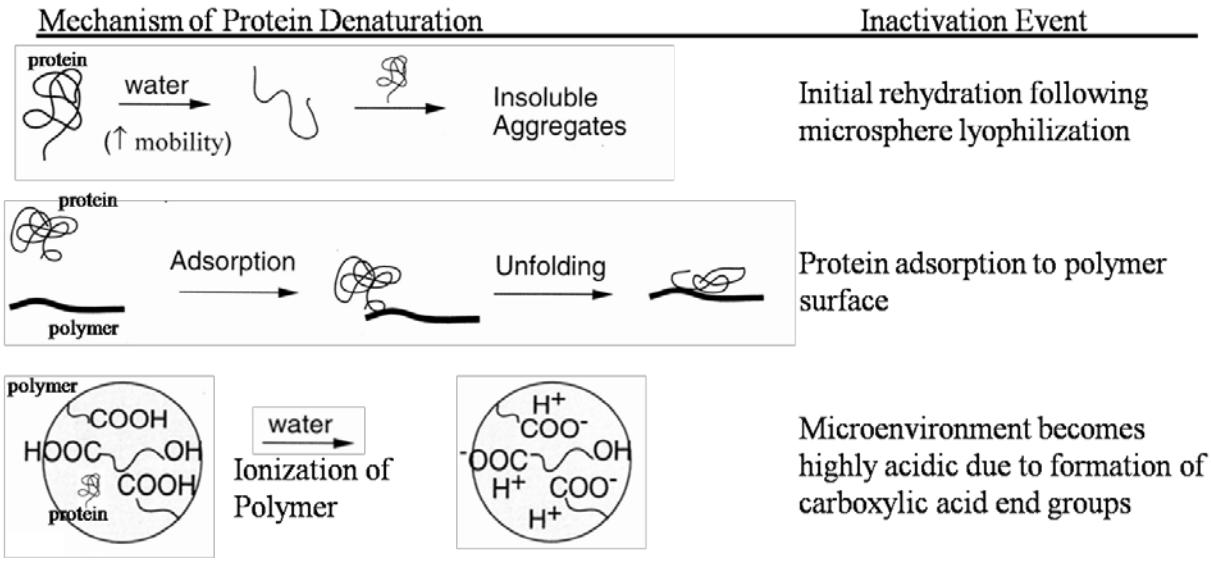

Figure 15. Potential mechanisms for protein denaturation during microsphere fabrication and protein release (Image modified from [207]).

3.1.4 Modeling GDNF release with Lysozyme

Lysozyme was chosen as a model for characterizing protein delivery from DW microspheres because of its small size (14.6 kD), which is similar to several neurotrophic factors (GDNF: 15 kDa [181], NGF: 26 kDa [182], BDNF: 12.3 kDa [183], and CNTF: 20.4 [184]). Additionally, the bioactivity of lysozyme can be easily quantified by measuring the enzymatic lytic activity on *Micrococcus lysodeikticus*. Because lysozyme bioactivity is easily measured and lysozyme has a similar size and isoelectric point to neurotrophic factors, lysozyme is an ideal protein for optimizing microsphere fabrication protocols.

3.1.5 Chapter Aims

It is hypothesized that a sustained delivery of GDNF applied directly to the site of nerve injury will result in an improved regeneration of lost nerve tissue. To evaluate this hypothesis, it was necessary to develop a delivery system that would release bioactive GDNF for a sustained period. With this goal, the purpose of the work described within this chapter was to optimize a microsphere delivery system such that GDNF was delivered for at least 60 days, the approximate period required for proximal nerve stumps to transverse the 1.5 cm interstump gap assuming a growth rate of 0.25 mm per day.

Investigation of microsphere delivery included the preparation of both single walled and DW microspheres. Two model proteins, BSA and lysozyme were encapsulated in single walled

microspheres. Release kinetics were evaluated from microspheres of variable PLGA comonomer ratio and molecular weight as well as microspheres encapsulating additives for protein stabilization. DW microspheres were prepared from PLGA and PLLA and encapsulated the model protein lysozyme. Design specifications for double walled microspheres included a PLGA core and PLLA shell with encapsulated protein localized to the microsphere core. To confirm the distribution of lysozyme within the polymer core, fluorescently labeled bovine serum albumin was encapsulated and localization to a particular polymer component was confirmed through fluorescent microscopy. Release studies were conducted to determine the long term release kinetics of the DW microspheres and the bioactivity of lysozyme was confirmed for the extended release period. In addition, co-encapsulates were evaluated as a method of protecting and stabilizing encapsulated model proteins during microsphere fabrication in order to improve liberated protein bioactivity.

3.2 METHODS

3.2.1 Reagents

All chemicals were analytical grade or purer and were purchased from commercial suppliers. Poly(vinyl alcohol) (average Mw 9,000-10,000, 80% hydrolyzed), poly(DL-lactide-co-glycolide) (lactide:glycolide (50:50), mol wt 40,000-75,000 units), Fluorescein Isothiocyanate Conjugated Bovine Albumin (FITC-BSA) (A9771), lysozyme from chicken egg white, Docusate Sodium Salt (AOT) (D1685), Dichloromethane, Ethyl Acetate, Phosphate Buffered Saline (PBS), Potassium Phosphate (Anhydrous, P-5379) and Micrococcus lysodeikticus (ATCC 4698),

sodium dodecyl sulfate (SDS) (minimum 98.5%, L4509), polyethylene glycol (avg mol wt 400, P3265) were all purchased from Sigma-Aldrich (St. Louis, MO). Poly-L-lactide (0.90 – 1.20 dL/g) was purchased from DURECT Corporation (Pelham, AL). The Micro Bicinchoninic Acid (BCA) Protein Assay Kit (23235) was purchased from Pierce (Rockford, IL). 228 mm Pasteur Pipettes were purchased from Wheaton (Millville, NJ). Dimethyl Sulfoxide (DMSO) was purchased from Thermo Fisher Scientific (Pittsburgh, PA).

3.2.2 Preparation of single walled, PLGA microspheres

Single walled microspheres were prepared using a standard double-emulsion (W/O/W) technique (Figure 16). The primary emulsion was formed by adding protein (20 mg of either BSA or lysozyme in 200 μL aqueous solution) to PLGA dissolved in dichloromethane (200 mg in 4 mL). The mixture was immediately sonicated for 10 seconds at 35% power using a 750 Watt probe sonicator. The second emulsion was formed by addition of the first emulsion to a 60 mLs of a 2% (w/v) solution of aqueous Poly(vinyl alcohol) (PVA). The solution was homogenized for 1 minute at 5,200 rpm using a Silverson homogenizer. The resulting emulsion was added to 80 mLs of a 1% PVA solution stirring continuously for 3 hours at 600 rpm. The resulting microspheres were washed 4 times with water and freeze dried using a Labconco freeze dry system (Kansas City, MO).

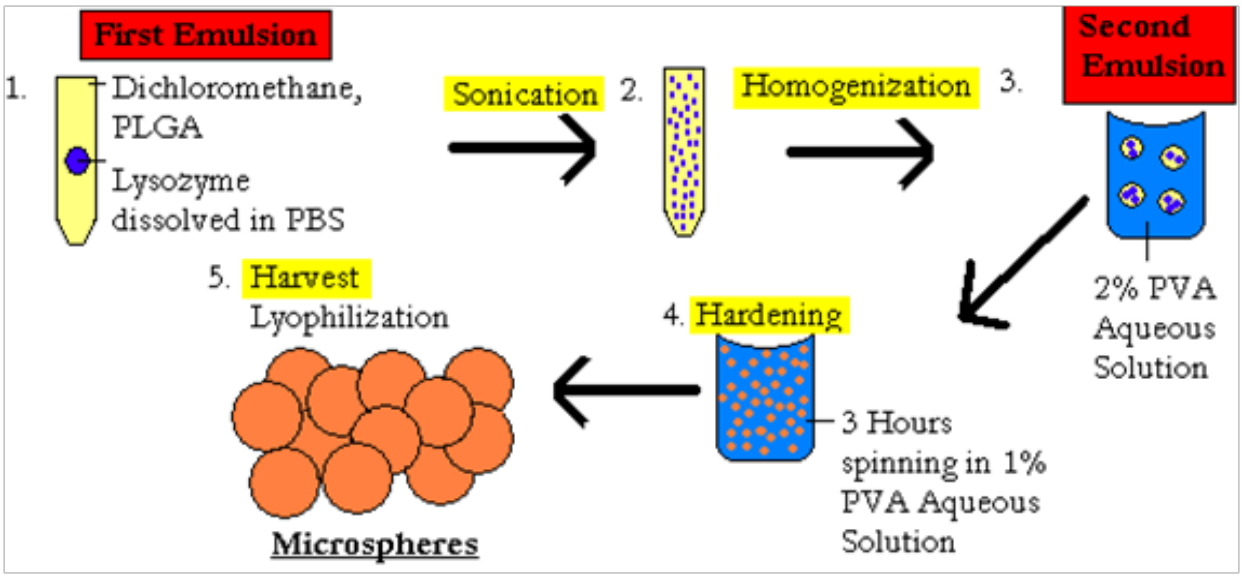

Figure 16. Preparation of single walled PLGA microspheres

3.2.2.1 Optimization of process parameters on single walled microsphere encapsulation

To determine the effect of polymer properties on microspheres prepared with constant operating conditions (*e.g.* geometry of beakers, agitation rate, and temperature), PLGA of varying co-monomer ratio and molecular weight was investigated with a primary emulsion of BSA in 2% aqueous PVA (Table 5). Microspheres were prepared with each PLGA ratio as described in Section 3.2.2.

Table 5. PLGA polymers used for fabricating single walled microspheres

PLGA lactide:glycolide monomer ratio	*Molecular Weight (M_w)*	*Inherent Viscosity (dL /g)*
50:50	5,000 – 15,000	0.15 – 0.25
50:50	40,000 – 75,000	0.61
65:35	40,000 – 75,000	0.61
75:25	66,000 – 107,000	0.63

The effect of additives on lysozyme encapsulation efficiency and release kinetics was investigated using stabilizing proteins such as human serum albumin (HSA) and surfactants such as poly(ethylene glycol) and docusate sodium salt (AOT). Microsphere preparation followed standard protocol as described in Section 3.2.2 with the exception that the primary emulsion of protein dissolved in 200 μL of PBS additionally contained coencapsulates as described in Table 6.

Table 6. Additives used in single walled microsphere fabrication

Coencapsulates	*Primary aqueous phase*	*Rationale*	*Reference*
HSA (10 mg), PEG 400 (120 μl)	16 mM Citrate Buffer (pH = 5.0)	Large protein for improved lysozyme stabilization	[183]
AOT (10 mg)	dI H_2O	Improves lysozyme solubility in DCM	[181]

Finally, single walled microspheres encapsulating GDNF were prepared using PLGA (65:35) and the surfactant AOT in a 1:30 molar ratio of GDNF (5 μg) to AOT (1.09 mg). The primary emulsion of GDNF and AOT contained DI water instead of either PBS or PVA as was used in previous microsphere formulations.

3.2.2.2 Microsphere characterization

Microspheres were examined morphologically by scanning electron microscopy (SEM). Microspheres were mounted on metal stubs using double-sided copper tape, coated with gold using a Cressington 108 Auto (Cressington, Watford UK) and then viewed with a JEM-6330F (JEOL, Peabody, MA) scanning electron microscope operating at 5 kV acceleration. The diameter distribution was measured using a Multisizer 3 Coulter Counter.

For each batch of microspheres, the final product weight (MS_{final}) was recorded. Microsphere batch efficiency (final batch yield as compared to initial product input, $MS_{initial}$) was calculated using equation 1.

$$\frac{MS_{final}}{MS_{initial}} \times 100\% \quad (1)$$

The drug loading of single walled PLGA microspheres was determined using methods described by Sah et al., [210]. A known weight of microspheres was first dissolved in 2 mL dimethyl sulfoxide (DMSO) for 1 hour. A 10 mL solution of 0.05 N NaOH solution in 0.5% (w/v) sodium dodecyl sulfate (SDS) was then added to the DMSO solution and mixed for an additional hour. Fractions of the clear DMSO/NaOH/SDS protein solution were then evaluated with a BCA assay. Known concentrations of protein dissolved in DMSO/NaOh/SDS were used

for standard curve production. From the standard curve, the total amount of loaded protein ($Weight_{Drug}$) was determined. Drug loading was then calculated using equation 2**.**

$$\frac{Weight_{Drug}(grams)}{Weight_{MS_{final}}(grams)} \times 100\% \quad (2)$$

3.2.2.3 *In vitro* release of encapsulated proteins

10 mg PLGA microspheres were incubated in 1mL PBS at 37°C. Following incubation, the microspheres were centrifuged for 10 minutes at 1000 rpm and the PBS was removed, leaving a microsphere pellet at the bottom of the eppendorf tube. The PBS was refreshed following each time point and the released protein concentration within the collected PBS was determined using a BCA assay.

3.2.3 Preparation of double-walled microspheres

3.2.3.1 Selection of PLGA and PLLA solvent for DW microsphere preparation

Microspheres were fabricated using the three solvents listed in Table 7. Two distinct polymer solutions of (50:50) PLGA and PLLA were prepared in glass vials. A single phase emulsion was then created by adding a 10% (w/v) PLGA (0.15 grams) solution in organic solvent to a 10% PLLA solution (1:1 polymer mass ratio) and sonicated for 20 seconds. This homogenous oil-in-oil emulsion was added drop-wise through a Pasteur pipette to 200mL of aqueous 0.5% poly(vinyl alcohol) solution stirring at 900 rpm for three hours. After this time, the polymer microspheres were collected through centrifugation (1000 rpm for 10 minutes) and

washed three times. Finally, the microspheres were lyophilized and stored in a desiccant at -20ºC.

Table 7. Properties of solvents for microsphere preparation

Solvent	*Chemical Formula*	*Boiling Point (°C)*	*Dielectric Constant*
Ethyl Acetate (EA)	$CH_3C(=O)\text{-}O\text{-}CH_2CH_3$	77	0.894
Dichloromethane (DCM)	CH_2Cl_2	40	1.326
Tetrahydrofuran (THF)	$(CH_2)_4O$	66	0.886

Table 8 describes the three polymer combinations used for double walled microsphere preparation as ordered in increasing polarity. Microspheres prepared with THF as the solvent for PLLA could not be produced with a 10% (w/v) solution due to the low solubility of polymer in solvent. Therefore, a 3.5% (w/v) PLLA solution in THF was utilized while maintaining the 1:1 mass ratio of PLGA to PLLA. Resulting microspheres were sectioned and examined for evidence of polymer separation using SEM as described in Section 3.2.4.1. To determine the localization of encapsulated protein within the polymer compartments, microsphere batches 1 through 3 were prepared by encapsulating 4 mg of fluorescently labeled albumin (FITC-BSA). To evaluate release kinetics, microspheres of identical solvent formulation were prepared encapsulating 20 mg lysozyme. When encapsulating protein within microspheres, protein in dry,

lyophilized form was added directly to the PLGA dissolved completely in solvent, vortexed, and placed in ice for 20 minutes before the PLGA and PLLA solutions were mixed.

Table 8. Solvent combinations for PLGA and PLLA in DW microsphere fabrication

Batch Number	*PLGA Solvent*	*PLLA Solvent*
1	DCM (17.5% w/v)	DCM (10% w/v)
2	EA (17.5% w/v)	DCM (10% w/v)
3	DCM (17.5% w/v)	THF (3.5% w/v)

3.2.3.2 Effect of PLGA solution concentration on polymer phase separation

To determine how PLGA solution concentration (w/v) affects polymer phase separation between the microsphere core and shell, double walled microspheres were prepared with varying PLGA solution concentrations ranging from 10% to 20% in 2.5% increments (batch numbers 4 – 8). A 10% PLLA solution in dichloromethane (0.15 grams PLLA in 1.5 mL DCM) was used for all microsphere batches. The PLGA to PLLA mass ratio was held constant at 1:1. For evaluation of PLGA solution concentration on microsphere release kinetics, lysozyme was encapsulated by adding 20 mg of protein (as a dry powder) directly to PLGA dissolved in dichloromethane.

Following microsphere preparation, the batch yield was calculated for each microsphere formulation using equation 1. Additionally, the external surface and internal architecture of

microspheres was observed through SEM (detailed methods in Section 3.2.4.1). Due to the limited capacity of coulter counters to measure large particles, the diameter distribution of microspheres prepared with a 20% PLGA solution was determined using Image-J analysis of SEM photo images [165]. Finally, *in vitro* microsphere release studies were performed as described in Section 3.2.4.3.

3.2.3.3 Co-encapsulation of additives for improved protein bioactivity

To improve the bioactivity of released protein samples, additives (Table 7) were used as coencapsulates with lysoyme, or subsequently GDNF. Because AOT and HSA both interact with the structure of lysozyme, possibly obstructing the enzyme ligand binding site prior to encapsulation and thus reducing lysozyme bioactivity upon release, preliminary studies were performed to determine the optimal molar ratios of additive to model protein such that the bioactivity of encapsulant was maintained.

Optimization of AOT and HSA molar ratio for lysozyme bioactivity

An initial bioactivity assay was performed on varying molar ratios of lysozyme:additive (AOT or HSA) to determine the optimum amount for encapsulation. This bioactivity assay was developed on the principle that the enzyme, lysozyme, causes the lysis of intact Micrococcus lysodeikticus cells. Therefore, the units of active lysozyme per mL solution were calculated by determining the solution turbidimetric rate. To accomplish this, three reagents were created: 1) 66 mM potassium phosphate buffer, pH 6.24 at 25ºC (Potassium phosphate in D.I. water), 2) 0.015% (w/v) Micrococcus lysodeikticus cell suspension in reagent 1, and 3) A range of 0 - 1000 units/mL in 100 unit increments of lysozyme enzyme solution in reagent 1. Previous analysis of lysozyme bioactivity revealed that the measured turbidmetric rate is highly temperature sensitive.

Therefore, all bioactivity measurements of lysozyme solutions were taken after the samples had reached a temperature of 37°C. For measuring the turbidimetirc rate, 0.1 mL of lysozyme solution was added to 2.5 mLs of solution (2) in a cuvette. The cuvette was immediately covered, mixed well and placed in a spectrophotometer. The change in measured absorbance at A_{450}nm was recorded for the initial 5 minutes (Thermo Spectronic GENESYS 10 Bio spectrophotometer).

For determining the percent activity of each lysozyme/additive solution, 200 units of lysozyme (0.0957 mg/mL) were dissolved in 1 mL of PBS (positive control) or PBS containing a specified amount of AOT or HSA in eppendorf tubes (molar ratios of lysozyme : AOT tested: 1:1, 1:2, 1:3, 1:4, 1:5, 1:10, 1:20. Molar ratios of lysozyme:HSA tested: 1:50, 1:100, in addition to those ratios listed for AOT). The solutions were mixed well and incubated at 37°C for 48 hours. This time period was required as the bioactivity of lysozyme was significantly affected by the protein binding of additive and no additional activity affects were seen after this time. After the initial incubation period, the eppendorf tubes were maintained at 37°C in a water bath as the bioactivity assay was performed as described above. The activity of fresh lysozyme dissolved in PBS alone was normalized to 100% and the activity of each additive / lysozyme solution was normalized to this value.

Preparation of microspheres encapsulating lysozyme with AOT

Four unique batches of DW microspheres were prepared encapsulating protein (either FITC-BSA or lysozyme) alone (batch 9) or in a 1:2 molar ratio with AOT (batch 10). Because AOT is stored as a thick waxy solid, lysozyme could not be mixed homogeneously with AOT in solid form. Therefore, lysozyme and AOT were mixed thoroughly in sterile water and lyophilized to produce a well mixed protein powder. For consistency, lysozyme was prepared in

an identical manner when microspheres were prepared without surfactant. The bioactivity of lyophilized lysozyme immediately prior to encapsulation was confirmed using the analysis method described above. Following protein solution lyophilization, either lysozyme or lysozyme with AOT solids were added to a 20% PLGA (50:50) solution (0.2 grams in 1 mL of dichloromethane). The protein/PLGA product was vortexed for ~30 seconds to achieve a homogenous mixture. The PLGA mixture was then poured into a glass vial containing a 20% PLLA solution (0.2 grams in 1 mL of dichloromethane) and sonicated for an additional 20 seconds. This oil-in-oil emulsion was added drop-wise through a Pasteur pipette to 200mL of aqueous 0.5% poly(vinyl alcohol) solution stirring at 900 rpm for three hours. After this time, the polymer microspheres were collected through centrifugation (1000 rpm for 10 minutes) and washed three times. Finally, the microspheres were lyophilized and stored in a desiccant at -20ºC.

3.2.3.4 Double walled microencapsulation of Glial Cell Line-Derived Neurotrophic Factor

Preliminary batches of double walled microspheres encapsulating GDNF were fabricated with GDNF, AOT and HSA as described by Jiang et al., [211] (batch 11). To create a single, homogenous protein/additive powder, 100 mg of AOT, 7 mg of HSA and 40 µl of GDNF (0.1 mg/mL) were combined in 3 mL of sterile dI H_2O. The solution was mixed well and added drop wise into a glass dish supported by a floatation device immediately above liquid nitrogen. After solidification, the dish was immediately placed in a container for lyophilization. Once all of the liquid had completely sublimed from the protein/additive mixture, the solid powder was added to a 10% (w/v) solution of PLGA dissolved in DCM and microspheres were prepared as described in Section 3.2.3. Additional microspheres were prepared using a reduced volume of AOT, with the final molar ratio of GDNF to AOT being 1:2 (batch 12).

Double walled microspheres were subsequently prepared encapsulating GDNF and HSA in a 1:10 molar ratio. Protein and stabilizer were combined in solution as described above and lyophilized, creating a single protein powder. This powder was then added to a 17.5% (w/v) solution of PLGA in DCM over ice. The polymer and GDNF mixture were allowed to thoroughly mix for 20 minutes before the PLGA was combined with a 10% PLLA solution and microspheres were prepared as previously described. To determine if cloud point induction of the two polymers combined in a single oil phase would improve encapsulation, a second batch of double walled microsphere were prepared using an identical GDNF / HSA powder (batch 13). After the two polymer solutions and protein were mixed in a single glass vial through vortexing, 100% ethanol was added drop wise to the oil emulsion until the solution was slightly turbid, indicating that the polymers had begun to phase separate. This polymer solution was immediately vortexed for 20 seconds and then added drop-wise to the aqueous PVA solution, forming microspheres as previously described. Identical microspheres were prepared without cloud point induction (batch 14).

3.2.4 Microsphere characterization

3.2.4.1 Morphological assessment with scanning electron microscopy

Double walled microspheres were examined morphologically by scanning electron microscopy (SEM). Microspheres were mounted on metal stubs using double-sided copper tape, coated with gold using a Cressington 108 Auto (Cressington, Watford UK) and then viewed with a JEM-6330F (JEOL, Peabody, MA) scanning electron microscope operating at 5 kV acceleration. Microsphere diameter distribution was determined using Image-J analysis of SEM photo images [165].

To view the internal architecture of the DW microspheres, the microspheres were suspended in an aqueous solution of 20% gelatin, 5% glycerin for 2-3 hours at 37ºC as described by Rosner et al [97]. The suspension was then placed into a mold and frozen over liquid nitrogen. The gelled suspension was removed from the mold, sectioned to 40 µm sections using a cryotome at -30ºC and mounted onto a metal SEM stub. Sections were dehydrated, coated as described above and imaged using SEM.

3.2.4.2 Determining protein localization and microsphere polymer orientation

Fluorescence microscopy was used to observe protein localization within the DW microspheres. Microspheres encapsulating FITC-BSA were sectioned to 30 µm sections as described in 3.2.4.1 and mounted onto glass slides for visualization. Fluorescent light microscopy was then employed to visualize the encapsulated FITC-BSA within the microsphere sections.

In order to confirm the polymer composition of the microsphere core and shell, a solvent-specific dissolution study was conducted. The polymer PLLA is insoluble in ethyl acetate (EA), while PLGA is soluble in EA. Therefore, DW microspheres were sectioned as described above and mounted onto metal stubs using double-sided copper tape. After the microsphere samples were secured onto the metal stubs, the samples were inverted, exposing the microspheres to EA for 2 days. The copper tape was not affected by this procedure. After this period the stubs were thoroughly dehydrated and imaged with SEM. Because the PLGA component of the DW microsphere was dissolved, either PLLA spherical cores or PLLA hemispheres were expected to remain.

3.2.4.3 *In vitro* protein release studies

To determine the protein release kinetics from DW microspheres, 10 mg of microspheres were incubated in 1mL PBS at 37°C. Following incubation, the microspheres were centrifuged for 10 minutes at 1000 rpm and the supernatant was removed. For measuring the lysozyme content of the releasate, a micro BCA protein analysis assay was performed. For this assay, 1 mL of lysozyme standard (or sample solution) and 1 mL of the micro BCA working reagent were combined in a test tube and mixed well. All of the standard lysozyme samples as well as the release samples were incubated simultaneously in a water bath for 1 hour at 60°C. After this period, the protein solutions were cooled to room temperature and 200 µL from each sample were transferred to a 48 well plate and read with a plate reader at 562 nm (Tecan Spectraflour).

Lysozyme bioactivity

To ensure the encapsulated lysozyme remained active following release from the DW microspheres, a lysozyme bioactivity assay was performed as described in Section 3.2.3.3 for each time point of supernatant collection. To determine the percent bioactivity, the known protein concentration of each microsphere release sample was calculated through Micro BCA analysis. The lysozyme stock solution used to create the standard curve for determining the lysozyme concentration with the BCA assay was identical to the solution used to produce the standard curve for the lysozyme bioactivity assay. Therefore, for each sample assayed, the known protein concentration and the measured protein bioactivity were determined. To calculate the percent bioactivity, the measured bioactivity was divided by the theoretical bioactivity based on the known protein concentration and this number was multiplied by 100%.

In vitro GDNF release

To determine the release kinetics of GDNF from the PLGA/PLA double-walled microspheres, 10mg of microspheres were placed into eppendorf tubes and incubated in 1 mL PBS at 37°C. At specified time points, the microspheres were vortexed, centrifuged for 10 minutes at 1000 rpm and the supernatant was replaced with fresh PBS. The amount of soluble GDNF in the collected samples was analyzed using an enzyme linked immunosorbent assay (ELISA) manufacturer's instructions. The optical density was recorded at 450 nm in an ELISA plate reader (Tecan, NC). The GDNF concentrations were calculated against a 6-point standard curve, then adjusted to picograms of GDNF per milligram of microspheres.

3.2.4.4 *In vitro* degradation of double walled microspheres

Degradation of DW microspheres was analyzed under the same conditions as the protein release studies in Section 3.2.4.3. Microspheres were incubated in PBS at 37°C for 6 months. At 1 week and subsequent monthly intervals the microspheres were collected through centrifugation and examined through SEM using the protocol described in Section 3.2.4.1.

3.2.5 Statistical analysis

Results are expressed as the mean ± standard deviation. Analysis of variance (ANOVA) was used to determine statistical significance between experimental groups. The least significant difference method was used for multiple comparisons with $p < 0.05$.

3.3 RESULTS

3.3.1 Single walled microspheres: effect of PLGA on microsphere properties and BSA release

Single walled PLGA microspheres were fabricated using a double emulsion (W/O/W) solvent evaporation method, with the primary emulsion containing BSA dissolved in 2% PVA solution. Microspheres were prepared using PLGA of 3 different lactide to glycolide monomer ratios and 2 polymer molecular weights. Drug loading for microsphere batches was 13.5 %, 11.1 %, 7.5 % and 9.0 % for batch A, B, C, and D respectively. The average batch yield and mean diameter are recorded in Table 9. The external surface of microspheres comprised of 50:50 high molecular weight (HMW) PLGA appeared smooth and nonporous. Encapsulation of BSA did not alter the external microsphere morphology (Figure 17).

Table 9. Properties of single walled microspheres prepared of variable PLGA

Batch ID	*PLGA*	*Batch Yield % (w/o BSA); (w/ BSA)*	*Diameter Range µm (w/o BSA); (w/ BSA)*
A	***50:50, LMW***	65.3 (1 batch) ; 78.4 ± 18.6	6.08 ± 2.52 ; 8.61 ± 4.05
B	***50:50, HMW***	79.4 ± 6.9 ; 67.9 ± 7.0	7.26 ± 2.43 ; 7.88 ± 3.13
C	***65:35***	64.4 (1 batch) ; 74.4 ± 8.5	10.01 ± 4.40 ; 10.50 ± 9.44
D	***75:25***	77.7 ± (1 batch) ; 84.0 ± 2.6	10.12 ± 3.95 ; 11.58 ± 5.29

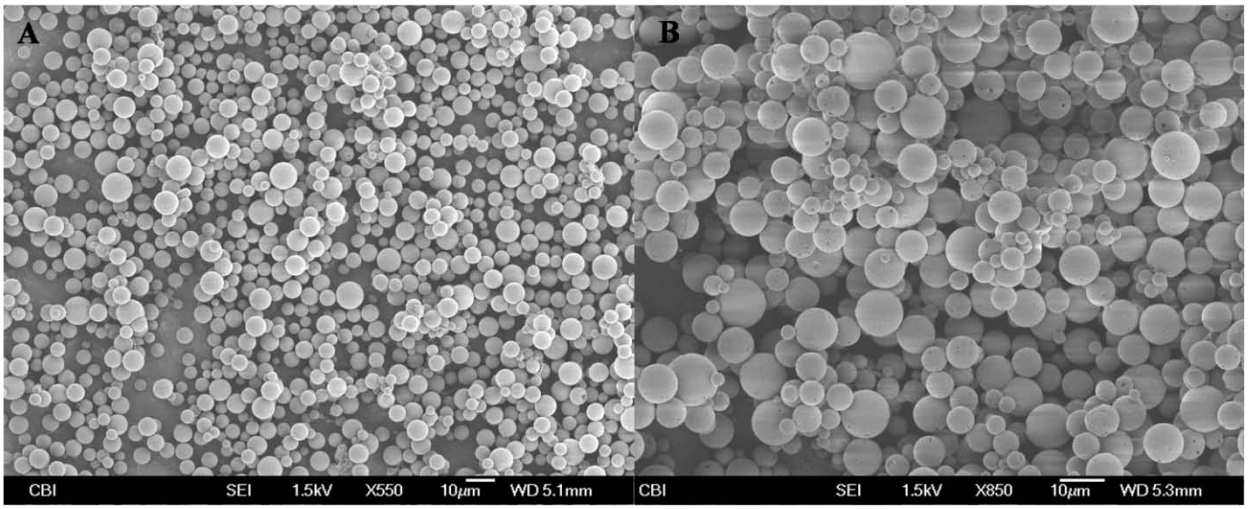

Figure 17. Scanning electron micrograph of single walled PLGA (50:50, HMW) microspheres (A) and microspheres of identical formulation encapsulating BSA (B).

3.3.1.1 *In vitro* release kinetics as affected by varying PLGA monomer ratio

The liberation of BSA from single walled PLGA microspheres was evaluated by measuring the protein concentration of PBS solution following microsphere suspension and incubation at 37°C. An initial burst of BSA release was seen in all four batches of PLGA microspheres (Figure 18). The percent released following 1 day incubation was 22.3%, 78.9%, 72.3%, and 70.1% of the total encapsulated protein for batch A, B, C, and D (respectively). While microsphere release from batch B, C, and D plateaued following 7 days of release, BSA release from batch A was nearly linear between day 1 and day 22. Following day 25 of the release period, microspheres of batch B released an additional 2.5% of the total encapsulated protein. Similarly, batch C released 3% and batch D released 0.2% beyond day 25. However,

batch A consisting of microspheres prepared with 50:50 low molecular weight (LMW) PLGA released an additional 20% of total encapsulated protein beyond day 25.

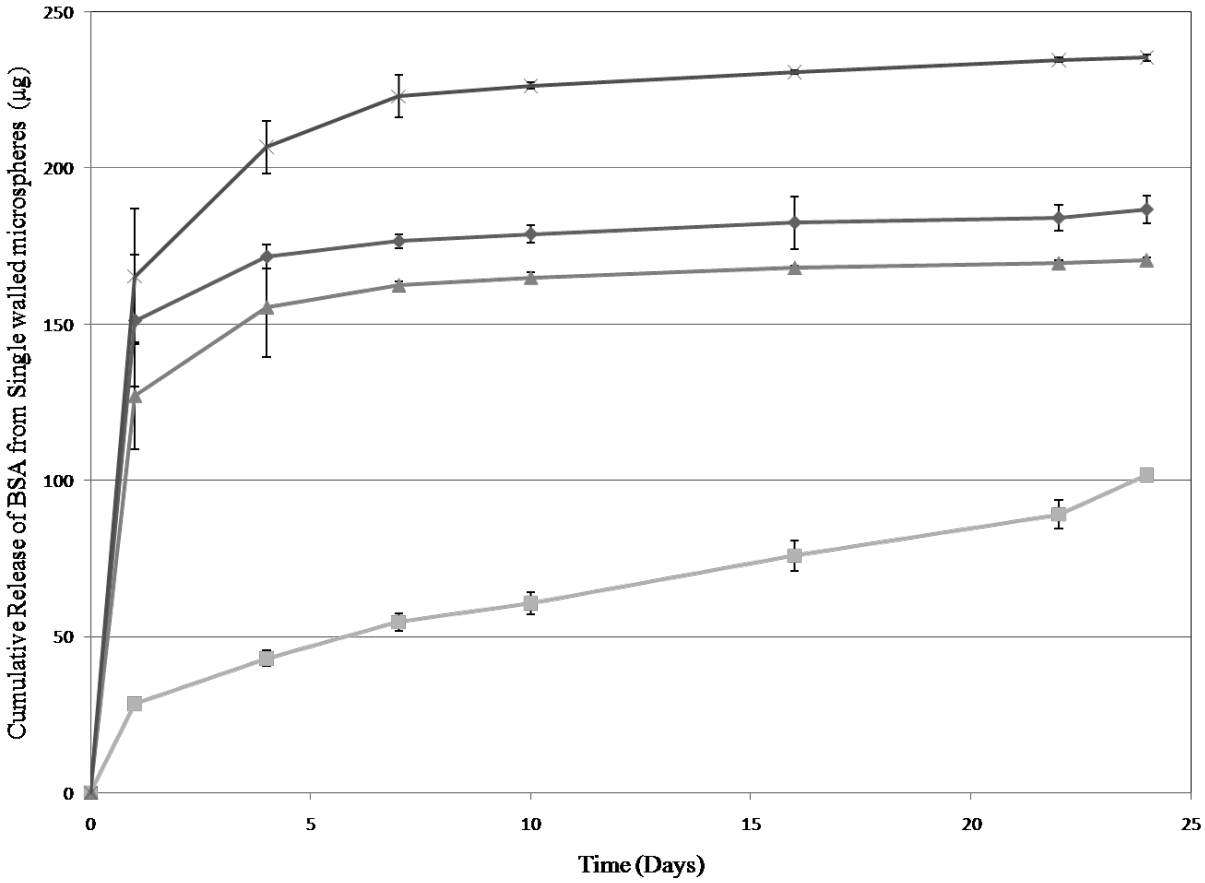

Figure 18. Cumulative release of BSA from single walled microspheres of variable PLGA physical properties. (▭) batch A, (◆) batch B, (▲) batch C, and (X) represents batch D. Data is presented as mean ± standard deviation (n = 3 measurements for each batch of microspheres).

3.3.2 Single walled microspheres: effect of additives on lysozyme release kinetics

Double emulsion microspheres were prepared as described in Section 3.2.2 with (65:35) PLGA and a primary emulsion of 20 mg of lysozyme in PBS without additives or with either AOT or HSA with PEG. The average batch yield ranged between 71% and 80%, with no additive formulation offering a significant improvement in batch yield. However, microspheres encapsulating lysozyme with HSA and PEG resulted in a decrease in protein loading (4%) as compared to lysozyme encapsulated alone (10.7%) or with AOT (11.0) (Table 10).

Table 10. Batch yield and drug loading of single walled microspheres encapsulating lysozyme with additives.

Batch ID	***Encapsulate(s)***	***Batch yield (%)***	***Protein loading (%)***
E	***None***	71.0 ± 19.6	NA
F	***Lysozyme***	76.9 ± 8.9	10.7
G	***Lysozyme, AOT***	71.1 ± 6.5	11.0
H	***Lysozyme, HSA, PEG400***	80.0 (1 batch)	4.0

Single walled microspheres produced with all 4 formulations of encapsulants resulted in similarly normal distributions of microsphere diameter range as indicated in Figure 19, however microspheres of batch E were observed in low frequency at diameters above 20 μm. The

diameter distribution of batch H shows peaks at higher diameters due to the measurement of aggregates of microspheres.

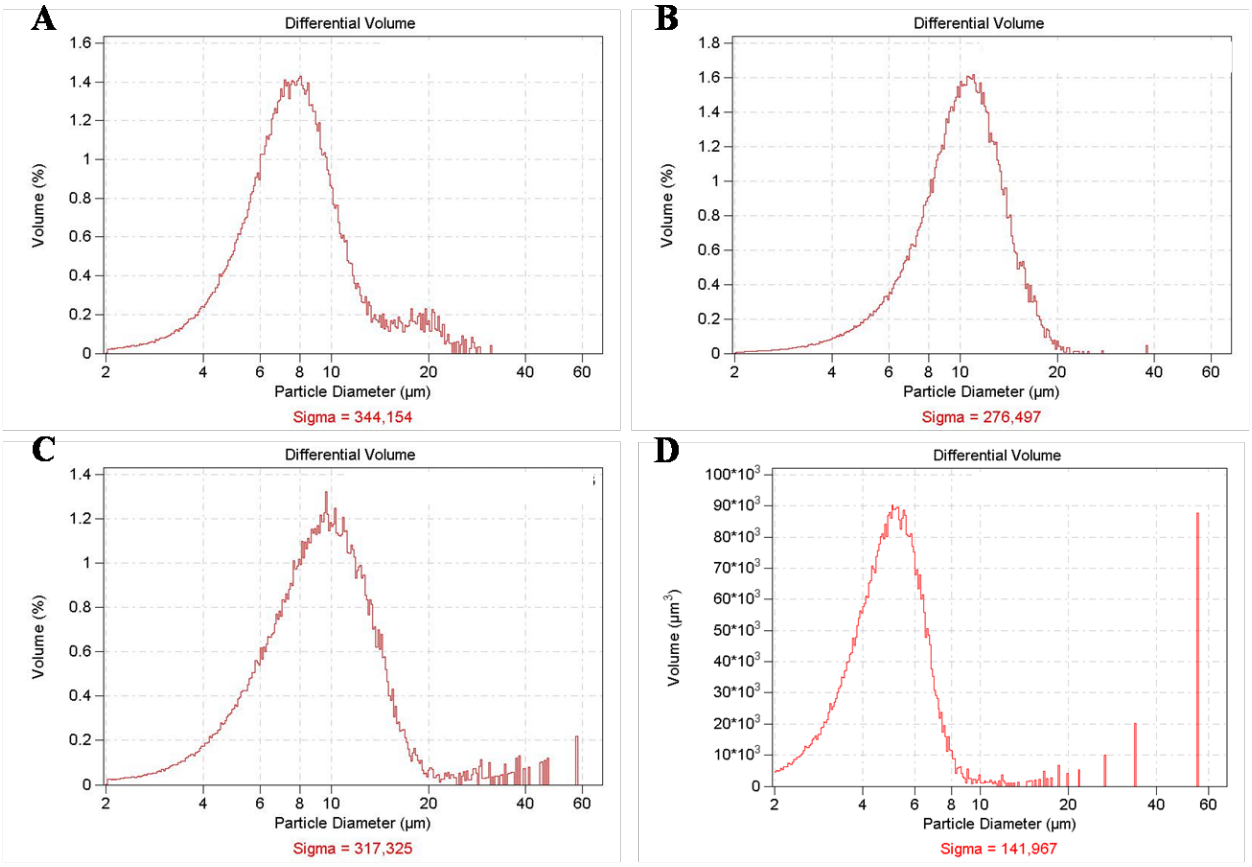

Figure 19. Diameter distributions of single walled PLGA microspheres for batch E (A), batch F (B), batch G (C) and batch H (D).

3.3.2.1 Scanning electron microscopic assessment of single walled PLGA microspheres with additives

Scanning electron micrographs of the external surface of single walled (65:35) PLGA microspheres prepared without encapsulants, batch E, reveal that microspheres generally have a smooth surface and are nonporous. However, microspheres are present in low frequency which possess large pores in the surface as indicated with a white arrowhead (Figure 20A). Additionally, large irregularly shaped microspheres are also visible as indicated with a white arrow. Similar to batch E, SEM images of microspheres encapsulating only lysozyme, batch F, also reveal a porous microsphere surface, although the diameter distribution does not appear to contain large malformed microspheres as was seen with batch E. However, microspheres of batch F have slightly non-spherical geometries.

Micrographs of microspheres prepared with lysozyme and AOT (batch G) reveal a large number of microspheres with concave regions (white arrow). However, unlike the alternative microsphere formulations, the external surface of batch G appears to be smooth and nonporous.

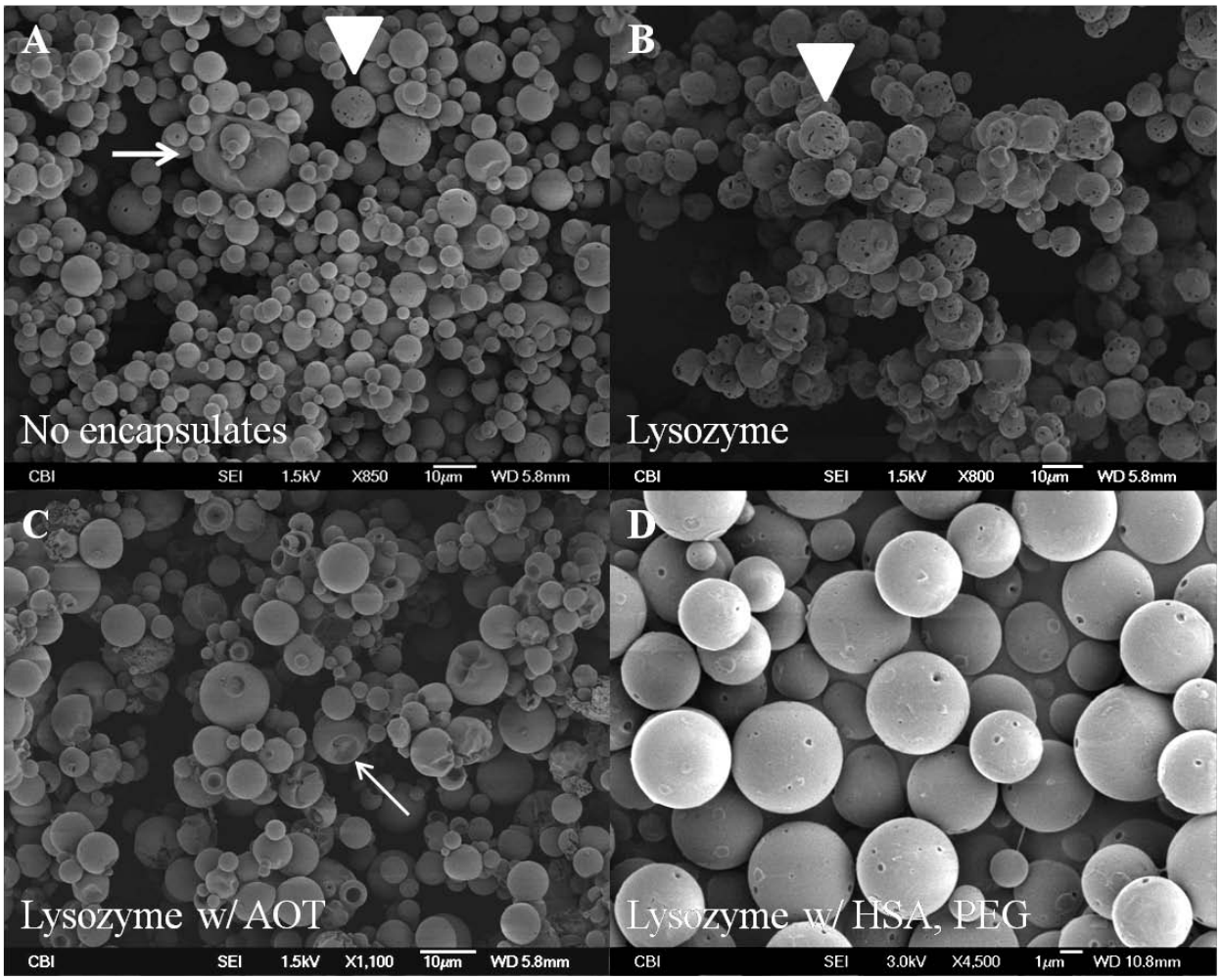

Figure 20. **S**canning electron micrographs of single walled (65:35) PLGA microspheres for batch E (A), batch F (B), batch G (C) and batch H (D). Irregularities in spherical morphology is indicated with white arrow head. Concave regions in microsphere surface are indicated with white arrows.

3.3.2.2 *In vitro* release kinetics as affected by addition of protein coencapsulates

Lysozyme release from single walled microspheres was evaluated over a time period of 75 days *in vitro* (Figure 21). Protein release from microspheres encapsulating lysozyme with or without additives resulted in an initial burst as was seen with single walled microspheres encapsulating BSA without co-encapsulants. The greatest percent of total encapsulated protein lost following the first day on incubation in PBS occurred in microspheres of batch E, where 86% of the total lysozyme encapsulated was lost after 1 day. Encapsulation of lysozyme with AOT and HSA (batch F) does not appear to decrease the initial burst of lysozyme, as 85% of the total encapsulated material was lost. However, addition of AOT in a 1:1 mass ratio to lysozyme in the primary emulsion (batch G) did decrease the initial percent release, with only 44% of the encapsulated protein being liberated on the first day of microsphere suspension. Beyond day 1, batch G experienced a sustained lysozyme release that continued to day 75 after which time the subsequent release samples were negligible.

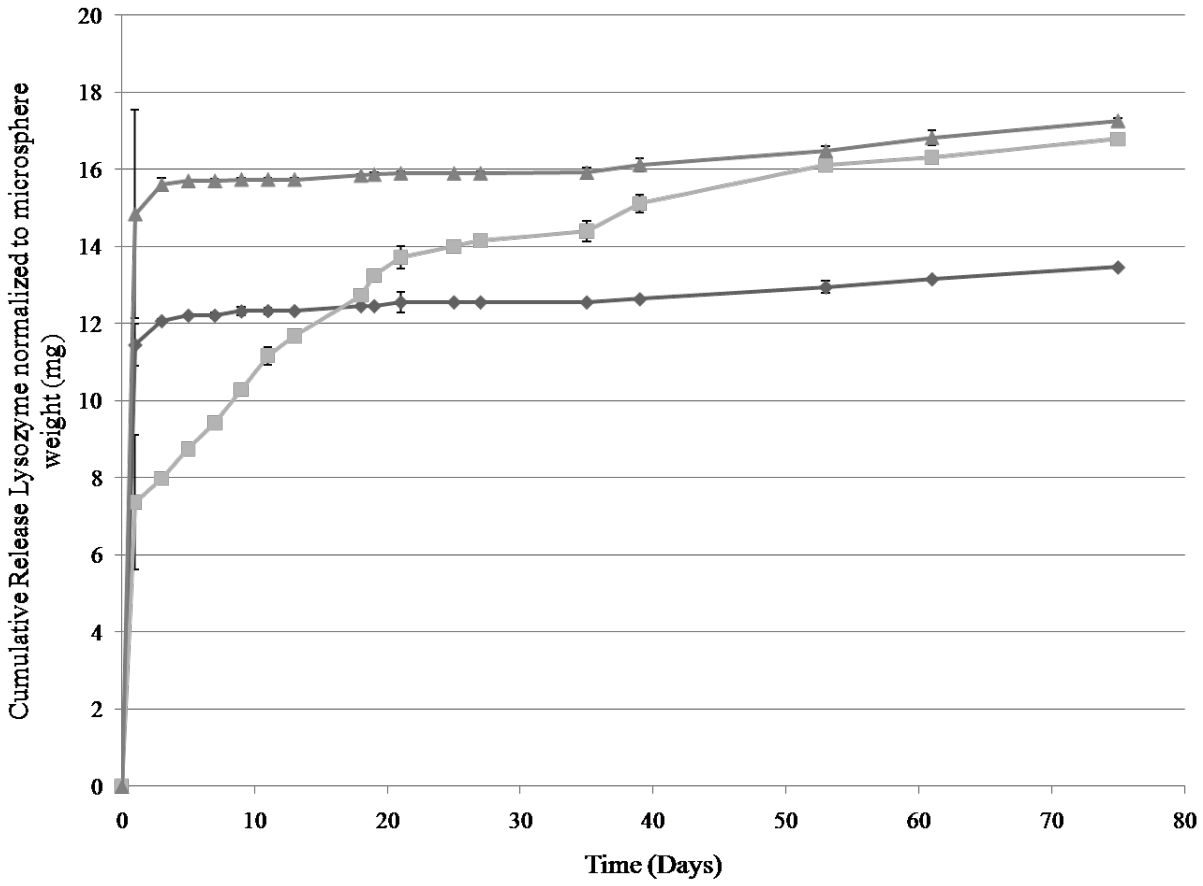

Figure 21. Cumulative release of lysozyme from single walled microspheres. (▲) batch F, (■) batch G, (◆) batch H. Data is presented as mean ± standard deviation (n = 3 measurements for each batch of microspheres).

3.3.3 Single walled microspheres encapsulating GDNF

Double emulsion (65:35) PLGA microspheres were prepared encapsulating GDNF with the primary emulsion containing AOT in a 1:30 molar ratio of GDNF to AOT in DI water. Microspheres were prepared with a batch yield of ~80% and drug loading of $2.3 * 10^{-5}$ % (or ~230 pg GDNF per mg microspheres).

3.3.3.1 SEM assessment of PLGA microsphere morphology and diameter distribution

Micrographs used to visualize microsphere morphology for single walled PLGA microspheres encapsulating GDNF reveal a smooth, nonporous external surface (Figure 22A). Generally, the microspheres possess a spherical shape with an average diameter of 6.3 ± 3.8 μm (Figure 22B).

3.3.3.2 *In vitro* release kinetics of PLGA microspheres encapsulating GDNF

Single walled (65:35) PLGA microspheres encapsulating GDNF in a 1:30 molar ratio with AOT result in release kinetics of an initial burst (~70%) at day 1 followed by a sustained release until day 20 (Figure 22C). Beyond this point, no measureable amount of GDNF was liberated from the microspheres.

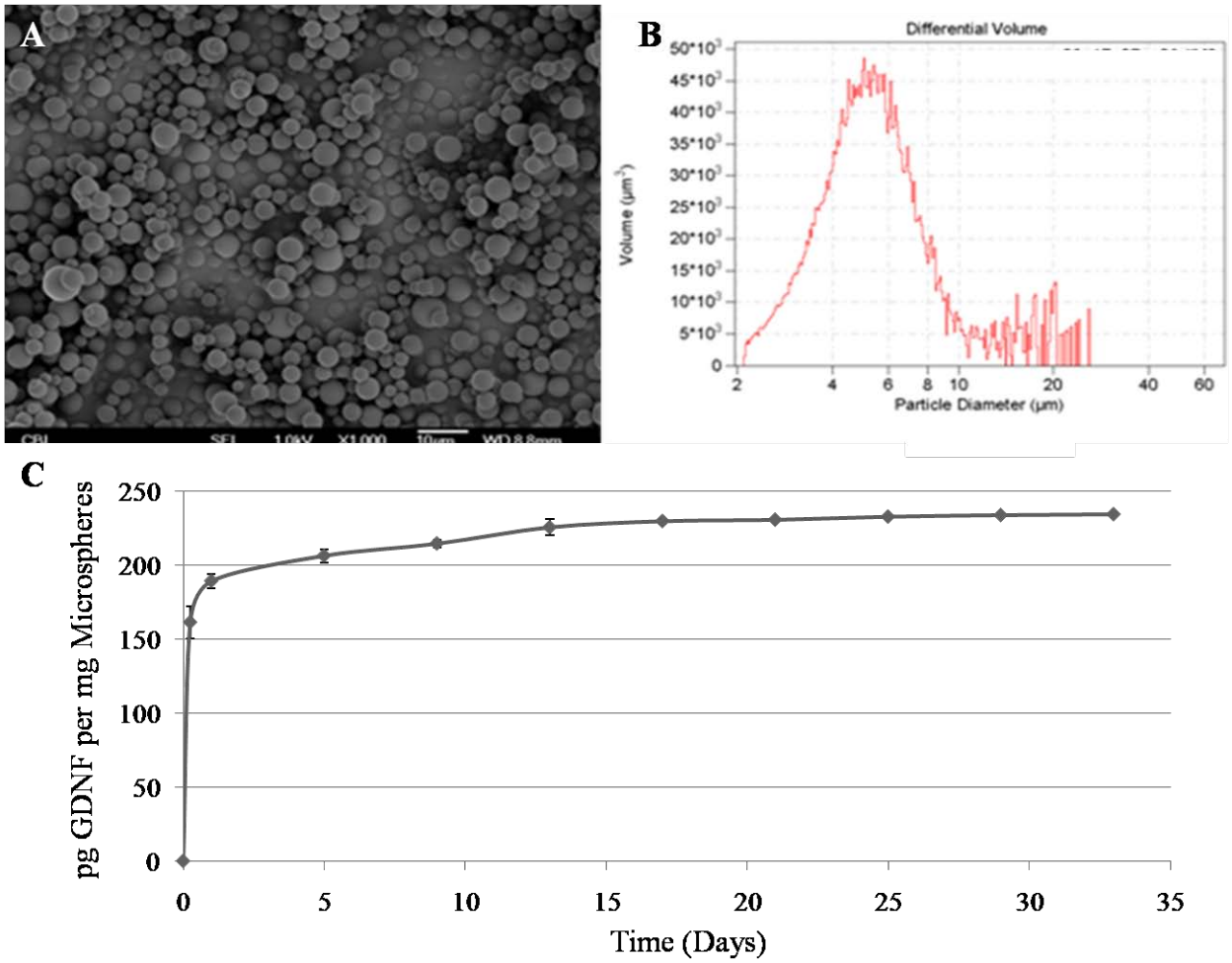

Figure 22. A) Scanning electron micrograph of single walled PLGA microspheres encapsulating GDNF. B) Diameter distribution of microspheres. C) *In vitro* cumulative release of GDNF from single walled microspheres.

3.3.4 Double walled microspheres: Selection of polymer solvent on protein localization and polymer orientation

DW microspheres were prepared using an oil-in-oil-in-water emulsion technique. The microspheres were prepared using a 1:1 weight ratio of PLGA to PLLA in solvent. To determine the appropriate organic solvent for creating a two phase microsphere with a PLGA core encapsulating protein and a PLLA shell, microspheres were prepared with combinations of dichloromethane, ethyl acetate and tetrahydrofuran (batches 1 – 3, Table 8). Scanning electron micrographs of microspheres prepared with dichloromethane for dissolution of both PLGA and PLLA (batch 1) reveal two distinct polymer walls with the microsphere shell completely engulfing the microsphere core indicating complete polymer separation (Figure 23A). Additionally, light micrographs of batch 1 microspheres encapsulating FITC-BSA show protein localization within the microsphere core (Figure 23B). SEM assessment of batch 2 microspheres also reveals two unique polymer walls with complete phase separation between the external shell and inner polymer core (Figure 23C). Figure 23D shows protein localization within the polymer core as visualized with fluorescent microscopy.

Double walled microspheres were not produced reproducibly with the solvent combination of DCM (PLGA) and THF (PLLA). SEM analysis of batch 3 microspheres revealed the production of microspheres with two polymer walls in low frequency as compared to the majority of microspheres which were non-engulfing and were composed of a single polymer (Figure 23E). The internal architecture of single polymer microspheres was rough and appeared to have a porous structure. In addition, for those microspheres seen which were composed of two polymer walls, fluorescent micrographs reveal protein localization in the outer polymer shell (Figure 23F).

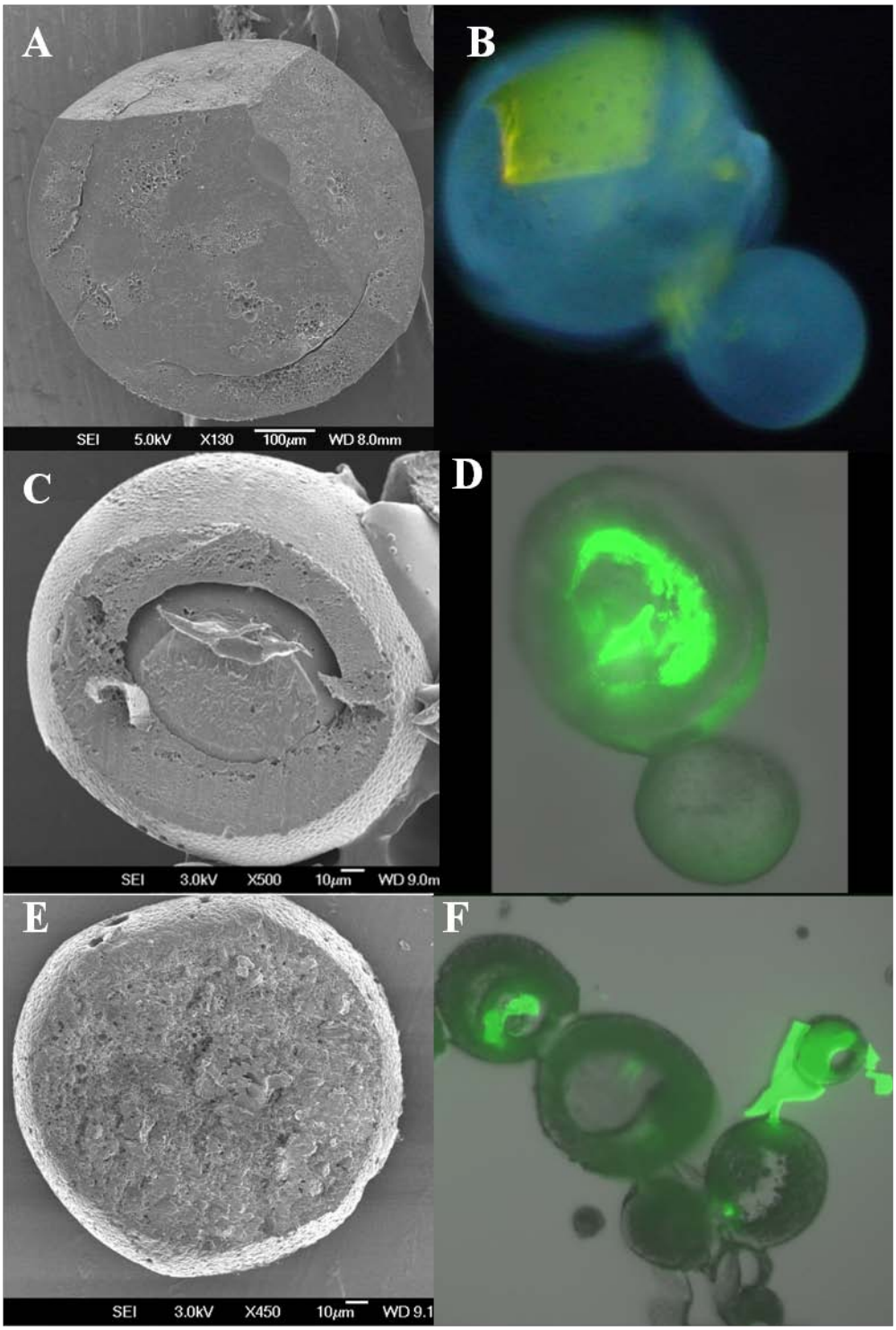

Figure 23. SEM and fluorescent visualization of cross sections of batch 1 (A, B), batch 2 (C, D) and batch 3 (E, F) microspheres. Fluorescent micrographs were taken at 40X.

3.3.4.1 Effect of polymer solvent on lysozyme release kinetics

Long term release studies were performed on batch 1 – 3 microspheres to determine the release profile of the encapsulated protein lysozyme (Figure 24). Microsphere release profiles for all three batches show a sustained release of lysozyme beyond 90 days of incubation in PBS at 37 °C. After 1 day release, lysoayme liberation from batch 1 and 2 was 4.4% and 5.8%, respectively while release of lysozyme from batch 3 was 11.5% at day 1. Beyond day 1, all three batches of microspheres produced a slow, gradual release of encapsulant until day 35, when batch 1 and 2 produced a rapid increase in lysozyme release rate. Lysozyme release from microspheres of batch 1 continued at an accelerated rate until day 70, when the release rate leveled and only negligible amounts of protein released beyond day 91. Lysozyme release for batch 2 microspheres was greatest between days 35 and 49, after which protein release slowed and was nearly linear until day 91, after which lysozyme release was no longer measured. Finally, lysozyme release from microspheres of batch 3 demonstrated a sustained, low rate of protein release for the duration of time over which protein samples were measured, with only a small increase in release rate seen between day 28 and 42. Drug loading as calculated with equation 2 was 21.1% for batch 1, 14.7% for batch 2, and 3% for batch 3.

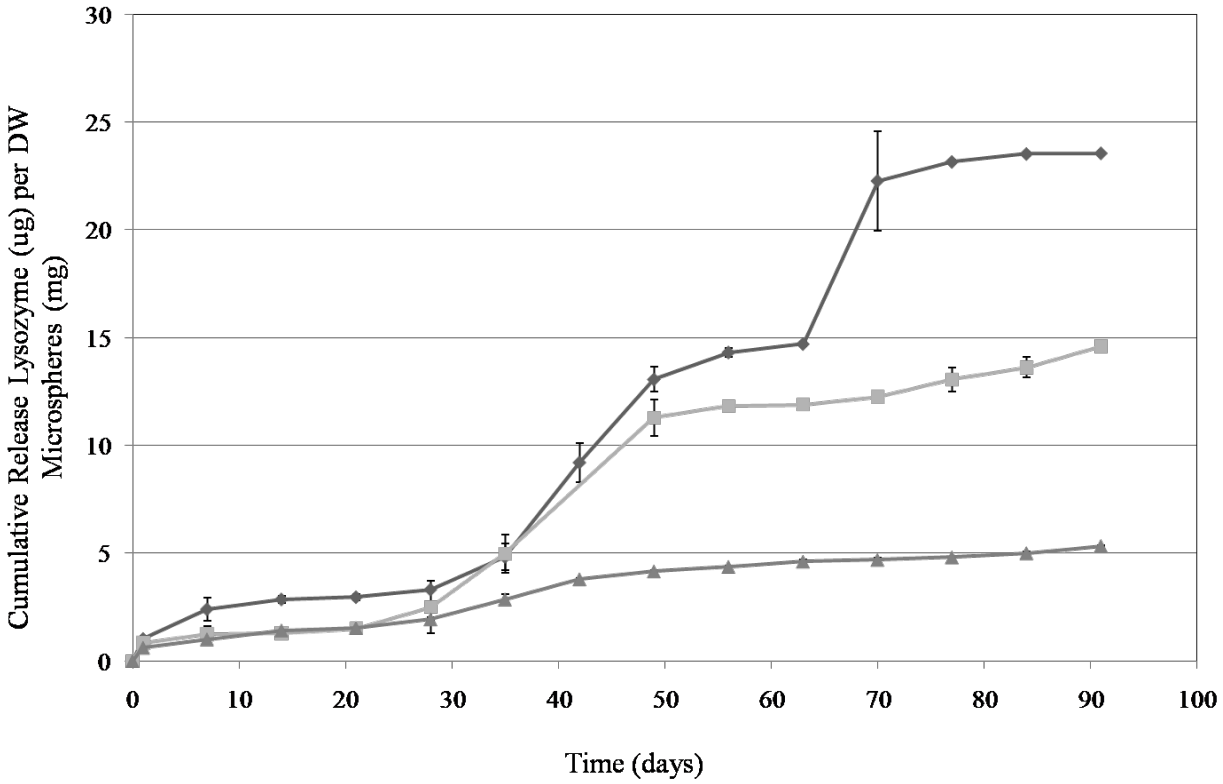

Figure 24. Cumulative *in vitro* release of lysozyme from microspheres of batch 1 (♦), batch 2 (▫) and batch 3 (▲).

3.3.5 Double walled microspheres: assessment of PLGA solution concentration on lysozyme release kinetics

DW microspheres were fabricated with the most efficient protein loading using dichloromethane as the solvent for both PLGA and PLLA. Initial microsphere batches were produced with a 20% PLGA solution and a 10% PLLA solution in a 1:1 polymer mass ratio. The external surface of the microspheres appeared smooth and non-porous (Figure 25A). The microspheres were manufactured with an average yield of ~50 ± 8 % (N = 12). The mean microsphere diameter was 81 ± 34 µm with the majority of microsphere ranging between 50 – 75 µm (Figure 25B).

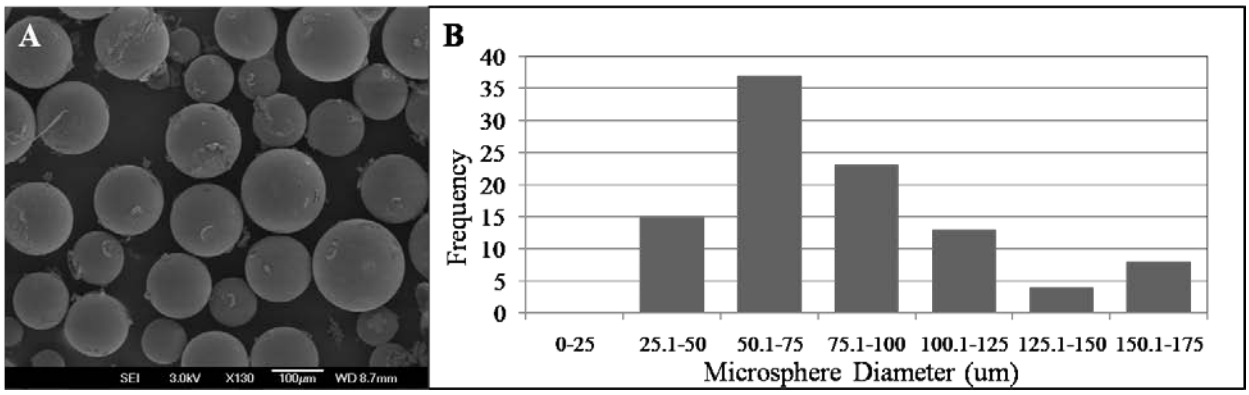

Figure 25. A) Scanning electron micrograph of 20% PLGA, 10% PLLA DW microspheres. B) Size distribution of double walled microspheres.

To determine the effect of variable PLGA solution concentrations on polymer phase separation, 4 additional microsphere batches were produced using PLGA in concentrations from

10% to 17.5% (w/v) in 2.5% increments. The batch yield for each microsphere formulation is presented in Table 11. For each presented microsphere batch type, three replicate batches of microspheres were prepared except for batch 8, where n = 20. Scanning electron micrographs of microsphere cross sections show a double walled microsphere morphology for all variations of PLGA solution concentration (Figure 26). However, microspheres formed with a low to intermediately viscous PLGA solution resulted in reduced polymer phase separation between the core and shell microsphere components. Microspheres prepared using 10% PLGA (Figure 26A), 12.5% PLGA (Figure 26B) and 15% PLGA (Figure 26C) show a high frequency of PLGA spherulitic occlusions within the PLLA shell. Additionally, large holes (white arrow heads) can be seen in both the PLLA microsphere shell and the PLGA microsphere core. Double walled microspheres produced with 17.5% (Figure 26D) and 20% (Figure 26E) PLGA solutions, polymer phases which were more viscous when dissolved in dichloromethane, produced microspheres of dense polymer compartments and a low frequency of PLGA spheres within the PLLA shell.

Table 11. Microsphere characterization: Batch Efficiency.

PLGA % w/v Solution Concentration	*% Batch Yield*
10 %	60.16 ± 12.58 %
12.5 %	66.96 ± 1.31 %
15 %	60.48 ± 13.56 %
17.5 %	61.57 ± 10.82 %
20 %	50.25 ± 8.41 %

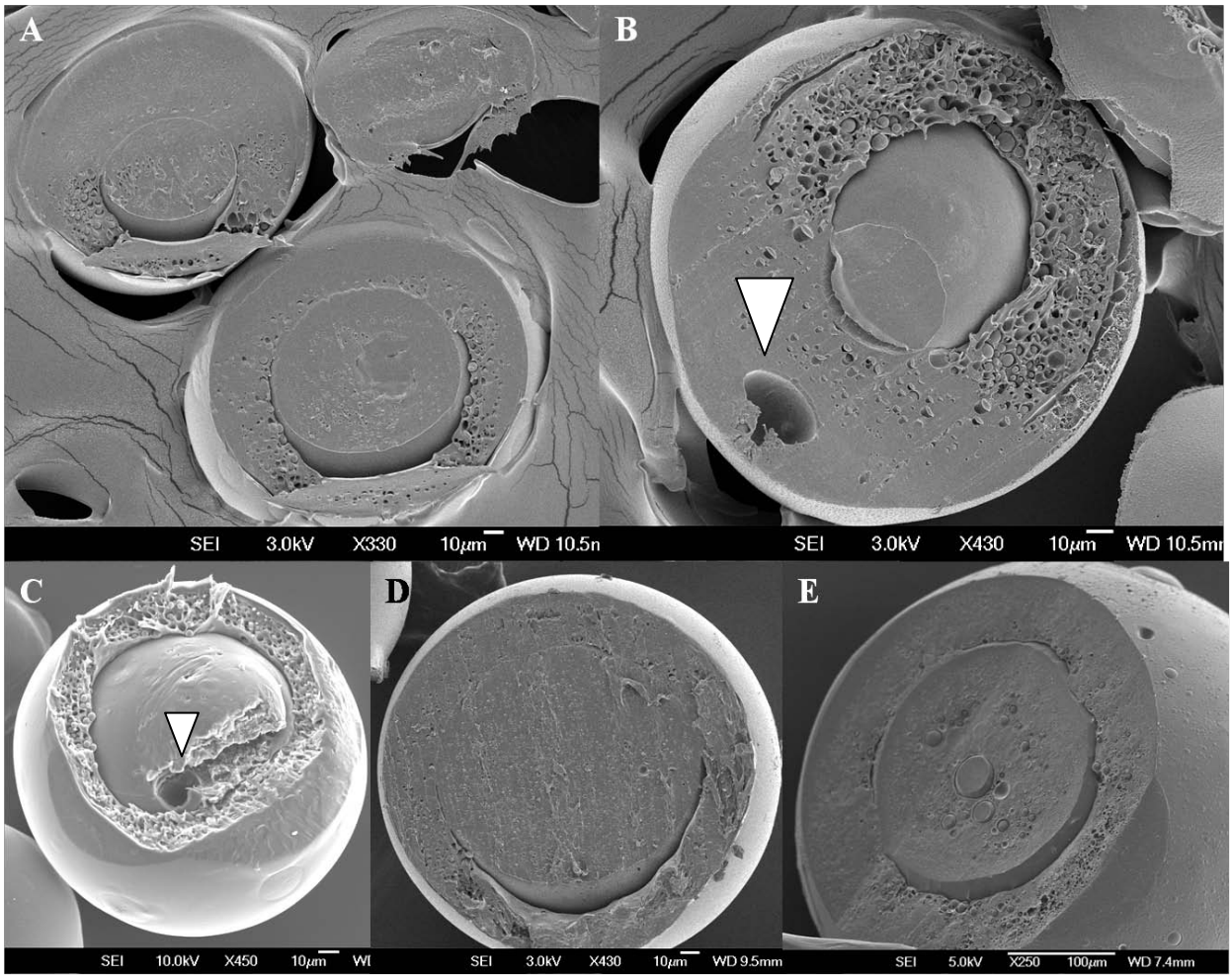

Figure 26. Scanning electron micrographs of double walled microspheres prepared with 10% PLLA in DCM and A) 10% PLGA (w/v), B) 12.5% PLGA, C) 15% PLGA, D) 17.5% PLGA and E) 20% PLGA in DCM. White arrow heads indicate large air occlusions in microspheres following polymer hardening.

3.3.5.1 Internal architecture

The scanning electron micrographs depicting microspheres treated for 48 hours with ethyl acetate shown in Figure 27 demonstrate a PLLA hemisphere with partial mass loss within the external microsphere shell, indicating incomplete polymer phase separation during the dynamic process of microsphere hardening. Microspheres produced with low PLGA solution concentration (10% to 15%) resulted in uniform microsphere shell coatings with small diameter spaces where PLGA spheres had existed. SEM images of microspheres produced with highly viscous PLGA solutions reveal heterogeneous microsphere shells with large holes following solvent removal of PLGA. Upon incubation of microspheres in aqueous solution, PLGA degrades before PLLA, resulting in mass loss from the microsphere shell and the formation of pores.

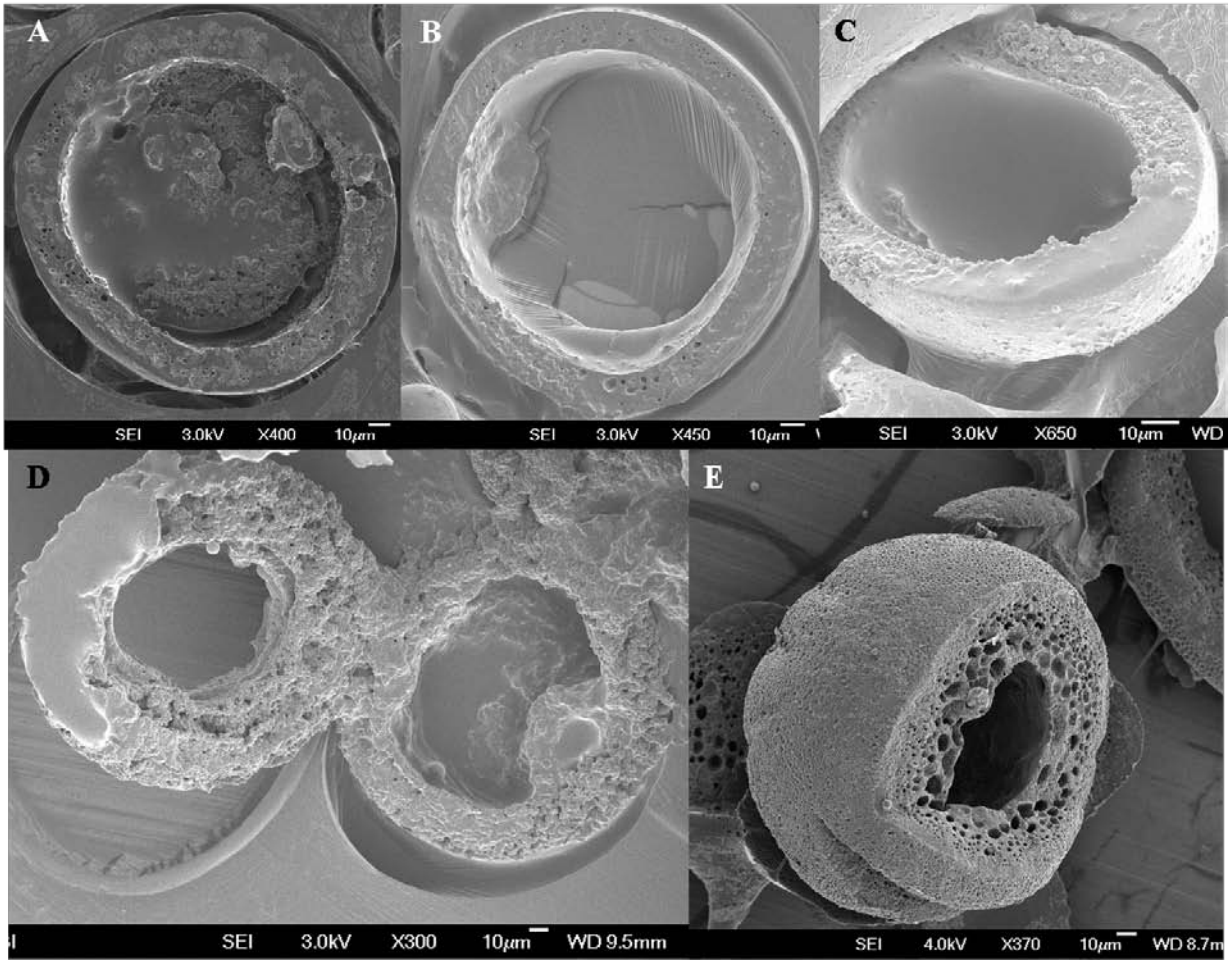

Figure 27. Scanning electron micrographs of double walled microspheres following treatment with ethyl acetate. A) 10% PLGA (w/v), B) 12.5% PLGA, C) 15% PLGA, D) 17.5% PLGA and E) 20% PLGA in DCM.

3.3.5.2 Microsphere degradation

Degradation studies were performed for DW microspheres prepared with 20% PLGA and 10% PLLA in DCM with and without encapsulated lysozyme (Figure 28 and 29 respectively). Following 1 week incubation *in vitro* (Figure 28A), the external PLLA surface of the spheres appeared very smooth and dense. Large quantities of adherent protein were evident on the surface of microspheres (Figure 29A). The shell appeared to roughen by 1 month and large craters formed (Figure 28B). Beyond 2 months of degradation, the shell continuity was compromised by large cracks (Figure 28C). In contrast, the PLGA core began to degrade within the first month of incubation in PBS and by month 3 the PLGA material was completely absent (Figure 28D). Micrographs taken after 3 months also reveal incomplete polymer separation in the microsphere layers as large spaces are evident within the microsphere PLLA shell due to PLGA degradation. Though the PLGA core degrades within the first few months of incubation, the PLLA shell maintained an overall spherical structure until month 5 (Figure 28F) when the material began to crumble and large macropores were evident. Following 6 months of *in vitro* degradation, a small percentage of intact PLLA microsphere shells remain while the majority of microspheres have broken apart (Figure 28G). The presence of encapsulated lysozyme did not alter the degradation process of double walled microspheres.

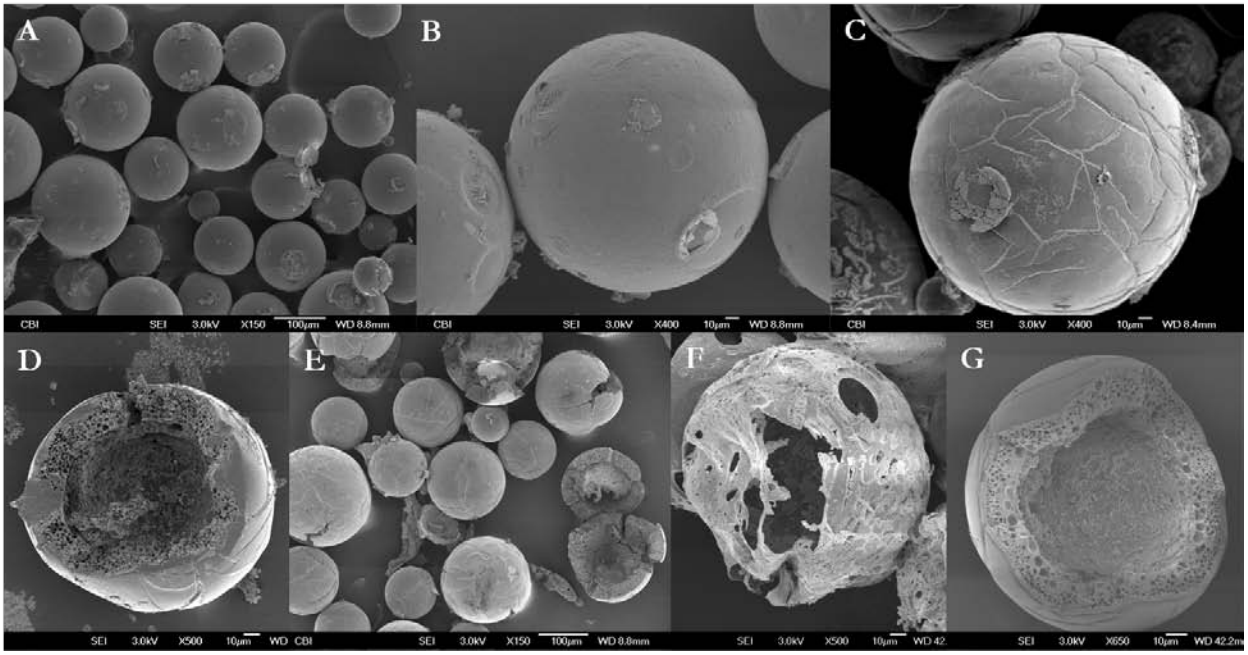

Figure 28. Scanning electron micrographs of double walled microspheres without encapsulated proteins incubated in PBS for 1 week, (A) followed by monthly intervals to 6 months (B – G).

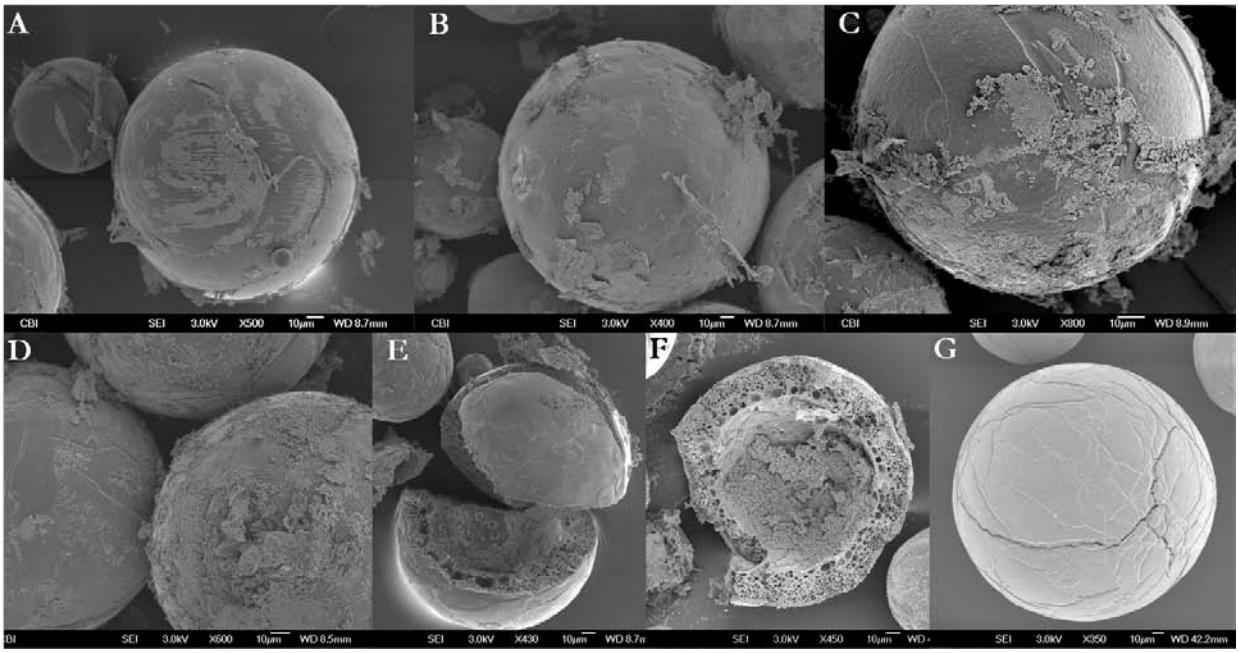

Figure 29. Scanning electron micrographs of double walled microspheres with encapsulated lysozyme incubated in PBS for 1 week, (A) followed by monthly intervals to 6 months (B – G).

3.3.5.3 *In vitro* release kinetics

The formation of pores in the microsphere shell impacted lysozyme release kinetics as shown in the protein release studies (Figure 30). The cumulative release of lysozyme from 10% PLGA microspheres by day 56 is 19.5 μg protein per mg microspheres, while 12.5% PLGA micropsheres released only 12 μg per mg microspheres. DW microspheres produced with 15% and 17.5% PLGA had reduced liberation of lysozyme as compared to 12.5% and 10% PLGA. At day 56, 15% PLGA microspheres released only 5.7 μg protein per mg microspheres. Lysozyme release from 17.5% PLGA microspheres was similar to that of 15% PLGA solution, with 6.3 μg protein liberated per mg microspheres. Therefore, PLGA solution concentration affected not only the pore structure within the PLLA shell, but also the overall protein loading of microsphere batches. Encapsulation efficiency for microspheres of successively increasing concentrations of PLGA were: 23.5%, 14.6%, 6.5%, 6.5%, and 4.3% for batch 4 – 8 respectively.

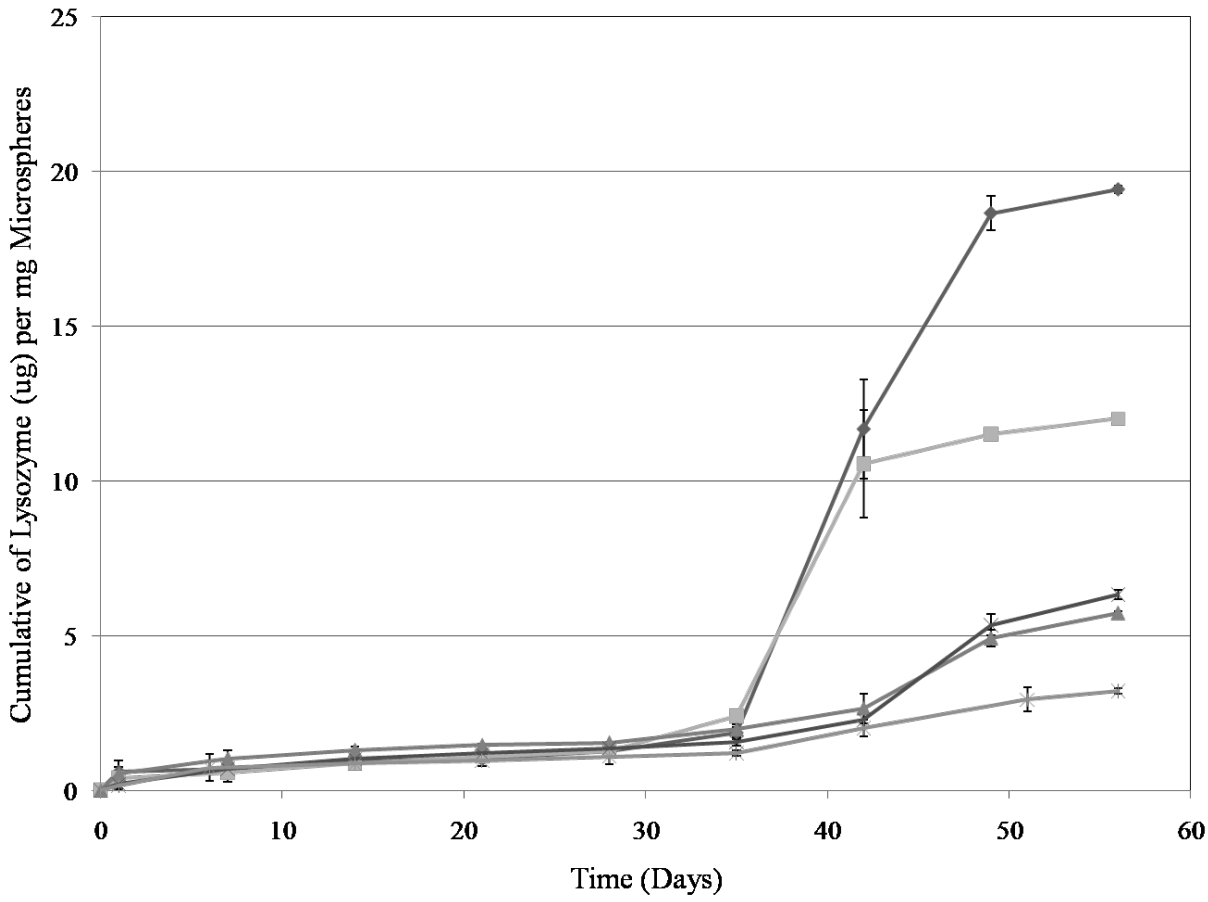

Figure 30. Cumulative release of lysozyme from double walled microspheres prepared with 10% PLLA solutions and 10% PLGA (◆), 12.5% PLGA (■), 15% PLGA (▲), 17.5% GDNF (*), 20% PLGA (X).

3.3.6 Double walled microspheres: effect of co-encapsulates

Additives such as the surfactant AOT and the large, stabilizing protein human serum albumin were investigated as co-encapsulants for double walled microsphere preparation.

3.3.6.1 Optimization of Lysozyme : AOT molar ratio

A bioactivity assay with specified molar ratios of lysoyme to AOT was performed using a Micrococcus lysodeikticus solution (Figure 31). Results suggest that a 1:2 (93% activity) and 1:3 (91% activity) molar ratio of lysozyme to AOT had significantly higher activity when compared to all other molar ratios of lysozyme:AOT tested ($p < 0.05$). The activity assay further indicated that AOT molar ratios of 1:1, 1:4, 1:5, and 1:20 all had similarly reduced activity (85%, 80%, 79% and 78%, respectively). The 1:10 solution of lysozyme to AOT appeared to have the lowest percent activity, with only 70% measured activity as compared to identical lysozyme concentration in PBS solution ($p < 0.003$ for all compared groups). From this study, DW microspheres were prepared using a 1:2 molar ratio of lysozyme to AOT.

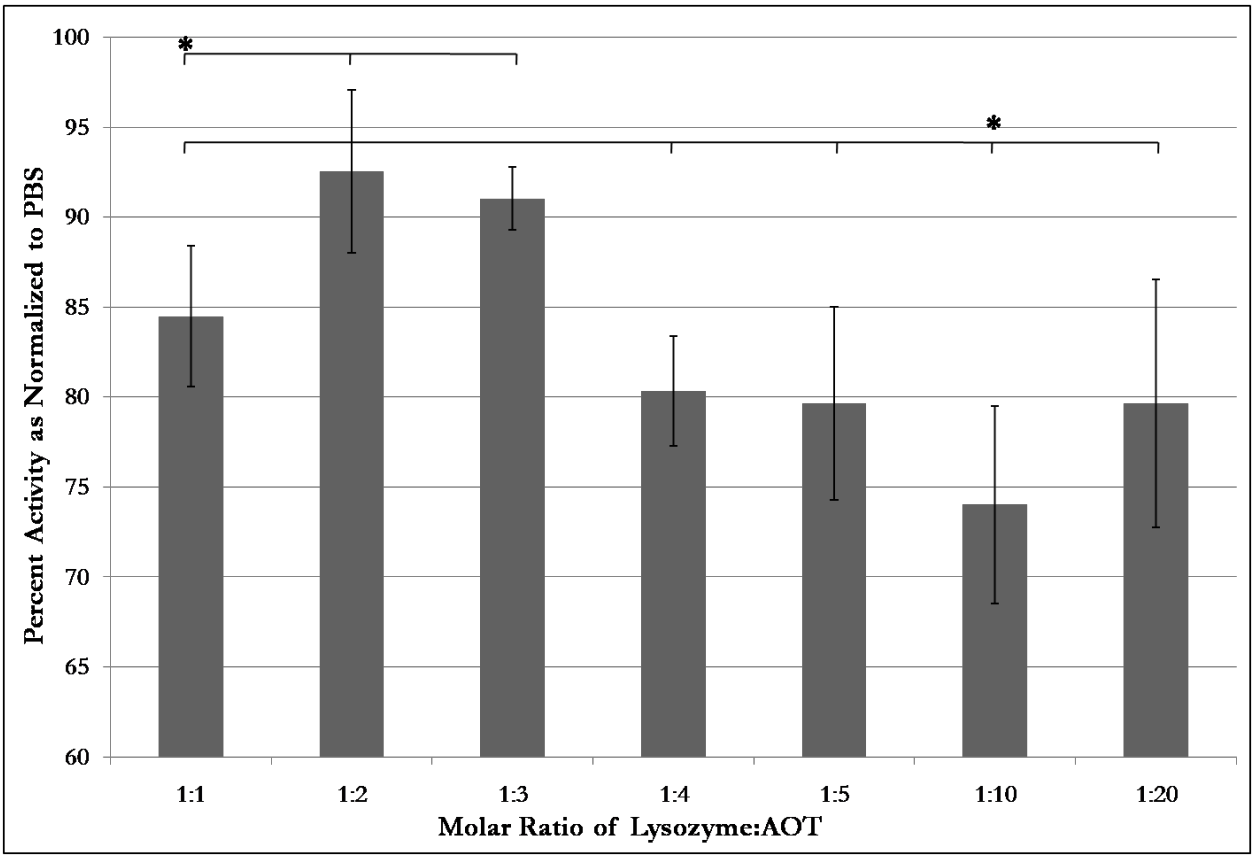

Figure 31. Measured bioactivity of lysozyme in PBS solution with varying molar ratios of lysozyme to the surfactant AOT. Error bars represent mean ± standard deviation for n = 4. Significance between groups is indicated by astersisks ($p < 0.05$).

3.3.6.2 Effect of docusate sodium salt on protein localization and microsphere polymer orientation

Light micrographs of DW microspheres encapsulating only fluorescently labeled albumin revealed protein localization within the polymer core (Figure 32A). However, when FITC-BSA was encapsulated with the surfactant AOT, the protein was detected in the microsphere shell (Figure 32B). Dissolution studies in which the microspheres were first sectioned and subsequently treated with ethyl acetate, a solvent which dissolves PLGA and not PLLA, revealed

the PLGA component of the microspheres was largely restricted to the internal microsphere core when AOT was not used for encapsulation. The scanning electron micrograph depicting microspheres treated for 48 hours with ethyl acetate shown in Figure 32C demonstrates a PLLA hemisphere with partial mass loss within the external microsphere shell. Scanning electron micrographs of DW microspheres encapsulating both lysozyme and AOT reveal solid polymer spheres remain following treatment with ethyl acetate for 48 hours (Figure 32D).

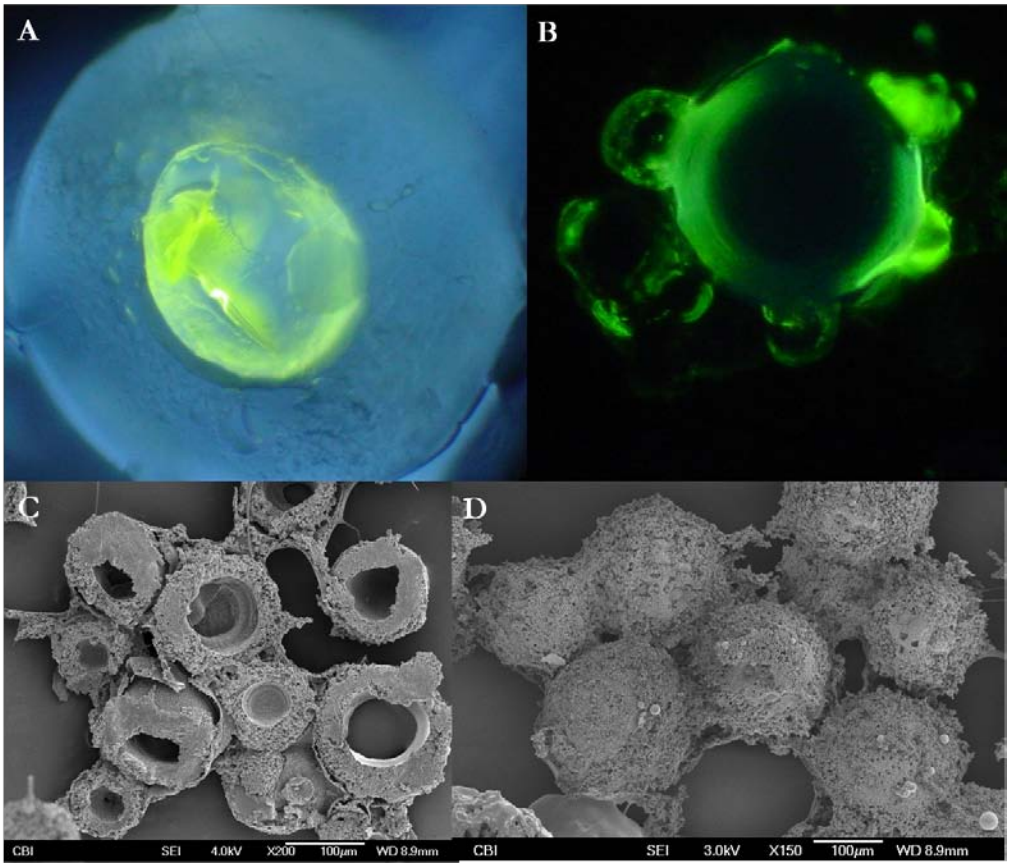

Figure 32. Fluorescent micrograph of double walled microsphere encapsulating FITC-BSA (A) and with FITC-BSA in a 1:2 molar ratio with AOT (B). Scanning electron micrographs of double walled microspheres encapsulating FITC-BSA (C) and FITC-BSA with AOT (D) following treatment with ethyl acetate.

3.3.6.3 Microsphere degradation *in vitro*

Degradation studies were performed for DW microspheres encapsulating lysozyme with the surfactant AOT. The degradation of microspheres encapsulating lysozyme with AOT (Figure 33) was markedly different from that seen with lysozyme alone (Figure 29). Microsphere surfaces after 1 week incubation *in vitro* were very rough (Figure 33A) and it is evident that the PLGA/PLLA orientation was reversed. The PLGA shell was mostly degraded following 1 month incubation (Figure 33B) and was almost completely absent after 2 months (Figure 33C). At month 3 (Figure 33D), the PLLA core seemed to have surface adherent protein that was not evident at 4 months (Figure 33E). As the degradation of the remaining PLLA core continued, the surface pores increased in size and by month 6 only single polymer PLLA spheres remained that were deeply cratered (Figure 33G).

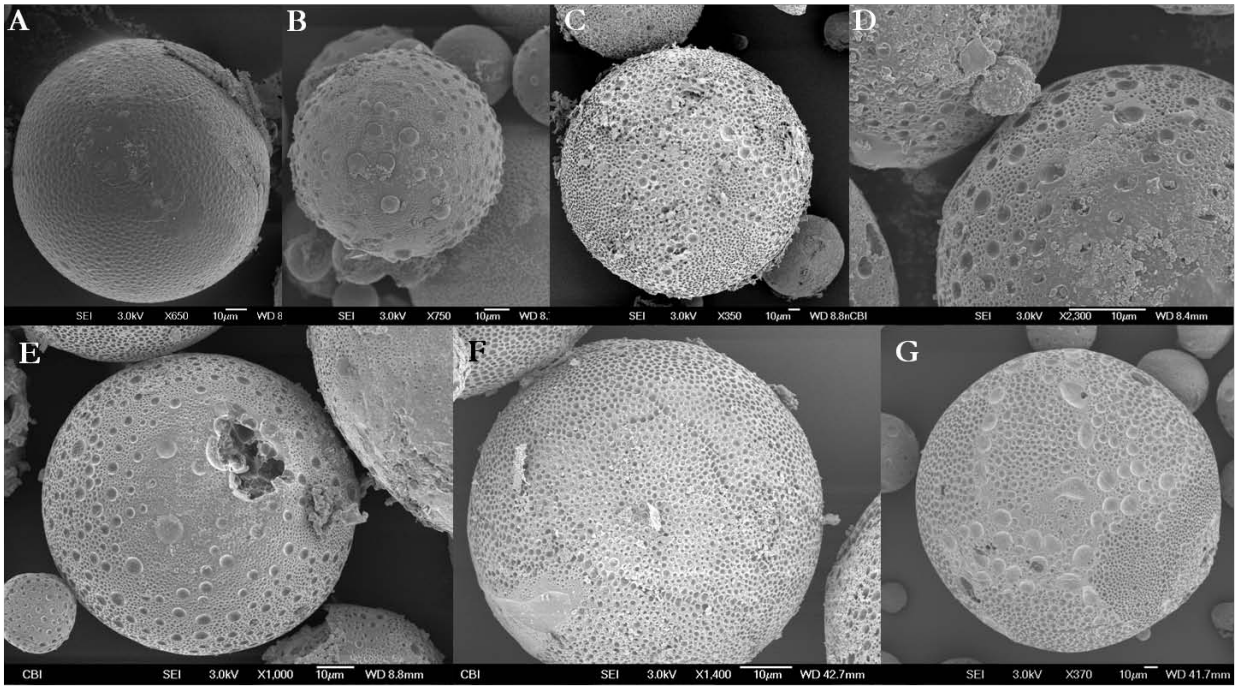

Figure 33. Scanning electron micrographs of double walled microspheres with encapsulated lysozyme and AOT incubated in PBS for 1 week, (A) followed by monthly intervals to 6 months (B – G).

3.3.6.4 *In vitro* release kinetics

The long-term delivery of lysozyme was measured following microsphere incubation in PBS at 37°C. At specified time points, the microspheres were centrifuged and the PBS was aspirated and analyzed with a Micro BCA protein assay. Protein release studies were performed on two unique batches of microspheres with lysozyme to assess fabrication consistency (Figure 34). Microspheres demonstrated an extended release of lysozyme for over 140 days. The drug loading efficiency was ~12% and microsphere drug loading capacity was .005%. The release profile revealed a small burst release of lysozyme within the first week of microsphere

incubation *in vitro*. This was followed by a slower, sustained release until day 36. At this point, ~16% of the encapsulated lysozyme was released from the microspheres. Between day 40 and day 100 of the release profile an additional 77% of encapsulated lysozyme was released. Beyond day 100, only small residual amounts of lysozyme were measured. The release profile of lysozyme between multiple batches of DW microspheres appeared consistent.

Lysozyme encapsulated with the surfactant AOT in a 1:2 molar ratio produced a significantly different release profile (Figure 34). Within the first week of incubation, ~37% of the encapsulated lysoyme was released, followed by an additional 37% before day 40. Between day 40 and day 100, 17% of the encapsulated lysozyme was released in a near linear order. Drug loading efficiency for lysozyme encapsulated with AOT was 12.8% and drug loading capacity was 0.006%.

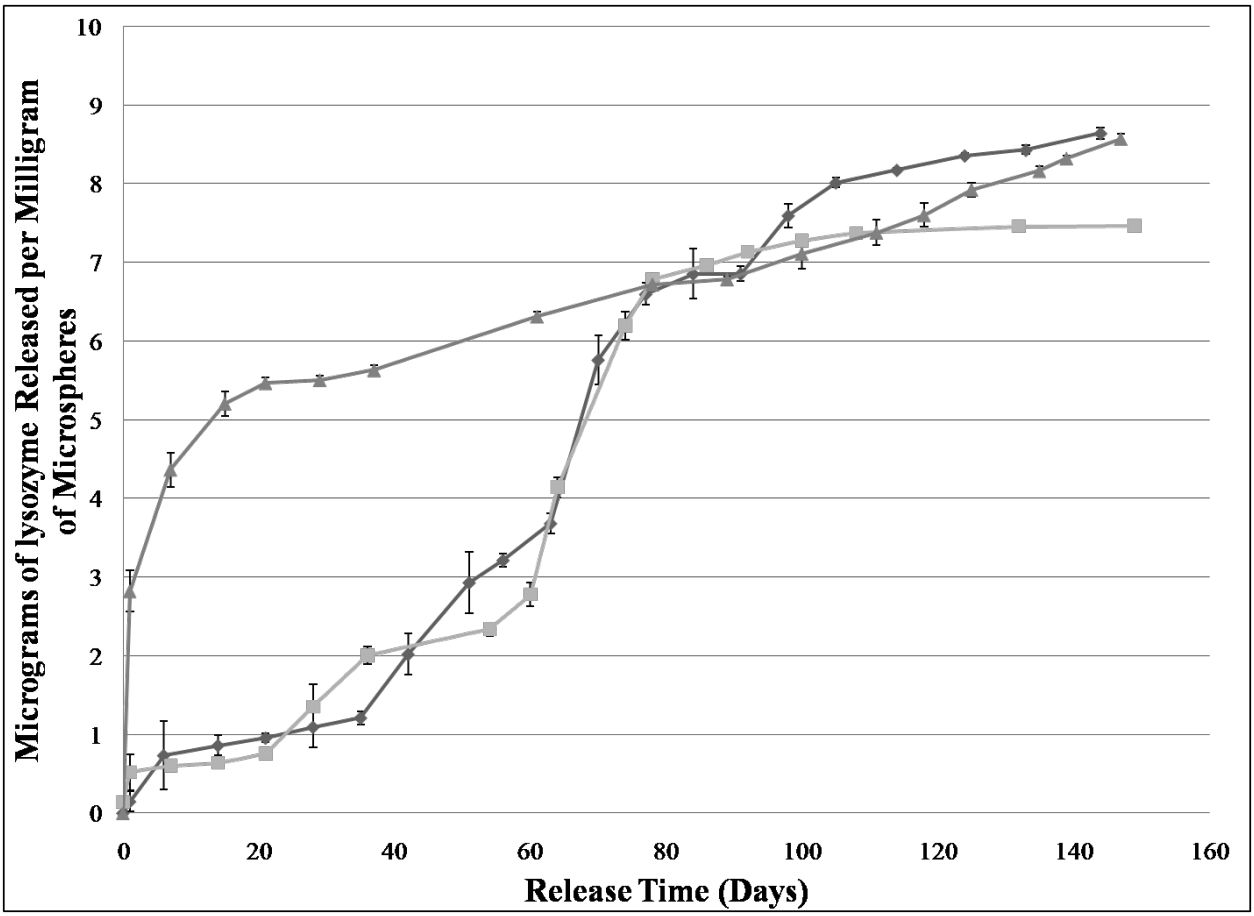

Figure 34. Release of lysozyme from double walled microspheres. Lysozyme was encapsulated in two unique batches of microspheres without AOT (▪ and ◆) and with AOT (▲). Error bars represent standard deviation (n = 3 measurements for each batch of microspheres).

3.3.6.5 Lysozyme Bioactivity

The bioactivity of lyophilized lysozyme was assessed immediately prior to encapsulation and was not significantly different from freshly dissolved lysozyme ($p = 0.66$). When microspheres were prepared with lysozyme independently, 82 ± 5 % of bioactivity was maintained following 1 week release from DW micropsheres (Figure 35). The lysozyme mean activity decreased slightly to ~73 ± 7 % at day 13, and then increased to measured activity levels above 100% between day 34 and 53 of the release studies, however the release activity for lysozyme encapsulated alone was not significantly different between day 1 and day 60 ($p > 0.05$). Beyond day 60, the lysozyme activity decreased significantly to ~65% ($p < 0.001$) and then decreased again at day 70 to ~17.0% ($p = 0.0012$). The bioactivity of lysozyme release beyond day 90 was no longer detectable.

Lysozyme encapsulated with the surfactant AOT had significantly reduced bioactivity at day 1 (47%) and day 7 (47%) as compared to lysozyme encapsulated alone ($p < 0.01$) (Figure 35). Bioactivity of released lysozyme samples increased after this period and was not significantly different from lysozyme activity when encapsulated alone ($p > 0.05$).

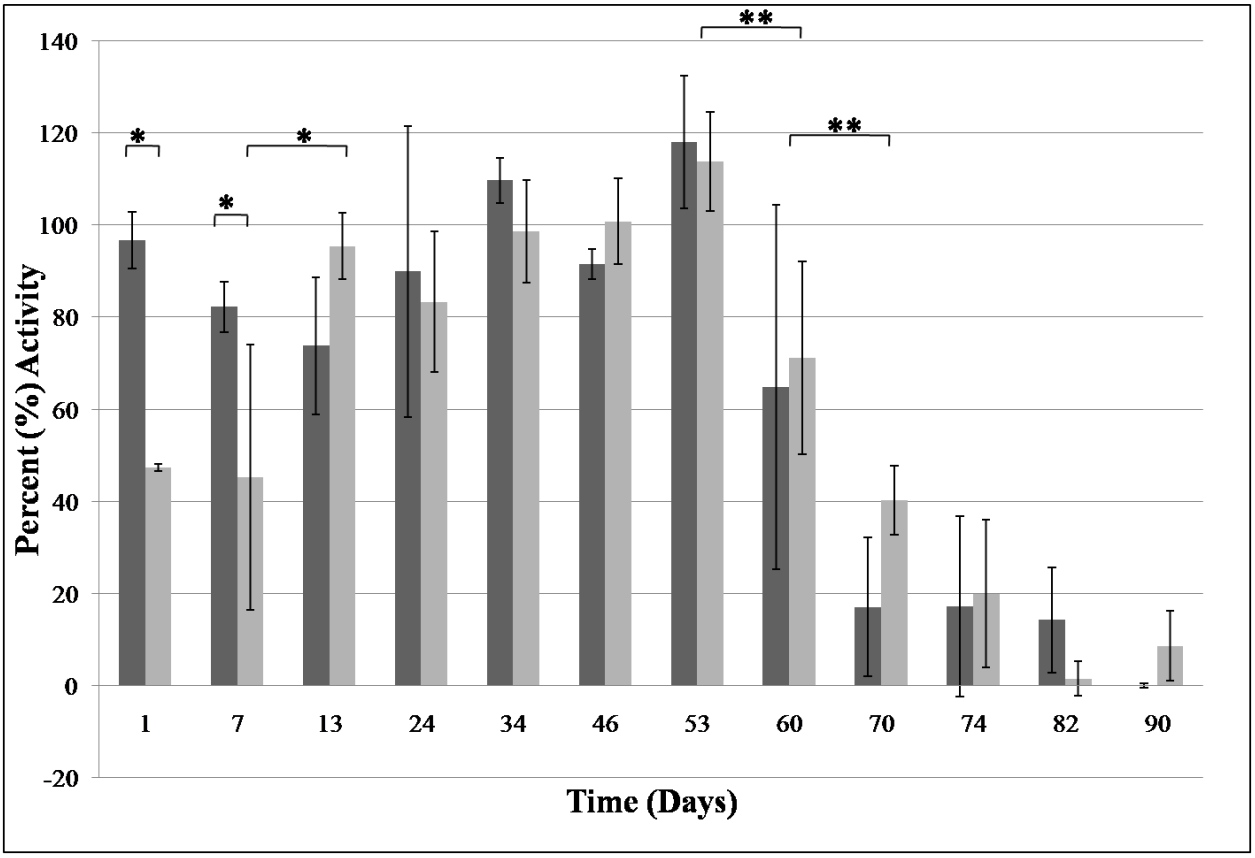

Figure 35. Measured percent bioactivity measurements for (■) lysozyme samples without AOT or (■) lysozyme with AOT released from double walled microspheres after incubation in PBS, mean ± standard deviation. Single asterisks represent statistical significance between individually compared groups. Double asterisks represent significant differences between time points for both microsphere groups ($p < 0.05$).

3.3.6.6 Double walled microsphere encapsulation of GDNF with AOT

GDNF was encapsulated in double walled 15% PLGA, 15% PLLA microspheres with the surfactant AOT. Batch 11 of GDNF microspheres was prepared with 7 mg HSA and 100 mg AOT as coencapsulants with 40 µl (0.1 mg/mL) GDNF as described by Jiang et al [193]. Microspheres of this preparation formulation were generated with a batch efficiency of 54.6%.

Scanning electron micrographs of double walled microspheres reveal heterogeneity in resulting microsphere morphology. Microspheres were produced with both a single polymer composition (Figure 36A) and a double walled morphology (Figure 36B). DW microspheres had a thick shell coating and show large holes in the polymer layer continuity.

Microspheres of batch 12 consisted of 15% PLGA, 15% PLLA with 7 mg HSA, 40 μl GDNF and a 1:2 molar ratio of AOT (2.37 μg). Micrographs of microspheres reveal two polymer microspheres with both complete core engulfment (Figure 36C) as well as partial engulfment (Figure 36D). Additionally, the external shell of double walled microspheres is rough and appears porous with small spheres of PLGA evident within the external shell layer.

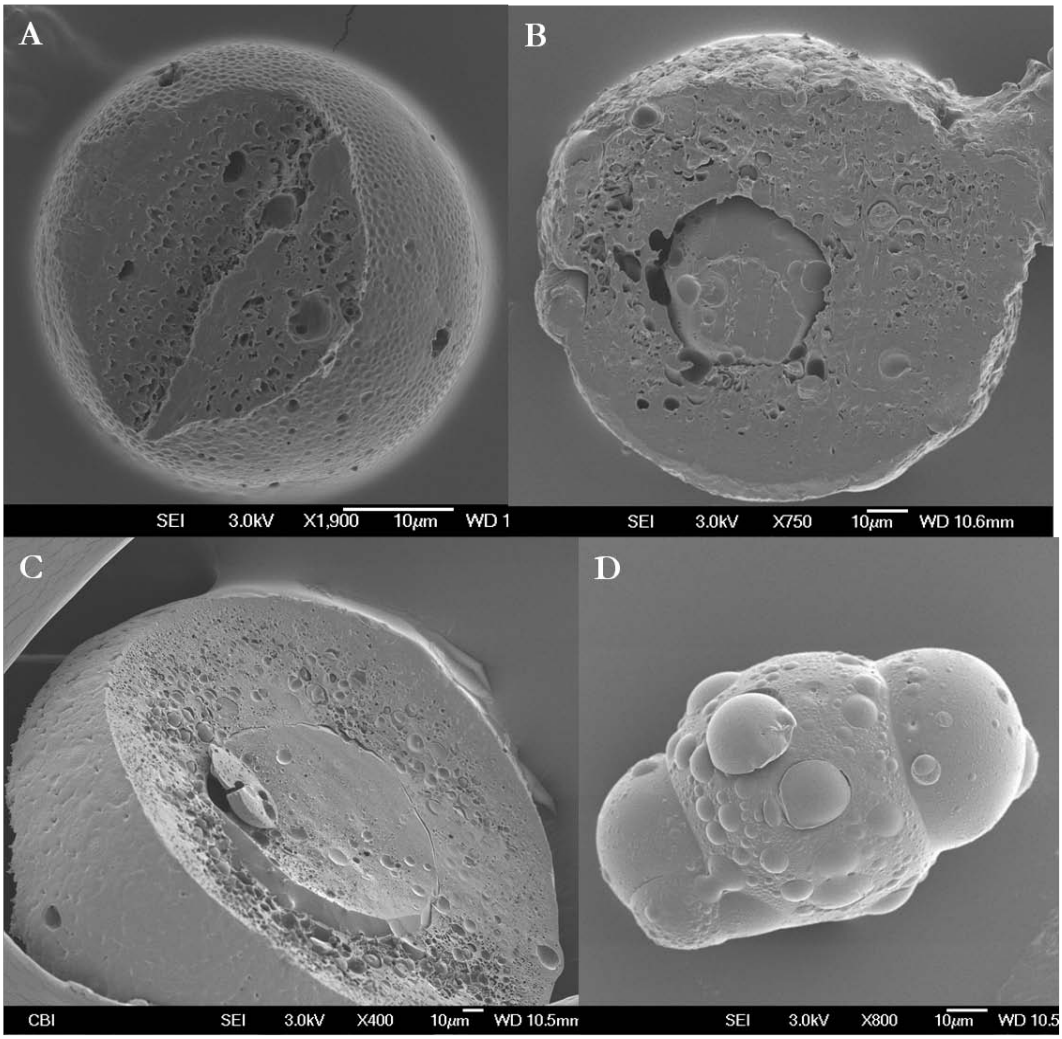

Figure 36. Scanning electron micrographs of batch 11 double walled microspheres encapsulating GDNF (A and B) and batch 12 double walled microspheres with GDNF in a 1:2 molar ratio with AOT (C and D).

The long term liberation of GDNF from double walled microspheres was measured following analysis of PBS collected following microsphere incubation *in vitro*. The release profile indicates an initial burst release of GDNF from batch 11 during the first day of microsphere incubation, with 4.8 ± 0.4 ng GDNF measured per mg microspheres (Figure 37). Following the initial burst, GDNF was released with near zero-order kinetics until day 40 and by day 64 had a cumulative release of 6.4 ± 0.02 ng GDNF per mg microspheres. GDNF release from batch 12 microspheres consists of two periods of accelerated release. After 1 day in solution, ~15% of the total encapsulated GDNF was released and by day 35, ~59% of the encapsulated GDNF was liberated. After this point, there was a second period of increased lysozyme release until day 57, when at this time point, almost 99% of the encapsulated GDNF was released. The cumulative release of GDNF for 64 days of incubation in PBS was ~4.5 ± 0.006 ng per mg of double walled microspheres. This represents a total drug loading of 0.0006% and 0.0004% for batch 11 and 12 respectively.

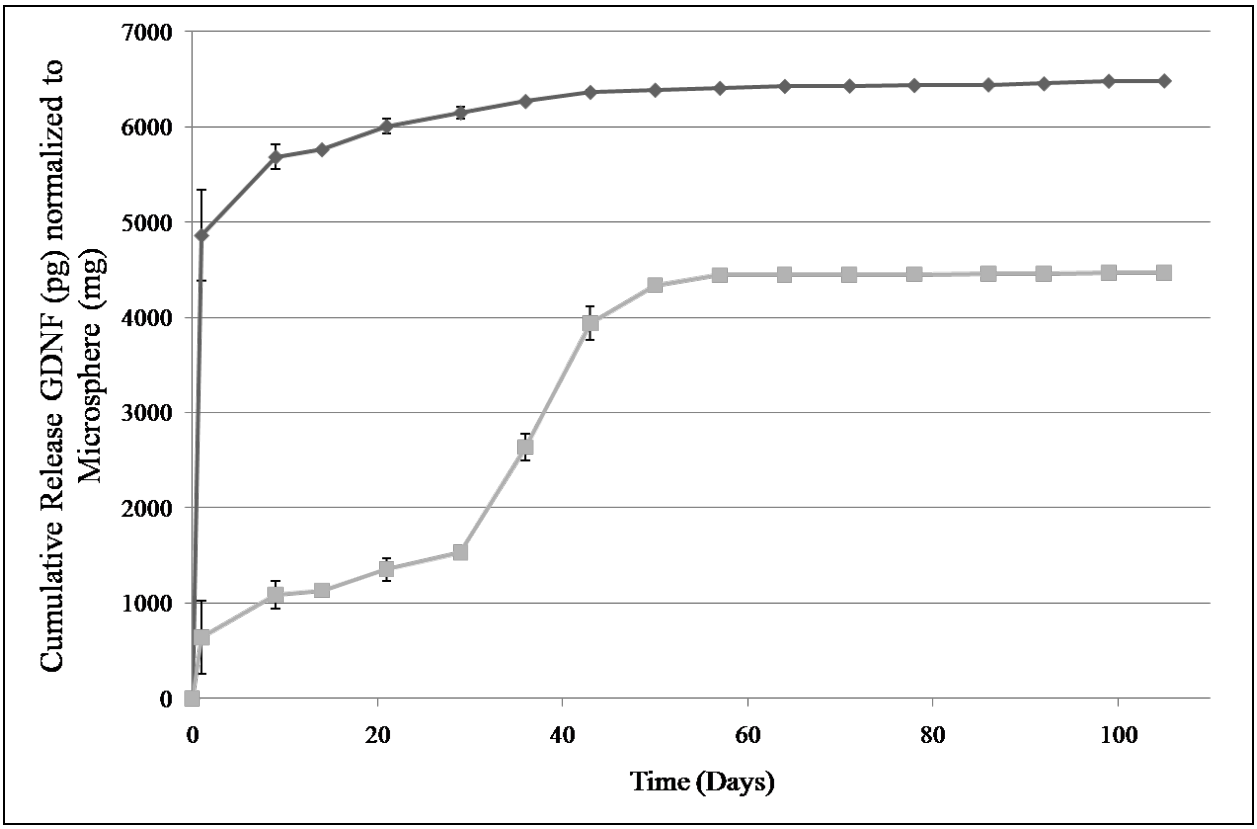

Figure 37. *In vitro* release of GDNF from double walled microspheres (◆ , batch 11; 100 mg AOT) and (■ , batch 12; 1:2 ratio of GDNF:AOT). Error bars represent standard deviation, with 4 unique release measurements per batch of microspheres.

3.3.7 Optimization of lysozyme : HSA molar ratio

A bioactivity assay with specified molar ratios of lysoyme to HSA was performed using a Micrococcus lysodeikticus solution (Figure 38). Following incubation of lysozyme with HSA in PBS for 48 hours, the protein solution was added to a standard solution of lyophilized bacteria and the change in solution absorbance was measured. All results were normalized to fresh lysozyme suspended in an identical PBS solution. Results indicate that HSA improved the stability of lysozyme in solution and therefore increased the measured *in vitro* bioactivity, as all recorded measurements of bioactivity were above lysozyme alone in solution. The mean recorded bioactivity of lysozyme with HSA was greatest at a 1:50 ratio of lysozyme to HSA, with the average bioactivity being ~111 ± 4.8 %, which was significantly greater than a 1:2 ratio (105 ± 1.63%), a 1:3 ratio (106 ± 2.8%), a 1:4 ratio (106 ± 3.2%) and a 1:20 ratio of lysozyme to HSA (107 ± 3.2%). Bioactivity of lysozyme in solution was recorded with four repetitions and statistical significance was established with $p < 0.05$.

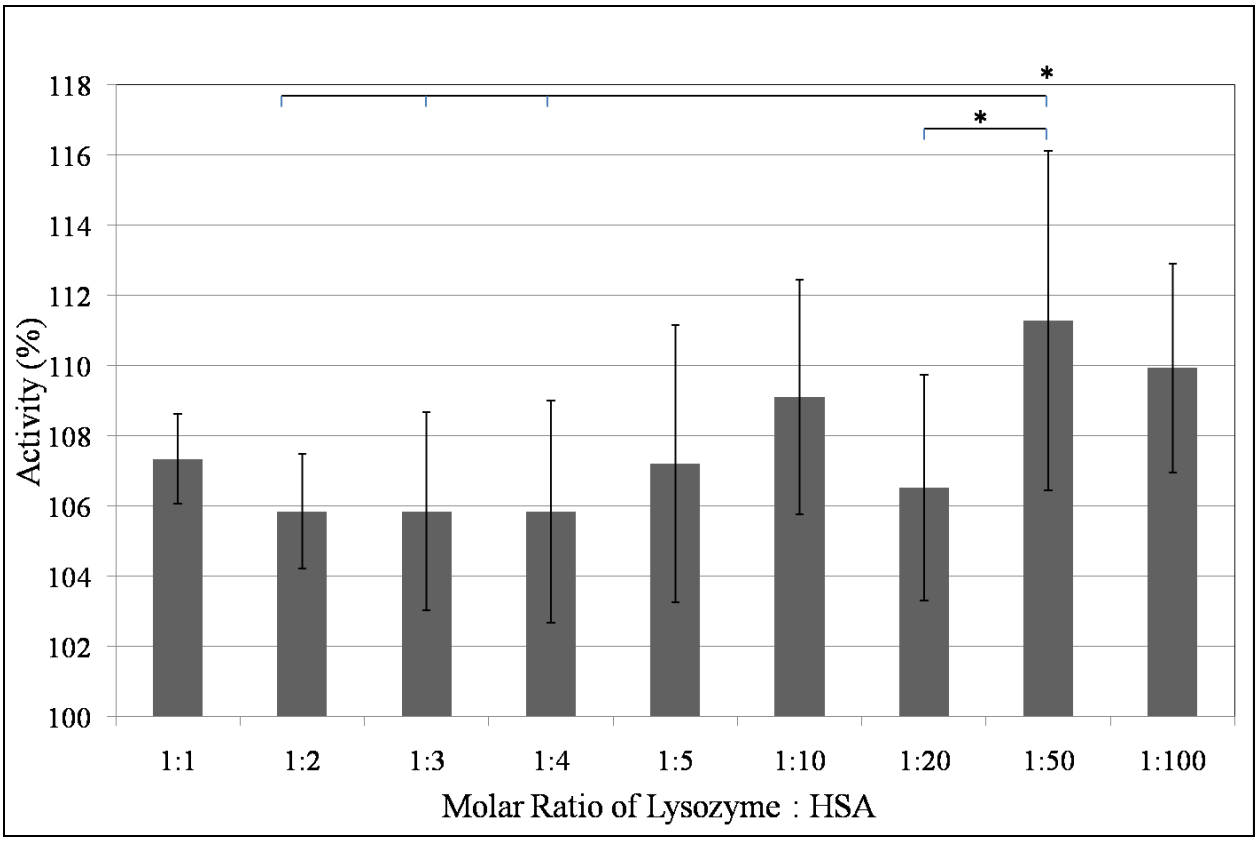

Figure 38. Measured bioactivity of lysozyme in PBS solution with varying molar ratios of lysozyme to HSA. Error bars represent mean ± standard deviation for n = 4. Significance between groups is indicated by astersisks ($p < 0.05$).

3.3.7.1 Double walled microspheres encapsulation of GDNF with HSA

Double walled microspheres were prepared with 17.5% PLGA, 10% PLLA and encapsulated GDNF with HSA as a coencapsulant. Batch 13 microspheres were produced with 85.7% microsphere efficiency and resulted in microspheres that had two distinct polymer walls (Figure 39 A and B). Large holes are evident within the PLGA core while the PLLA shell appears smooth and dense. The external surface of the microsphere shell is rough, with a large number of protuberances. Batch 14 microspheres were produced with 84.7% yield efficiency and also produced microspheres of two distinct polymer layers in high frequency. As was evident with batch 13, large holes are evident in the PLGA core. However, the external microsphere shell is smooth and dense and appears to contain only small traces of PLGA that was not able to fully phase separate.

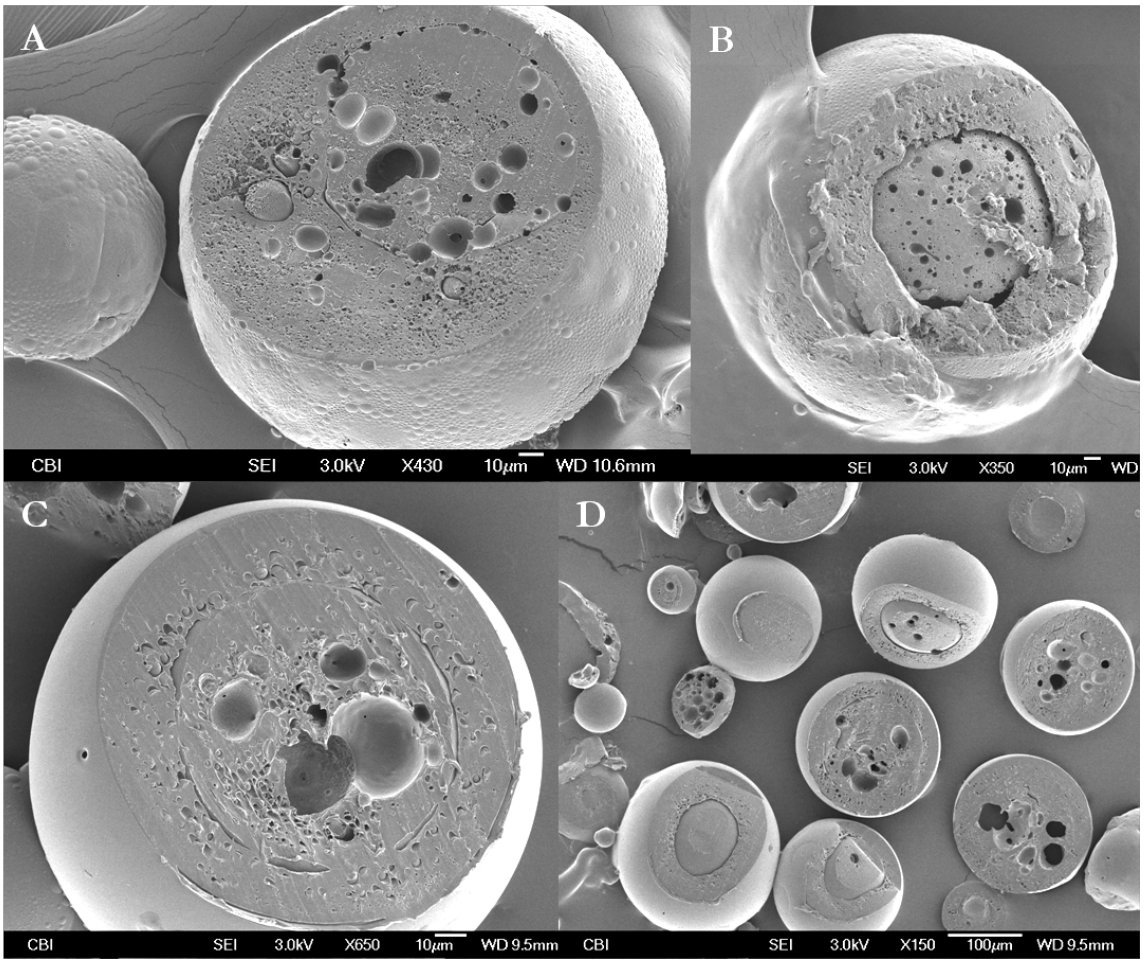

Figure 39. Scanning electron micrographs of double walled microspheres encapsulating GDNF with HSA. A and B) Double walled microspheres produced with cloud point induction. C and D) Double walled microspheres produced without induction of phase separation.

Long term release studies of GDNF encapsulated with HSA reveal two phase protein release for both batches 13 and 14 of microspheres. For those microspheres produced with cloud point induction (batch 13), protein release following 1 day incubation resulted in a burst with ~53% of the total encapsulated GDNF released into solution. GDNF release between day 1 and 28 was nearly continuous with ~80% of GDNF released by day 28. Following a second period of accerlerated protein release, all measurable amounts of GDNF were released by day 63 *in vitro*. Protein release from batch 14 microspheres showed two periods of rapid protein release with little to negligible GDNF liberation in between At day 1, ~29% of the total encapsulated protein was released followed by a plateau until day 35, when the release profile appears nearly zero order. This period of release occurred between day 35 and day 50, when ~98.5% of the encapsulated GDNF was released. The drug loading for batch 13 and 14 respectively was $8.2x10^{-4}$ % and $4.5x10^{-4}$ %.

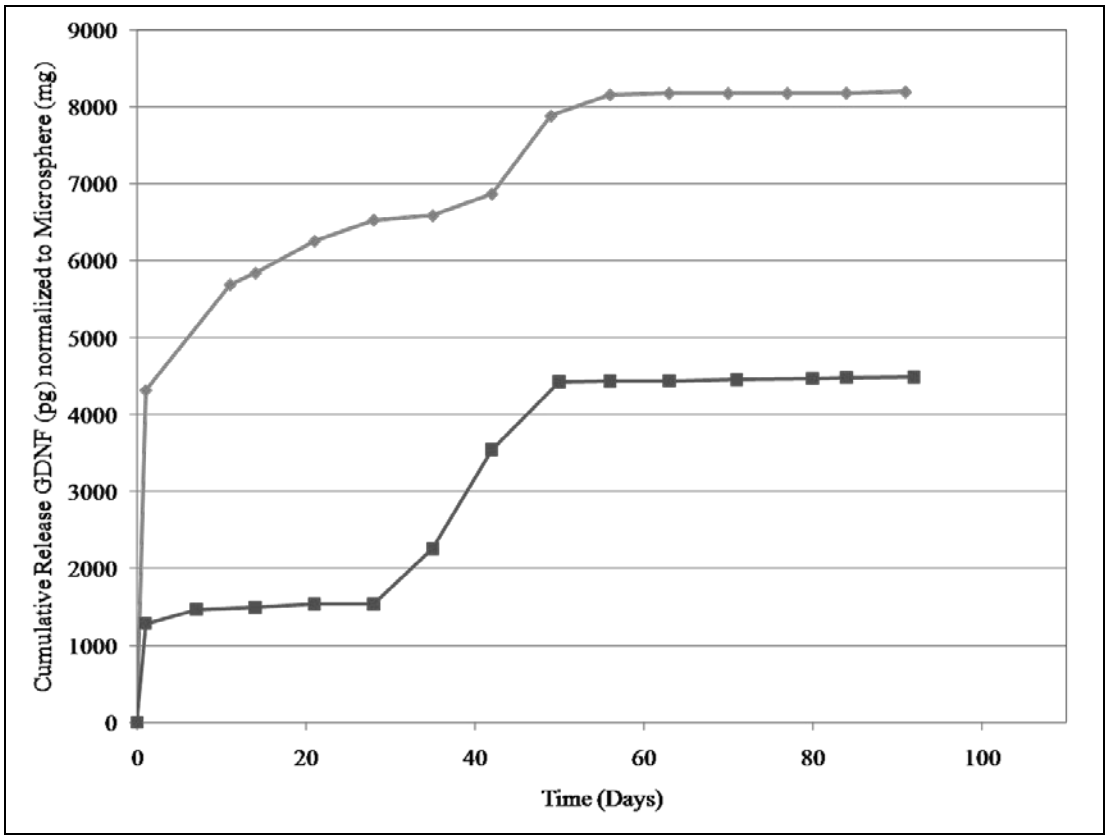

Figure 40. *In vitro* release of GDNF from double walled microspheres (◆ , batch 13; cloud point induction) and (■ , batch 14; no cloud point induction). Error bars represent standard deviation, with 4 unique release measurements per batch of microspheres.

3.4 DISCUSSION

There are several manufacturing factors within solvent evaporation methods for microsphere fabrication that influence the physical properties of the microsphere product and thus the drug release profile. Such factors include the selection of fabrication materials such as polymer type, solvent, encapsulated protein and surfactant choice. Depending on the selected

permeation of these manufacturing factors, microsphere size distribution, surface morphology, porosity, encapsulation efficiency and protein release kinetics can all be influenced [212].

GDNF has been successfully encapsulated in single walled microspheres by Ward et al., [192], Fu et al., [181], Aubert-Pouessel et al., [183] and Tatard et al., [213]. By using single emulsion and double emulsion PLGA microspheres, Fu et al., were not able to avoid burst release of GDNF such that blood serum levels in rats showed significant protein delivery beyond 2 days. Our results show that even with optimization of PLGA selection (65:35 lactide to glycolide molar ratio) and coencapsulation of surfactants shown to delay model protein release, the burst release of GDNF from single walled microspheres was not improved upon. Therefore, the use of double walled microspheres as a method for improved GDNF release kinetics was investigated.

While DW microspheres were originally formed from poly(1,3-bis(*p*-carboxyphenoxypropane)-co-sebacic anhydride) 20:80 and poly(lactic acid) [204] more chemically similar polymer pairs such as PLLA and PLGA have also been used [199, 201, 203, 214, 215]. The benefit of using PLGA and PLLA for DW microspheres includes the polymers proven biocompatibility and toxicologically safe degradation products (lactic and glycolic acid) [182]. Furthermore, PLGA and PLLA used in combination create a DW microsphere that is both a reservoir and bioerodible matrix system. When the DW microsphere is added to an aqueous environment, the PLLA microsphere shell presents a barrier and suppresses water diffusion throughout the microsphere, limiting the initial protein release [216]. Within the two polymer microsphere layers, the PLGA microsphere core undergoes bulk erosion first (Figures 28 and 29), allowing water molecules to permeate into the amorphous regions of the polymer matrix and release the encapsulated protein through diffusion. However, the degradation of PLLA is much

slower than PLGA (50:50) due to increased polymer crystallinity and hydrophobicity [217], which results in a temporary reservoir system from which the protein diffuses outward through the PLLA pores and is released with kinetics approaching first order [199].

Double walled microspheres were produced using an oil-in-water single emulsion process. This method depends on the creation of a two polymer solution in a single, continuous phase in which phase separation occurs. The two polymers used for microsphere preparation were PLGA and PLLA. The desired polymer configuration for the microsphere core and shell was one of PLGA engulfed by PLLA. The effect of three volatile solvents on polymer phase separation was investigated as a method of engineering polymer orientation within the double walled microspheres. After the selection of appropriate polymer solvents, separate solutions of PLGA (10 – 17.5% w/v) and PLLA were prepared in order to dictate the extent to which the two polymers were able to phase separate within each droplet of the single emulsion solution. Finally, additives were investigated as a method of protecting the encapsulated protein and thus improve the bioactivity of liberated proteins *in vitro*.

For selection of polymer solvent for DW microsphere preparation, it was hypothesized that the polymer dissolved in the more hydrophilic solvent would phase separate toward the aqueous environment and would therefore become the microsphere shell. Therefore, solvent combinations of Table 8 were selected such that the most hydrophobic solvent within combinations was used for PLGA dissolution. Polymer combinations of PLGA and PLLA dissolved in dichloromethane or PLGA in ethyl acetate and PLLA in DCM resulted in the desired polymer orientation and protein localization with the PLGA core. However, the solvent combination of DCM for PLGA and THF for PLLA was used, the resulting microspheres were heterogeneous in polymer orientation with the majority of microspheres having a PLLA core and

a PLGA shell. Although, the encapsulated protein remained within the PLGA microsphere layer, because the PLGA composed the microsphere shell, the localization of protein was not optimal for our purposes. Because the protein loading within microspheres prepared with only DCM (21.1%), was greatly improved over microspheres prepared with ethyl acetate and dichloromethane (14.7%), future microspheres were produced using dichloromethane for both PLGA and PLLA.

The percent concentration of PLGA was further investigated as a method of tailoring the release kinetics of lysozyme from microspheres. As shown in Figure 27, the degree of phase separation between PLGA and PLLA during the dynamic process of polymer separation and hardening is affected by the concentration of PLGA in dichloromethane used for the primary oil-in-oil emulsion. Low concentrations of PLGA, 10% and 12.5% PLGA, result in the formation of small, interconnected pores upon PLGA degradation form the microsphere shell. Accordingly, when the PLGA degrades during protein release studies at day 35, there is an increase in lysozyme liberation seen in microspheres prepared with 10% and 12.5% PLGA solutions. However, DW microspheres prepared with higher concentrations of PLGA showed large occlusions of PLGA within the PLLA shell due to an increase in polymer solution viscosity. As a result, large, isolated pores remained following PLGA degradation. Therefore, the liberation of lysozyme into release media was slowed from microspheres produced with highly viscous solutions of PLGA during the initial oil-in-oil emulsion preparation.

Despite the improved release kinetics that DW microspheres present as compared to standard, single-walled double emulsion microspheres, some of the drawbacks of encapsulating proteins with a solvent evaporation method continue to exist. During the DW microsphere fabrication process, the protein to be encapsulated is added directly to PLGA dissolved in an

organic solvent, potentially denaturing the protein. Furthermore, high energy mixing and addition of the dissolved protein and polymer solution to a large aqueous volume is still required. Therefore, the encapsulation procedure results in a substantial loss of expensive drug or protein materials. Because of this, additives for protein encapsulation have been investigated to maximize the recovered protein bioactivity following encapsulation.

Protein stabilizers such as cyclodextrins [218], poly(ethylene glycol) (PEG) [219], Rat Serum Albumin (RSA) [208] and AOT [181, 192, 193] have all been investigated as potential compounds for protecting a protein during the encapsulation procedure. For this study, docusate sodium salt was chosen because it was hypothesized that a continuous distribution of protein within the initial PLGA solution would lead to a decrease in protein aggregation and therefore an improvement in released lysozyme bioactivity. While other stabilizers were shown effective in minimizing protein denaturation during manufacturing of single polymer double-emulsion microspheres, protein encapsulation in DW microspheres required that lyophilized protein powder solubilize in a single-phase polymer solution. Fu et al., have shown previously that AOT dramatically increases the solubility of lysozyme in dichloromethane and when used to fabricate single-walled microspheres resulted in enhanced protein partitioning within PLGA in organic solvent [181].

However, it has also been documented that anionic surfactants, such as AOT, can cause a decrease in enzyme stability at temperatures near 37°C [220]. Literature reports that there is an initial interaction between the negatively charged regions of surfactants (such as the two negatively charged arms of AOT) with the cationic amino-acid residues of lysine, histidine and arginine [221]. In an oil-based solution, such as dichloromethane, the conformation of lysozyme changes slowly to maximize the number of exposed hydrophobic regions. If an abundance of

AOT is added to the lysozyme solution such that the cationic sites of lysozyme are saturated, AOT will also bind to the exposed hydrophobic regions of lysozyme and can disrupt the secondary structure of the protein folding, especially the α-helices [221]. In an effort to determine the optimal concentration of AOT for encapsulation, a bioactivity study was conducted using various molar ratios of lysozyme to AOT. While Fu et al., reported that a 1:30 molar ratio of protein to AOT was optimal for protein solubility in the single phase of PLGA and solvent, our bioactivity studies of lysozyme in solution with various molar ratios of AOT revealed that an excess of surfactant decreased the protein bioactivity. Because we consider protein bioactivity a priority for our delivery system, we chose to conduct our experiments with a 1:2 molar ratio of lysozyme to AOT.

DW microsphere degradation studies revealed an unexpected effect of AOT on the process of polymer phase separation (Figures 29 and 33). After one week *in vitro*, microspheres encapsulating lysozyme alone displayed a smooth surface with adherent lysozyme. However, microspheres encapsulating both lysozyme and AOT resulted in a surface covered with protuberances indicating incomplete phase separation between PLLA and PLGA. By validating the polymer orientation through dissolution studies (Figure 32) and from the progression of microsphere degradation micrographs, it is evident that the polymer orientation seen previously with lysozyme-loaded microspheres had reversed. Instead of DW microspheres containing a core of PLGA and a PLLA shell, microspheres encapsulating lysozyme and AOT resulted in a core composed mostly of PLLA and a PLGA shell.

Lysozyme release kinetics from the two microsphere samples reflect the reversal of polymer core and shell orientation. The release profile of lysoyme encapsulated alone from DW microspheres reveals that protein was delivered first from the surface of the microsphere,

followed by a slow rupture and formation of macropores in the PLLA microsphere shells. The slow, steady-state release of lysozyme between day 7 and day 35 reflects the high water uptake of the inner PLGA core and the slow release of lysozyme through PLLA micropores [215]. Lysozyme release between day 40 and day 100 is nearly zero-order and indicates that the PLGA core has undergone bulk degradation and the PLLA shell served as a rate-limiting barrier for continued lysozyme release.

Lysozyme encapsulated with the surfactant AOT in a 1:2 molar ratio resulted in an initial burst of lysozyme release within the first week. Therefore, there was a large amount of protein adherent to the surface of the microspheres during fabrication. Furthermore, within the first 40 days of microsphere incubation, nearly two-thirds of the encapsulated protein was lost. Because the PLGA shell degradation profile (Figure 29) closely matches the lysozyme release profile, it is most likely that a majority of lysozyme was encapsulated within the PLGA microsphere shell. Furthermore, the release profile of lysozyme beyond day 40 until day 100 was nearly zero order. This indicates that an additional quantity of lysozyme was also encapsulated within the PLLA microsphere core and was released through matrix diffusion.

Although we hypothesize that the inversion of microsphere release kinetics between sustained, nearly constant release from microspheres encapsulating only lysozyme and an initial lysozyme release within 20 days from microspheres with AOT is caused by the inversion of polymer orientation, additional mechanisms may be responsible. For example, it is possible that AOT interrupts the interaction between polymer and protein and allows for an increased concentration of non-adsorbed, soluble lysozyme within the DW microspheres. Because similar overall concentrations of lysozyme are released cumulatively, we feel that the primary mechanism affecting the lysozyme release kinetics is polymer orientation.

At present, the exact mechanism for reversal of the polymer orientation in the microsphere core and shell is not clear. We hypothesize that the increase in charge of the PLGA solution caused the polymer to reposition toward the aqueous solution and thus became the microsphere shell. During fabrication, the protein and surfactant were added as a powder to PLGA dissolved in dichloromethane; the solution was then vortexed very well and allowed to sit on ice for ~20 minutes. Therefore, lysozyme and AOT were adsorbed onto the PLGA prior to addition of PLLA. In dichloromethane, the PLGA with adsorbed protein would arrange itself to get an energy minimum and would hide the hydrophilic elements in the center of the polymer – protein aggregate. Because PLLA is a more hydrophobic polymer and because PLGA contained charged molecules, the PLGA most likely separated to the interior of polymer. However, when the PLGA – PLLA oil phase was emulsified with the aqueous solution for microsphere formation, PLGA with bound protein and AOT rearranged toward the water interface. This hypothesis is supported by both the initial burst release of protein adherent to the surface of the DW microspheres as well as the measured bioactivity of released lysozyme (Figure 35).

Alternatively, it is possible that polymer rearrangement occurred during emulsification of PLGA – PLLA in aqueous solution is due to a reduction in polymer viscosity because of AOT and not because AOT binds to PLGA. In addition to creating DW microspheres of 10% PLGA solution, we have also investigated fabricating microspheres using more concentrated polymer solutions with an increased viscosity. Microspheres of similar polymer orientation to those used in assessment of AOT have been constructed from both dilute PLGA solutions (10% w/v) and highly viscous polymer solutions (20% w/v) (Section 3.3.5; Figure 26). Therefore, a decrease in polymer solution viscosity is likely not responsible for the inversion of polymer orientation.

Within the first week of protein release from microspheres, the bioactivity of lysozyme encapsulated with the surfactant AOT was significantly reduced at both day 1 and day 7. Possible mechanisms of protein denaturation include damage to protein structure by the organic/aqueous interface as well as an increased molar ratio of lysozyme to AOT. Results from activity data from lysozyme encapsulated alone and the microsphere release profile present evidence that both mechanisms are responsible for the lysozyme/AOT decrease in activity. AOT caused an increase in surface adherent lysozyme (as indicated by the initial burst release from microspheres) which exposed a greater concentration of lysozyme to interface damage. Additionally, lysozyme released from microspheres encapsulating both protein and surfactant regained activity that was similar to protein encapsulated alone after 7 days. Therefore, it is probable that nearly all of the AOT encapsulated in microspheres was located near the surface and was released within the first week of *in vitro* studies.

Encapsulation of lysozyme with HSA did not appear to affect the bioactivity of lysozyme (Figure 38). Additionally, SEM assessment of microspheres encapsulating protein with HSA showed that two layered microsphere morphology was consistently produced within two unique batches of microspheres. Induction of polymer cloud point using ethyl acetate resulted in an increased drug loading 8.2×10^{-4} % as compared to 4.5×10^{-4} % for microspheres prepared without cloud point induction. However, GDNF release from microspheres prepared through cloud point induction resulted in an initial burst of protein from the microspheres followed by a sustained release until day 50. This release profile was distinct from microspheres prepared without cloud point induction, in which GDNF release closely resembled typical double walled release profiles as modeled with lysozyme.

3.4.1 Conclusions

DW microspheres were fabricated from two polymers of a similar chemical structure, PLGA and PLLA. Initial studies with microspheres encapsulating a fluorescent protein, FITC-BSA, indicated that protein localization was restricted to the PLGA core. In addition, protein release studies were performed using microspheres with the model protein lysozyme encapsulated alone or with the surfactant AOT. Degradation studies indicated that microspheres encapsulating lysozyme alone resulted in a microsphere core composition of PLGA and a shell composed of PLLA. In contrast, the polymer configuration for the microsphere core and shell were reversed due to AOT addition in the PLGA solution phase. The reversal of polymer orientation was evident in both the microsphere release kinetics as well as the bioactivity assay of lysozyme released from both microsphere samples. Lysozyme encapsulated with AOT caused the majority of encapsulated elements to be released from DW microspheres within the first 40 days of microsphere incubation *in vitro*. Alternatively, lysozyme encapsulated alone resulted in the majority of encapsulated protein release occurring between day 40 and day 100. The overall improvement in drug delivery through DW microspheres is promising. Because of the potential for scale-up with this simple manufacturing technique, the DW microparticles presented herein represent a method of encapsulation with great utility in an array of delivery applications.

3.5 FUTURE DIRECTIONS

Though DW microspheres encapsulating protein with AOT resulted in an improvement in protein release kinetics such that the initial burst release of protein was avoided, the DW

microsphere formulations described herein do not yet meet our requirements of delivery bioactive protein for the entire duration of long term studies for long gap peripheral nerve repair. Therefore, additional studies with alternative protein stabilizers such as trehalose or antacids such as magnesium hydroxide are currently under investigation. Trehalose has been shown to thermostabilize proteins such as BSA or other globular proteins composed mainly of α-helices such as lysozyme [222, 223]. By stabilizing the intermolecular O-H interactions responsible for the stability of the protein tertiary structure, Trehalose may prove fruitful as a method of improving encapsulated protein bioactivity following the initial freeze-drying procedure required for protein mixing with PLGA [223]).

Magnesium Hydroxide ($Mg(OH)_2$) has been used by several groups as a method of increasing the pH within the microsphere microenvironment during PLGA degradation and accumulation of acidic end groups [224]. Within PLGA microspheres, the acidic microenvironment has been shown to fall to as low as pH = 2 [225]. Previous work performed with lysozyme has shown that the bioactivity is decreased at such a low pH, and certainly less stabile proteins such as neurotrophic factors would be denatured at such a low pH. Therefore, $Mg(OH)_2$ will be investigated as a coencapsulate for improved bioactivity of lysozyme upon release form microspheres. The effect of antacid encapsulation will be investigated for protein release kinetics, microsphere degradation, and the long term bioactivity of released lysozyme.

4.0 INCORPORATION OF DOUBLE-WALLED MICROSPHERES INTO POLYMER NERVE GUIDES

4.1 INTRODUCTION

Though there has been a considerable amount of research in improving peripheral nerve guide design, commercially available nerve guides have not equaled the regenerative capacity of the nerve autograft in long gap peripheral nerve repair. While autografts (*e.g.* the sural nerve) have been used to bridge nerve defects of 6 cm or more [13], polymer based nerve guides are effectively used to regenerate nerves in gaps that span only 3 cm or less [8]. This barrier in gap length may reflect the unmet necessity for nerve guides to actively promote nerve regeneration through the lumen of the guide from the proximal to the distal nerve stump [151]. Therefore, in addition to providing mechanical support for regenerating nerves, nerve guides must also provide cues that guide axonal growth and, as a consequence, increase the rate at which nerves regenerate.

4.1.1.1 Substrate delivery from polymer nerve guides

The complex problem of targeting axonal outgrowth has led to the investigation of a variety of nerve guide materials, luminal fillers, cell therapies and combinations thereof [133]. One additional pathway toward enhancing axonal growth involves locally delivering drugs or

neurotrophic factors that promote nerve growth and survival. Growth factors have been delivered from nerve guides through several methods detailed in Table 12 (for review of these techniques, see [151] and [226]). Results from these preclinical studies have shown many beneficial effects of delivered growth factors for nerve regeneration. For example, the delivery of nerve growth factor (NGF) promotes sensory neuron survival, outgrowth and branching [102], ciliary neurotrophic factor (CNTF) aids in motor neuron survival and outgrowth [227] and glial cell line-derived neurotrophic (GDNF) has been shown to promote the regeneration of fibers originating from the spinal cord beyond what has been measured with NGF [228]. Because of the numerous promising reports following treatment of nerve injuries with neurotrophic factors, the delivery of such factors may be a potential method of surpassing the current length limitations in nerve regeneration.

Table 12. Methods of delivering growth factors within nerve guides.

Method of Protein Delivery from Nerve Guides	*Reference(s)*
Growth factor adsorbed to the nerve guide scaffold	[229]
Growth factors combined with the scaffold material during fabrication	[72]
Growth factor encapsulated in additional delivery system (rods or microspheres) that is incorporated into the nerve guide	[97, 99, 102, 228, 230-232]
Growth factor covalently immobilized onto the nerve guide surface	[101, 125, 233]
Co-implantation of an osmotic pump releasing growth factor	[234, 235]

4.1.2 Limitations of previous art

While strategies have been developed for protein delivery from polymer nerve guides, many conduit delivery systems lack a sustained and controlled release rate of bioactive proteins for the entire duration required for the axon to cross from the proximal to the distal nerve stump [72]. For example, Dodla and Bellamkonda implanted polysulfone nerve guides across a 20 mm defect with lipid microtubules capable of delivery NGF for only 18 days and saw no improvement in axonal elongation after 4 months [99]. Furthermore, because typical microspheres have low drug loading, Rosner et al., noted that a significant limitation for microsphere loading in the center lumen of guides was adequate space. For a target drug release of 1 ng/mL, the authors stated that for a nerve guide 1 mm in diameter, the construct's capacity prevented microsphere loading and transfected cells were used instead [97]. Therefore, several groups have constructed nerve guides with microspheres embedded in the nerve guide wall and have shown that growth factors can be delivered from nerve guides in this manner for almost 30 days [72, 100, 231].

4.1.3 Chapter Aims

In this chapter, double-walled microspheres comprised of poly(L-lactide) / poly(lactic-co-glycolic acid) were reproducibly incorporated into porous poly(caprolactone) nerve guides in a manufacturer controlled distribution. To confirm the distribution of microspheres within the nerve guide, fluorescently labeled bovine serum albumin (BSA) was encapsulated and visualized through fluorescent microscopy. Because particulate leaching is required to create the porous nerve guide walls, the minimum period required for sodium chloride removal was determined.

In vitro release studies were performed to determine the effect of the nerve guide macrostructure on release of a model protein, lysozyme.

4.2 METHODS

4.2.1 Reagents

All chemicals were analytical grade or purer and were purchased from commercial suppliers. Poly(vinyl alcohol) (average Mw 9,000-10,000, 80% hydrolyzed), poly(DL-lactide-co-glycolide) (lactide:glycolide (50:50), mol wt 40,000-75,000 units), Fluorescein isothiocyanate Conjugated Bovine Albumin (A9771) (FITC-BSA), lysozyme from chicken egg white, Dichloromethane, Ethyl Acetate, and Phosphate Buffered Saline (PBS) were all purchased from Sigma-Aldrich (St. Louis, MO). Poly-L-lactide (0.90 – 1.20 dL/g) was purchased from DURECT Corporation (Pelham, AL). The Micro Bicinchoninic Acid (BCA) Protein Assay Kit (23235) was purchased from Pierce (Rockford, IL).

4.2.2 Fabrication of poly(caprolactone) disks and nerve guides

4.2.2.1 PCL Disks

PCL disks were prepared to determine the effect of nerve guide macrostructure on lysozyme release from double walled microspheres. Briefly, 15 mg of double walled microspheres (detailed fabrication description in Section 3.2.3) were added to a circular well

(diameter = 1 cm, depth = 0.5 cm) of a custom made silicone mold (Figure 41A). Porous disks were created by dissolving 1.35 g PCL in 15 mL ethyl acetate. To the dissolved polymer solution, sodium chloride impregnation was accomplished by adding NaCl in a 80% (v/v) amount. 200 μl of the polymer slurry was added to each mold and mixed well to distribute the microspheres within the disk space. The ethyl acetate was allowed to evaporate and the sodium chloride was leached with distilled water.

4.2.2.2 Nerve Guides

PCL nerve guides were fabricated using a modification of previously reported methods (Section 2.2.2 and [236]). Glass capillary mandrels 1.5 mm in diameter were coated with a 17% w/v% aqueous solution of poly(vinyl alcohol) (PVA), air dried and then immersed into the polymer slurry (as described above) creating NaCl/PCL mandrel coatings. The ethyl acetate was allowed to evaporate for a minimum of ten minutes between successive mandrel immersions into the polymer slurry. After the completion of the dip-coating process, the resulting polymer conduits were submerged in distilled water for 5 hours to allow for salt and PVA dissolution, and the guides were removed from the glass mandrels. The final wall thickness after 6 successive immersions of the mandrels into the polymer solutions was 600 - 700 μms.

To incorporate double-walled microspheres into the inner half of the nerve guide wall (Figure 41B), 15 mg of double walled microspheres encapsulating either FITC-BSA (for visualization) or lysozyme (for protein release kinetics) were evenly spread onto a drawn grid on parchment paper (Figure 41C). After the first immersion of the glass mandrel into the PCL slurry, the ethyl acetate was allowed to evaporate for only 30 seconds leaving a semi-hardened polymer layer on the mandrel. The mandrel with semi-hardened polymer was then smoothly rolled across the microspheres on parchment paper. The PCL with embedded microspheres was

allowed to dry for ten minutes and then repeatedly coated with additional layers of polymer as done in nerve guides without microspheres.

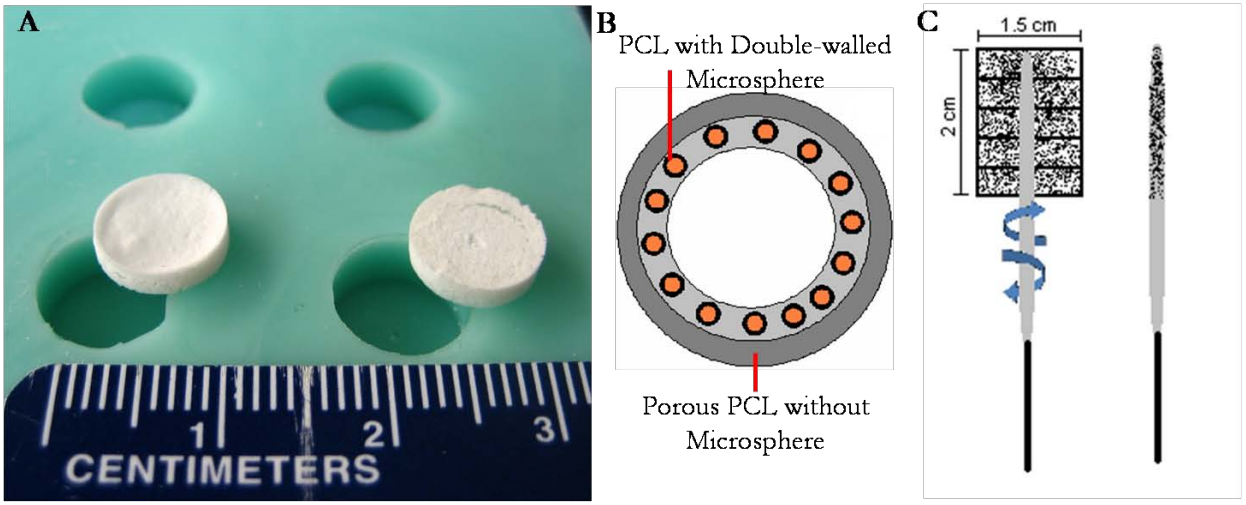

Figure 41. (A) Photograph of PCL disks following fabrication in custom made silicone mold. (B) Schematic of polymer orientation in double-walled microsphere. (C) Schematic of fabrication technique for incorporating double-walled microspheres into PCL nerve guide.

4.2.3 Evaluation of sodium chloride leaching from nerve guide walls

To determine the minimum amount of time required to leach the sodium chloride from the nerve guide walls, nerve guides were fabricated as described above (n = 5). After ethyl acetate evaporation overnight, each mandrel with the attached polymer guide was weighed. The mandrels were then immersed in distilled water in one hour increments. The dry weight of each

guide was recorded between successive salt leaching periods. Previous work has indicated that in an 80% porous nerve guide, very few closed pores exist from which remaining salt crystals could not dissolve [22].

4.2.4 *In vitro* release of lysozyme from PCL disks and nerve guides

To determine the effect of the nerve guide material on lysozyme release from double-walled microspheres, protein release kinetics were compared between a known weight of microspheres embedded in PCL disks to an equal weight of free microspheres in solution. To accomplish this, 15 mg of microspheres were first immersed in water for a period identical to that used to remove the salt particulates from the PCL disks. The microspheres were then collected and incubated in 1 mL PBS at 37°C. Following incubation, the microspheres were centrifuged for 10 minutes at 1000 rpm and the supernatant was removed. Five PCL disks prepared as described above were individually placed into wells of a 48 well plate. To each disk, 0.6 mL of PBS solution was added and the well plate was incubated for equal time periods as microsphere samples. To collect the releasate, the disks were removed using sterile forceps and transferred into clean wells where the PBS was refreshed.

To measure the release of lysozyme from double-walled microspheres in PCL nerve guides, nerve guides were fabricated as described in Section 2.4.2. After the guides were immersed in distilled water for 10 hours, the guides were cut to 2 cm lengths and added to a clean eppendorf tube. To each tube, 0.6 cm of PBS was added and the guides were incubated at 37°C for specified time increments. To collect the releasate, the guides were removed from each eppendorf tube using clean forceps and added to new tubes in which the PBS was refreshed.

For measuring the lysozyme content of the releasate, a micro BCA protein analysis assay was performed. Lysozyme standard or sample solution (1 mL) and 1 mL of the Micro BCA working reagent were combined in a test tube and mixed well. All of the standard lysozyme samples as well as the release samples were incubated simultaneously in a water bath for 1 hour at 60°C. After this period, the protein solutions were cooled to room temperature and 200 µL from each sample were transferred to a 48 well plate and measured with a plate reader at 562 nm (Tecan Spectrafluor, NC).

4.2.4.1 Statistical Methods

A minimum repetition value of five was used when measuring lysozyme release from PCL disks and nerve guides. Results are expressed as the mean ± standard deviation. Analysis of variance (ANOVA) was used to determine statistical significance between experimental groups. The least significant difference method was used for multiple comparisons with $p < 0.05$.

4.3 RESULTS

4.3.1 Minimization of salt leaching period

Leaching of sodium chloride from the nerve guide walls also results in a loss of protein from the microspheres. Therefore, it is desirable to minimize the immersion of nerve guides in water. Following fabrication of PCL nerve guides impregnated sodium chloride, the PCL guides were immersed in distilled water for one hour increments. Figure 42 indicates that the majority (97%)

of NaCl was removed from the nerve guide wall after one hour of immersion in water. Beyond 5 hours, no amount of measurable NaCl was further removed. To validate the final PCL nerve guide weight, the guides were weighed after 60 hours of immersion in water and the final weight was unchanged.

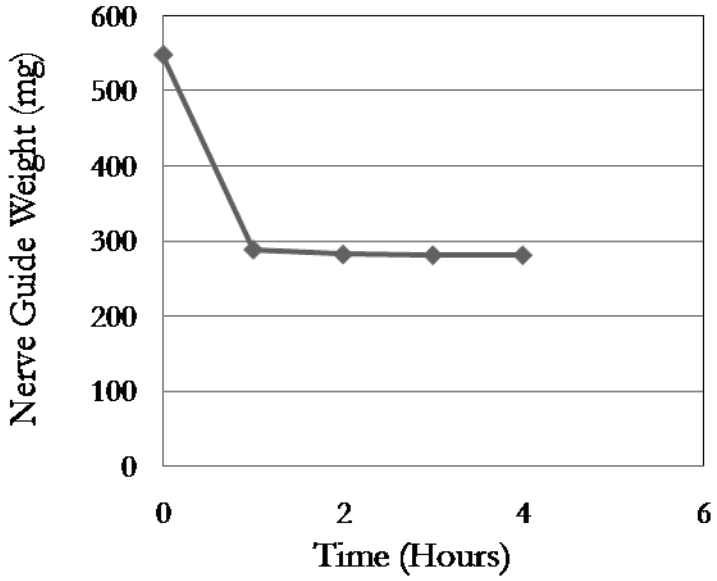

Figure 42. Weight of nerve guides following NaCl impregnation and removal by leaching in distilled water for specified time points. (Mean ± std dev, N=5).

4.3.2 Incorporation of double-walled microspheres into PCL nerve guides

A novel rolling technique was used to embed double-walled microspheres into PCL nerve guides for sustained protein release. Fluorescently labeled BSA was encapsulated in the double-walled

microsphere to visualize microsphere distribution within the nerve guide wall. Fluorescent microscopy images were then taken of the microspheres and overlaid with light microscopy images of the polymer nerve guide. As seen in Figure 43A, by smoothly rolling the nerve guide mandrel across the microspheres and performing several consecutive immersions of the mandrel into the polymer solution, a nerve guide was created with microspheres distributed evenly along the luminal wall of the nerve guide. Because PLA is not soluble in ethyl acetate, the rounded morphology of the microspheres was maintained following nerve guide fabrication (Figure 43B).

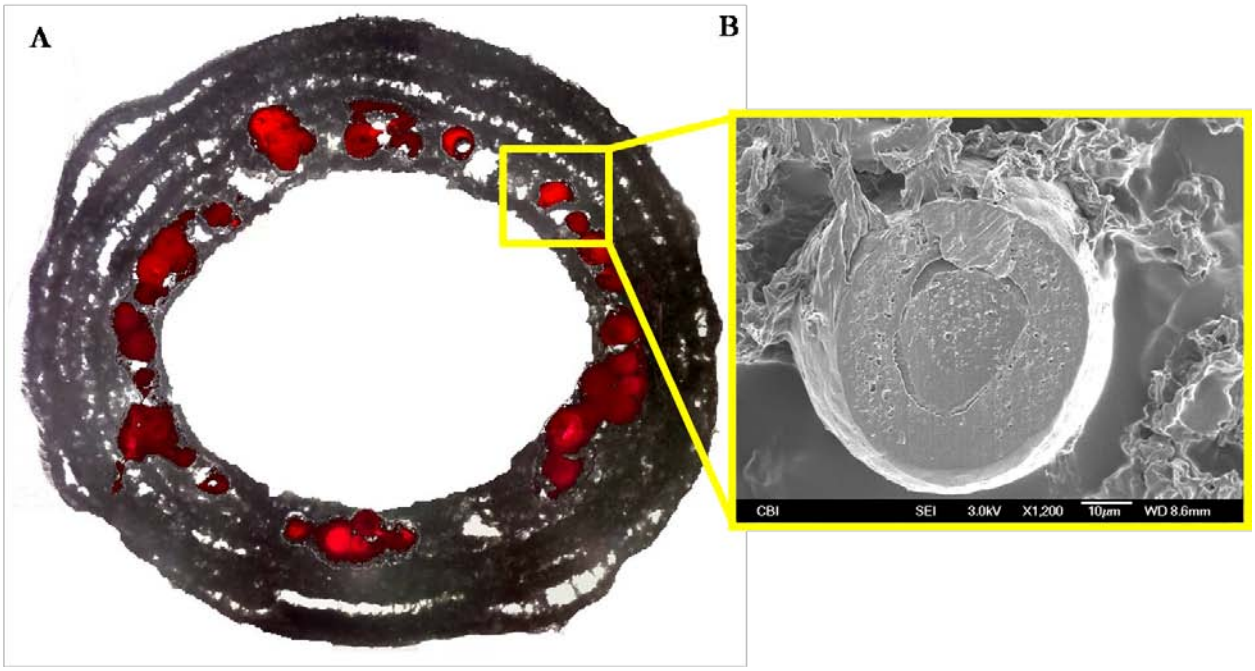

Figure 43. (A) Compilation of brightfield and fluorescent micrographs taken at 10X. Multiple images of both the nerve guide and FITC-BSA encapsulated in double-walled microspheres were used to overlay fluorescent images on brightfield prior to realignment of figures. (B) Scanning electron micrograph of double-walled microsphere following incorporation into PCL nerve guides.

4.3.3 Lysozyme release from double-walled microspheres embedded in PCL

A known weight of double-walled microspheres was incorporated into PCL disks to measure the effects of nerve guide macrostructure on protein release. Lysozyme was released from microspheres in a significantly higher concentration than from microspheres embedded in PCL ($p < 0.05$, $n=5$). The cumulative amount of protein released at day 35 was not significantly different between free floating microspheres and microspheres in disks ($p > 0.05$) (Figure 44A).

To analyze the long-term release of protein from PCL nerve guides, 15 mg of double-walled microspheres identical to those used in the disks were embedded into the walls of 5 individually prepared nerve guides. The lysozyme release pattern from nerve guides was similar to that from microspheres alone (Figure 44B). There was a gradual, sustained release of lysozyme until day 36 when ~45% of the total lysozyme was released. After this period, there was an increase in release rate and by day 49, 90% of lysozyme was released. No detectable amount of lysozyme was measured beyond day 56.

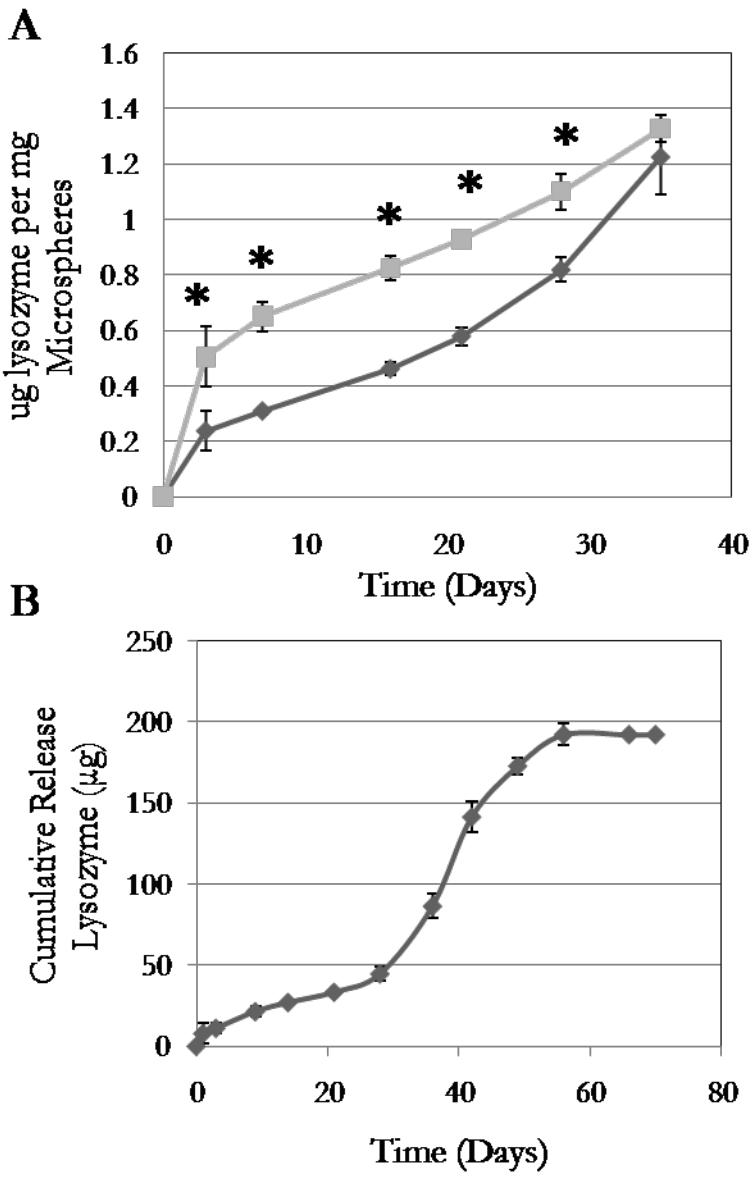

Figure 44. (A) Cumulative release of lysozyme from PCL disks ( ) and microspheres suspended in buffer solution ( ) (mean ± std dev, N=5). Asterisks indicate statistical differences between microspheres that were suspended in solution and those embedded in disks ($p < 0.05$). (B) Cumulative release of lysozyme from nerve guides with double-walled microspheres (mean ± std dev, n = 5).

4.4 DISCUSSION

Typical microsphere release kinetics include an initial burst release of protein within the first 24 hours of placement in aqueous solution either *in vitro* or *in vivo*. To increase the time over which protein is released, PLGA microspheres were coated with an additional layer of polymer (e.g. PLLA), creating a double-walled microsphere. With this technique, the encapsulated growth factor is protected in the core of the two-layered core-shell microsphere structure. Furthermore, by localizing a growth factor to the core of the double-walled microsphere, the amount of material through which the protein must diffuse through is increased thus slowing the protein release rate. In addition, double-walled microspheres with a core of PLGA and a PLLA shell is an effective method of incorporating the microspheres into PCL nerve guide walls. PLLA is not soluble in ethyl acetate, the solvent used to create the PCL / NaCl slurry for nerve guide fabrication and therefore protects the microspheres from dissolution during nerve guide fabrication.

In the present study, we have demonstrated that microspheres can be reproducibly incorporated into PCL nerve guides in a distribution that was easily tailored to manufacturer specifications. While the nerve guide with FITC-BSA microspheres in Figure 43A depicts microspheres embedded along the luminal edge of the guide, it would also be possible to create a homogeneous distribution of microspheres in the nerve guide wall. Furthermore, microspheres encapsulating multiple growth factors could be used such that the inside layer of microspheres releases neurotrophic factors while the external microspheres release vascular endothelial growth factor (VEGF) for promotion of revascularization of the injured nerve. Additionally, because the microspheres are organized by distribution on parchment paper, it would also be possible to

create gradient distributions of microspheres along the longitudinal axis to mimic the release of growth factors from Schwann cells within the distal nerve stump.

Because the initial release of protein from double walled microspheres at day 1 is typically less than 25% of the total encapsulated material, the required leaching period of 5 hours appears adequate for our nerve guide delivery system. Additionally, lysozyme release studies from microspheres embedded in PCL disks suggest that the nerve guide material delays the initial release of protein into the aqueous environment, presumably because the protein is trapped within the porous architecture of the nerve guide wall.

4.4.1 Limitations

In the creation of our PCL nerve guides, it was initially hypothesized that this effect of nerve guide macrostructure on the initial protein release kinetics would be of benefit for our application, as the initial burst of protein from the microspheres (Figure 44A) would be delayed and closer to first-order. However, lysozyme release from DW microspheres within nerve guide walls was no longer detectable after 54 days while previous work has shown that microspheres suspended in PBS release protein for >80 days (Figure 34). It is possible that released protein adsorbs to the PCL surface upon release and is entrapped within the nerve guide wall. Initial exposure of the PCL guide surface to blood proteins following implantation *in vivo* would likely minimize protein adsorption upon release from microspheres.

4.5 CONCLUSIONS

The polymer orientation of double-walled microspheres protected the microsphere morphology during PCL nerve guide fabrication. The microsphere core was composed of PLGA while the shell was PLLA, a polymer that is insoluble in ethyl acetate which was used to create the PCL / NaCl slurry. Nerve guides embedded with microspheres encapsulated with FITC-BSA show a homogeneous distribution of microspheres along the inner luminal circumference of the guide and SEM analysis indicate that the mechanical integrity of the microspheres was maintained. The nerve guides created within this experiment indicate potential for examining the effect of a variety of growth factors within long gap peripheral nerve defects.

5.0 *IN VIVO* DELIVERY OF GLIAL CELL LINE-DERIVED NEUROTROPHIC FACTOR WITHIN A DEGRADABLE POLYMER NERVE CONDUITS FOR LONG GAP PERIPHERAL NERVE REPAIR IN THE RODENT ANIMAL MODEL

5.1 INTRODUCTION

Glial cell line-derived neurotrophic factor (GDNF) is related structurally to the transforming growth factor beta (TGF–β) superfamily and was first identified as a survival factor for dopaminergic neurons of the midbrain [156]. GDNF signals through a multicomponent receptor complex consisting of a glycosyl-phosphatidylinositol (GPI-) anchored coreceptor (GFRα1 through 4) as a ligand binding component and a receptor tyrosine kinase (RET) signaling component [237]. Following homodimeric binding of GDNF with GFRα1, the RET receptor further dimerizes and initiates several canonical signaling pathways including the Ras-MAPK (mitogen activated protein kinase), the phosphatidylinositol-3 kinase (PI3K)-Akt, the PLC-γ and the Src pathways [238].

In addition to the crucial role GDNF has within the development and function of the central nervous system, GDNF has further demonstrated efficacy in promoting the survival of motor and sensory neurons [239, 240]. Knock-out mice lacking GDNF die at birth with a 40% loss in viscerosensory neurons and a postnatal loss of myelinated mechanoceptors [240]. Furthermore, GDNF may have an important role in motor neuron target innervations, as an

overexpression has been shown to induce a hyperinnervation of neuromuscular junctions [241]. In addition to serving as a survival factor for neurons, GDNF also promotes proliferation, migration and differentiation of Schwann cells [242].

5.1.1 *In vivo* use of GDNF in animal models for peripheral nerve repair

The efficacy of GDNF toward improving peripheral nerve regeneration through nerve guidance conduits has been evaluated in preclinical studies (Table 13). In a 2007 study by Patel et al., chitosan scaffolds blended with laminin-1 and 5μg GDNF were implanted across a 10 mm gap in the Lewis rat sciatic nerve [123]. After 12 weeks, the chitosan / GDNF guides resulted in decreased gastrocnemius muscle atrophy and restoration of functional strength that was comparable to autograft controls. Behavioral testing indicated GDNF treatment groups regained sensation and improved gait kinematics. In addition, silicone conduits filled with GDNF gene modified Schwann cells have resulted in significantly improved nerve conduction velocity, number and density of regenerated nerves, and the thickness of the myelin sheath of regenerated nerves than that seen in controls across a 10 mm defect in the Wistar rat [155]. Finally, nerve guides with a GDNF releasing rod increased the number of myelinated axons and the overall number of regenerated axons was four-fold higher than nerve guides with NGF [103].

Table 13. Investigation of GDNF for peripheral nerve repair *in vivo*.

Animal Model	*Conclusion*	*Reference*
8 mm sciatic nerve gap in adult Sprague-Dawley rats	GDNF increased motor neuron survival and regenerated myelinated axons.	Chen et al., 2001 [117]
1 mm gap in Wistar rat facial nerve	GDNF promoted axonal branching from motor neurons.	Streppel et al., 2002 [118]
8 mm gap in Wistar rat facial nerve	GDNF promoted axonal maturation.	Barras et al., 2002 [119]
15 mm gap in Wistar rat sciatic nerve	GDNF increased the number of myelinated axons and the overall number of regenerated axons was four-fold higher than with NGF.	Fine et al., 2002 [103]
Transection and coaptation in Sprague-Dawley rat sciatic nerve	GDNF increased the rate of sensory recovery than with NGF and aFGF.	Jubran et al., 2003 [121]
10 mm gap in Wistar rat sciatic nerve	GDNF improved nerve conduction velocity, the number and density of reinnervated axons, the area of regenerated nerve and the thickness of myelin sheath of the regenerated nerves.	Ping et al., 2003 [122]
10 mm gap in Lewis rat sciatic nerve	GDNF resulted in decreased gastrocnemius muscle atrophy and restoration of functional strength that was comparable to autograft controls. GDNF treatment groups regained sensation and improved gait kinematics.	Patel et al., 2007 [123]
3 mm gap in sciatic nerve of adult male Wistar rats	GDNF resulted in improved nerve fiber diameter.	Piquilloud et al., 2007 [124]
13 mm gap in Lewis rat sciatic nerve	GDNF-containing fibrin resulted larger nerve fiber diameters compared to NGF-containing guides.	Wood et al., 2009 [125]

5.1.2 Rationale of using the 1.5 cm rat sciatic nerve model for evaluating nerve regeneration

Transection of the sciatic nerve in the rat is the most often employed animal model for peripheral nerve regeneration studies [243]. Therefore, it is advantageous for the investigation presented within this dissertation to use the rat sciatic nerve gap model so that a fair comparison can be made between the regenerative capabilities of our guide to those documented for animal models. In addition, strain differences in the rodent model have been carefully considered and the Lewis rat was selected as a model specifically because of the length of available sciatic nerve tissue available for removal in the Lewis rat. A 2007 study by Rupp et al., showed that the distance from the most proximal visible point of the sciatic nerve to the point at which the sciatic nerve divides into the tibial and peroneal nerves is longer on average in the Lewis rat compared to Sprague-Dawley, Fischer 344, Wistar-Han, Lewis or Nude rats [243]. Therefore, the sciatic nerve can be transected as a single epineuria which simplifies the path for the regenerating nerve fibers within the guidance conduit.

Though many authors initially state the limitations in currently employed nerve guides (guides are only useful for bridging short defects), there is a conflict that arises in the animal models used to test the efficacy of nerve guides under investigation. The criteria often used to determine success in terms of axon regeneration and functional recovery of the muscle are tested in rat sciatic nerve gaps of 1 cm or less. However, it is well known that the probability of observing regeneration depends strongly on the gap length and regeneration can occur in an unfilled nonporous silicone tube in a defect model of this size. Therefore, it is difficult to extrapolate the impact of involved factors being tested when regeneration is also present without such altered combinations of porosity, delivery of growth factors, incorporation of Schwann cells

or extracellular matrix. As such, a 1.5 cm defect was used in the described *in vivo* studies because regeneration is not observed in empty defects.

5.1.3 GDNF in human clinical trials

Currently, four clinical trials have been performed utilizing GDNF for the treatment of Parkinson's disease [244] or Progressive Supranuclear Palsy [245]. Within these studies, GDNF was continuously infused via catheter either intracerebrally or intraputaminally. Side effects of GDNF therapy included nausea, loss of appetite, cutaneous sensory disturbances and psychiatric symptoms [246]. Post study evaluation of the delivery method utilized in the clinical trials performed in rhesus monkeys determined that GDNF delivery by a point source (catheter) led to an uneven distribution of the administered growth factor, with tissue levels of GDNF dropping exponentially from distances beyond the single opening in the catheter [244]. Therefore, the development of an improved GDNF delivery system would have utility in not only our nerve guide application discussed here, but also within the broader field of growth factor delivery for treatment of a variety of neurodegenerative diseases.

5.1.4 Chapter aims

It is hypothesized that a sustained delivery of GDNF applied directly to the site of injury will result in an improved regeneration of lost nerve tissue. This hypothesis is based on the following observations. First, nerve injury results in rapid up-regulation of GDNF by Schwann cells in distal segments of lesioned sciatic nerve [156]. Second, GDNF has been shown to prevent avulsion-induced motorneuron death following complete nerve transection whereas nerve growth

factor (NGF), brain-derived neurotrophic factor (BDNF), and insulin-like growth factor (IGF) all failed to enhance cell survival or cell size [126]. Third, GDNF treatment with guidance channels following spinal cord injury resulted in a reduction of reactive astrocytosis and macrophage accumulation [120]. Finally, histological comparison of nerve guides implanted with and without added GDNF showed that nerve guides releasing GDNF increased nerve fiber number, fiber diameter, and additionally myelin thickness was improved, an indication of improved nerve regeneration [103, 119].

To evaluate this hypothesis, poly(caprolactone) (PCL) nerve guides were fabricated as described within Section 4.2.2.2 with double walled microspheres encapsulating GDNF described in Section 3.3.7.1. To approximate the dosage of GDNF released from the PCL nerve guides, *in vitro* release studies were performed using the complete nerve guide/microsphere system. Nerve guides delivering GDNF were then implanted into a 1.5 critical size nerve defect in the adult rat sciatic nerve.

To assess the initial efficacy of the nerve guide design, a short-term, 6 week pilot study was performed to ensure that bioactive GDNF was delivered to the site of nerve ligation. Subsequently, a long-term, 16 week assessment of nerve regeneration across a similar long gap defect with GDNF therapy was performed. Nerve repair was evaluated through functional assessment of toe-spread, joint angle range of motion, gastrocnemius contraction force and gastrocnemius wet weight. Histological evaluation of nerve repair included assessment of Schwann cell and neurofilament location with immunohistochemistry, evaluation of tissue integration and organization throughout the lumen of the regenerated nerve with Masson's trichrome stain, and quantification of axon fiber density and g-ratio.

5.2 METHODS

5.2.1 Reagents

In addition to those reagents previously listed, Gel Mount (G0918), Xylene, monoclonal anti-S100, and monoclonal anti-neurofilament were all purchased from Sigma-Aldrich (St. Louis, MO). The Masson's trichrome kit was purchased from American MasterTech (Modesto, CA).

5.2.2 *In vitro* release of GDNF from Nerve guides with Double walled microspheres

Twenty PCL nerve guides with double-walled microspheres encapsulating GDNF were prepared as described in Section 4.2.2.2. Following fabrication, the PCL polymer was allowed to dry completely and NaCl leaching was performed by immersing the guides in sterile DI water for 5 hours. Nerve guides were then removed from glass mandrels used during initial preparation and cut to 1.7 cm lengths. From this group of nerve guides, 4 were randomly selected for measuring *in vitro* GDNF release kinetics. The remaining 16 were implanted into the experimental group of animals as described in Section 5.2.3.

Long term release studies were performed to approximate the amount of GDNF released during the duration of the *in vivo* studies. To accomplish this, nerve guides were individually added to clean eppendorf tubes. To each tube, 0.6 mL of PBS was added and the guides were incubated at 37°C for specified time increments. To collect the releasate, the guides were removed from each eppendorf tube using clean forceps and added to clean tubes with fresh PBS.

The amount of soluble GDNF from the collected samples was analyzed using an enzyme linked immunosorbent assay (ELISA) manufacturer's instructions as described in Section

3.2.4.3. The optical density was recorded at 450 nm in an ELISA plate reader (Tecan, NC). The GDNF concentrations were calculated against a 6-point standard curve, then adjusted to picograms of GDNF per milligram of microspheres.

5.2.3 Surgical technique

Following the guidelines of the University of Pittsburgh Institutional of Animal Care and Use Committee, 54 male Lewis rats (250-300 g, Harlan Labs) were used to evaluate the efficacy of GDNF released from PCL nerve guides for improved nerve regeneration. To implant the guide, each rat was anesthetized with an intraperitoneal injection of sodium pentobarbital (50 mg/kg). The sciatic nerve was then exposed with a muscle splitting incision of the gluteal muscle. The nerve was sharply transected ~0.5 cm from the proximal bifurcation and 0.5 cm of tissue was excised. After the proximal and distal nerve stumps were allowed to retract, the exposed fascicles were trimmed and sutured with 10-0 prolene epineurial mattress stitch 1 mm into each end (Figure 45A) of a 1.7 cm nerve guide, creating a 1.5 cm defect (Figure 45B). The gluteal muscle and skin were then closed with 4-0 vicryl suture.

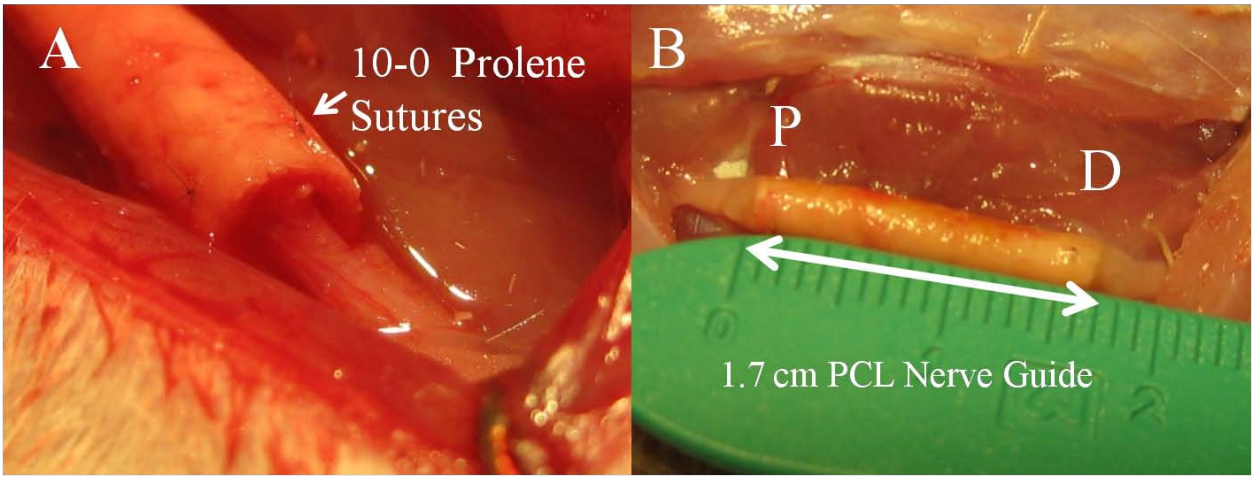

Figure 45. (A) Photograph of distal sciatic nerve stump sutured 1mm into PCL conduit using a mattress stitch. Prolene sutures are indicated with white arrow. (B) Photograph of PCL guide at time of implantation. Ruler indicates nerve guide is 1.7 cm in length. Nerve stumps were inserted 1 mm into each end of nerve guide.

For *in vivo* studies, two time points were used; a 6 week time point for evaluation of guide design and a longer 16 week study to evaluate the effects of GDNF release on nerve regeneration. For the initial 6 week pilot study, animals were randomly divided evenly amongst two groups, one of which received conduits with microspheres encapsulating GDNF (n = 3) and the other group received identical conduits with empty microspheres as a negative control (n = 3). Animals used for the subsequent 16 week study were divided amongst three groups, animals receiving an isograft (n = 16), animals receiving nerve guides with empty microspheres (n = 16), and animals receiving PCL guides with encapsulated GDNF (n = 16).

5.2.4 Functional assessment of nerve regeneration

Functional reinnervation of the lower limb muscles was assessed through four methods: Sciatic functional index, video gait kinematics, gastrocnemius muscle contraction force, and gastrocnemius wet weight. Sensory reinnervation was evaluated with a timed response to hot water.

5.2.4.1 Sciatic Functional Index

Beginning at week 6, rats were in an enclosed walkway (30 x 100 x 15 cm) ending in a darkened cage/box weekly as seen in Figure 46A [247]. Baseline measurements were recorded at week 0, prior to surgery. The rats were initially allowed two or three conditioning trials to become acclimated to the track. White paper was cut to the appropriate dimensions and placed on the bottom of the track. The rat's hind feet were painted with nontoxic paint (Figure 46B), and the animal was allowed to walk down the track, leaving its hind footprints on the paper. The following measurements were taken from the footprints (as shown in Figure 46C and D, from [247]) to determine the sciatic functional index (SFI):

a) distance from the heel to the third toe, the print length (PL);

b) distance from the first to the fifth toe, the toe spread (TS);

c) distance from the second to the fourth toe, the intermediary toe spread (ITS).

All three measurements are taken from the experimental (E) and normal (N) sides [248]. Several prints of each foot will be obtained on each track, and the data will then be entered into the SFI equation 3:

$$SFI = -38.3\frac{(EPL-NPL)}{NPL} + 109.5\frac{(ETS-NTS)}{NTS} + 13.3\frac{(EIT-NIT)}{NIT} - 8.8 \quad (3)$$

An SFI of 0 is normal, while an SFI of -100 indicates total impairment [249]. Total impairment may result from a complete transection of the sciatic nerve. The walking track analysis provides a direct relationship between individual hind limb muscle function and print measurements [250].

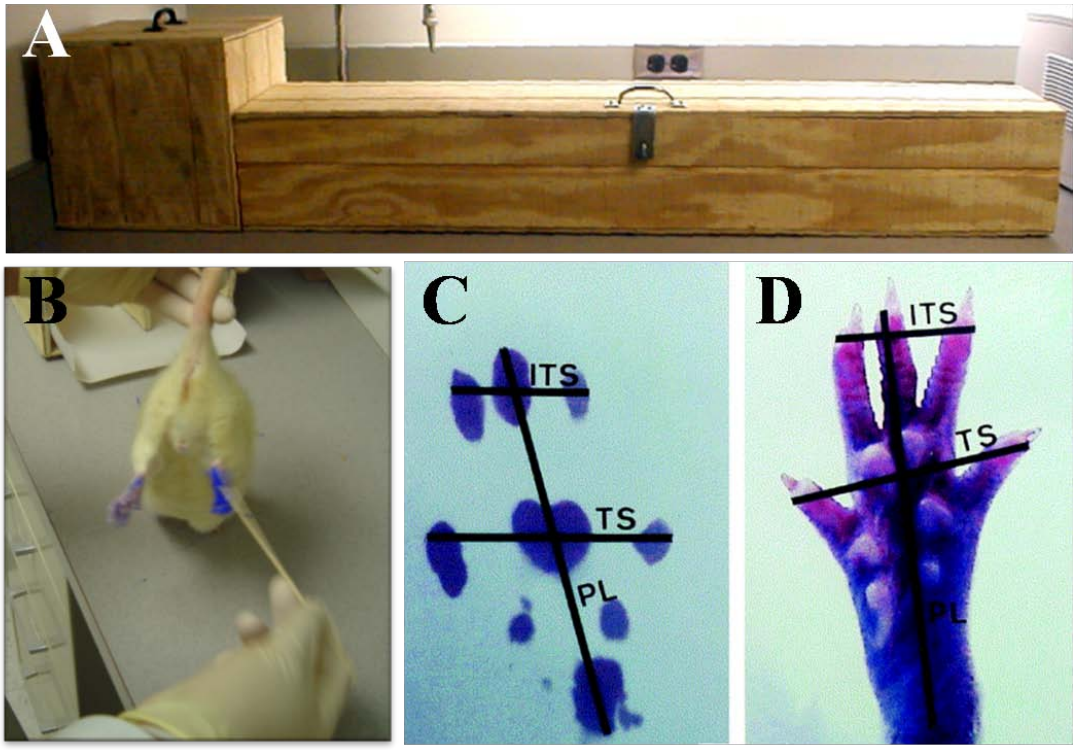

Figure 46. (A) Photo of walking track used for SFI evaluation. (B) Photo of method used for painting animals' back feet. (C and D) Photo of animal print and hind foot with SFI variables indicated (from [247]).

5.2.4.2 Video Gait kinematics

A high-speed (100 full frames per second) digital video camera (Fujinon, HF12.5HA-1B) was used to record motion of the hindlimb during walking along a 10 cm wide runway (Figure 47A). Black ink marks of contrast (3 mm diameter) or reflective markers (Figure 47B) were positioned over the iliac crest, greater trochanter, knee, ankle, and fifth metatarsal-phalangelal joints. During each test, the rat was positioned at one end and encouraged to walk the length of the 60 cm runway. This procedure is repeated until 15 – 20 steps were recorded with the rat walking straight forward (Figure 47C). Figure 48 shows an image taken from the high-speed video of a rat walking on the runway. A custom Matlab program (gratefully provided by Dr. Douglas Weber and Dennis Bourbeau) was used to automatically track the location of each mark of contrast in all frames of the video. The marker locations were then used to construct line segments connecting each pair of adjacent markers. Intersegmental joint angles for the hip, knee, and ankle joints were calculated using equation 4.

$$\theta = a\cos\frac{A \cdot B}{|A||B|} \tag{4}$$

In this equation, the vectors A and B denote the line segments proximal and distal to the joint. The intersegmental angle (θ) was computed as the inverse cosine of the dot product of vectors A and B, normalized by their respective lengths. The joint angular position and velocity trajectories were computed from the measured marker positions. The range of motion during both flexion and extension were measured for each joint during each step cycle. These measures were then used for comparing gait kinematics across time points and treatment groups.

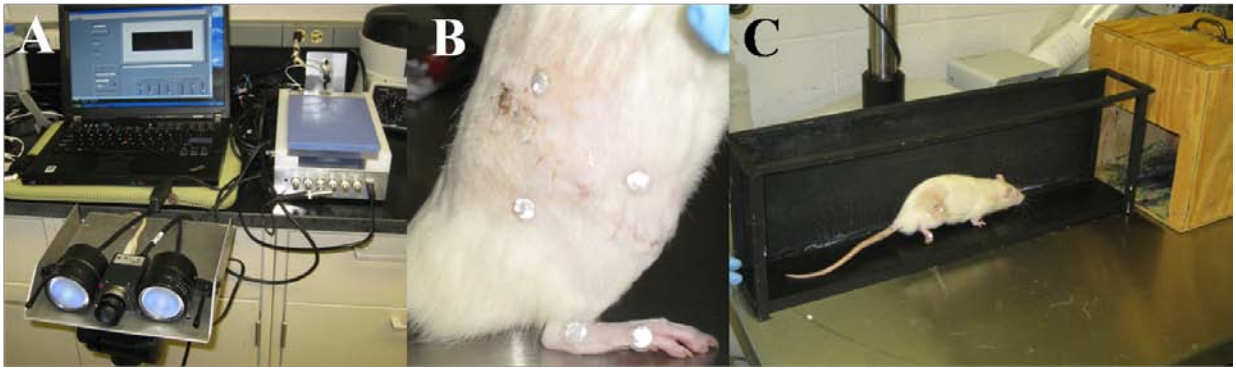

Figure 47. (A) Photo of high speed camera with equipment for data acquisition used for recording videos of animal gait. (B) Photo of anatomical placement of reflective markers for calculating joint angles during gait. (C) Photo of rat traversing walkway while being video recorded for gait analysis.

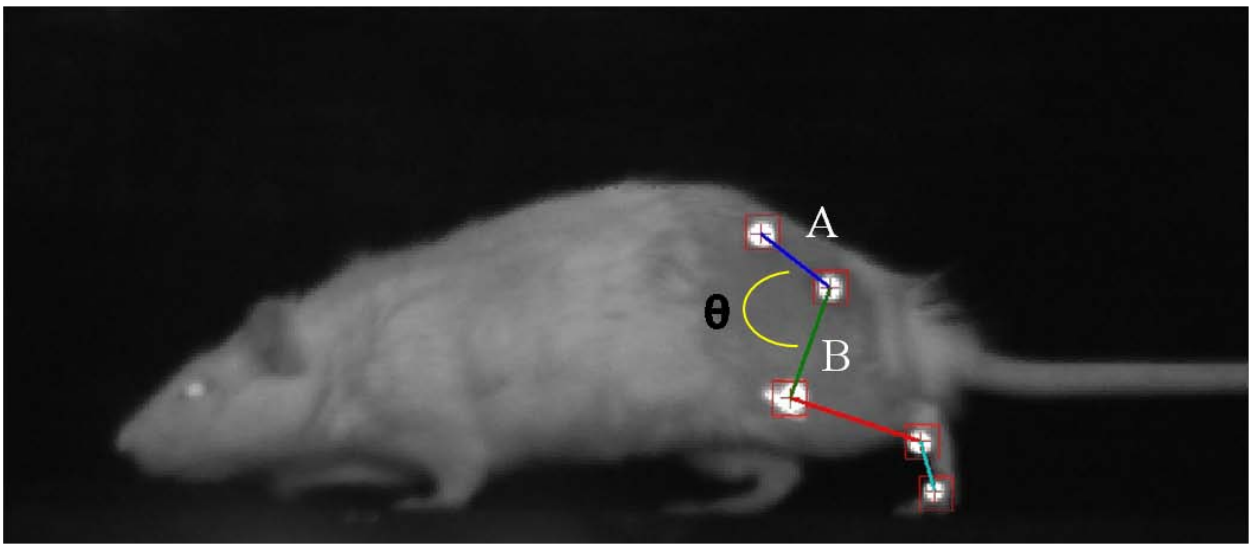

Figure 48. Image of rat captured during plantarflexion immediately prior to initiatin the swing phase. Line segments connect each of the 5 reflective markers. Representative vectors indicated with A and B are used to calculate the intersegmental joint angle θ.

5.2.4.3 Timed response to sensory stimuli

Sensory recovery following nerve regeneration was assessed throughout the duration of the 16 week animal study. At weekly intervals, animals were observed for indications of sensory innervations using a preliminary behavioral test. Animals were placed atop a raised metal grid and observed as they moved freely across the bars. The non-injured foot from experimental animals was able to grip each bar and the corresponding leg was able to support weight. However, an injured foot without sensory innervations could not sense the presence of the bar. The behavior of each animal atop the grid was evaluated using three points of criteria: the foot was successfully placed on the bar, the foot responded to and gripped the metal bar, forward progress over the grid was made following successful placement of an injured foot on the bar. If any of the following criteria were met, the sensory innervation was subsequently quantified using a hot water test.

To compare the degree of sensory reinnervation within experimental groups, a hot water test was performed. A glass dish with water at 60°C was prepared. Each animal was blindfolded using a cotton towel and first the experimental and then the control foot was placed into the water bath. The response time required by each animal to retract the foot from the bath was recorded and the difference in response time between injured and control legs was calculated.

5.2.4.4 Gastrocnemius contraction force

Immediately prior to sacrifice, animals were anesthetized with sodium pentobarbital and the injured sciatic nerve was exposed with a muscle splitting incision made following the scar line remaining from graft or guide implantation. After freeing the isograft or regenerated nerve from the superficial and underlying muscle tissues, a 1.5 mm diameter nerve cuff (Microprobe, Inc. Gaithersburg, MD. Cat # NC(1.5)24) was placed around the nerve. Because the implanted

nerve conduit enclosed the regenerated nerve, the PCL material had to be carefully removed such that sufficient nerve material was available for contact with the nerve cuff. The lower gastrocnemius was then completely isolated from the anterior and posterior tibialis muscles and the Achilles tendon was cut and fastened to a force transducer using a transfixation stitch and 4-0 silk sutures. Finally, to completely stabilize the femur position, the animal's foot, knee and back were immobilized on the data acquisition board using 16-0 gauge needles (Figure 49A). Prior to obtaining the muscle contraction force, the tension of the suture used to connect the gastrocnemius muscle to the force transducer was optimized for obtaining the maximum force possible.

The sciatic nerve was then stimulated (World Precision Instruments. Sarasota, FL. Model A320R) with a nerve cuff containing 4 points of contact and the generated muscle force was recorded from the data acquisition board (National Instruments, Model USB6009) using a custom Matlab program by Dennis Bourbeau and Dr. Douglas Weber (Figure 49B). The difference in force between baseline and stimulated measurements for 5 consecutive recordings was then calculated and optimized for the strongest stimulation points of contact between the nerve cuff and the sciatic nerve.

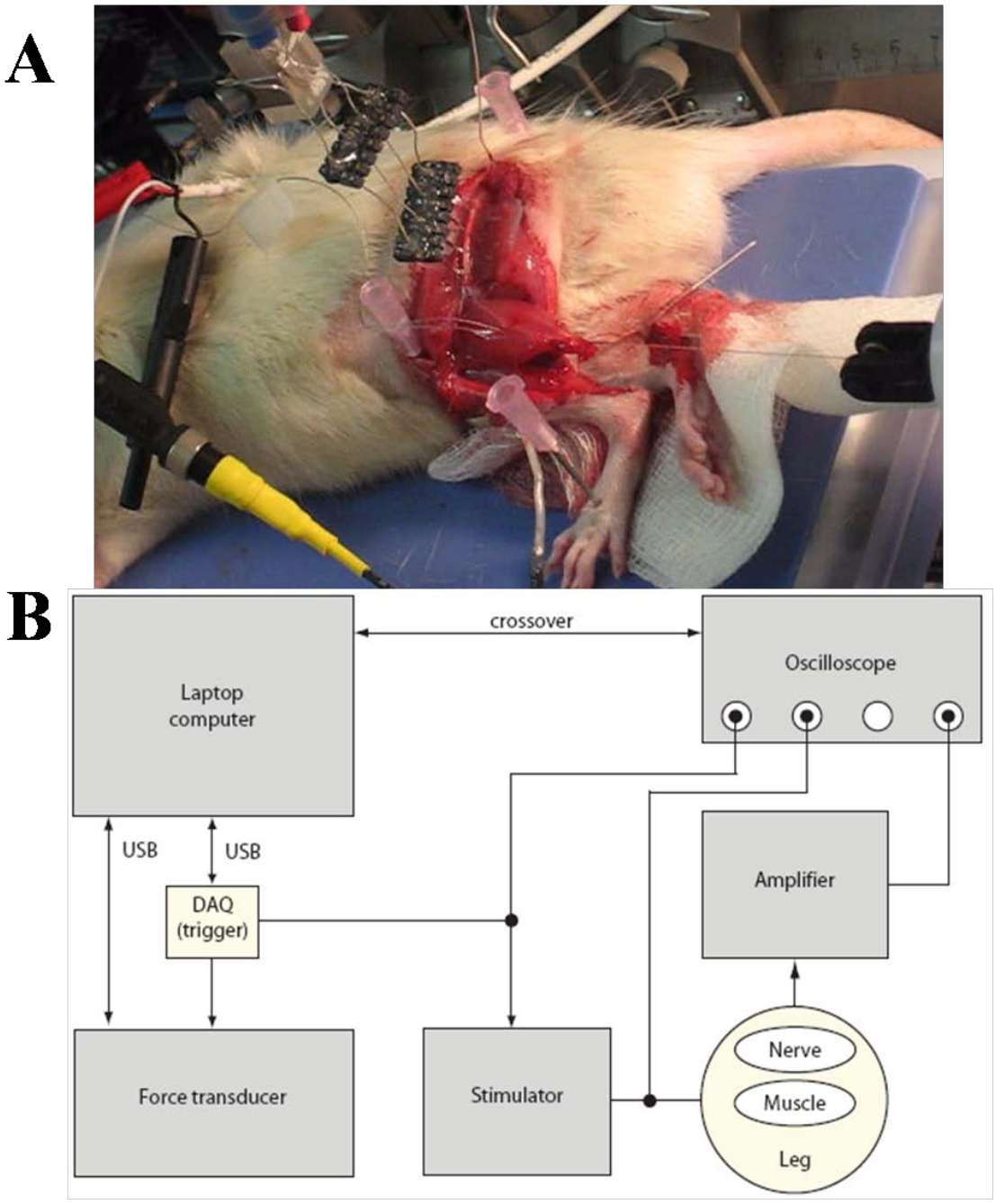

Figure 49. (A) Photo of rat prepared on data acquisition board for muscle contraction force recordings. (B) Schematic of equipment organization for stimulating the sciatic nerve and obtaining muscle contraction force recordings.

5.2.4.5 Gastrocnemius muscle weight

At the predetermined sacrifice date for each group of animals (6 weeks or 16 weeks), the animals were euthanized with an overdose of sodium pentobarbital (100 mg/kg IP). A longitudinal incision in the lower leg, parallel to the extension of the Achilles tendon and gastrocnemius (gastroc) muscle, was made followed by a dissection of the skin which adequately exposed the gastroc muscle. The two proximal tendonous insertions of the gastroc in the femoral area were identification and sectioned. The distal gastroc insertion in the heel through the Achilles tendon was then severed for the extraction of the gastroc muscle. The wet muscle mass of the unoperated contralateral control was compared to the muscle mass of the gastroc from the injured leg.

5.2.5 Histological assessment of nerve regeneration

At specified study time points, animals were sacrificed with an overdose of sodium pentobarbital and the implanted guides were harvested and immediately immersed in a fixative. Nerves prepared for paraffin embedding for Masson's trichrome stain (MTC) and immunohistochemistry (IHC) were fixed in 4% paraformaldyhyde. Samples prepared for histomorphometry analysis were fixed in 2.5% gluteraldehyde. After the tissue samples were immersed in fixative for at least 24 hours, the samples were washed with PBS and post-fixed in 1% osmium tetroxide for either 2 hours in sample preparation for MTC and IHC analysis or 48 hours for those samples prepared for histomorphometry. Nerve specimens were then dehydrated with increasing concentrations of ethanol (30% to 100%) and sectioned with a sharp razor blade at the proximal nerve stump (PS), the proximal (PG), middle (MG) and distal (DG) regions of the nerve conduit, and at the distal nerve stump (DS) (Figure 50A). The sections were then

embedded in paraffin or epoxy in descending order (Figure 50B) and sectioned at thicknesses of 3 μm (IHC, MTC) or 0.5 μm (histomorphometry).

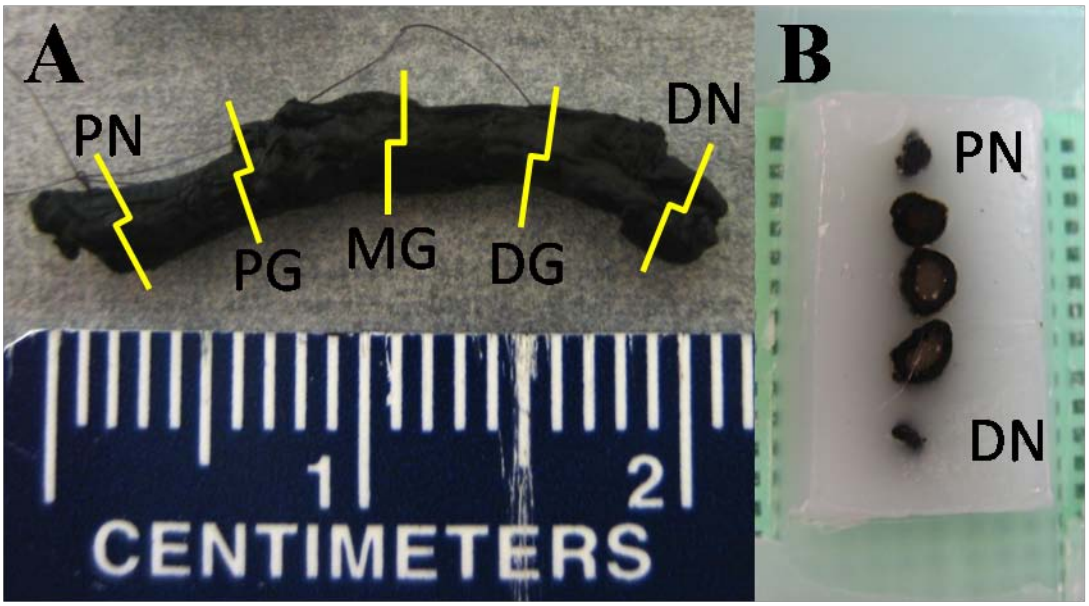

Figure 50. (A) Photograph of explanted nerve and conduit at 6 weeks. Guide has been fixed and treated with osmium tetroxide. Dashed likes indicate the proximal nerve stump (PS), the proximal (PG), middle (MG) and distal (DG) regions of the nerve conduit, and at the distal nerve stump (DS) where transverse cuts were made for histology. (B) Photograph of sectioned nerve guide embedded in paraffin.

5.2.5.1 Masson's Trichrome

For analysis of cellular and tissue infiltration of the nerve conduits, nerve sections from the negative control and experimental animals were stained for Masson's Trichrome. Sectioned

nerves were first deparaffinized with Xylene and rehydrated with decreasing percent ethanol solutions (100% followed by 90% and then DI water). Solutions from a Masson's trichrome kit were then used according to the protocol published by Di Scipio et al. [251].

5.2.5.2 Immunohistochemistry

For fluorescent visualization of S-100 protein (Schwann cells), neurofilament proteins (axons), and ED1 (macrophages), IHC was performed on explanted nerve samples. Paraffin embedded specimens fixed in osmium tetroxide were first deparaffinized as described above and then etched with H_2O_2 for ten minutes as described in [251]. The samples were then blocked with 5% FBS with 0.02% triton-X in PBS for one hour at room temperature. Primary antibodies were then added overnight at 4°C (1:400, 1:200 and 1:200 respectively in 2.5% FBS and 0.02% triton-X in PBS). The samples were then washed three times with PBS and the secondary antibody was added for one hour at room temperature (1:1000 in 2.5% FBS and 0.02% triton-X in PBS). The samples were then washed thrice again and the nuclei were detected using DAPI (0.6 μg / mL). The slides were then mounted with a fluorescent mounting media.

5.2.5.3 Histomorphometry

Nerve sections were fixed using 2.5% gluteraldehyde, embedded in epon and cut to 0.5 μm cross-sections using an ultramicrotome (Reichert Ultracut). Sections were then mounted onto glass slides and stained with 1% toluidine blue dye for imaging. A Hitachi (model KP-M1AN) digitizing camera was mounted on a Zeiss Primo Star microscope for image acquisition. A 100X oil immersion objective lens was used to produce digital images at a final magnification of 1000X, with a pixel size of 0.125 μm as calibrated with a stage micrometer.

The Leco IA32 Image Analysis System (Leco, St. Joseph, MI) with custom calculation routines (macros) was used as developed by Hunter et al., [252]. 8-bit monochrome images were acquired and thresholded for determining myelin composition as detailed in Figure 51 from [252]. As described by Hunter et al., manual adjustments were made to photomicrographs displayed on an attached monitor such that debris and nonviable nerve fibers were removed (Figure 51D, from [252]). Viable axons were defined as dark myelin rings enclosing clear fiber areas devoid of debris or cell nuclei. Myelin width, axon width, and fiber diameter were then automatically calculated through software analysis of red and green bitplane identifiers. From these primary measurements, g-ratio (the ratio of the axonal diameter divided by the diameter of the axon and its myelin sheath) and nerve fiber density (fiber number/mm^2) were calculated.

5.2.6 Statistical Analysis

Results are expressed as the mean ± standard deviation. Analysis of variance (ANOVA) was used to determine statistical significance between experimental groups. The least significant difference method was used for multiple comparisons with $p < 0.05$.

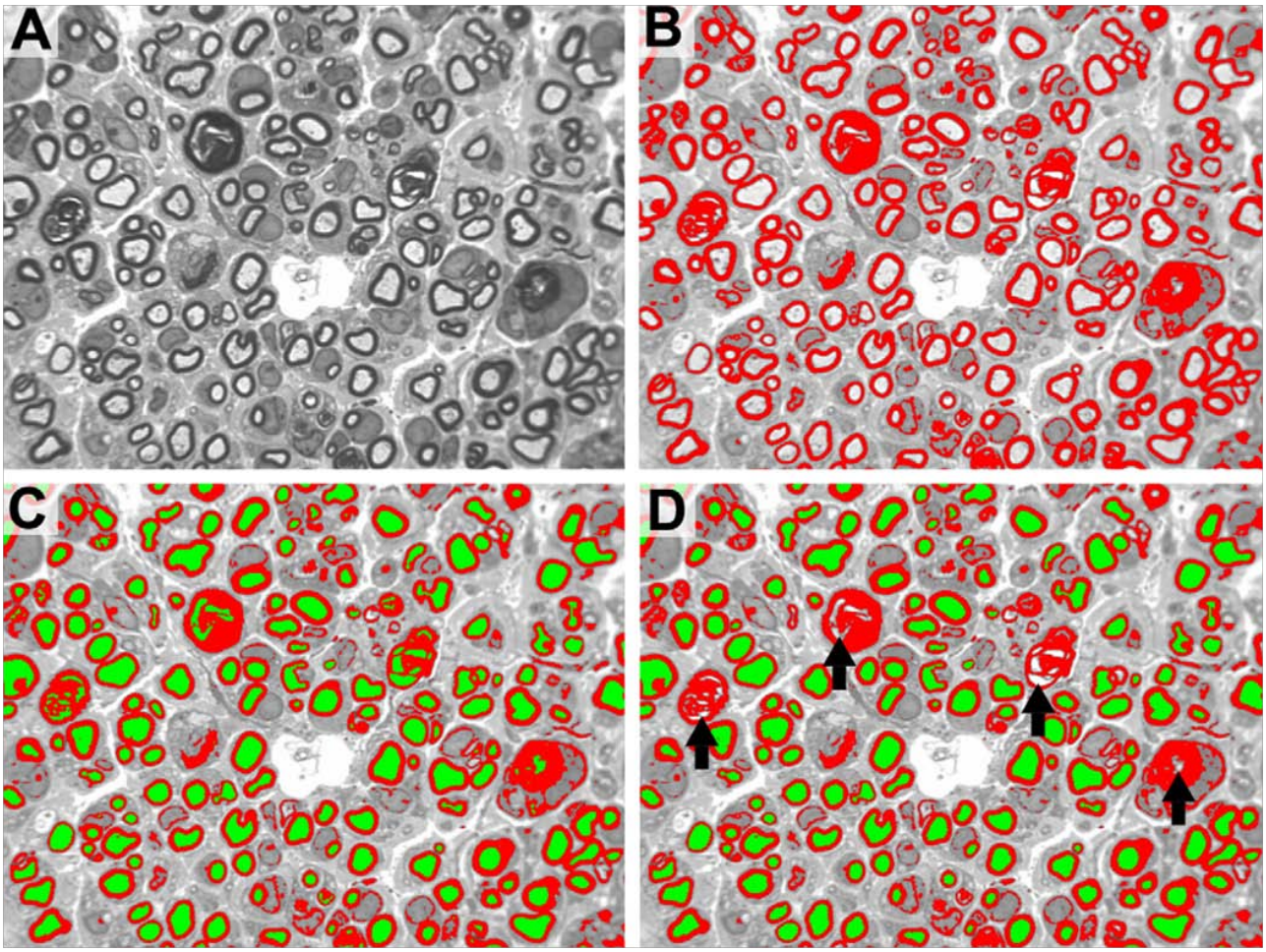

Figure 51. (A) Original high magnification micrograph of native nerve. (B) Micrograph with overlaying red myelin bitplane as manually adjusted during the initial thresholding step for myelin identification. (C) Micrograph with overlaying red and green bitplanes for axon identification. (D) Manual elimination of nonviable axons as indicated with black arrows. (Images are from [252])

5.3 RESULTS

5.3.1 *In vitro* release of GDNF from PCL Nerve guides

Long term release studies of GDNF form PCL nerve guides with double-walled microspheres were performed to approximate the release profile of the growth factor *in vivo*. Nerve guides embedded with double-walled microspheres encapsulating GDNF were incubated in PBS and released growth factor was quantified using an ELISA system. As shown in Figure 52, the release of GDNF from the PCL nerve guides did not exhibit the typical burst release profile seen in single walled microsphere studies. At day 3, only ~2.9% of the total released protein is liberated into solution. GDNF release is nearly linear until day 56, at which point ~89.0% of the total growth factor is released. After this point, GDNF release is consistent to day 112, when the 16 week *in vivo* studies were complete. Assuming that the majority of microspheres weighed for nerve guide preparation were successfully embedded and secured into the nerve guide walls, the encapsulation efficiency for GDNF nerve guide production was ~1%. Further, using double walled microsphere GDNF loading as determined in Section 3.3.7.1, only ~5% of the total expected GDNF was released from the PCL nerve guides at the completion of the *in vitro* measurements.

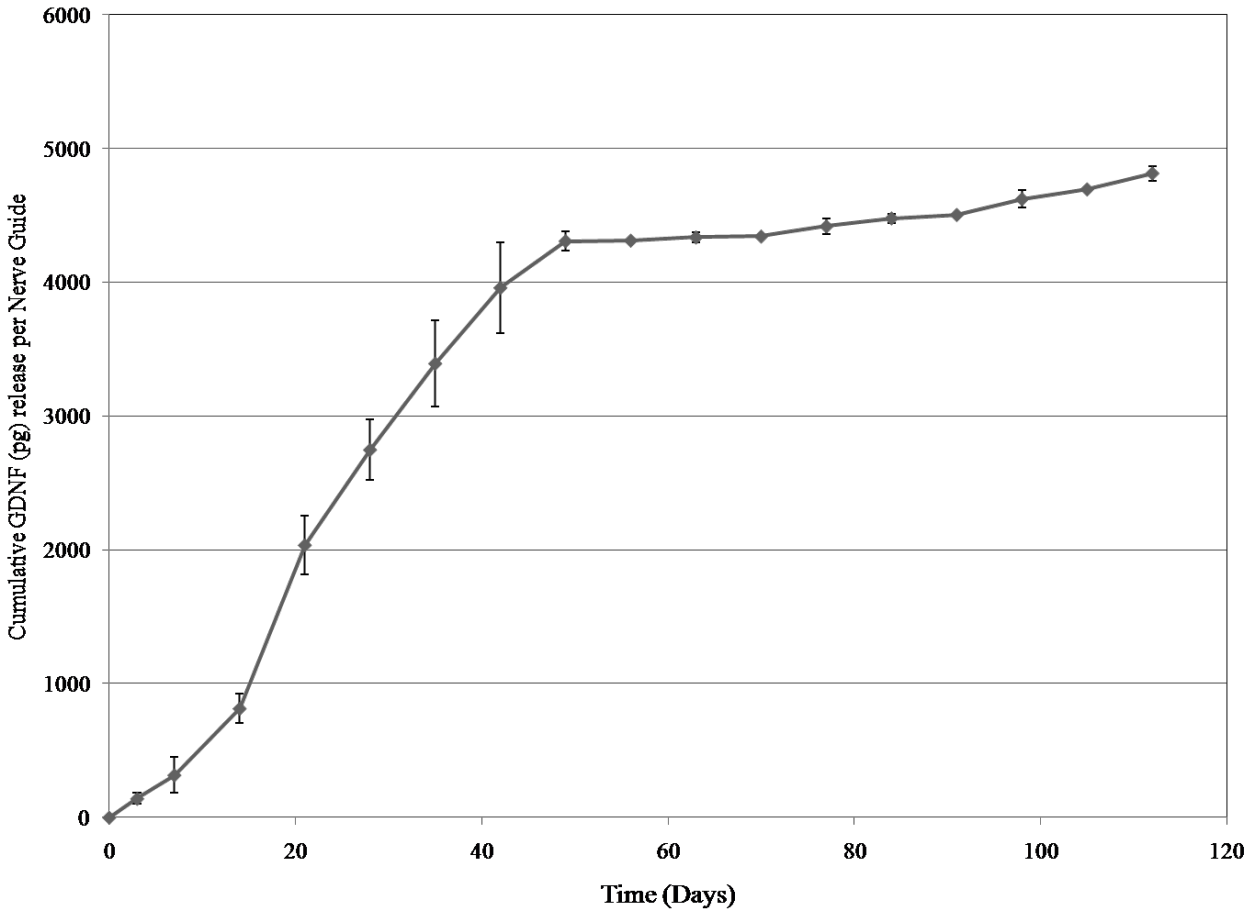

Figure 52. Cumulative release of GDNF (pg) from double walled microspheres embedded in PCL nerve guides (1.7 cm in length). Values expressed as mean ± std dev (n = 4).

5.3.2 Implantation of PCL nerve guides

Upon exposure of the injured sciatic nerve at sacrifice, remaining PCL conduits were soft and pliable and both sutures intact. Nerve guides were well vascularized with a soft fibrous coating (Figure 53A). The proximal and distal ends of the nerve guides were completely sealed

with a fibrous capsule and small neuromas are apparent at both guide ends. Prior to separating the nerve guide from the regenerated nerve, a pinch test was administered proximal to any anastamosis to determine if a muscle reflex could be observed. In 70% of the animals treated with an empty PCL conduit, a lower limb reflex was observed. However, often the regenerated nerve through the negative control conduits was delicate, and attempts to remove the conduit for placement of a nerve cuff resulted in disruption in nerve continuity. It was also noted that the regenerating nerve grew adjacent or into the porous walls of the PCL conduit.

Nerve guides implanted with GDNF releasing microspheres were also observed as well vascularized and sheathed in a soft fibrous coating. Results from a preliminary pinch test indicated that lower limb reinnervation was seen in 100% of the experimental animals. Furthermore, the nerves appeared to grow through the open lumen of the nerve guides and could be easily separated from the conduits for electrophysiology studies (Figure 53B).

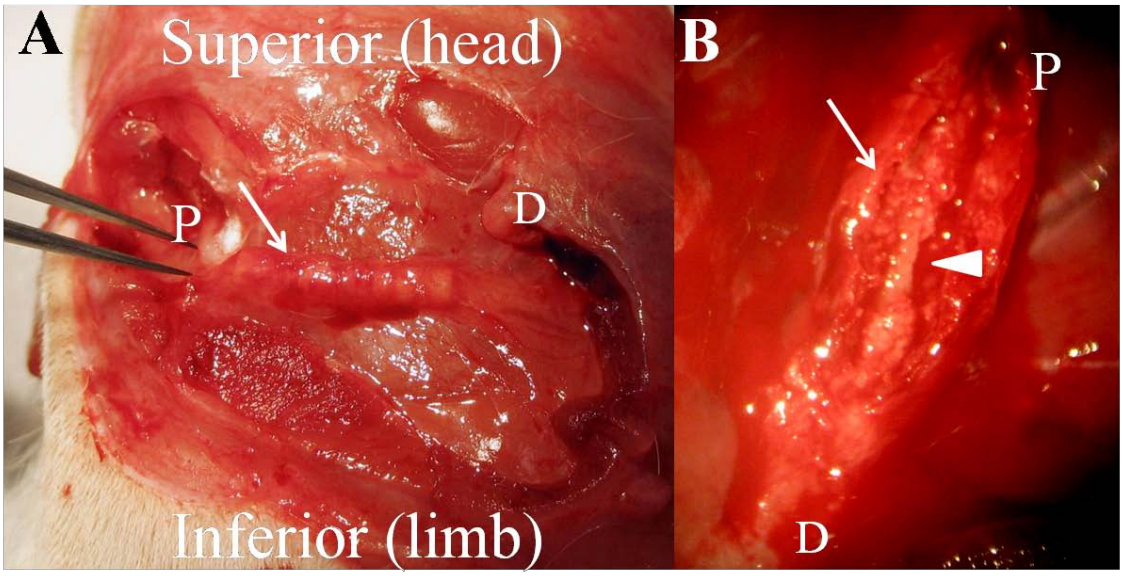

Figure 53. Photo of exposed empty PCL nerve guide 16 weeks after implantation (white arrow). The proximal and distal ends of the guide are indicated with the characters P and D. (B) Photo of GDNF releasing PCL nerve guide (white arrow) that has been longitudinally sectioned revealing regenerated nerve (white arrow head).

5.3.3 Functional analysis of nerve regeneration

5.3.3.1 Sciatic functional index

After 9 weeks post surgery, the sciatic functional index was recorded at weekly intervals (Figure 54). Previous work has shown that no improvement in gait should be expected before this time point (Appendix A). Considering that a SFI value of 0 is healthy and -100 is completely non-functional, animals from both the experimental treatment group (GDNF microspheres) and those with empty PCL guides (negative controls) showed impaired gait

patterns at week 9. The SFI value for animals of the GDNF group was -71.3 ± 15 (n = 16), which was not statistically considered different from the empty guides which had an SFI of -80.3 ± 7 (n = 3). There was no statistical difference in the measured SFI values throughout the duration of the study period. Additionally, there was no significant improvement in SFI value between timepoints for the duration of the study.

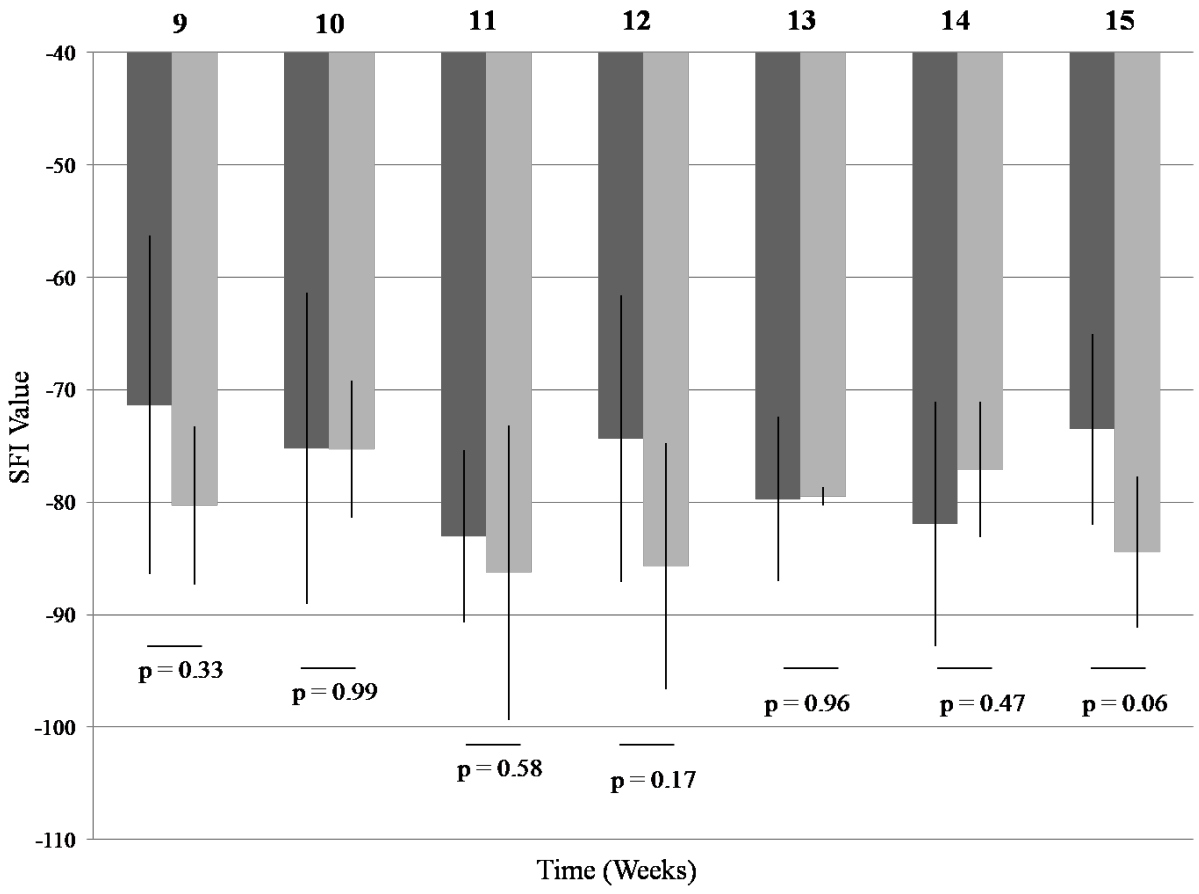

Figure 54. Calculated SFI values for animals receiving GDNF conduits (■), and empty control conduits (■). Values are expressed as mean ± std dev.

5.3.3.2 Gait kinematic Analysis

Gait kinematics from animals receiving a PCL nerve guide without growth factor (n = 3) and animals which received GDNF releasing guides (n=16) following sciatic nerve injury shows that motion of the hip joint is similar in the two animal groups within both the swing and stance phase of the gait cycle (Figure 55A and 55B). Hyperflexion of the hip is required to compensate for weakness in the distal part of the leg, which is impaired by the injury to the sciatic nerve (mid-femur). Thus, dramatic differences are evident at the knee (Figures 55C and 55D) and ankle (Figures 55E and 55F). Injured animals are unable to generate muscle force to extend the knee, reaching only ~90̊ of extension during stance (Figure 55C) compared to 130̊ in the healthy animal. Further evidence of muscle weakening is evident at the ankle. Normally, the ankle is flexed during the swing phase to lift the foot, but the ankle of an injured animal extends during swing (Figure 55E). This ankle extension is caused by gravity when the hip flexes to swing the leg forward. The range of motion (RoM) between experimental and negative control animals was not significantly different between groups at any time point.

5.3.3.3 Timed response top sensory stimuli

Rats were observed to have regained a small degree of sensory innervations beginning at week 14 using visual analysis of rat behavior while maneuvering a challenging metal grid. At week 15, animals were further assessed for sensory recovery using a hot water test. Animals receiving a GDNF guide had a mean response time to sensory stimuli of 0.93 ± 1.32 seconds (n = 16) while animals receiving control PCL guides were significantly slower in response time with an average recorded time of 3.64 ± 1.93 seconds ($p = 0.02$, n = 3) (Figure 56).

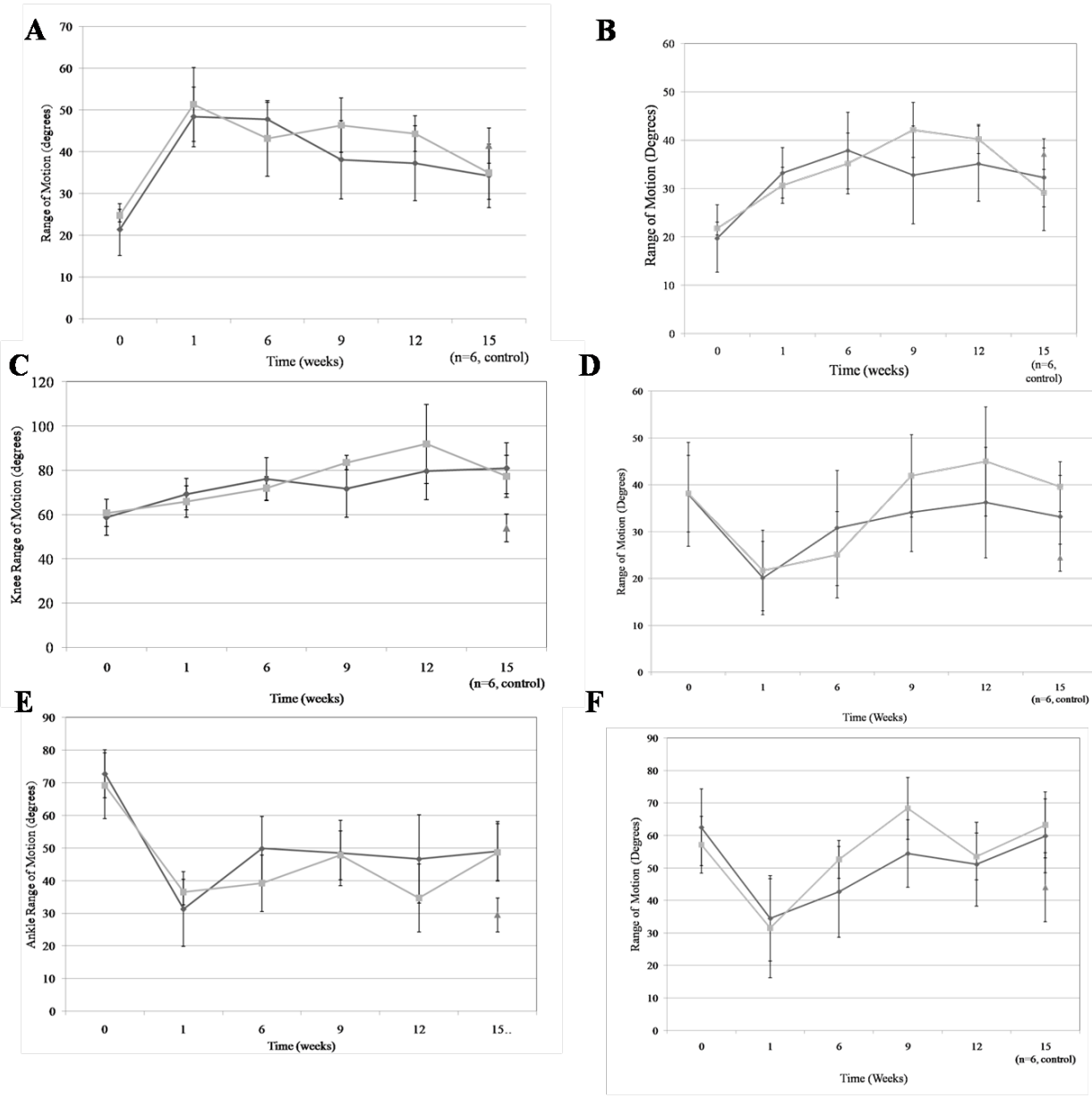

Figure 55. Hip range of motion (degrees) at baseline (week 0) and sequential timepoints following injury for swing phase (A) and stance phase (B) of the gait cycle. Knee range of motion during swing (C) and stance (D). Ankle range of motion (degrees) in swing (E) and stance (F). For all graphs, GDNF animals are represented with (♦), control PCL guides are (■) and isografts at week 15 are (▲).

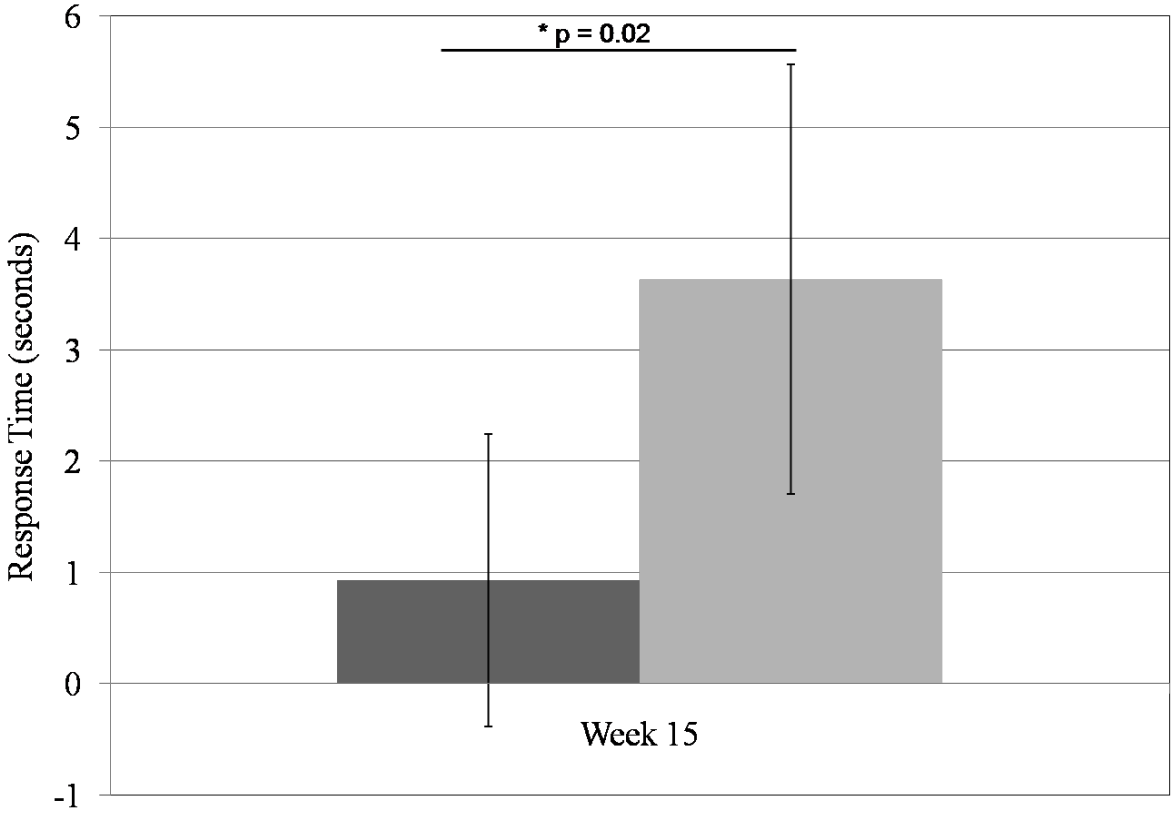

Figure 56. Mean response time required by animals receiving a GDNF rleasing conduit (■) and control PCL guides (■). Values are expressed as mean ± std dev with significant differences marked with an asterisk.

5.3.3.4 Gastrocnemius Contraction Force

The mean measured gastroc contraction force was 0.59 ± 0.28 N, 0.44 ± 0.22 N, and 0.07 ± 0.07 N for animals treated with an isograft (n = 11), a nerve conduit with GDNF (n = 6) and animals treated with a PCL conduit and no growth factors (n = 7), respectively. The average

contraction force between isograft animals and those within the experimental GDNF group was not significantly different (p = 0.1754) while both of these groups showed significantly improved contraction force above negative control animals (Figure 57).

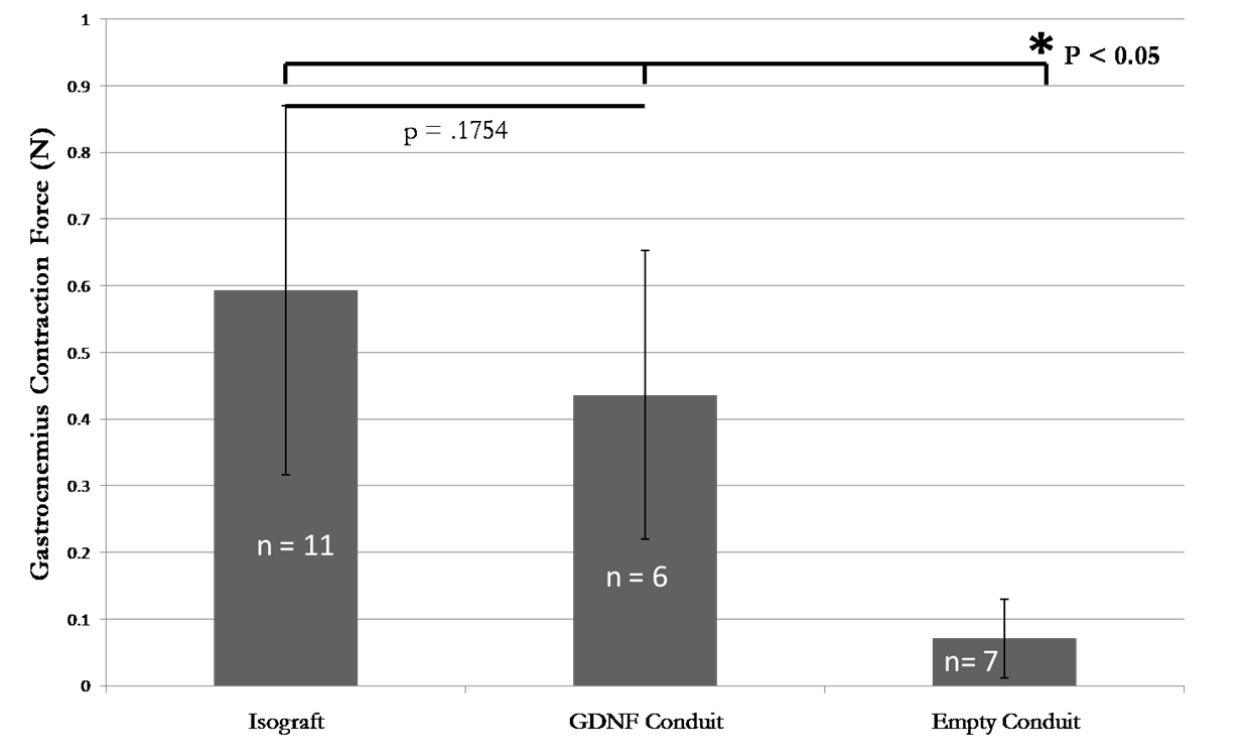

Figure 57. Average gastrocnemius contraction force (N) with error bars representing standard deviation.

5.3.3.5 Gastrocnemius muscle weight

The wet weight of recovered gastroc muscles from injured legs as normalized to contralateral uninjured controls are recorded in Table 14. The normalized values of muscles from animals treated with isografts as a positive control for nerve regeneration were statistically higher than both the experimental GDNF group as well as the PCL guides without growth factor delivery ($p < 0.01$).

Table 14. Recorded wet weights of injured gastrocnemius muscle as normalized to contralateral control. (Asterisk indicates statistical significance from experimental groups, $p < 0.01$)

Treatment Description	*Gastrocnemius wet weight (%)*
Isograft (positive control)	46.6 ± 12.4 *
GDNF Nerve Guides (experimental group)	24.8 ± 5.7
Empty PCL conduits (negative control)	21. 7 ± 4.4

5.3.4 Histological assessment of nerve regeneration

5.3.4.1 Masson's Trichrome

6 week pilot study

PCL nerve guides with double-walled microspheres were implanted across a 1.5 cm defect in the sciatic nerve to determine the initial effects of GDNF delivery on nerve regeneration. The presence of cellular infiltration, tissue formation and collagen content within the implanted conduits was visualized through Masson's trichrome stain. At low magnification (Figure 58A), transverse images of proximal segments of PCL conduits implanted without encapsulated GDNF showed a thin collagen capsule surrounding the nerve guide (arrow). Within the lumen of the guide, there is incomplete tissue integration and a lack of intercellular fibers. High magnification images (Figure 58B) reveal the presence of blood vessels (arrow head) and localization of cells near the inner surface of the nerve guide. There does not appear to be a measureable number of nerve fibers present and the majority of infiltrating cells, such as fibroblasts and macrophages, are organized around the nerve guide wall and surround the microspheres (MS). Neither the experimental nor control guide appear to illicit a strong inflammatory response.

Visualization of nerve guides implanted with double-walled microspheres releasing GDNF show a higher concentration of intercellular fibers and tissue formation at the proximal segment of the guide (Figure 58C). Though connective tissue does not appear to be organized, high magnification images of the center of the nerve guide reveal the presence of cells throughout the entire interior of the guide (Figure 58D). The presence of a blood vessel located near a microsphere in the nerve guide wall is indicated with a white arrow head.

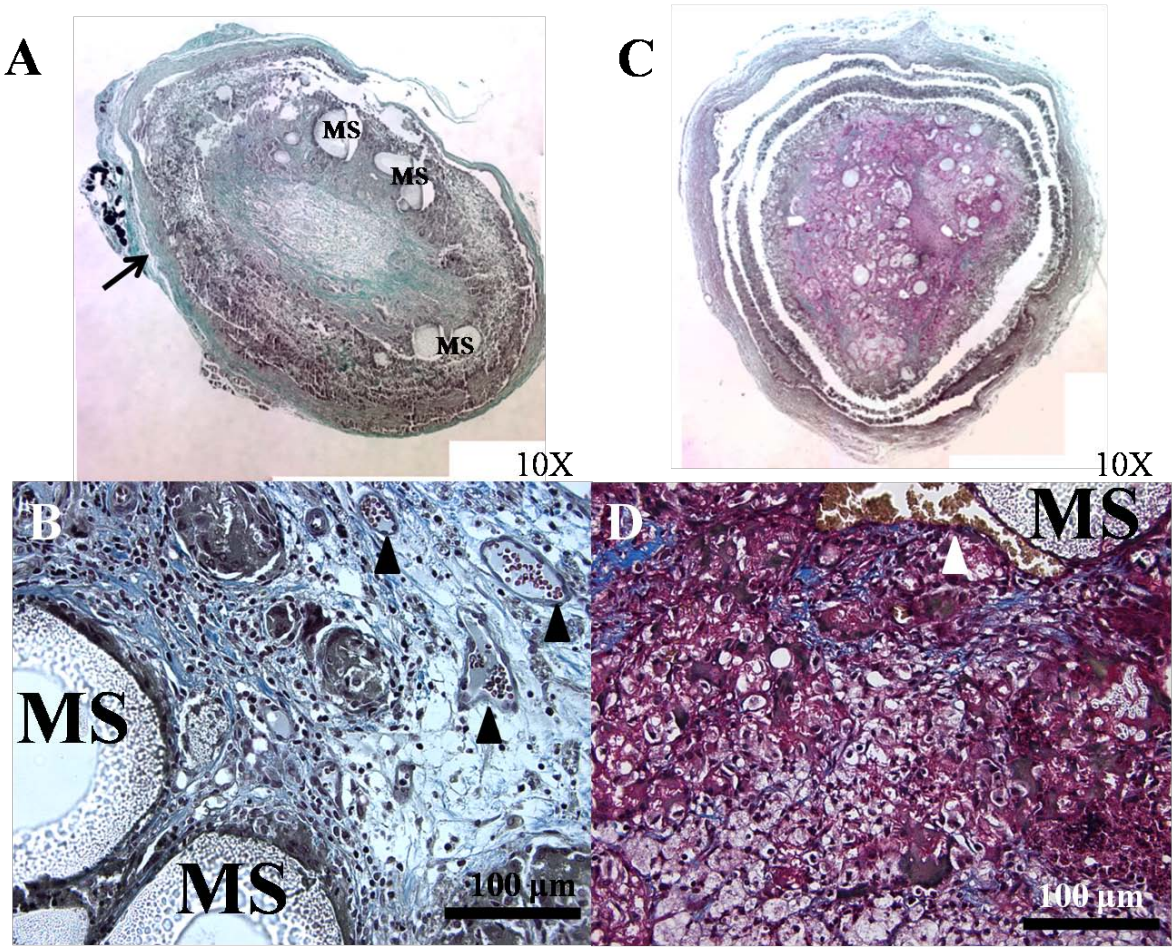

Figure 58. (A and C) Compilation of brighfield micrographs taken of a transverse section of the proximal segment guides visualized with Masson's trichrome stain. To create the final image, a series of 10X images were realigned and blended using photoshop CS3. (A) Negative control guides. Microspheres are labeled as "MS." The collagen capsule surrounding the implanted guide is labeled with an arrow. (C) Guides releasing GDNF. (B and D) High magnification brightfield micrographs taken of the lumen of explanted nerve guides from negative controls (B) and guides releasing GDNF (D). Blood vessels are labeled with an arrow head. Scale bars are 100µm.

In the distal region of the implanted nerve guides, the empty conduit shows very little tissue formation in the lumen of the guide (Figure 59A) in comparison to guides releasing GDNF (Figure 59B). Analysis of high magnification light micrograph images confirm that in negative control guides, there is an absence of intercellular fibers and cells in the lumen of the guide (Figure 59C). In GDNF conduits (Figure 59D), tissue infiltration is not as developed as was seen in the same proximal nerve segment, however there was an increase in collagen content and intercellular fibers above the negative controls.

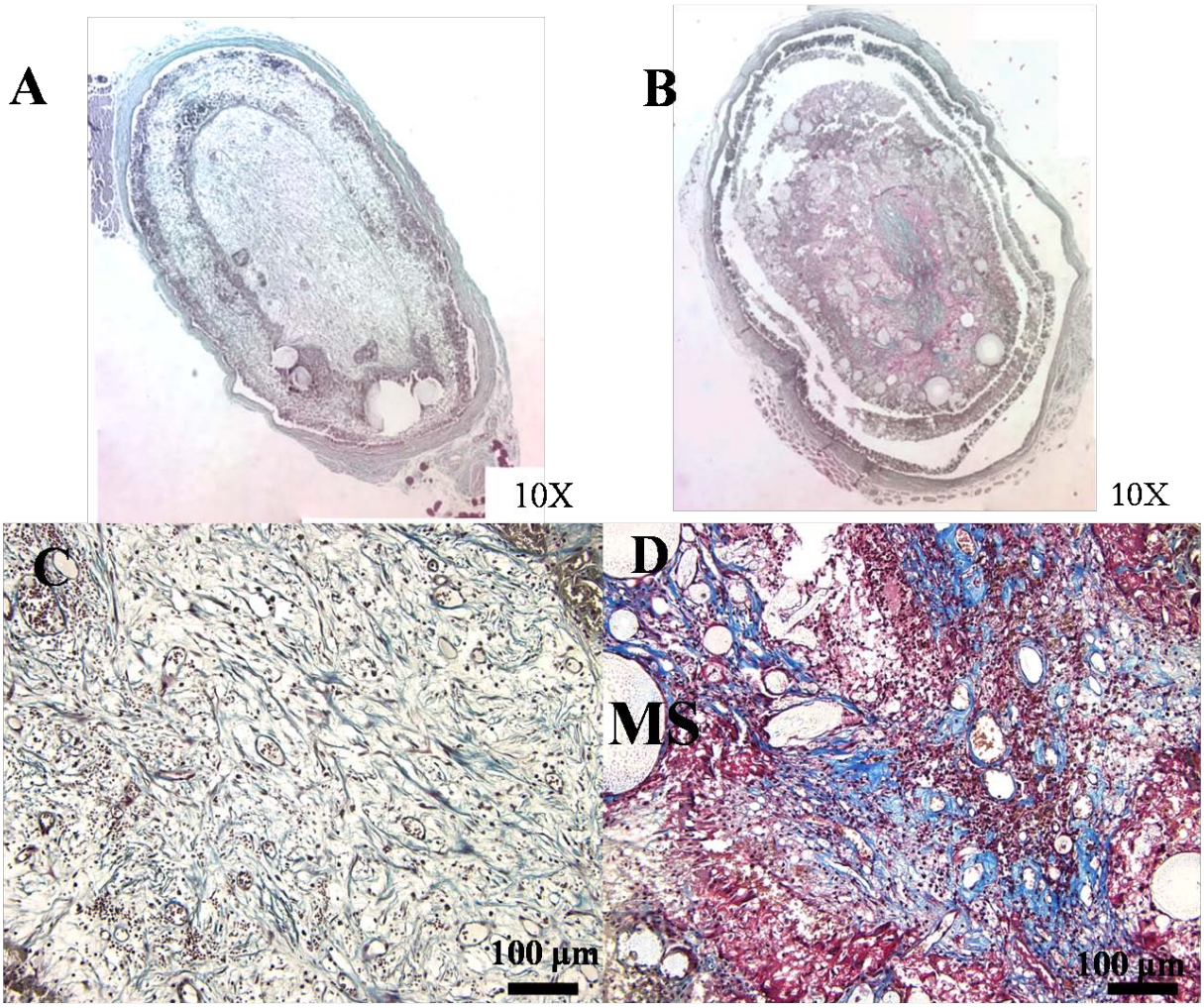

Figure 59. (A and B) Compilation of brightfield micrographs taken of a transverse section of the distal segment of guides visualized with Masson's trichrome stain. (A) Negative control guides and (B) guides with GDNF. (C and D) High magnification brightfield micrographs taken of the lumen of explanted nerve guides from negative controls (C) and guides releasing GDNF (D). Scale bars are 100 µm.

16 Week, Long Term Study

The regeneration of nerve across a 1.5 cm defect was also evaluated at a longer time point of 16 weeks. Low magnification transverse sections of the proximal portion of negative control conduits reveal a high degree of collagen content within the lumen of the guide (blue) with tissue integration throughout the entirety of the guide lumen (Figure 60A). Regenerated nerve is evident near the PCL nerve guide wall (black box) and as evident at higher magnification, is disorganized and sparse (Figure 60B). Nerve tissue is also evident within the lumen of nerve guides releasing GDNF, however, fibers are located in the center of the lumen surrounded by newly formed tissue (black circle, Figure 60C). High magnification light micrographs reveal a large number of small nerve fibers that are well organized and thinly myelinated (Figure 60D).

Low magnification brightfield images of transverse sections from control PCL guides reveal that regenerated nerve tissue was not evident within mid (Figure 61A) or distal segments (Figure 61B). Tissue integration appears incomplete and few blood vessels are observed. However, in both the mid and distal regions of conduits releasing GDNF, there was regenerated nerve tissue within the lumen of the guides. Low magnification micrographs of the midline of explanted conduits (Figure 61C) shows collagen formation and tissue integration supporting the regenerated nerve fibers seen at higher magnification within Figure 61D. Additionally, nerve tissue is also evident within distal regions of the GDNF releasing conduits within both low (Figure 61E) and high magnification (Figure 61F) micrographs.

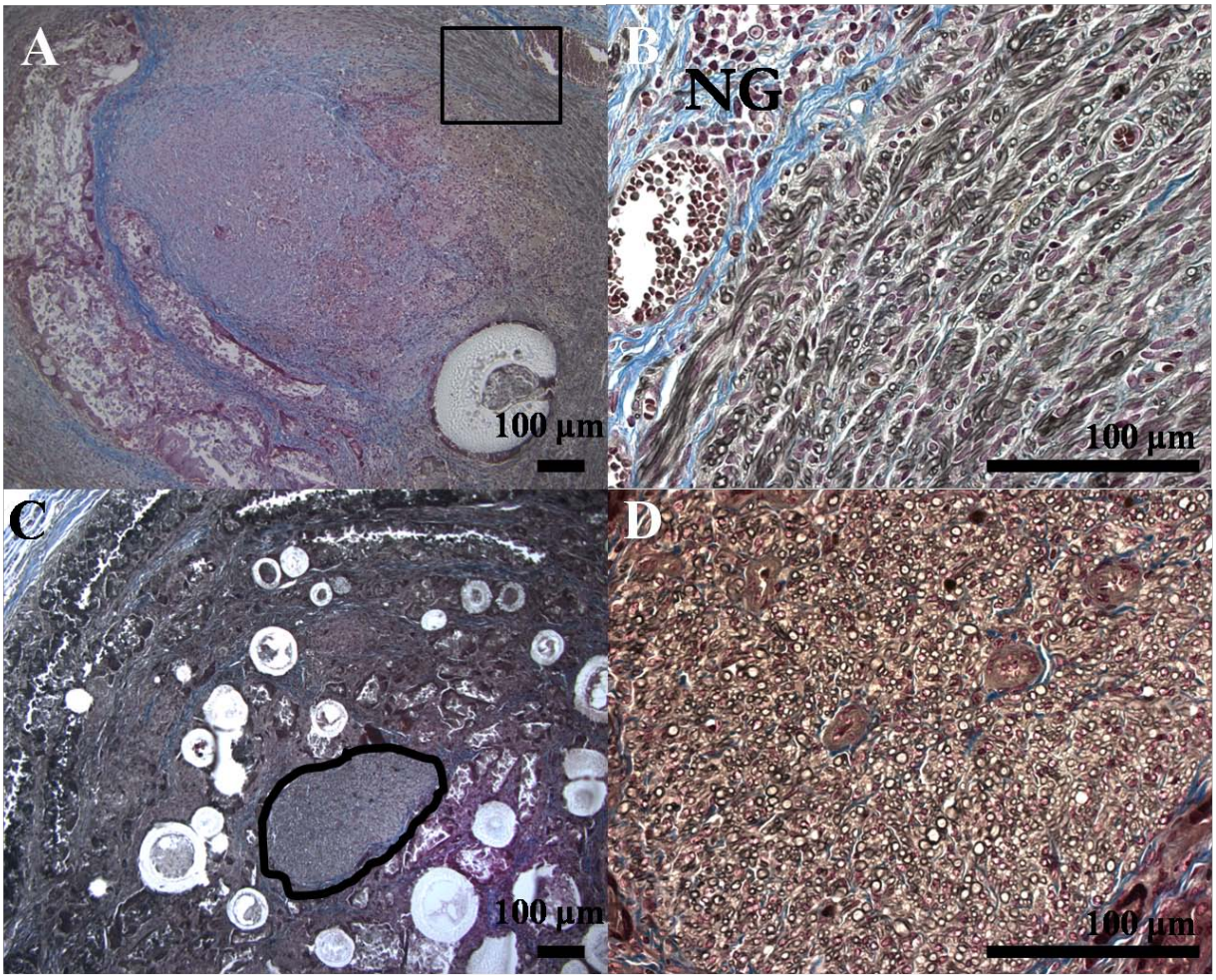

Figure 60. Transverse sections of the proximal segment of guides explanted after 16 weeks as visualized with Masson's trichrome stain. (A) Low magnification brightfield micrographs taken of negative control guides with regenerated nerve tissue indicated within black box. (B) High magnification micrographs showing detailed nerve tissue organization. (C) Low magnification transverse section from guides releasing GDNF with centrally located nerve tissue circled in black. (D) High magnification brightfield image of nerve fiber organization following GDNF treatment. Scale bars are 100 µm.

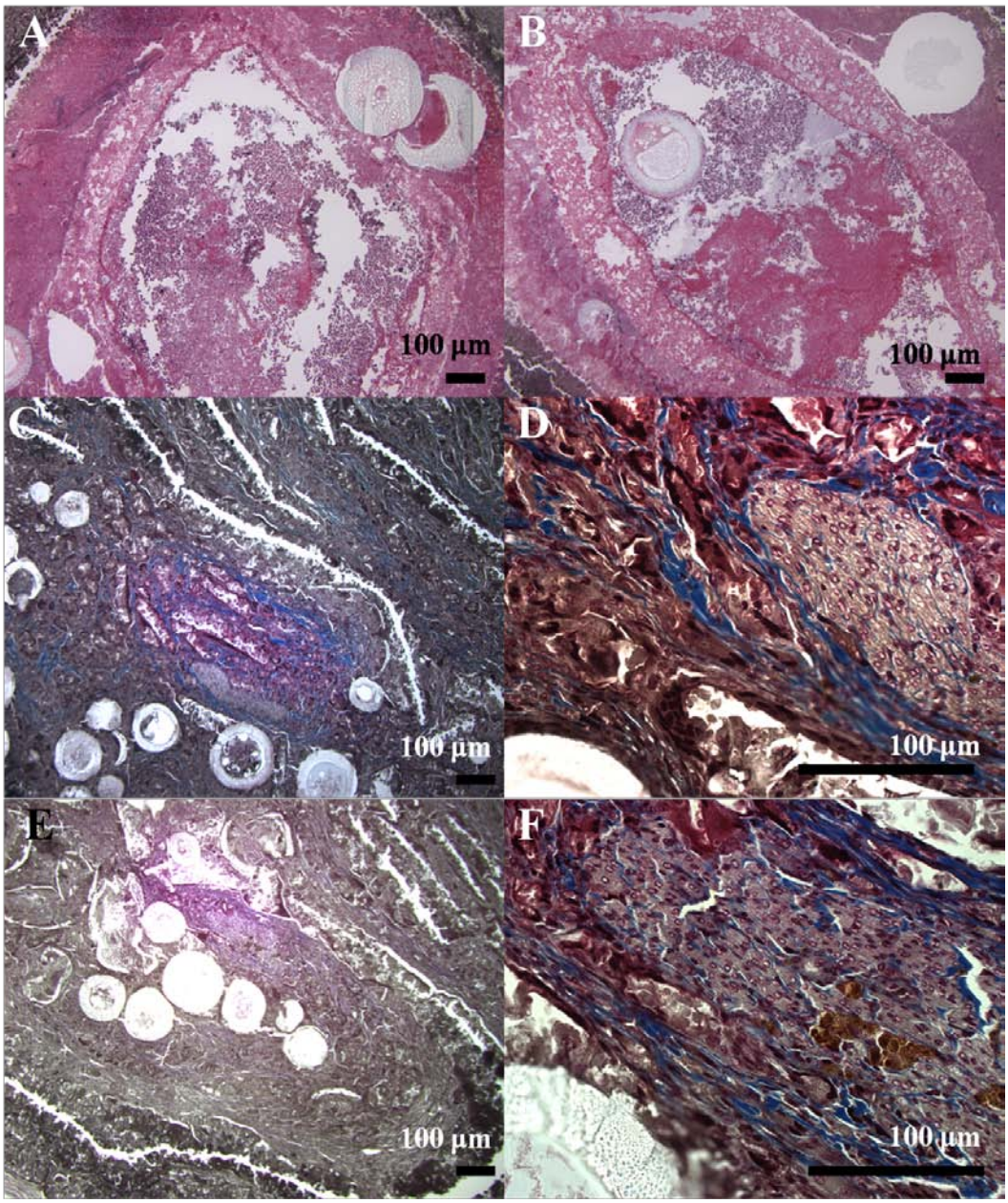

Figure 61. Transverse sections from guides explanted 16 weeks post injury visualized with Masson's trichrome stain. Low magnification brightfield micrographs taken of negative control guides from the mid (A) and distal (B) sections of the explanted guide. (C) Low magnification mid transverse section from guides releasing. (D) High magnification brightfield image of nerve fiber organization following GDNF treatment. (E) Low magnification distal transverse section from guides releasing. (F) High magnification brightfield image showing detail nerve fiber organization from within GDNF guides. Scale bars are 100 µm.

5.3.4.2 Immunohistochemical analysis

6 week, Pilot Study

Results from immunohistochemical analysis of nerve sections treated with anti-S100 antibodies showed that Schwann cells were present in the proximal nerve guide segment in both negative control and nerves that received guides with GDNF microspheres. However, as seen in Figure 62A, the distribution of Schwann cells in control guides was largely restricted to the middle of the nerve guide. Within the lumen of nerve guides releasing GDNF, Schwann cells are evident not only in the center of the conduit, but also surrounding the microspheres (Figure 62B). At higher magnification, Schwann cells (red) are visualized surrounding the double-walled microspheres releasing GDNF (Figure 62D) but are not present around non-encapsulating control microspheres (Figure 62C).

Analysis of the distal regions of the explanted nerve guide reveal the presence of Schwann cells in the lumen of only those guides releasing GDNF. In Figure 62E, DAPI staining of nuclei reveals the presence of cell nuclei in lower frequency than in control guides as compared to GDNF guides (Figure 62F). Also evident in Figure 62F is the presence of Schwann cells in GDNF guides not seen in the negative control guides.

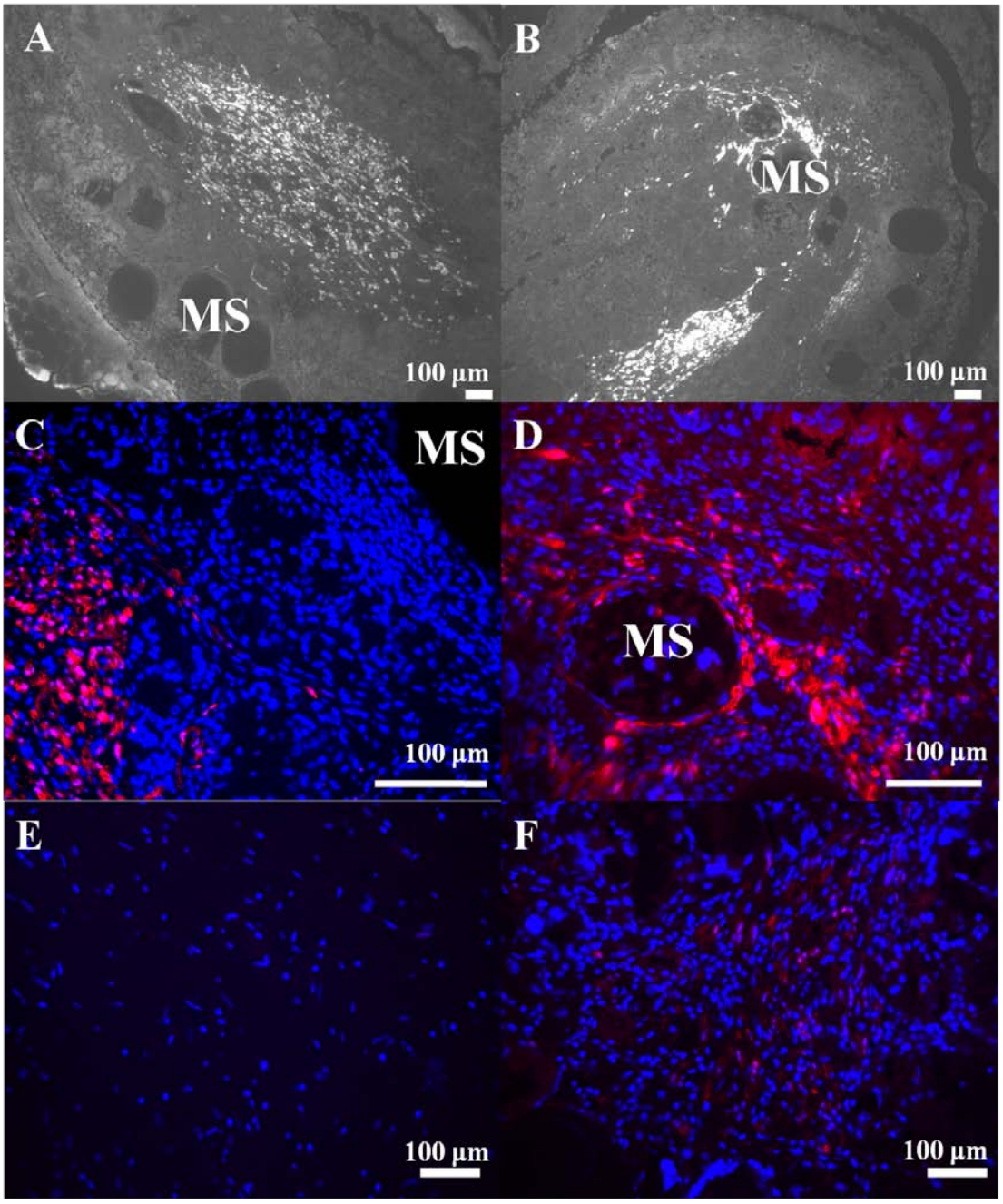

Figure 62. (A and B) Black and white fluorescent micrograph showing Schwann cells (visualized with S100). (A) Proximal transverse section of negative control guides. (B) Proximal section of guides release GDNF). (C) High magnification fluorescent micrograph of double-walled microsphere encapsulating GDNF. (E and F) Fluorescent micrographs from distal segment of explanted nerve tissue. (E) negative control and (F) GDNF releasing nerve guides. Red indicates S100 labeling of Schwann cells. DAPI is blue. Scale bars are 100 µm.

16 week, Long Term Study

Nerve tissue was evident in the proximal region of explanted conduits 16 weeks after sciatic nerve transection and conduit implantation. Fluorescent images reveal the presence of both nerve fibers (neurofilament proteins: green) and Schwann cells (S-100: red) in both negative control PCL guides and guides releasing GDNF. However, nerve tissue within control PCL guides (Figure 63A) was localized to the internal border of the nerve guide wall and appears disorganized, while nerve tissue was centrally located and well organized within GDNF releasing guides (Figure 63B). Schwann cells and nerve fibers were not detectable within the middle (Figure 63C) or distal segments (Figure 63E) of control nerve guides, while robust Schwann cell populations were observed across the entire length of GDNF releasing guides (Figures 63D and F).

To determine if macrophages were also present within and surrounding the implanted PCL conduits, IHC was performed using antibodies against CD68, a known macrophage marker. Throughout each observed section from control PCL guides, macrophages were not observed to preferentially localize around double walled microspheres were instead found in higher frequency throughout the conduit wall and surround blood vessels (Figure 64A). However, in nerve guides with microspheres encapsulating GDNF, macrophages, like Schwann cells were seen in high frequency immediately surrounding the double walled microspheres (Figure 64B). This observation suggests that bioactive GDNF was delivered and had a chemotactic affect on endogenous macrophages.

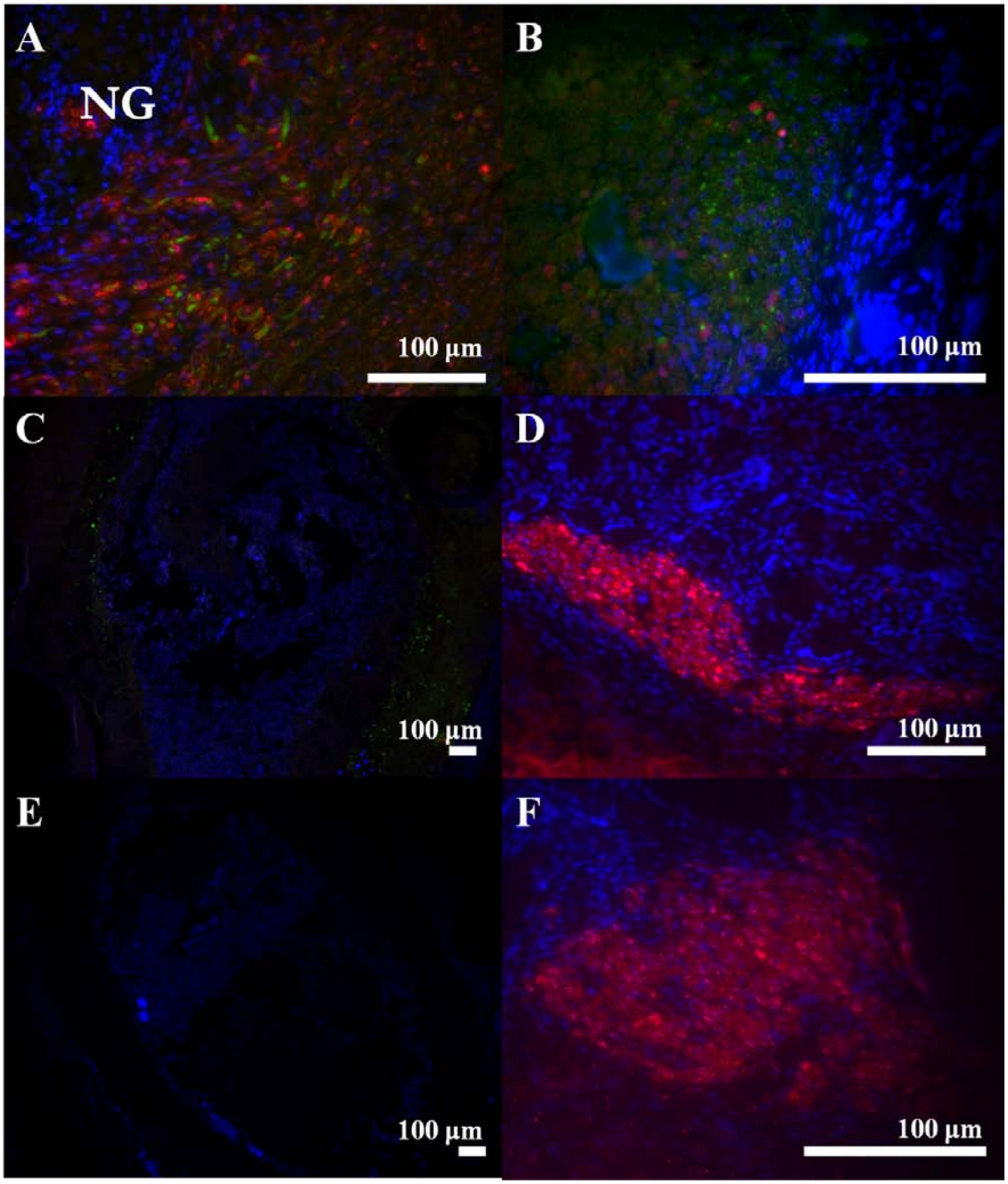

Figure 63. Fluorescent micrographs of proximal transverse sections of negative control guides (A) and guides releasing GDNF (B). Fluorescent micrograph from middle segment of control (C) and GDNF (D) nerve guides. Distal transverse section from negative control (E) and GDNF releasing nerve guides (F). Red indicates S100 labeling of Schwann cells. Neurofilament proteins within nerve fibers are green. DAPI is blue. Scale bars are 100 µm.

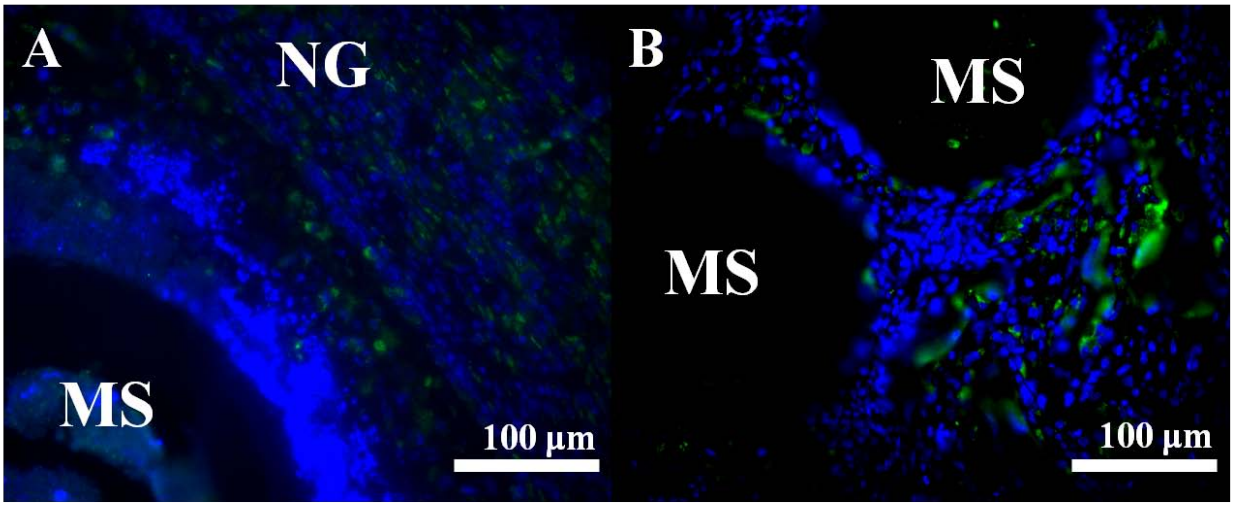

Figure 64. Fluorescent micrograph of transverse sections of explanted PCL conduits. Distribution of macrophages (CD68, green) within control PCL guides (A) and guides releasing GDNF (B). Microspheres are indicated with the characters "MS" while the nerve guide luminal edge is marked with "NG." Scale bars represent 100 µm.

5.3.4.3 Axon morphometric and histological analysis

Monochrome images of the proximal nerve stump, proximal isograft or nerve guide, distal isograft or nerve guide, and distal nerve stump were acquired and thresholded to identify viable axons. Using semi-automated software, myelin width, axon width, and fiber diameter were calculated. From these primary measurements g-ratio and nerve fiber density (fiber number/mm^2) were determined. Within the isograft, positive control nerve samples, the g-ratio of axons was consistent within each section from the proximal nerve stump to the distal nerve stump with a measured range of 0.40 to 0.42 (Figure 65A). The g-ratio of nerve fibers within GDNF releasing guides were higher for all measured transverse sections, with average values of 0.53, 0.54, 0.55, and 0.44 for the PNS, PG, MG and DNS sections respectively. These measured values from GDNF guides approach an uninjured g-ratio range of 0.6 to 0.7 (gray bar). Fibers

from control PCL guides were observed to have a lower g-ratio value within both the proximal nerve stump (0.47) and the proximal segment (0.45) of the explanted nerve guide. No fibers were evident in the mid or distal regions of negative control PCL guides for measurement calculations.

Evaluation of nerve fiber density throughout the length of explanted nerve samples shown in Figure 65B reveals an increased density of fibers per mm^2 for both the GDNF and control nerve guides as compared to isograft positive controls, an indication of axonal sprouting from regenerating nerves (Figure 65B). As seen in fiber g-ratio results, isograft sections had a small range of fiber densities (~11,300 to 12,200) progressing from the proximal to the distal nerve stumps indicating limited axonal sprouting occurred within the graft. Within GDNF and control nerve guides, nerve fiber densities were calculated confirmed early Masson's trichrome observation of improved nerve regeneration through PCL conduits releasing GDNF. The density of fibers within GDNF releasing guides was higher than negative control guides for all measured segments and there were no viable nerve fibers in negative control nerve guides beyond the mid region of the explanted conduits (Figure 66).

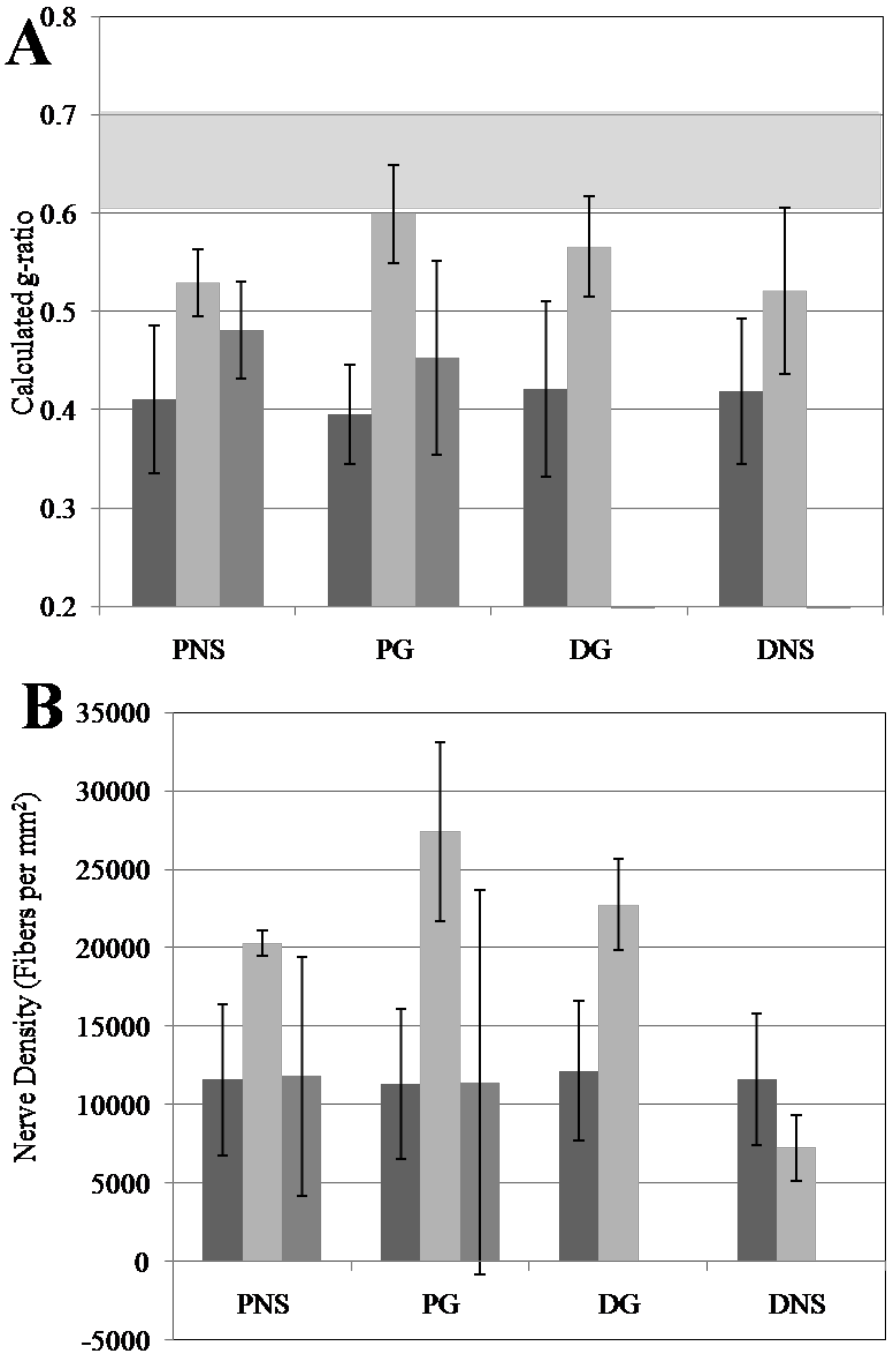

Figure 65. (A) Calculated g-ratio of fibers within transverse segments of the proximal nerve stump (PNS), proximal graft or guide (PG), distal graft or guide (DG) and distal nerve stump (DNS). (B) Calculated nerve fiber density (fibers per mm^2). Treatment groups are isograft (■), GDNF nerve guide (■) and control nerve guide (■). Values are expressed as mean ± std dev. Gray horizontal bar indicates normal, uninjured g-ratio values.

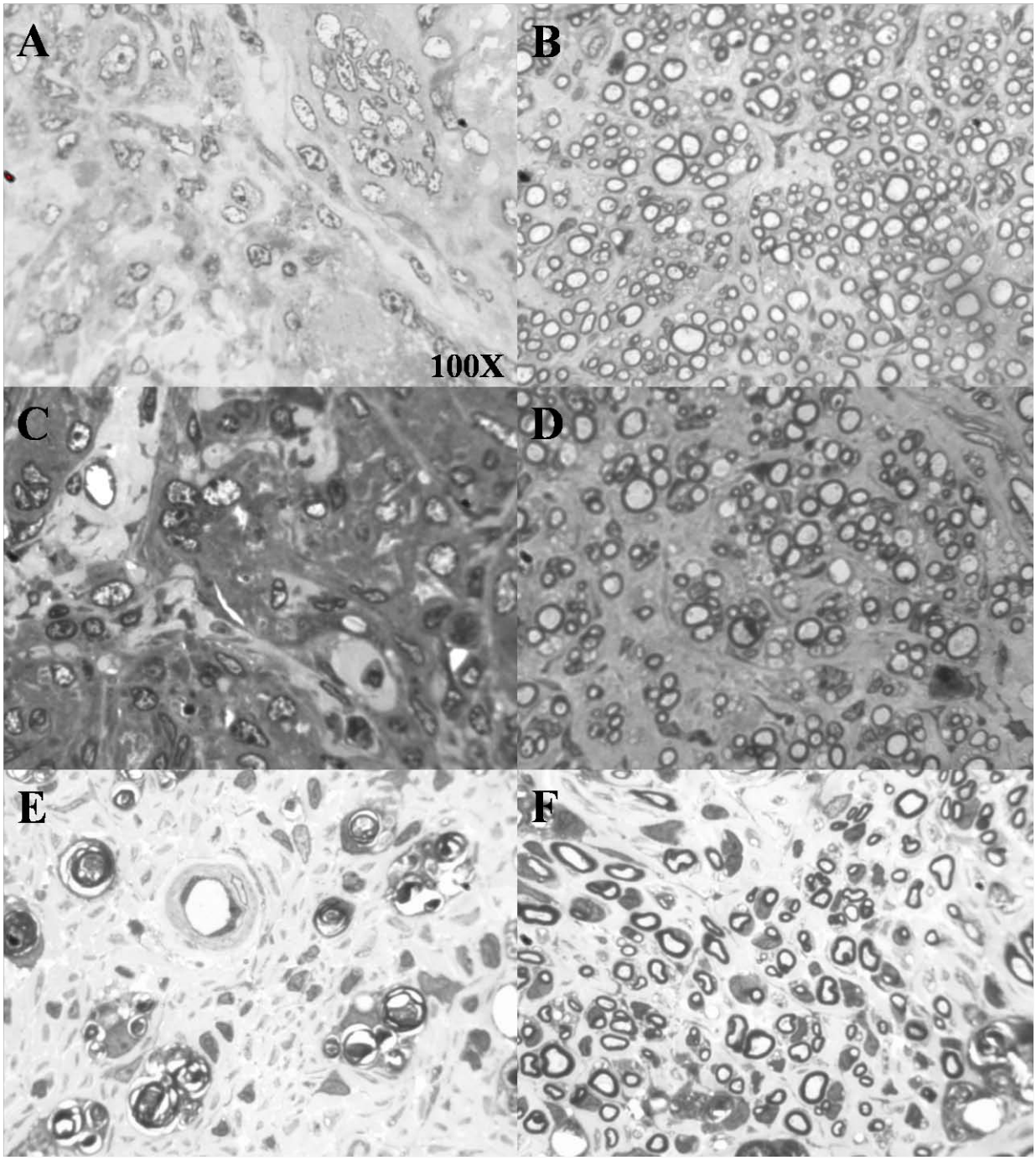

Figure 66. High magnification (100X) light micrographs of transverse sections of explanted nerve following 16 weeks *in vivo*. Mid-conduit nerve tissue from negative control PCL guides (A) and guides releasing GDNF (B). Distal-conduit nerve tissue from negative control PCL guides (C) and guides releasing GDNF (D). Distal nerve stump of negative control PCL guides (E) and GDNF releasing guides (F).

5.4 DISCUSSION

While the benefits of many different neurotrophic factors have been assessed in sciatic nerve defects (e.g. NGF, BDNF, CNTF) we chose to initially implant nerve guides releasing GDNF because of the promising results described in literature. GDNF is a neuroprotective growth factor secreted by Schwann cells in distal segments of peripheral nerves following injury [156]. In addition, GDNF has been shown to prevent avulsion-induced motorneuron death following complete nerve transection whereas nerve growth factor (NGF), brain-derived neurotrophic factor (BDNF), and insulin-like growth factor (IGF) all failed to enhance cell survival or cell size [126]. Finally, GDNF treatment with guidance channels following spinal cord injury resulted in a reduction of reactive astrocytosis and macrophage accumulation [120].

Our initial *in vitro* release studies suggest that GDNF was delivered throughout the preliminary 6 week pilot study period used to determine the efficacy of our novel nerve guide design. Furthermore, histological evaluation of explanted conduits suggest that bioactive GDNF was delivered to endogenous cell populations and markedly improved cellular integration and tissue formation across the nerve injury. While nerve gaps treated with empty microsphere conduits resulted in incomplete fibrotic tissue formation and scattered fibroblast – like cells in the center of proximal segment of the excised nerve guides, nerve guides releasing growth factor reveal an increase in cellular infiltration and tissue integration within the lumen of the conduits. In addition, tissue integration in the distal segments of nerve guides was markedly improved in guides releasing GDNF. High magnification micrographs of the central portion of transverse segments (Figure 59C and 59D) reveal an overall increase in cellular infiltration and collagen content following GDNF treatment. This increase in collagen content potentially supplied an

improved scaffold for Schwann cell migration and supported axonal outgrowth during longer 16 week *in vivo* studies.

Detection of Schwann cell localization with immunofluorescence indicated that Schwann cells were present in proximal segments of PCL nerve guides. Fluorescent micrographs of control guides show a significant number of Schwann cells within the lumen of the guide (Figure 62A) and Schwann cells do not appear to localize to the conduit wall or microspheres (Figure 62C). Nuclear staining (DAPI) within the conduit center reveal a large presence of additional cell populations which most likely include fibroblasts and macrophages but were not positive for antibodies against neurofilament antibodies (Figure 62C). However, micrographs of nerve guides with GDNF microspheres show a population of Schwann cells encircling the microspheres, an indication of targeted migration of Schwann cells toward a source of GDNF (Figure 62B and 62D). This result is significant for two reasons. First, a cellular response to the encapsulated growth factor suggests that the released GDNF is bioactive and has not been completely denatured through the nerve guide fabrication process. Second, the migration of Schwann cells, presumably from the lumen of the conduit, indicates that GDNF is being delivered to the lumen of the nerve guide in a physiologically relevant concentration and is not entirely entrapped within the porous nerve guide structure.

Nerve guides encapsulating GDNF also resulted in the presence of Schwann cells at the distal portion of transverse sections of explanted tissue that was not observed in control guides (Figure 62E and 62F). Fluorescent micrographs of the central portion of the nerve guide reveal an increase in both cellular infiltration and cells positive for antibodies against S-100 protein in experimental guides while there were no detectable positive for S-100 in control guides. The presence of Schwann cells in the distal segment of experimental nerve guides could be a result of

either Schwann cell proliferation or migration. Though GDNF is typically utilized in nerve regeneration as trophic factor for nerve fibers and as a promoter of axonal growth [242] and branching [253, 254], GDNF also causes a marked proliferation and migration of Schwann cells [254, 255]. The effect of GDNF is RET (receptor tyrosine kinase) independent and instead, GDNF signaling mechanisms directly in Schwann cells through a GPI-anchored coreceptor (GFR-α1) and neural cell adhesion molecule (NCAM) [255]. Additionally, downstream signaling protein kinases (PKA) participates in GDNF transcription, and therefore, GDNF promotes a positive feedback loop for autocrine signaling in Schwann cells. This autocrine feedback loop has been reported to further enhance Schwann cell migration and myelination [256], both of which are important events in nerve regeneration.

Finally, not only were Schwann cells observed to localize around double-walled microspheres, macrophages were also seen with high frequency surrounding microspheres. During Wallerian degeneration, both endogenous Schwann cells and macrophages proliferate and phagocytose axonal debris within endoneurial tubes, an important process for providing regenerating axons an optimal environment for outgrowth. In addition to this function, both cell types release growth factors which have chemotactic affects on directing axonal outgrowth [257]. Because the number of cells which secrete growth factors was improved within the experimental guides, the concentration of axonal growth promoting factors within the site of nerve injury may have been further increased in addition to exogenous GDNF delivery.

Measured outcomes from functional analyses of nerve regeneration through nerve conduits also reflect improved nerve regeneration within GDNF releasing guides. Upon the initial exposure of the site of nerve injury, nerve tissue was seen exiting the distal end of implanted conduits in only 70% of the control PCL guides, while 100% of the animals implanted

with GDNF releasing guides had nerve trunks throughout the length of the conduits and integrating into the distal target muscles. In addition, the measured gastrocnemius contraction force, an indication of muscle atrophy and reinnervation, was significantly improved by a difference of 6-fold in animals treated with GDNF releasing conduits as opposed to those which received empty PCL conduits. Markedly, the contraction force between animals treated with isografts, considered to be the gold standard for nerve repair, was not significantly different from animals receiving GDNF releasing conduits.

Analysis of muscle reinnervation through quantification techniques of rat gait proved challenging using the techniques described herein. No significant difference in SFI measurements or joint angle range of motion was measured between the GDNF experimental group and the negative control. Partly, this is due to the early time points at which rat gait was assessed. Because the experiments described here were designed to detect improvement in nerve regeneration due to growth factor delivery, it was necessary to use an animal sacrifice date that would preclude the natural ability of rats to regenerate nerve without treatment, known as the blow-through effect. While rats have a number of positive attributes which make them ideal for evaluating therapies for nerve regeneration, they also have been reported in literature as having a superior capacity for regenerating nerve across large defects [258]. Therefore, if lengthy time points are used, given enough time, nerve regeneration in negative control groups will eventually catch up to experimental groups. Therefore, it may have been possible to see improvements in animal toe spread or joint angle range of motion given more time for muscle reinnervation in experimental animals.

In addition to evaluating animal recovery at early time points within the long term 16 week study, several experimental difficulties were encountered when using SFI analysis for

quantifying nerve regeneration. The animal of experimental choice, the rat, has several behavioral instincts that can cause obtaining clear, easily measured footprints difficult. The first innate behavior pertains to self- grooming and the rats' natural desire to trim the toe nails with the teeth. When the lower leg has lost sensation, the rat may either autotomize the toes causing severe mutilation or will cease to trim the nails resulting in extremely long toe nails to develop over time (Figure 67A). While the strain of rat can be varied to one which has less incidence of autotomy, such as the Lewis rat [259], a rat that produces elongated nails can cause the print length to appear much longer than it should be measured (Figure 67B). Additionally, flexion contractures occur in early stages of nerve regeneration and prevent any toe markings from being left on paper (Figure 67C). Contractures occur when the sciatic nerve fails to reinnervate proper connections during nerve regeneration [260] and result in these animals being discarded from the data pool. Finally, animals that have lost the ability to walk with a raised heel, as is typical rat gait, develop blisters and sores on the heel which cause the animal discomfort or may cause the resulting foot print to appear wider than it might otherwise be (Figure 67D). The described examples of compounding foot deformities overtime can lead to gait compensatory behaviors such as foot inversion or eversion that are difficult to measure through SFI. Therefore, a more global view of the rat gait kinematics throughout nerve regeneration may be used in conjunction or separate of SFI to more adequately describe functional recovery following nerve repair.

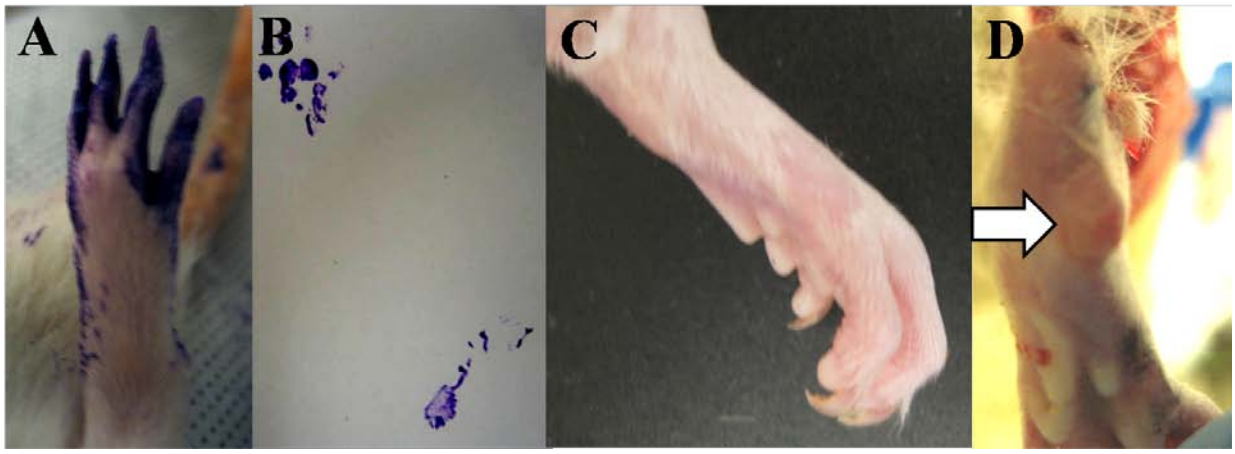

Figure 67. (A) Photo of rat foot with lengthened toe nails which results from the cessation of self-grooming. (B) Photo of incomplete foot print of injured right leg. (C) Photo of a flexion contracture, a common occurrence in early stages of nerve regeneration which result in an inability to evaluate animal print. (D) Photo of a sore (white arrow) on the bottom of a foot on the side of sciatic nerve injury.

The development of a technique for analyzing gait kinematics through video recording was undertaken as a method of circumventing those challenges seen with SFI measurement. However, unique obstacles were presented within this method of gait analysis. First, animal behavior is fickle, and often animals were observed as walking with a unique head position, speed, or step pattern. In addition, animals would traverse the walkway only a few times before losing interest in the activity and could not be trained to proceed with a smooth gait pattern despite incentives provided by the operator. Because of this, step cycles were used for measuring joint angles from only those steps which were consecutive and were determined to be of a walking nature (at least one foot always on the ground). The use of a treadmill would greatly improve the consistency seen in joint angle measurements and may allow this technique

to be a more robust method for detecting early improvements in gait kinematics following lower limb nerve injury.

Because of the unique difficulties that occur within each of the various methods used for assessment of functional recovery following nerve injury, it is suggested here that multiple techniques be employed such that diverse measurements are pooled to provide the strongest indicators of lower limb muscle control. SFI is a simple method of obtaining gross estimations of lower limb muscle control. Video assessment of gait kinematics provides a much deeper understanding of animal behavior and uncovers compensatory behavior. With further optimization, these tools may prove invaluable when used with sensory evaluation to track animal recovery throughout the duration of *in vivo* studies of therapeutics for nerve repair. In addition to these tests which can be performed across multiple time points, end point assessment of muscle contraction force is a critical method of quantifying muscle reinnervation that does not depend on animal behavior. When these tools are used in combination with the multiple histological techniques described herein, it is possible to strongly support or dismiss claims of regenerative effects of a wide number or therapeutics.

5.4.1 Conclusions

GDNF was successfully encapsulated in double-walled microspheres and released in a controlled manner for over 100 days *in vitro*. The overall efficacy of incorporating microspheres into the luminal wall of PCL nerve guides was confirmed with GDNF in the rat sciatic nerve model. Functional evaluation of animals at weekly intervals revealed no significant differences in toe spread measurements between animals treated with the GDNF releasing conduits or the control conduits. Furthermore, though calculated joint angles showed an overall improvement in animal

gait toward baseline levels, no significant difference between the experimental group and negative controls were measured. However, evaluation of sensory reinnervation following nerve injury showed a significant increase in animal response time to stimuli within the group of animals treated with GDNF releasing guides. Furthermore, the measured gastrocnemius contraction force in animals treated with GDNF was significantly higher than negative controls and was not significantly different from the isograft positive control group.

Histological assessment of explanted conduits after 16 weeks further showed that tissue integration within GDNF releasing nerve guides was improved above negative controls and resulted in a greater concentration of intercellular fibers and collagen content within the lumen of the guides. In addition, fluorescent and brightfield images showed nerve fibers throughout the entire length of guides releasing GDNF, while no nerve fibers were detectable beyond the middle region of negative control guides. Furthermore, a localization of Schwann cells and macrophages around microspheres encapsulating GDNF indicates that bioactive GDNF was being released from our delivery system. Therefore, the results reported within this dissertation support our original hypothesis that; the delivery of Glial Cell Line-Derived Neurotrophic Factor (GDNF) from nerve guides results in improved functional recovery above negative controls in the *in vivo* environment following large axonal defects in the peripheral nervous system.

5.5 FUTURE DIRECTIONS

While initial studies for evaluating nerve repair have been conducted with a single growth factor, this technique could lend itself useful for evaluating delivery systems for additional growth factors or combinations thereof. The nerve guide delivery system described within this

dissertation has been optimized in terms of guide manufacturing parameters for the sustained delivery of small proteins in general. Additionally, both large (BSA) and small proteins (lysozyme, GDNF) were successfully encapsulated within double walled microspheres. As the nerve guide design is modular, the PCL conduits described herein lend themselves easily toward investigation of a variety of different therapeutics for improved nerve regeneration.

6.0 DISCUSSION

The work described within this dissertation presents a novel method for delivering growth factors from biodegradable polymeric nerve guides for peripheral nerve repair. To accomplish this, a poly(caprolactone) (PCL) scaffold was combined with microspheres composed of poly(lactic-co-glycolic acid) (PLGA) and poly(l-lactide) (PLLA) in a novel fabrication method that utilized physical properties unique to each polymer. A brief summary of each specific aim required to produce the final engineered nerve conduit for sustained protein delivery is presented below. Future studies involving the nerve guide delivery device are then discussed.

6.1 SUMMARY OF RESULTS

6.1.1 Specific Aim 1: Optimizing Nerve Guide Manufacturing Parameters

The objective of Specific Aim 1 was to quantify the *in vitro* effect of nerve guide porosity percentage and wall thickness on growth factor and nutrient diffusion through PCL nerve guide walls. This work was necessary as highly porous nerve guide walls have been shown as a necessary feature of nerve guide design because it is critical to allow for the diffusion of blood nutrients and oxygen into the site of nerve injury. However, as the guide was also intended to deliver and maintain small molecular weight proteins at high concentration within the lumen of

the guide, wall porosity had to be limited to prevent growth factor loss. Lysozyme was used as a representative small molecular weight protein to model growth factor diffusion and glucose, a small hydrophilic molecule was used to model blood nutrients.

Initial optimization experiments resulted in the highest glucose diffusion from guides of 80% porosity with pore diameter ranging between 10 - 38 μm. Additionally, it was determined that at high porosity percentages, decreasing the pore diameter was a measurable method of decreasing the lysozyme permeability of PCL nerve guides while not creating a loss of glucose permeability. PCL fouling studies were used to optimize the desirable nerve guide wall thickness. Results indicated that nerve guides of 0.6 mm thickness decreased the loss of lysozyme to almost 10% without significantly diminishing glucose permeability. Based on the results of this study, nerve guides of 80% porosity percentage with 10 – 38 μm pore diameter and 0.6 mm wall thickness were used for subsequent *in vivo* studies.

6.1.2 Specific Aim 2: Development of a Microsphere Based GDNF Delivery System

The objective of specific aim 2 was to develop a nerve guide that delivers encapsulated proteins for the duration required for regenerating peripheral nerve axons to reach the distal nerve stump following transection and creation of a long gap nerve defect (1.5 cm). This was accomplished by first developing a microsphere delivery system for sustained protein release and then incorporating the microspheres into the polymer nerve guide wall such that the mechanical integrity of both polymer components, the nerve guide and the microspheres, was maintained.

Double walled microspheres encapsulate proteins within a polymeric core that is encased by a second polymer, thus increasing the amount of material through which the liberated protein

must diffuse, and subsequently slowing the release rate. To delivery bioactive proteins over a sustained period (at least 60 days), microspheres were prepared with various polymer solvents, polymer solution concentrations and co-encapsulants. Results demonstrate that double walled microspheres with a poly(lactic-co-glycolic acid) core containing the encapsulated protein and a poly(L-lactide) shell are produced when dichloromethane is selected as the solvent for both solubilizing both polymers. Further, protein release from the micropsheres can be significantly slowed when an increased solution concentration of PLGA is used in the initial oil-in-oil phase of microsphere preparation. Finally, coencapsulants such as human serum albumin can be used to stabilize delicate growth factors during microsphere fabrication without decreasing protein bioactivity or altering the microsphere polymer orientation.

It was important for reproducible nerve guide fabrication that microspheres were created with a PLGA core and PLLA shell so that microspheres could be combined with PCL for nerve guide preparation. Because PLLA is not soluble in ethyl acetate, the solvent used to create the PCL/NaCl slurry for nerve guide fabrication, the microsphere morphology was protected from dissolution during nerve guide fabrication. Our results show that we can incorporate microspheres into PCL nerve guides in a manner that does not harm the morphology of microspheres and results in reproducible protein release profiles. Additionally, the distribution of microspheres within the nerve guide walls can be easily tailored. For example, microspheres can be homogenously distributed along the nerve guide wall, or embedded in a gradient distribution to release an increasing concentration of growth factor along the longitudinal axis. While the nerve guides were tailored for locally delivering GDNF to injured nerves, the overall design with which PCL nerve guides were engineered allows for incorporation of varying

microsphere concentration, location and encapsulated substance. Therefore, our guides could be used to test a variety of therapeutics for nerve repair.

6.1.3 Specific Aim 3: *In vivo* Delivery of GDNF in Long Gap Peripheral Nerve Defects

Our overall goal was to quantify the *in vivo* effect of GDNF delivery from a PCL nerve guide in terms of histological and functional regeneration of the sciatic nerve across a critical size (1.5 cm) defect. An *in vivo* pilot study was first performed to determine if bioactive GDNF was sufficiently delivered from implanted nerve guides and if any improvements in nerve tissue regeneration could be detected within the nerve guides. In a 6 week pilot study, PCL nerve guides with GDNF were used to bridge a rat sciatic nerve defect and resulted in an increase in tissue integration in both the proximal and distal segments of the lumen of the nerve guide and an increase in Schwann cells in the distal region of the guide. Migration of Schwann cells toward double-walled microspheres indicated that bioactive GDNF was encapsulated and delivered to the internal environment of the nerve guide. Because of these positive preliminary outcomes, the long term effects of GDNF delivery were assessed over a 16 week period.

Results from our 16 week *in vivo* study supported our initial hypothesis that localized GDNF delivery to an injured nerve would improve nerve regeneration in terms of both functional recovery and nerve histomorphometry. Four methods of functional evaluation were used to assess recovery of animals following nerve injury. Two of these methods, sciatic functional index and video assessment of gait kinematics, were used to track behavioral changes in rats at defined time points throughout the duration of the study. Neither of these methods was able to detect significant improvements in rat gait between experimental and negative control nerve

guides. However, recordings of gastrocnemius contraction force of anesthetized rats showed a 6-fold increase in contraction force of animals treated with GDNF above the negative control guides. Because the wet weights of harvested gastrocnemius muscles following the completion of the study were not significantly different, the improvement in contraction force suggests that perhaps the target muscles of animals treated with GDNF were innervated with an increased number of nerve fibers allowing for a greater recruitment of muscle fibers for contraction. Further histological analysis of explanted gastroc muscles for neuromuscular junctions could be performed to explore this hypothesis.

Explanted nerves were examined with a variety of histological techniques to further examine the morphology of regenerated nerve tissue. Transverse sections of proximal, middle and distal regions of explanted conduits were visualized with Masson's trichrome stain and showed an overall increase in tissue integration at the middle and distal lengths of GDNF releasing guides as compared to PCL guides containing DW microspheres without encapsulated GDNF controls. Semi-thin (500 nm) sections of tissue architecture from within PCL guides further confirmed that nerve fiber density was greater in the middle and distal regions of GDNF releasing guides. Finally, visualization of Schwann cells and Neurofilament proteins with immunofluorescence revealed a higher degree of nerve tissue organization within nerve guides releasing GDNF, with tissue located in the center of the explanted conduit as opposed to negative control guides which produced nerve tissue only along the surface of the conduit. The distribution of nerve fibers within the guides may reflect the overall improvement in tissue in growth with GDNF treatment. Presumably, axons within GDNF guides were provided with an enhanced collagen and tissue scaffold for support of migration and elongation, and thus resulted in increased outgrowth throughout the entire length of the experimental conduits.

6.2 FUTURE DIRECTIONS

The delivery of growth factors from nerve guides is one technique used to improve nerve regeneration. At the conclusion of our *in vivo* studies, it was concluded that axonal elongation was supported within GDNF releasing guides in part by inner luminal tissue formation that served as a platform for axonal extension across the large nerve defect. This hypothesis is supported by the documented importance of scaffolds for cell migration for nerve repair [36]. Within the first week of injury, fibrin cables are formed to bridge the proximal and distal nerve stumps. The fibrin bridge is critical for migration of Schwann cells, fibroblasts and macrophages, which are ultimately responsible for the regeneration of nerve fibers [261]. We now plan to evaluate the potential benefits of incorporating a luminal filler within our GDNF releasing nerve guides across long peripheral nerve gaps. We hypothesize that incorporation of a scaffold for cellular and axonal migration at the time of guide implantation would further increase the rate of nerve regeneration across breaks in nerve continuity.

Fibrin [262], collagen [263-265], laminin [266-268], keratin [269, 270] and hyaluronic acid [271, 272] have all been used to provide structural support and topographical cues for axonal elongation. In collaboration with the Wake Forest Institute of Regenerative Medicine, we intend to investigate GDNF delivering guides in combination with keratin gels within rat sciatic nerve defects. Sierpinski et al., have reported keratin-based gels as having regulatory molecules which are useful for cell attachment and migration [270]. Within this study, Schwann cell proliferation and migration were significantly increased above negative controls using keratin derived from wool fibers. Additionally, in a 4 mm tibial nerve defect in Swiss Webster mice, keratin gels within silastic tubing resulted in a reduced nerve conduction delay and an increased compound motor action potential as compared to both silastic tubes filled with saline as well as

autograft controls [269, 270]. While the use of a short nerve gap, 4 mm, allowed for the recovery of all animals given enough time, early study results suggest that keratin is a promising material for further improving the quality of nerve regeneration within our PCL nerve guides.

In addition to natural materials for luminal fillers, our lab is also developing novel thermo-sensitive hyaluronic acid based hydrogels for use within PCL conduits. Poly(N-isopropylacrylamide) (p-NIPAAm) is a thermo-sensitive polymer that undergoes a coil-to-globule phase transition at temperatures above the lower critical solution temperature of ~32°C [273]. When copolymerized with hyaluronic acid, p-NIPAAm-HA is biodegradable and would therefore provide space for regenerating tissue within the lumen of nerve guides. Additionally, because p-NIPAAm-HA is liquid at room temperature, this gel could serve as an injectable method for initial support for cells migrating within the open conduit lumen from the two nerve stumps.

It is our ultimate goal to transition the novel GDNF delivering nerve conduit to an implantable device for use in humans. As initially conceived, the nerve guide described within this dissertation would be considered a combination product; it is a scaffold that also contains a drug delivery system and is implanted as a single entity. Because our nerve guide combines both a device and a drug, there are additional challenges to obtaining regulatory clearance. However, the device materials, poly(caprolactone), poly(lactic-co-glycolic acid) and poly(lactide) and the delivered drug, GDNF, have been studied in humans, and therefore have previously acquired data that may be leveraged to support the safety of the combined materials in this product. Therefore, there is great promise for the progression of our described nerve guide toward clinical studies. Additional studies that would be necessary before this goal is met would include an analysis of lot-to-lot variation in drug loading and growth factor release. In addition, it is

required that 80% of the encapsulated growth factor be recovered, regardless of the matrix. Therefore, additional studies are needed to improve the overall encapsulation efficiency of GDNF within the microsphere/nerve guide system as well as to increase the quantity of protein that is liberated from the guides. Further investigation into potential co-encapsulants and protein stabilizers would therefore be of great utility before additional preclinical *in vivo* investigations are performed.

APPENDIX A

DEVELOPMENT OF AN *IN VITRO* MODEL FOR EVALUATING NERVE REGENERATION WITH DORSAL ROOT GANGLION EXPLANTS

As a method for performing preliminary analyses on factors which promote nerve elongation, we have preformed intial work towards developing a three dimensional *in vitro* model of axonal elongation. An *in vitro* model of nerve regeneration would be useful as a method of comparing variable growth factors, growth factor doses or gradients of growth factors with high repetition and short time periods. Within our proposed *in vitro* design, an explanted dorsal root ganglion is suspended within an agarose gel adjacent to a nerve guide such that axons extend through the lumen of the nerve guide. This 3-D culture method is advantageous to existing two dimensional culture systems because horizontal neurite sprouting can be used as an internal control. Therefore, the unique extent to which each DRG is capable of sprouting neurites can be accounted for when determining directed neurite outgrowth. It was our intentions that this 3-D model for axonal outgrowth be used prior to *in vivo* studies to reduce study variables and therefore decrease the number of experimental animals.

A.1 METHODS

For *in vitro* analysis, dorsal root ganglion (DRG) explants from one month (21 – 29 day old) male Lewis rats were used. Following a complete laminectomy for removal of the spinal column, the column was cut in half following along the sagittal axis and DRGs were dissected away from the surrounding connected and nerve tissue. Prior to the DRG isolation process, agarose gels were prepared with a 1% (w/v) stock solution in dI water (Invitrogen Ultrapure LMP Agarose, 15517-022). To dissolve the agarose, water was continuously stirred and heated to 60°C. The solution was then sterilized by filtration and added in 2 mL volumes to each well of a 24 well plate. During DRG isolation, well plates with gel were incubated at 37°C so as to prevent solidification. Immediately after isolation, DRGs were suspended in the gel and placed at 4°C to allow the gel to solidify. Neurobasal media with B27 supplements was then added to the well. Following 2 hours of incubation, standard media was replaced with neurobasal media containing 50ng/mL Nerve Growth Factor (NGF).

To optimize axonal outgrowth, four agarose gel concentrations were prepared: 0.25%, 0.50%, 0.75% and 1.0%. Additionally, to minimize the exposure time of DRGs to low temperations, 5 time points of 4°C incubation were investigated: 3min to 15 min in 3min increments. Finally, the addition of both collagen and laminin to the agarose gels were investigated as a method of further improving the structural support of axonal extension. To a 0.5% agarose gel, either 33µl of laminin, 20µl collagen (rat tail) or both were added in soluble form per mL of agarose solution.

For DRG visualization, immunofluorescence was used with FITC conjugated lectin-IB4 and antibodies against cGRP receptors. After DRGs were incubated for at least 48 hours in NGF containing culture media to allow axonal sprouting, whole explants were fixed in 4%

paraformaldehyde for 4 hours and then rinsed twice with PBS for 5 minutes each wash. FITC-conjugated lectin IB-4 (3.125 μg/mL) in solution was then added overnight at 4ºC after which the tissue was washed thrice with PBS for 5 minutes each wash. The tissue was then permeabilized with 0.5% triton-X in a 5% Horse Serum solution for 15 minutes and primary antibodies against cGRP were added at a 1:200 dilution in 2.5% horse serum in PBS. Following two additional washes in PBS with 0.2% Tween, anti-mouse secondary antibodies were added at a 1:1000 dilution in PBS with horse serum and incubated for one hour. The tissue was then washed two more times and incubated with DAPI (0.6 μg/mL) for 30 minutes. Finally, the tissue explants were washed and mounted for fluorescent microscopy.

A.2 RESULTS

Following initial preparation of 4 concentrations of agarose gels, it was observed that 0.25% agarose gels did not fully solidify and could not physically support DRGs without the gel settling on the bottom of the well plate due to gravity. Furthermore, 1.0% agarose solutions produced a very firm gel that inhibited axonal outgrowth. Excellent axonal outgrowth was seen using DRGs in gels prepared from 0.5% agarose solution (Figure A1), and therefore gels of this concentration were used for future studies. In addition, it was observed that both 0.5% and 0.75% solutions of agarose began to gel following a 6 min incubation at 4°C and were completely solidified by 9 min.

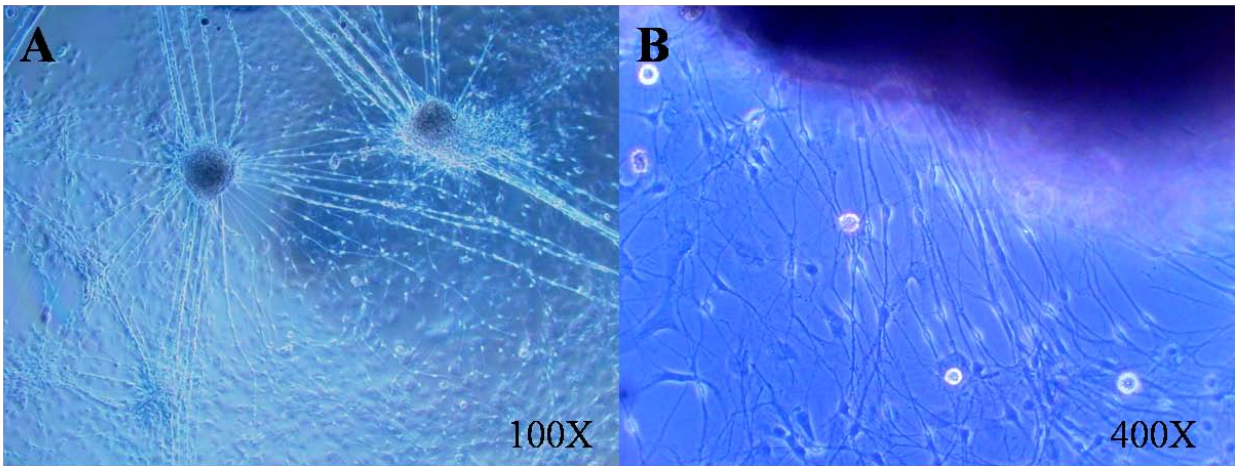

Figure A 1. Low (A) and high (B) magnification brightfield micrographs of explanted dorsal root ganglion in gel composed of 0.75% agarose in dI water.

Addition of extracellular matrix proteins that have been shown to support axonal elongation *in vitro* was also investigated as a method of improving DRG axonal sprouting. The greatest extent of axonal extension was observed using 0.5% agarose solutions containing 20 µl per mL rat tail collagen (Figure A2).

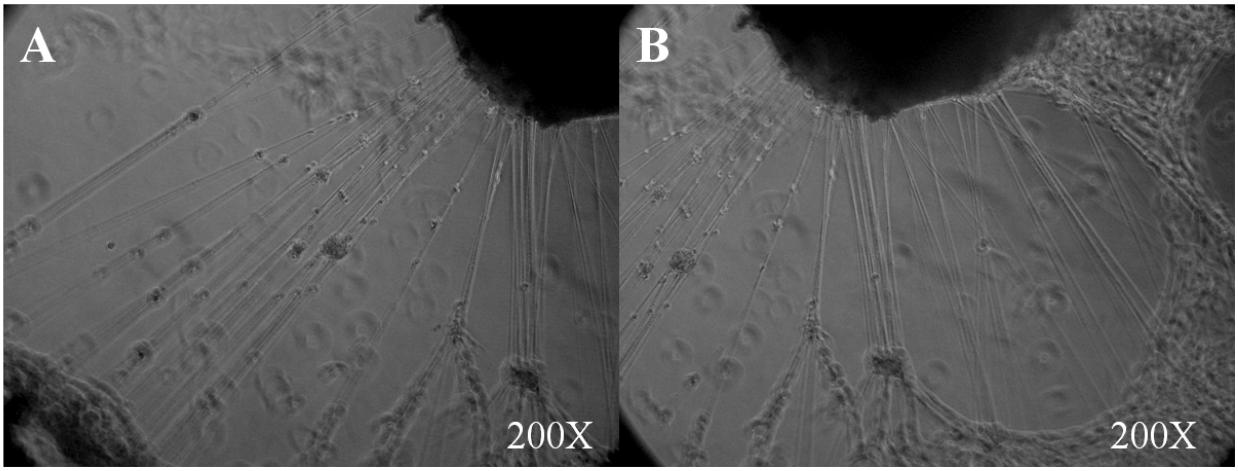

Figure A 2. (A) Brightfield Micrographs of a DRG with extended axons in a 0.5% Agarose gel with 20µl per mL collagen. (B) DRG is rotated to show extent of axonal sprouting.

Because dorsal root ganglion explants contain a heterogeneous population of sensory neurons, it was necessary to confirm that explants contained a population of cells which would respond to applied neurotrophins that do not specifically target sensory axons. Therefore, immunofluorescense was used to identify neural cells which possess receptors for neutrophins such as NGF (cGRP, red) and glial cell-line derived neurotrophic factor (GDNF) (Lectin IB4, green). Following addition of lectin-IB4 and antibodies against cGRP, positive identification of cells responsive to both NGF and GDNF were observed (Figure A3).

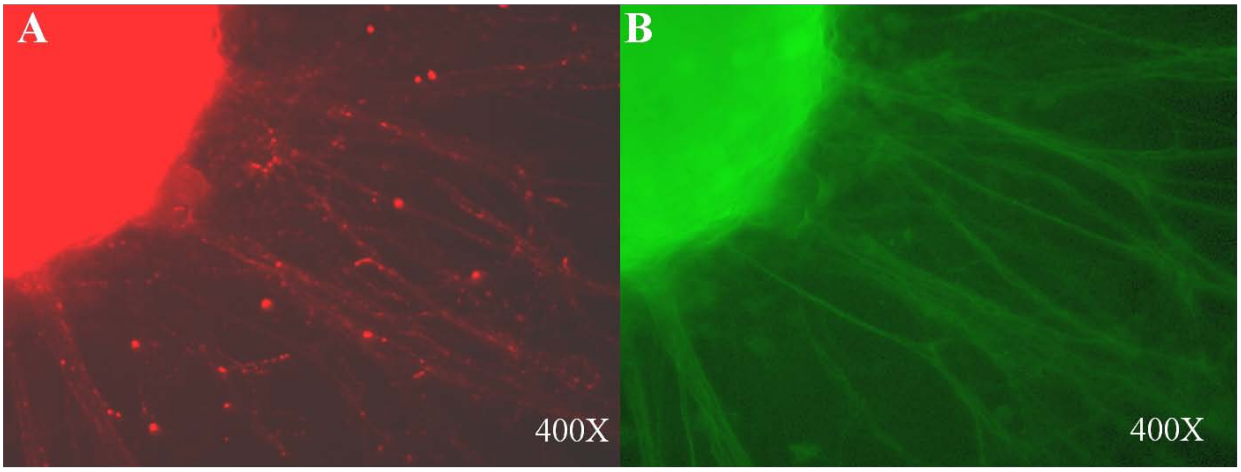

Figure A 3. Fluorescent micrographs of dorsal root ganglion explants. (A) Positive staining for cGRP, indicating cells which are responsive to NGF. (B) Positive staining for lectin IB4, an indication that a population of neurons have receptors for GDNF.

A.3 DISCUSSION

Optimization of the culture methods used for obtaining axonal sprouting from explanted dorsal root ganglion from rats was a necessary first step for the development of our *in vitro* model of nerve regeneration. It is our intentions to create a method of quantifying the capacity of exogenously applied neurotrophins to promote axonal elongation, and therefore we can test a larger number of factors before *in vivo* experiments are performed.

Figure A4 shows a schematic of our design for such an *in vitro* model. Within the agarose gel in which the DRG explants is suspended, a PCL nerve guide containing neurotrophin

delivering microspheres will be vertically fixed so that one end is on the gel-surface interface beneath the DRG while the distal end is located on the gel-well plate interface. The DRGs will be placed in the unsealed end of the guide and cultured for 2 weeks after which the nerve guide will be removed from the gel and fixed for histological analysis. It is our hypothesis that growth promoting cues delivered from the nerve guides will diffuse throughout the gel and promote neurite sprouting into conduits, which can then can be quantified in terms of length and number through sectioning in paraffin and immunofluorescence. This apparatus could be used to compare potential growth factors, growth factor dosages, or homogenous versus gradients of growth factors.

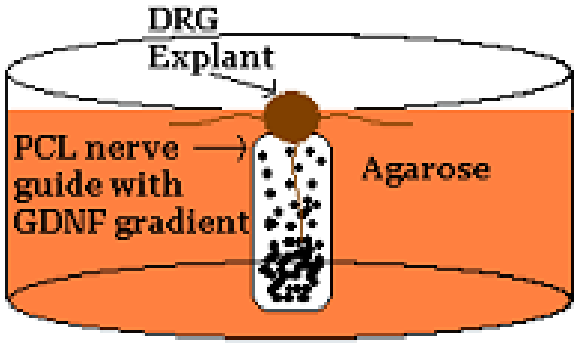

Figure A 4. Schematic of *in vivo* model of axonal outgrowth using a dorsal root ganglion explants suspended in an agarose gel with growth factor releasing conduits.

APPENDIX B

COMPARISON OF VIDEO GAIT KINEMATICS AND SCIATIC FUNCTIONAL INDEX FOR THE QUANTITATIVE ASSESSMENT OF FUNCTIONAL RECOVERY FOLLOWING NERVE TRANSECTION AND REPAIR

One of the most common animal models reported in literature for peripheral nerve injury is the transection of the sciatic nerve in the rat species, which leads to a loss of muscle innervation and sensory defects in the lower leg. The sciatic functional index (SFI) has become a standard tool after almost three decades of development and allows a more complete assessment of therapeutic interventions following lower limb peripheral nerve injury. However, as discussed in Section 5.4, the use of SFI has problems in the implementation of this technique.

Also introduced within Chapter 5 is a novel technique for the analysis of the gait kinematics during both the stance phase and swing phase in the rat gait cycle using video recording of animal movements. Video capturing with a high-speed digital camera allows the fine movements of the rat to be recorded during every portion of the gait cycle. This digital information is tracked and plotted automatically via hind limb markers so as to allow the computation of joint angles and velocities. The parameters measured in video analysis are thus not limited by contractures, exo-rotation, or autotomy as are those by other methods of functional

analysis such as the sciatic functional index (SFI). Video gait analysis evaluates function of more proximal musculature, which are reinnervated prior to the distal musculature of the limb. Consequentially this can be used to detect subtle differences in plantar flexion and dorsiflexion following recovery from nerve injury and repair.

In order to determine if video analysis of gait kinematics could be used in place of SFI measurements, a direct comparison of animal recovery following a sharp transection and repair of the right sciatic nerve was performed. The recovery of injured animals were compared to an additional group receiving a sham operation to determine if the method of nerve exposure, a gluteal muscle splitting incision, also affected gait patterns. Our goal was to determine which method of assessment detected functional recovery at early time points or with less variability so as to result in statistically significant differences between animal gait patterns.

B.1 METHODS

In the experimental group (n=6), the sciatic nerve was sharply transected and repaired with epineurial sutures. SFI and gait kinematics as described in Section 5.2.4.1 and Section 5.2.4.2 respectively, were used for functional assessment prior to surgery and every week after until sacrifice at 9 weeks post-op. In the control group (n=6), the sciatic nerve was exposed but uninjured and functional assessments were conducted at weeks 0, 1, 3, and 5.

B.2 RESULTS

Animals were excluded from SFI measurements due to formation of contractures at week 6 (1 of 6), week 7 (2 of 6) and week 9 (4 of 6) (Figure B1). Assessment of reinnervation in male Lewis rats revealed a decrease in SFI measurements over the first two weeks following sciatic nerve transection. By week 9, animals had recovered to within ~37% of uninjured measurements (Figure B2A). Analysis of SFI measurements from individual rats shows a consistent trend with measured SFI values across all 6 animals (Figure B2B).

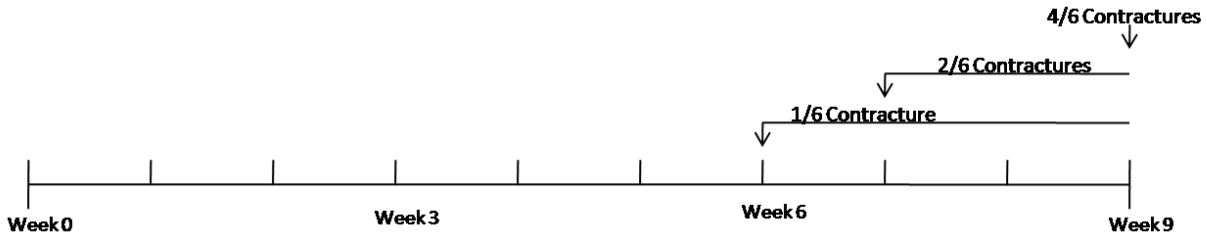

Figure B 1. Schematic of the occurrence of flexion contractures during nerve regeneration following sciatic nerve transection. Animals with contractures were excluded from data pool.

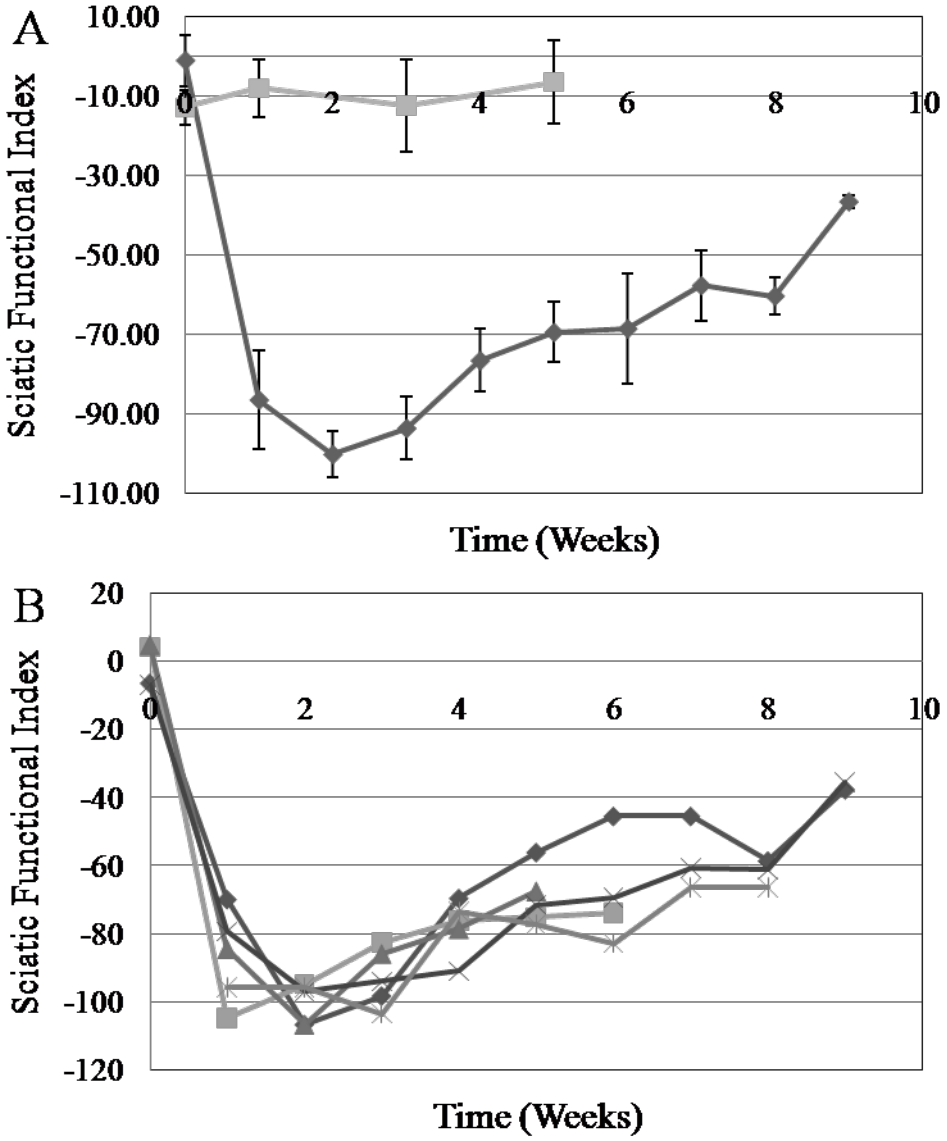

Figure B 2. (A) SFI measurements of animals receiving a sciatic nerve injury (◆) as compared to sham animals (■). Data is expressed as mean ± std dev (B) SFI measurements for rats (n = 6) receiving sciatic nerve transection to show consistency in animal recovery trends. Rat 1 (◆), rat 2 (■), rat 3 (▲), rat 4 (X), rat 5 (*), rat 6 (●).

Initial observations of gait kinematic analysis of the experimental group revealed a sharp increase in ankle range of motion (ROM) within the stance phase of the gait cycle following the first postoperative week (Figure B3A). As animals lost the ability to maintain the raised paw position that is typical for rat gait, the heel dropped and the knee collapsed on the foot in an effort to bear weight. During the swing phase of the gait cycle, a loss of active plantarflexion resulted in a decreased ankle ROM from 1 to 4 weeks post-op (Figure B3B).

Analysis of joint angle range of motion was difficult to assess for the knee and hip measurements due to a lack of deviation of range of motion measurements between the experimental animal and measurements from the group of animals receiving a sham procedure. This challenge occurred because analysis could only be performed on one experimental animal, further trends in rat gait following injury cannot be adequately predicted. Due to technical difficulties, this study should be repeated in order to fully describe hind limb loss of function following nerve injury.

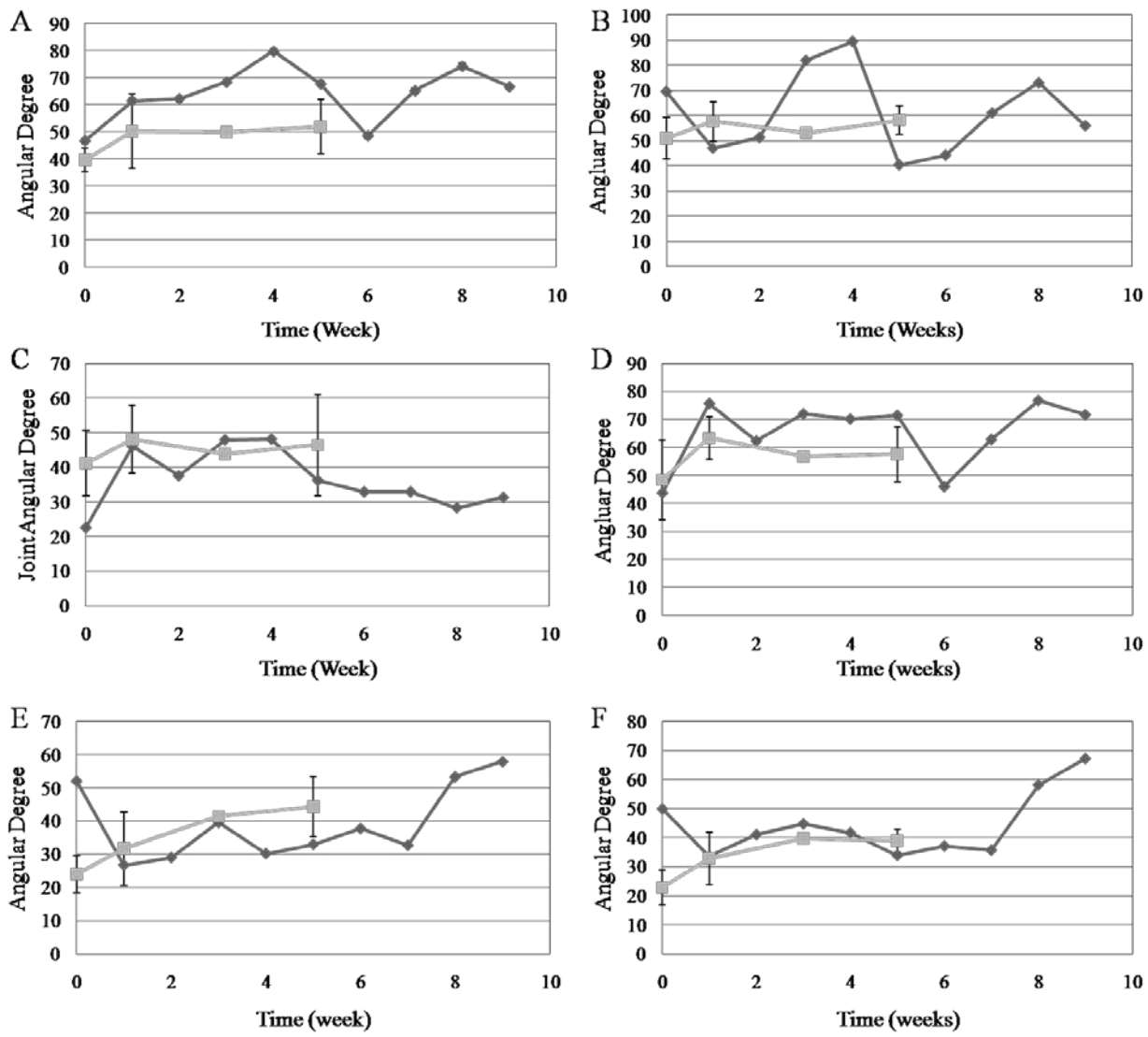

Figure B 3. Joint range of motion (degrees) at baseline (week 0) and sequential timepoints following injury (♦) or sham (▭) procedures. (A) Ankle range of motion during stance phase (A) and swing phase (B) of the gait cycle. Knee range of motion during stance (C) and swing (D). Hip range of motion (degrees) in stance (E) and swing (F).

B.3 DISCUSSION

Video gait kinematics analysis of hind limb function was developed to more thoroughly describe functional recovery in the rat following sciatic nerve injury. Nerve reinnervation as measured through SFI requires a large number of animals to be tested due to the inability to measure lower limb function once contractures occur. However, limitations persist within the presented video assessment method. The validity of joint ROM measurements was highly dependent on the velocity of the animals and was difficult to control for using a simple runway. In addition, it was difficult to place static markers on the skin of the animal to represent the knee joint in a dynamic measurement. This is due to the natural fluidity with which the skin moves across the knee joint. Therefore, evaluation of animals receiving our experimental nerve guides was performed using black ink for marking the five anatomical joint locations. Because we were unable to conclusively show that video measurement of gait kinematics could replace SFI measurements, video gait kinematics were used in conjunction with SFI measurements for detecting nerve regeneration between our final experimental groups.

BIBLIOGRAPHY

[1] S. Ichihara, Y. Inada, T. Nakamura, Artificial nerve tubes and their application for repair of peripheral nerve injury: an update of current concepts. Injury 39 (2008) 29-39.

[2] D.B.Y. Syme, N.M. Corcoran, D.M. Bouchier-Hayes, A.J. Costello, Hope springs eternal: cavernosal nerve regeneration. BJU International 97(1) (2006) 17-21.

[3] D. Slutsky, V. Hentz, Peripheral Nerve Surgery: Practical Applications, Churchill Liningstone Elsevier, Philadelphia, PA, 2006.

[4] H. Rosberg, L. Dahlin, Epidemiology of hand injuries in a middle-sized city in southern Sweden: a retrospective comparison of 1989 and 1997. Scandanavian Journal of Plastic and Reconstructive Surgery and Hand Surgery 38(6) (2004) 347-355.

[5] G. Lundborg, A 25-year perspective of peripheral nerve surgery: Evolving neuroscientific concepts and clinical significance. The Journal of Hand Surgery 25(3) (2000) 391-414.

[6] H.E. Rosberg, K.S. Carlsson, S. HöjgÅrd, B. Lindgren, G. Lundborg, L.B. Dahlin, Injury to the human median and ulnar nerves in the forearm - analysis of costs for treatment and rehabilitation of 69 patients in southern sweden. The Journal of Hand Surgery: Journal of the British Society for Surgery of the Hand 30(1) (2005) 35-39.

[7] K. Watanabe, T. Tsukagoshi, M. Kuroda, Y. Hosaka, Nerve conduit using fascia-wrapped fibrocollagenous tube. Journal of Reconstructive Microsurgery 17(5) (2001) 363-368.

[8] B. Schlosshauer, L. Dreesmann, H.-E. Schaller, N. Sinis, Synthetic Nerve Guide Implants in Humans: A Comprehensive Survey. Neurosurgery 59(4) (2006) 740-748.

[9] C.E. Schmidt, J.B. Leach, Neural Tissue Engineering: Strategies for Repair and Regeneration. Annual Review of Biomedical Engineering 5(1) (2003) 293-347.

[10] J.K. Terzis, K.L. Smith, The Peripheral Nerve: Structure, Function and Reconstruction, Hampton Press, New York, NY, 1990.

[11] R. Barker, S. Dunnett, Neural Repair, Transplantation and Rehabilitation, Psychology Press, Cambridge, UK, 1999.

[12] W.J.a.C.L.S. Germann, Principles of Human Physiology, Pearson Education, Inc Benjamin Cummings, San Francisco, 2005.

[13] D. Kim, R. Midha, J. Murovic, R. Spinner, Nerve Injuries: Operative Results from Major Nerve Injuries, Entrapments, and Tumors, Saunders Elsevier, Philadelphia, 2008.

[14] S. Sunderland, Nerves and Nerve Injuries, The Williams and Wilkins Company, Baltimore, 1968.

[15] J.D. Stroncek, W.M. Reichert, in: W. M. Reichert (Ed.), Indwelling Neural Implants, Taylor & Francis Group, LLC, 2008.

[16] S. Maggi, J. Lowe, S. Mackinnon, Pathophysiology of nerve injury. Clinics in Plastic Surgery 30(2) (2003) 109-126.

[17] R.P. Bunge, Tissue culture observations relevant to the study of axon-Schwann cell interactions during peripheral nerve development and repair. J Exp Biol 132(1) (1987) 21-34.

[18] R. Nancy, B. Richard P, G. Luis, Schwann Cell Proliferation In Vitro. Annals of the New York Academy of Sciences 486(Neurofibromatosis) (1986) 170-181.

[19] M.B. Clark, M.B. Bunge, Cultured Schwann cells assemble normal-appearing basal lamina only when they ensheathe axons. Developmental Biology 133(2) (1989) 393-404.

[20] F.J. Rodríguez, N. Gómez, G. Perego, X. Navarro, Highly permeable polylactide-caprolactone nerve guides enhance peripheral nerve regeneration through long gaps. Biomaterials 20(16) (1999) 1489-1500.

[21] J. Cai, X. Peng, K.D. Nelson, R. Eberhart, G.M. Smith, Permeable guidance channels containing microfilament scaffolds enhance axon growth and maturation. Journal of Biomedical Materials Research Part A 75A(2) (2005) 374-386.

[22] H. Millesi, in: G. E. Omer, M. Spinner and A. L. Van Beek (Eds.), Management of Peripheral Nerve Problems, W.B. Saunders Company, Philadelphia, PA, 1998.

[23] H. Seddon, Surgical Disorders of the Peripheral Nerves, Longman Group Ltd, New York, NY, 1975.

[24] M.G. Burnett, E.L. Zager, Pathophysiology of Peripheral Nerve Injury: A Brief Review: Nerve Injury Classification. Neurosurg Focus. 16(5) (2004) 1-7.

[25] S. Hall, Axonal regeneration through acellular muscle grafts. Journal of Anatomy 190(1) (1997) 57-71.

[26] S. Sunderland, Nerve Injuries and Their Repair: A Critical Appraisal, The Bath Press, Aon, Great Britain, 1991.

[27] X. Navarro, M. Vivó, A. Valero-Cabré, Neural plasticity after peripheral nerve injury and regeneration. Progress in Neurobiology 82(4) (2007) 163-201.

[28] T.M. Myckatyn, S.E. MacKinnon, A review of research endeavors to optimize peripheral nerve reconstruction. Neurological Research 26 (2004) 124-138.

[29] J.W. Faweett, R.J. Keynes, Peripheral Nerve Regeneration. Annual Review of Neuroscience 13(1) (1990) 43-60.

[30] R.V. Weber, S.E. MacKinnon, Bridging the Neural Gap. Clinics in Plastic Surgery 32 (2005) 605-616.

[31] S.K. Lee, S.W. Wolfe, Peripheral Nerve Injury and Repair. J Am Acad Orthop Surg 8(4) (2000) 243-252.

[32] A. Dellon, S. Mackinnon, An alternative to the classical nerve graft for the management of the short nerve gap. Plastic and Reconstructive Surgery 82(5) (1988) 849-856.

[33] M.F. Meek, J.H. Coert, Clinical Use of Nerve Conduits in Peripheral-Nerve Repair: Review of the Literature. J reconstr Microsurg 18(02) (2002) 097-110.

[34] J.S. Taras, S.M. Jacoby, Repair of Lacerated Peripheral Nerves With Nerve Conduits. Techniques in Hand & Upper Extremity Surgery 12(2) (2008) 100-106.

[35] G. Ciardelli, V. Chiono, Materials for Peripheral Nerve Regeneration. Macromolecular Bioscience 6(1) (2006) 13-26.

[36] M.B. Chen, F. Zhang, W.C. Lineaweaver, Luminal Fillers in Nerve Conduits for Peripheral Nerve Repair. Annals of Plastic Surgery 57(4) (2006) 462-471.

[37] L.A. Pfister, M. Papaloïzos, H.P. Merkle, B. Gander, Nerve conduits and growth factor delivery in peripheral nerve repair. Journal of the Peripheral Nervous System 12(2) (2007) 65-82.

[38] T.W. Hudson, G.R.D. Evans, C.E. Schmidt., Engineering Strategies for Peripheral Nerve Repair. Orthopedic Clinics of North America 31(3) (2000).

[39] M. Bunge, R. Bunge, N. Kleitman, A. Dean, Role of peripheral nerve extracellular matrix in Schwann cell function and in neurite regeneration. Developmental Neuroscience 11(4-5) (1989) 348-360.

[40] S. Archibald, C. Krarup, J. Shefner, S. Li, R. Madison, A collagen-based nerve guide conduit for peripheral nerve repair: an electrophysiological study of nerve regeneration in rodents and nonhuman primates. The Journal of Comparative Neurology 306(4) (1991) 685-696.

[41] E.L. Whitlock, S.H. Tuffaha, J.P. Luciano, Y. Yan, D.A. Hunter, C.K. Magill, A.M. Moore, A.Y. Tong, S.E. Mackinnon, G.H. Borschel, Processed allografts and type I collagen conduits for repair of peripheral nerve gaps. Muscle & Nerve 39(6) (2009) 787-799.

[42] S. Li, S. Archibald, C. Krarup, R. Madison, Peripheral nerve repair with collagen conduits. Clinical Materials 9(3-4) (1992) 195-200.

[43] S.W.P. Kemp, S. Syed, S.K. Walsh, D.W. Zochodne, R. Midha, Collagen Nerve Conduits Promote Enhanced Axonal Regeneration, Schwann Cell Association, and Neovascularization Compared to Silicone Conduits. Tissue Engineering Part A 0(0).

[44] S. Felix, F. Hisham, W. Gerald, K. Gerburg, Collagen nerve conduits - Assessment of biocompatibility and axonal regeneration. Bio-Medical Materials and Engineering 15(1) (2005) 3-12.

[45] O. Alluin, C. Wittmann, T. Marqueste, J.-F. Chabas, S. Garcia, M.-N. Lavaut, D. Guinard, F. Feron, P. Decherchi, Functional recovery after peripheral nerve injury and implantation of a collagen guide. Biomaterials 30(3) (2009) 363-373.

[46] B. Harley, M. Spilker, J. Wu, K. Asano, H. Hsu, M. Spector, I. Yannas, Optimal degradation rate for collagen chambers used for regeneration of peripheral nerves over long gaps. Cells Tissues Organs 176(1-3) (2004) 153-165.

[47] K. Wang, I. Nemeth, B. Seckel, D. Chakalis-Haley, D. Swann, J. Kuo, D. Bryan, C.J. Cetrulo, Hyaluronic acid enhances peripheral nerve regeneration in vivo. Microsurgery 18(4) (1998) 270-275.

[48] B. Seckel, D. Jones, K. Hekimian, K. Wang, D. Chakalis, P. Costas, Hyaluronic acid through a new injectable nerve guide delivery system enhances peripheral nerve regeneration in the rat. Journal of Neuroscience Research 40(3) (1995) 318-324.

[49] Z. Ahmed, S. Underwood, R.A. Brown, Nerve Guide Material Made from Fibronectin: Assessment of in Vitro Properties. Tissue Engineering 9(2) (2003) 219-231.

[50] T. Hashimoto, Y. Suzuki, M. Kitada, K. Kataoka, S. Wu, K. Suzuki, K. Endo, Y. Nishimura, C. Ide, Peripheral nerve regeneration through alginate gel: analysis of early outgrowth and late increase in diameter of regenerating axons. Experimental Brain Research 146(3) (2002) 356-368.

[51] P. Zhang, C. Zhang, Y. Kou, X. Yin, H. Zhang, B. Jiang, The Histological Analysis of Biological Conduit Sleeve Bridging Rhesus Monkey Median Nerve Injury with Small Gap. Artificial Cells, Blood Substitutes, and Biotechnology: An International Journal 37(2) (2009) 101 - 104.

[52] L. Pfister, E. Alther, M. Papaloïzos, H. Merkle, B. Gander, Controlled nerve growth factor release from multi-ply alginate/chitosan-based nerve conduits. European Journal of Pharmaceutics and Biopharmaceutics 69(2) (2008) 563-572.

[53] F. Xie, Q. Feng, L. Bin, G. Kai, L. Guo, X. Shen, In vitro and in vivo evaluation of a biodegradable chitosan-PLA composite peripheral nerve guide conduit material. Microsurgery 28(6) (2008) 471-479.

[54] V. Maquet, D. Martin, B. Malgrange, R. Franzen, J. Schoenen, G. Moonen, R. Jérôme, Peripheral nerve regeneration using bioresorbable macroporous polylactide scaffolds. Journal of Biomedical Materials Research 52(4) (2000) 639-651.

[55] T. Hadlock, C. Sundback, R. Koka, D. Hunter, M. Cheney, J. Vacanti, A novel, biodegradable polymer conduit delivers neurotrophins and promotes nerve regeneration. Laryngoscope 109(9) (1999) 1412-1416.

[56] P. Scherman, M. Kanje, L.B. Dahlin, Local Effects on Triiodothyronine-Treated Polyglactin Sutures on Regeneration across Peripheral Nerve Defects. Tissue Engineering 10(3-4) (2004) 455-464.

[57] M.F. Meek, J.H. Coert, US Food and Drug Administration/Conformit Europe-Approved Absorbable Nerve Conduits for Clinical Repair of Peripheral and Cranial Nerves. Annals of Plastic Surgery 60(4) (2008) 466-472.

[58] G. Lundborg, L.B. Dahlin, N. Danielsen, R.H. Gelberman, F.M. Longo, H.C. Powell, S. Varon, Nerve regeneration in silicone chambers: Influence of gap length and of distal stump components. Experimental Neurology 76(2) (1982) 361-375.

[59] R. Kakinoki, N. Nishijima, Y. Ueba, M. Oka, T. Yamamuro, Relationship between axonal regeneration and vascularity in tubulation -- an experimental study in rats. Neuroscience Research 23(1) (1995) 35-45.

[60] R.D. Madison, C. da Silva, P. Dikkes, R.L. Sidman, T.-H. Chiu, Peripheral nerve regeneration with entubulation repair: Comparison of biodegradeable nerve guides versus polyethylene tubes and the effects of a laminin-containing gel. Experimental Neurology 95(2) (1987) 378-390.

[61] P. Robinson, B. van der Lei, H. Hoppen, J. Leenslag, A. Pennings, P. Nieuwenhuis, Nerve regeneration through a two-ply biodegradable nerve guide in the rat and the influence of ACTH4-9 nerve growth factor. Microsurgery 12(6) (1991) 412-419.

[62] M. Lanzetta, A. Gal, B. Wright, E. Owen, Effect of FK506 and basic fibroblast growth factor on nerve regeneration using a polytetrafluoroethylene chamber for nerve repair. International Surgery 88(1) (2003) 47-51.

[63] X. Navarro, F. Rodríguez, R. Labrador, M. Butí, D. Ceballos, N. Gómez, J. Cuadras, G. Perego, Peripheral nerve regeneration through bioresorbable and durable nerve guides. Journal of the Peripheral Nervous System 1(1) (1996) 53-64.

[64] B. Schlosshauer, D. Lars, HE Schaller, N Sinis, Synthetic Nerve Guide Implants in Humans: A Comprehensive Survey.[Review]. Neurosurgery 59(4) (2006) 740-748.

[65] M. Neubauer, M. Hacker, B.-K. Petra;, B. Weiser, C. Fischback, M.B. Schulz, A. Goepferich, T. Blunk, Adipose Tissue Engineering Based ON Mesenchymal Stem Cells and basic Fibroblast Growth Factor in vitro. Tissue Engineering 11(11/12) (2005) 1840 - 1851

[66] D. Hutmacher, T. Woodfield, P. Dalton, J. Lewis, in: C. v. Blitterswijk (Ed.), Tissue Engineering, Academic Press, San Diego, CA, 2008.

[67] B.J. Bender M, Waddell R, Doctor J, Marra K, Multi-channeled Biodegradable Polymer/Cultisphere Composite Nerve Guides. Biomaterials 25 (2004) 1269-1278.

[68] G.E. Rutkowski, C.A. Heath;, Development of a Bioartificial Nerve Graft. II. Nerve Regeneration in Vitro. Biotechnology Progress 18(2) (2002) 373-379.

[69] G.R.D. Evans, K. Brandt, M.S. Widmer, L. Lu, R.K. Meszlenyi, P.K. Gupta, A.G. Mikos, J. Hodges, J. Williams, A. Gürlek, A. Nabawi, R. Lohman, C.W. PatrickJr, In vivo evaluation of poly(-lactic acid) porous conduits for peripheral nerve regeneration. Biomaterials 20(12) (1999) 1109-1115.

[70] C. Jie, P. Xuejun, D.N. Kevin, E. Robert, M.S. George, Permeable guidance channels containing microfilament scaffolds enhance axon growth and maturation. Journal of Biomedical Materials Research Part A 75A(2) (2005) 374-386.

[71] M.S. Widmer, P.K. Gupta, L. Lu, R.K. Meszlenyi, G.R.D. Evans, K. Brandt, T. Savel, A. Gurlek, C.W. PatrickJr, A.G. Mikos, Manufacture of porous biodegradable polymer conduits by an extrusion process for guided tissue regeneration. Biomaterials 19(21) (1998) 1945-1955.

[72] Y. Yang, L. De Laporte, C.B. Rives, J.-H. Jang, W.-C. Lin, K.R. Shull, L.D. Shea, Neurotrophin releasing single and multiple lumen nerve conduits. Journal of Controlled Release 104(3) (2005) 433-446.

[73] C.-J. Chang, S.-h. Hsu, The effect of high outflow permeability in asymmetric poly(dl-lactic acid-co-glycolic acid) conduits for peripheral nerve regeneration. Biomaterials 27(7) (2006) 1035-1042.

[74] A.P. Pego, A.A. Poot, D.W. Grijpma, J. Feijen, Copolymers of trimethylene carbonate and -caprolactone for porous nerve guides: Synthesis and properties. Journal of Biomaterials Science, Polymer Edition 12 (2001) 35-53.

[75] S.I. Jeong, B.-S. Kim, S.W. Kang, J.H. Kwon, Y.M. Lee, S.H. Kim, Y.H. Kim, In vivo biocompatibilty and degradation behavior of elastic poly(-lactide-co-[var epsilon]-caprolactone) scaffolds. Biomaterials 25(28) (2004) 5939-5946.

[76] P. Plikk, S. MÃlberg, A.-C. Albertsson, Design of Resorbable Porous Tubular Copolyester Scaffolds for Use in Nerve Regeneration. Biomacromolecules 10(5) (2009) 1259-1264.

[77] Y.-Z. Bian, Y. Wang, G. Aibaidoula, G.-Q. Chen, Q. Wu, Evaluation of poly(3-hydroxybutyrate-co-3-hydroxyhexanoate) conduits for peripheral nerve regeneration. Biomaterials 30(2) (2009) 217-225.

[78] M.P. Prabhakaran, J.R. Venugopal, T.T. Chyan, L.B. Hai, C.K. Chan, A.Y. Lim, S. Ramakrishna, Electrospun Biocomposite Nanofibrous Scaffolds for Neural Tissue Engineering. Tissue Engineering Part A 14(11) (2008) 1787-1797.

[79] W. Wei, I. Soichiro, M. Atsushi, I. Shizuko, S. Kenichi, H. Yuiro, T. Junzo, Influences of mechanical properties and permeability on chitosan nano/microfiber mesh tubes as a scaffold for nerve regeneration. Journal of Biomedical Materials Research Part A 84A(2) (2008) 557-566.

[80] S. Panseri, C. Cunha, J. Lowery, U. Del Carro, F. Taraballi, S. Amadio, A. Vescovi, F. Gelain, Electrospun micro- and nanofiber tubes for functional nervous regeneration in sciatic nerve transections. BMC Biotechnology 8(39) (2008) 1-12.

[81] I. Ahmed, H.-Y. Liu, P.C. Mamiya, A.S. Ponery, A.N. Babu, T. Weik, M. Schindler, S. Meiners, Three-dimensional nanofibrillar surfaces covalently modified with tenascin-C-derived peptides enhance neuronal growth in vitro. Journal of Biomedical Materials Research Part A 76A(4) (2006) 851-860.

[82] J.M. Corey, D.Y. Lin, K.B. Mycek, Q. Chen, S. Samuel, E.L. Feldman, D.C. Martin, Aligned electrospun nanofibers specify the direction of dorsal root ganglia neurite growth. Journal of Biomedical Materials Research Part A 83A(3) (2007) 636-645.

[83] S. Patel, K. Kurpinski, R. Quigley, H. Gao, B.S. Hsiao, M.-M. Poo, S. Li, Bioactive nanofibers: synergistic effects of nanotopography and chemical signaling on cell guidance. Nano Letters 7(7) (2007) 2122-2128.

[84] S. Chew, R. Mi, A. Hoke, K.W. Leong, Aligned Protein - Polymer Composite Fibers Enhance Nerve Regeneraton: A Potential Tissue-Engineering Platform. Advanced Functional Materials 17(8) (2007) 1288-1296.

[85] B.A. Harley, A.Z. Hastings, I.V. Yannas, A. Sannino, Fabricating tubular scaffolds with a radial pore size gradient by a spinning technique. Biomaterials 27(6) (2006) 866-874.

[86] Q. Ao, A. Wang, W. Cao, L. Zhang, L. Kong, Q. He, Y. Gong, X. Zhang, Manufacture of multimicrotubule chitosan nerve conduits with novel molds and characterization <I>in vitro</I>. Journal of Biomedical Materials Research Part A 77A(1) (2006) 11-18.

[87] Y. Yang, X. Gu, R. Tan, W. Hu, X. Wang, P. Zhang, T. Zhang, Fabrication and properties of a porous chitin/chitosan conduit for nerve regeneration. Biotechnology Letters 26(23) (2004) 1793-1797.

[88] C. Sundback, T. Hadlock, M. Cheney, J. Vacanti, Manufacture of porous polymer nerve conduits by a novel low-pressure injection molding process. Biomaterials 24(5) (2003) 819-830.

[89] B. Doubleday, P.P. Robinson, The Effect of NGF Depletion in the Neurotropic Influence Exerte by the Distal Stump Following Nerve Transection. Journal of Anatomy 186(3) (1995) 593-605.

[90] X. Cao, M.S. Shoichet, Investigating the synergistic effect of combined neurotrophic factor concentration gradients to guide axonal growth. Neuroscience 122(2) (2003) 381-389.

[91] M.J. Politis, K. Ederle, P.S. Spencer, Tropism in nerve regeneration in vivo. Attraction of regenerating axons by diffusible factors derived from cells in distal nerve stumps of transected peripheral nerves. Brain Research 253(1-2) (1982) 1-12.

[92] B.L. Eppley, R.V. Snyders, T.M. Winkelmann, D.G. Roufa, Efficacy of nerve growth factor in regeneration of the mandibular nerve: A preliminary report. Journal of Oral and Maxillofacial Surgery 49(1) (1991) 61-68.

[93] I. Whitworth, R. Brown, C. Doré, P. Anand, C. Green, G. Terenghi, Nerve growth factor enhances nerve regeneration through fibronectin grafts. Journal of Hand Surgery 21(4) (1996) 514-522.

[94] R. Heumann, S. Korsching, C. Bandtlow, H. Thoenen, Changes of nerve growth factor synthesis in nonneuronal cells in response to sciatic nerve transection. J. Cell Biol. 104(6) (1987) 1623-1631.

[95] M. Oudega, T. Hagg, Nerve Growth Factor Promotes Regeneration of Sensory Axons into Adult Rat Spinal Cord. Experimental Neurology 140(2) (1996) 218-229.

[96] S. Bu, J. Li, C. Hu, The influence of nerve growth factor on inferior alveolar nerves regeneration in the silicone tubes. Chinese Journal of Stomatology 34(4) (1999) 217-219.

[97] B.I. Rosner, R.A. Siegel, A. Grosberg, R.T. Tranquillo, Rational Design of Contact Guiding, Neurotrophic Matrices for Peripheral Nerve Regeneration. Annals of Biomedical Engineering 31(11) (2003) 1383-1401.

[98] X. Xu, H. Yu, S. Gao, H. Ma, K. Leong, S. Wang, Polyphosphoester microspheres for sustained release of biologically active nerve growth factor. Biomaterials 23(17) (2002) 3765-3772.

[99] M.C. Dodla, R.V. Bellamkonda, Differences between the effect of anisotropic and isotropic laminin and nerve growth factor presenting scaffolds on nerve regeneration across long peripheral nerve gaps. Biomaterials 29(1) (2008) 33-46.

[100] A. Piotrowicz, M.S. Shoichet, Nerve guidance channels as drug delivery vehicles. Biomaterials 27(9) (2006) 2018-2027.

[101] A.C. Lee, V.M. Yu, J.B. Lowe, M.J. Brenner, D.A. Hunter, S.E. Mackinnon, S.E. Sakiyama-Elbert, Controlled release of nerve growth factor enhances sciatic nerve regeneration. Experimental Neurology 184(1) (2003) 295-303.

[102] J. Bloch, E.G. Fine, N. Bouche, A.D. Zurn, P. Aebischer, Nerve Growth Factor- and Neurotrophin-3-Releasing Guidance Channels Promote Regeneration of the Transected Rat Dorsal Root. Experimental Neurology 172(2) (2001) 425-432.

[103] E.G. Fine, I. Decosterd, M. Papaloizos, A.D. Zurn, P. Aebischer, GDNF and NGF released by synthetic guidance channels support sciatic nerve regeneration across a long gap. European Journal of Neuroscience 15(4) (2002) 589-601.

[104] M. Sendtner, B. Holtmann, R. Kolbeck, H. Thoenen, Y. Barde, Brain-derived neurotrophic factor prevents the death of motoneurons in newborn rats after nerve section. Nature 360(6406) (1992) 757-759.

[105] S. Braun, B. Croizat, M. Lagrange, J. Warter, P. Poindron, Neurotrophins increase motoneurons' ability to innervate skeletal muscle fibers in rat spinal cord--human muscle cocultures. Journal of the Neurological Sciences 136(1-2) (1996) 17-23.

[106] M. Oudega, T. Hagg, Neurotrophins promote regeneration of sensory axons in the adult rat spinal cord. Brain Research 818(2) (1999) 431-438.

[107] J.G. Boyd, T. Gordon, A dose-dependent facilitation and inhibition of peripheral nerve regeneration by brain-derived neurotrophic factor. European Journal of Neuroscience 15(4) (2002) 613-626.

[108] M. Moir, M. Wang, M. To, J. Lum, D. Terris, Delayed repair of transected nerves: effect of brain-derived neurotrophic factor. Archives of Otolaryngology-Head and Neck Surgery 126(4) (2000) 501-505.

[109] E. Vögelin, J.M. Baker, J. Gates, V. Dixit, M.A. Constantinescu, N.F. Jones, Effects of local continuous release of brain derived neurotrophic factor (BDNF) on peripheral nerve regeneration in a rat model. Experimental Neurology 199(2) (2006) 348-353.

[110] D. Utley, S. Lewin, E. Cheng, A. Verity, D. Sierra, D. Terris, Brain-derived neurotrophic factor and collagen tubulization enhance functional recovery after peripheral nerve transection and repair. Archives of Otolaryngology-Head and Neck Surgery 122(4) (1996) 407-413.

[111] P. Ho, G. Coan, E. Cheng, C. Niell, D. Tarn, H. Zhou, D. Sierra, D. Terris, Repair with collagen tubules linked with brain-derived neurotrophic factor and ciliary neurotrophic factor in a rat sciatic nerve injury model. Archives of Otolaryngology-Head and Neck Surgery 124(7) (1998) 761-766.

[112] M. Sendtner, G. Kreutzberg, H. Thoenen, Ciliary neurotrophic factor prevents the degeneration of motor neurons after axotomy. Nature 345(6274) (1990) 440-441.

[113] N. Oyesiku, D. Wigston, Ciliary neurotrophic factor stimulates neurite outgrowth from spinal cord neurons. The Journal of Comparative Neurology 364(1) (1996) 68-77.

[114] S.G. Siegel, B. Patton, A.W. English, Ciliary Neurotrophic Factor Is Required for Motoneuron Sprouting. Experimental Neurology 166(2) (2000) 205-212.

[115] S.W. Levison, M.H. Ducceschi, G.M. Young, T.L. Wood, Acute Exposure to CNTFin VivoInduces Multiple Components of Reactive Gliosis. Experimental Neurology 141(2) (1996) 256-268.

[116] C. Winter, Y. Saotome, S. Levison, D. Hirsh, A Role for Ciliary Neurotrophic Factor as an Inducer of Reactive Gliosis, the Glial Response to Central Nervous System Injury. PNAS 92(13) (1995) 5865-5869.

[117] Z. Chen, Y. Chai, L. Cao, C. Lu, C. He, Glial cell line-derived neurotrophic factor enhances axonal regeneration following sciatic nerve transection in adult rats. Brain Res. 902(2) (2001) 272-276.

[118] M. Streppel, N. Azzolin, S. Dohm, O. Guntinas-Lichius, C. Haas, C. Grothe, A. Wevers, W.F. Neiss, D.N. Angelov, Focal application of neutralizing antibodies to soluble neurotrophic factors reduces collateral axonal branching after peripheral nerve lesion. European Journal of Neuroscience 15(8) (2002) 1327-1342.

[119] F. Barras, P. Pasche, N. Bouche, P. Aebischer, A.D. Zurn, Glial cell line-derived neurotrophic factor released by synthetic guidance channels promotes facial nerve regeneration in the rat. Journal of Neuroscience Research 70(6) (2002) 746-755.

[120] C. Iannotti, H. Li, P. Yan, X. Lu, L. Wirthlin, X. Xu, Glial cell line-derived neurotrophic factor-enriched bridging transplants promote propriospinal axonal regeneration and enhance myelination after spinal cord injury. Exp Neurol. 183(2) (2003) 379-393.

[121] M. Jubran, J. Widenfalk, Repair of peripheral nerve transections with fibrin sealant containing neurotrophic factors. Experimental Neurology 181 (2003) 204–212.

[122] P. Ping, Q. Li, D. Zhang, An experiment study on repair of peripheral nerve defects by GDNF gene modified Schwann cells. Zhonghua Zheng Xing Wai Ke Za Zhi 19(5) (2003) 369-372.

[123] M. Patel, L. Mao, B. Wu, P.J. VandeVord, GDNF-chitosan blended nerve guides: a functional study. Journal of Tissue Engineering and Regenerative Medicine 1(5) (2007) 360-367.

[124] G. Piquilloud, T. Christen, L.A. Pfister, B. Gander, M.Y. Papaloïzos, Variations in glial cell line-derived neurotrophic factor release from biodegradable nerve conduits modify the rate of functional motor recovery after rat primary nerve repairs. European Journal of Neuroscience 26(5) (2007) 1109-1117.

[125] M. Wood, G. Borschel, S.E. Sakiyama-Elbert, Controlled release of glial-derived neurotrophic factor from fibrin matrices containing an affinity-based delivery system. Journal of Biomedical Materials Research Part A 89A(4) (2009) 909-918.

[126] L. Li, W. Wu, L. Lin, M. Lei, R. Oppenheim, L. Houenou, Rescue of Adult Mouse Motorneurons from Injury-Induced Cell Death by Glial Cell Line-Derived Neurotrophic Factor. Proceedings of the National Academy of Sciences 92 (1995) 9771-9775.

[127] A. Hoke, T. Ho, T. Crawford, C. LeBel, D. Hilt, J. Griffin, Glial cell line-derived neurotrophic factor alters axon schwann cell units and promotes myelination in unmyelinated nerve fibers. J Neurosci. 23(2) (2003) 561-567.

[128] H. Sariola, M. Saarma, Novel functions and signalling pathways for GDNF. J Cell Sci 116(19) (2003) 3855-3862.

[129] P. Cordeiro, B. Seckel, S. Lipton, P. D'Amore, J. Wagner, R. Madison, Acidic fibroblast growth factor enhances peripheral nerve regeneration in vivo. Plastic and Reconstructive Surgery 83(6) (1989) 1020-1021.

[130] R.E. Friesel, T. Maciag, Molecular mechanisms of angiogenesis: fibroblast growth factor signal transduction. FASEB J. 9(10) (1995) 919-925.

[131] N. Danielsen, B. Pettmann, H. Vahlsing, M. Manthorpe, S. Varon, Fibroblast growth factor effects on peripheral nerve regeneration in a silicone chamber model. Journal of Neuroscience Research 20(3) (1988) 320-330.

[132] M. Timmer, S. Robben, F. Müller-Ostermeyer, G. Nikkhah, C. Grothe, Axonal regeneration across long gaps in silicone chambers filled with Schwann cells overexpressing high molecular weight FGF-2. Cell Transplantation 12(3) (2003) 265-277.

[133] R. Midha, C. Munro, P. Dalton, C. Tator, M. Shoichet, Growth factor enhancement of peripheral nerve regeneration through a novel synthetic hydrogel tube. Journal of Neurosurgery 99(3) (2003) 555 - 565.

[134] M. Hobson, C. Green, G. Terenghi, VEGF enhances intraneural angiogenesis and improves nerve regeneration after axotomy. Journal of Anatomy 197(Pt 4) (2000) 591-605.

[135] A. Dubuisson, R. Beuermann, D. Kline, Sciatic nerve regeneration across gaps within collagen chambers: the influence of epidermal growth factor. Journal of Microreconstructive Surgery 9(5) (1993) 346-347.

[136] D.N. Ishii, G.W. Glazner, S.F. Pu, Role of insulin-like growth factors in peripheral nerve regeneration. Pharmacology & Therapeutics 62(1-2) (1994) 125-144.

[137] M.-H. Chen, P.-R. Chen, M.-H. Chen, S.-T. Hsieh, F.-H. Lin, Gelatin-tricalcium phosphate membranes immobilized with NGF, BDNF, or IGF-1 for peripheral nerve repair: An in vitro and in vivo study. Journal of Biomedical Materials Research Part A 79A(4) (2006) 846-857.

[138] G. Glazner, A. Morrison, D. Ishii, Elevated insulin-like growth factor (IGF) gene expression in sciatic nerves during IGF-supported nerve regeneration. Brain Research. Molecular Brain Research 25(3-4) (1994) 265-272.

[139] H. Fansa, W. Schneider, G. Wolf, G. Keilhoff, Influence of insulin-like growth factor-I (IGF-I) on nerve autografts and tissue-engineered nerve grafts. Muscle & Nerve 26(1) (2002) 87-93.

[140] T.W. Hudson, S. Zawko, C. Deister, S. Lundy, C.Y. Hu, K. Lee, C.E. Schmidt, Optimized Acellular Nerve Graft Is Immunologically Tolerated and Supports Regeneration. Tissue Engineering 10(11-12) (2004) 1641-1651.

[141] H. Fansa, G. Keilhoff, G. Wolf, W. Schneider, B. Gold, Tissue Engineering of Peripheral Nerves: A Comparison of Venous and Acellular Muscle Grafts with Cultured Schwann Cells. Plastic and Reconstructive Surgery 107(2) (2001) 495-496.

[142] G. Keilhoff, F. Pratsch, G. Wolf, H. Fansa, Bridging Extra Large Defects of Peripheral Nerves: Possibilities and Limitations of Alternative Biological Grafts from Acellular Muscle and Schwann Cells. Tissue Engineering 11(7-8) (2005) 1004-1014.

[143] R.M. Smith, C. Wiedl, P. Chubb, C.H. Greene, Role of Small Intestine Submucosa (SIS) as a Nerve Conduit: Preliminary Report. Journal of Investigative Surgery 17(6) (2004) 339 - 344.

[144] F.G. Mondalek, B.J. Lawrence, B.P. Kropp, B.P. Grady, K.-M. Fung, S.V. Madihally, H.-K. Lin, The incorporation of poly(lactic-co-glycolic) acid nanoparticles into porcine small intestinal submucosa biomaterials. Biomaterials 29(9) (2008) 1159-1166.

[145] F.A. Court, L. Wrabetz, M.L. Feltri, Basal lamina: Schwann cells wrap to the rhythm of space-time. Current Opinion in Neurobiology 16(5) (2006) 501-507.

[146] M. Dezawa, Central and peripheral nerve regeneration by transplantation of Schwann cells and transdifferentiated bone marrow stromal cells. Anatomical Science International 77(1) (2002) 12-25.

[147] G.E. Rutkowski, C.A. Miller, S. Jeftinija, S.K. Mallapragada, Synergistic effects of micropatterned biodegradable conduits and Schwann cells on sciatic nerve regeneration. Journal of Neural Engineering 1(3) (2004) 151-157.

[148] S.-M. Kim, S.-K. Lee, J.-H. Lee, Peripheral Nerve Regeneration Using a Three Dimensionally Cultured Schwann Cell Conduit. Journal of Craniofacial Surgery 18(3) (2007) 475-488

[149] V. Guenard, N. Kleitman, T.K. Morrissey, R.P. Bunge, P. Aebischer, Syngeneic Schwann cells derived from adult nerves seeded in semipermeable guidance channels enhance peripheral nerve regeneration. J. Neurosci. 12(9) (1992) 3310-3320.

[150] F.J. Rodríguez, E. Verdú, D. Ceballos, X. Navarro, Nerve Guides Seeded with Autologous Schwann Cells Improve Nerve Regeneration. Experimental Neurology 161(2) (2000) 571-584.

[151] S.W.P. Kemp, S.K. Walsh, R. Midha, Growth factor and stem cell enhanced conduits in peripheral nerve regeneration and repair. Neurological Research 30 (2008) 1030-1038.

[152] S. Dazert, D. Kim, L. Luo, C. Aletsee, S. Garfunkel, T. Maciag, A. Baird, A.F. Ryan, Focal delivery of fibroblast growth factor-1 by transfected cells induces spiral ganglion neurite targeting in vitro. Journal of Cellular Physiology 177(1) (1998) 123-129.

[153] D. Emerich, S. Winn, P. Hantraye, M. Peschanski, E. Chen, Y. Chu, P. McDermott, E. Baetge, J. Kordower, Protective effect of encapsulated cells producing neurotrophic factor CNTF in a monkey model of Huntington's disease. Nature 386(6623) (1997) 395-399.

[154] Y. Nakahara, F. Gage, M. Tuszynski, Grafts of fibroblasts genetically modified to secrete NGF, BDNF, NT-3, or basic FGF elicit differential responses in the adult spinal cord. Cell Transplantation 5(2) (1996) 191-204.

[155] Q. Li, P. Ping, H. Jiang, K. Liu, Nerve conduit filled with GDNF gene-modified schwann cells enhances regeneration of the peripheral nerve. Microsurgery 26(2) (2006) 116-121.

[156] T. Iwase, C. Jung, H. Bae, M. Zhang, B. Solivan, Glial Cell Line Derived Neurotrophic Factor-Induced Signaling in Schwann Cells. Journal of Neurochemistry 94 (2005) 1488-1499.

[157] G. Terenghi, Peripheral nerve regeneration and neurotrophic factors. Journal of Anatomy 194(1) (1999) 1-14.

[158] J.S. Belkas, M.S. Shoichet, R. Midha, Peripheral nerve regeneration through guidance tubes. Neurological Research 26 (2004) 151-160.

[159] C.-B. Jenq, R.E. Coggeshall, Nerve Regeneration Through Holey Silicone Tunes. Brain Research 361 (1985) 233-241.

[160] C.-B. Jenq, L.L. Jenq, R.E. Coggeshall, Nerve Regeneration Changes with Filters of Different Pore Size. Experimental Neurology 97 (1987) 662-671.

[161] P. Aebischer, V. Guenard, S. Brace, Peripheral nerve regeneration through blind-ended semipermeable guidance channels: Effect of the molecular weight cutoff. Journal of Neuroscience 9 (1989) 3590-3595.

[162] G. Rutkowski, C.A. Heath, Development of a bioartificial nerve graft I. Design based on a reaction-diffusion model. Biotechnology Progress 18(2) (2002) 362-372.

[163] G.E. Rutkowski, C.A. Heath, Development of a Bioartificial Nerve Graft II. Nerve Regeneration in Vitro. Biotechnology Progress 18(2) (2002) 373-379.

[164] P.V. Grant, C.M. Vaz, P.E. Tomlins, L. Mikhalovska, S. James, S. Mikhalovsky, P. Vadgama, Physical Characterisation of a Polycaprolactone Tissue Scaffold, National Physical Laboratory, Teddington, Middlesex, UK, September 2005.

[165] W.S. Rasband, ImageJ, U. S. National Institutes of Health. http://rsb.info.nih.gov/ij/, Vol. 2008, Bethesda, Maryland, US, 1997-2008.

[166] P.-S. Liao, T.-S. Chen, P.-C. Chung, A Fast Algorithm for Multilevel Thresholding. Journal of Information Science and Engineering 17 (2001) 713-727.

[167] J. Suckale, M. Solimena, Pancreas islets in metabolic signaling – focus on the β-cell. Frontiers in Bioscience 13 (2008) 7156-7171.

[168] M. Friedman, Applications of the Ninhydrin Reaction for Analysis of Amino Acids, Peptides, and Proteins to Agricultural and Biomedical Sciences. J. Agric. Food Chem. 52(3) (2004) 385-406.

[169] A. Kugushev, Statistical Research Methods in the Life Sciences, Brooks/Cole Publishing Company, Pacific Grove, CA, 1998.

[170] J. Stankus, J. Guan, K. Fujimoto, W. Wagner, Microintegrating smooth muscle cells into a biodegradable, elastomeric fiber matrix. Biomaterials 735-744 (2006) 735-744.

[171] J. Sanchez, A. Tsuchii, Y. Tokiwa, Degradation of polycaprolactone at 50 °C by a thermotolerant Aspergillus sp. Biotechnology Letters 22(10) (2000) 849-853.

[172] M.J. Mondrinos, R. Dembzynski, L. Lu, V.K.C. Byrapogu, D.M. Wootton, P.I. Lelkes, J. Zhou, Porogen-based solid freeform fabrication of polycaprolactone-calcium phosphate scaffolds for tissue engineering. Biomaterials 27(25) (2006) 4399-4408.

[173] C.-H. Lu, W.-J. Lin, Permeation of protein from porous poly(ε-caprolactone) films. Journal of Biomedical Materials Research 63(2) (2002) 220-225.

[174] F.J. Rodriguez, Gomez, N., Perego, G., and Navarro, X., Highly permeable polylactide-caprolactone nerve guides enhance peripheral nerve regeneration through long gaps. Biomater. 20(16) (1999) 1489-1500.

[175] B.D. Ratner, A.S. Hoffman, F.J. Schoen, J.E. Lemons, Biomaterials Science: An Introduction to Materials in Medicine, Academic Press, San Diego, CA, 1996.

[176] V.V. Ranade, M.A. Hollinger, Drug Delivery Systems, CRC Press, University of California, Davis, 2004.

[177] K. Heilmann, Therapeutic Systems. Rate-Controlled Drug Delivery: Concept and Development, Stuttgart, New York, 1983.

[178] D.N. Hovland, Jr;, R.B. Boyd, M.T. Butt, J.A. Engelhardt, M.S. Moxness, M.H. Ma, M.G. Emery, N.B. Ernst, R.P. Reed, J.R. Zeller, D.M. Gash, D.M. Masterman, B.M. Potter, M.E. Cosenza, R.M. Lightfoot, Six-Month Continuous Intraputamenal Infusion Toxicity Study of Recombinant Methionyl Human Glial Cell Line-Derived Neurotrophic Factor (r-metHuGDNF) in Rhesus Monkeys. Toxicol Pathol 35(7) (2007) 1013-1029.

[179] D. Shirley, S. Williams, P. Santos, Brain-derived neurotrophic factor and peripheral nerve regeneration: a functional evaluation. Laryngoscope 106(5 Pt 1) (1996) 629 - 632.

[180] J.D. Bruce, H. Alan, M.B. Timothy, A.M. Wayne, M. Aurora, Effects of LIF dose and laminin plus fibronectin on axotomized sciatic nerves. Muscle & Nerve 23(9) (2000) 1356-1364.

[181] K. Fu, R. Harrell, K. Zinski, C. Um, A. Jaklenec, J. Frazier, N. Lotan, P. Burke, A.M. Klibanov, R. Langer, A potential approach for decreasing the burst effect of protein from PLGA microspheres. Journal of Pharmaceutical Sciences 92(8) (2003) 1582-1591.

[182] J.M. Anderson, M.S. Shive, Biodegradation and biocompatibility of PLA and PLGA microspheres. Advanced Drug Delivery Reviews 28(1) (1997) 5-24.

[183] A. Aubert-Pouëssel, M.-C. Venier-Julienne, A. Clavreul, M. Sergent, C. Jollivet, C.N. Montero-Menei, E. Garcion, D.C. Bibby, P. Menei, J.-P. Benoit, In vitro study of GDNF release from biodegradable PLGA microspheres. Journal of Controlled Release 95(3) (2004) 463-475.

[184] A.J. DeFail, C.R. Chu, N. Izzo, K.G. Marra, Controlled release of bioactive TGF-[beta]1 from microspheres embedded within biodegradable hydrogels. Biomaterials 27(8) (2006) 1579-1585.

[185] S.M. Royce, A. Morad, K.G. Marra, Incorporation of polymer microspheres within fibrin scaffolds for the controlled delivery of FGF-1. Journal of Biomaterials Science, Polymer Edition 15 (2004) 1327-1336.

[186] M. van de Weert, W.E. Hennink, W. Jiskoot, Protein Instability in Poly(Lactic-co-Glycolic Acid) Microparticles. Pharmaceutical Research 17(10) (2000) 1159-1167.

[187] S.P. Baldwin, W. Mark Saltzman, Materials for protein delivery in tissue engineering. Advanced Drug Delivery Reviews 33(1-2) (1998) 71-86.

[188] A.J. DeFail, H.D. Edington, S. Matthews, W.-C.C. Lee, K.G. Marra, Controlled release of bioactive doxorubicin from microspheres embedded within gelatin scaffolds. Journal of Biomedical Materials Research Part A 79A(4) (2006) 954-962.

[189] A. Jaklenec, A. Hinckfuss, B. Bilgen, D.M. Ciombor, R. Aaron, E. Mathiowitz, Sequential release of bioactive IGF-I and TGF-[beta]1 from PLGA microsphere-based scaffolds. Biomaterials 29(10) (2008) 1518-1525.

[190] M.K. Nkansah, S.Y. Tzeng, A.M. Holdt, E.B. Lavik, Poly(lactic-co-glycolic acid) nanospheres and microspheres for short- and long-term delivery of bioactive ciliary neurotrophic factor. Biotechnology and Bioengineering 100(5) (2008) 1010-1019.

[191] T.A. Hadlock, T. Sheahan, M.L. Cheney, J.P. Vacanti, C.A. Sundback, Biologic Activity of Nerve Growth Factor Slowly Released from Microspheres. J reconstr Microsurg 19(03) (2003) 179-184.

[192] M. Ward, A. Khoobehi, E. Lavik, R. Langer, M. Young, Neuroprotection of retinal ganglion cells in DBA/2J mice with GDNF-loaded biodegradable microspheres. Journal of Pharmaceutical Sciences 96(3) (2007) 558-568.

[193] C. Jiang, M. Moore, X. Zhang, H. Klassen, R. Langer, M. Young, Intravitreal injections of GDNF-loaded biodegradable microspheres are neuroprotective in a rat model of glaucoma. Molecular Vision 13 (2007) 1783-1792.

[194] F. Tewes, F. Boury, J.-P. Benoit, in: J. Swarbrick (Ed.), Drugs and the Pharmaceutical Sciences, Vol. 158, PharmaceuTech, Inc., Pinehurst, NC, 2006.

[195] D.H. Lewis, in: M. Chasin and R. Langer (Eds.), Biodegradable Polymers as Drug Delivery Systems, Vol. 45, Taylor & Francis, Chapel Hill, NC, 1990.

[196] R.P. Batycky, J. Hanes, R. Langer, D.A. Edwards, A theoretical model of erosion and macromolecular drug release from biodegrading microspheres. Journal of Pharmaceutical Sciences 86(12) (1997) 1464-1477.

[197] S.N. Rothstein, W.J. Federspiel, S.R. Little, A Simple Model Framework for the Prediction of Controlled Release from Hydrated Biodegradable Polymer Matrices. Journal of Materials Chemistry 18 (2008) 1873-1880.

[198] S.N. Rothstein, W.J. Federspiel, S.R. Little, A unified mathematical model for the prediction of controlled release from surface and bulk eroding polymer matrices. Biomaterials 30(8) (2009) 1657-1664.

[199] N.A. Rahman, E. Mathiowitz, Localization of bovine serum albumin in double-walled microspheres. Journal of Controlled Release 94(1) (2004) 163-175.

[200] E. Mathiowitz, R. Langer, Preparation of multiwall polymeric microcapsules, United States Patent, August 29, 1989 1989.

[201] E.C. Tan, R. Lin, C.-H. Wang, Fabrication of double-walled microspheres for the sustained release of doxorubicin. Journal of Colloid and Interface Science 291(1) (2005) 135-143.

[202] C. Berkland, A. Cox, K. Kim, D.W. Pack, Three-month, zero-order piroxicam release from monodispersed double-walled microspheres of controlled shell thickness. Journal of Biomedical Materials Research Part A 70A(4) (2004) 576-584.

[203] T.H. Lee, J. Wang, C.-H. Wang, Double-walled microspheres for the sustained release of a highly water soluble drug: characterization and irradiation studies. Journal of Controlled Release 83(3) (2002) 437-452.

[204] K.J. Pekarek, J.S. Jacob, E. Mathiowitz, Double-walled polymer microspheres for controlled drug release. Nature 367(6460) (1994) 258-260.

[205] C. Berkland, E. Pollauf, D.W. Pack, K.K. Kim, Uniform double-walled polymer microspheres of controllable shell thickness. Journal of Controlled Release 96(1) (2004) 101-111.

[206] J. Godbee, P. Weston, E. Mathiowitz, The effects of infiltration on protein release from multi-phase microspheres fabricated via solvent removal. Journal of Microencapsulation 19(6) (2002) 783-796.

[207] S.P. Schwendeman, M. Cardamone, A.M. Klibanov, R. Langer, in: M. S. Brandon (Ed.), Microparticulate Systems for the Delivery of Proteins and Vaccines, Vol. 77, Marcel Dekker, New York, 1996.

[208] C. Srinivasan, Y.K. Katare, T. Muthukumaran, A.K. Panda, Effect of additives on encapsulation efficiency, stability and bioactivity of entrapped lysozyme from biodegradable polymer particles. Journal of Microencapsulation 22(2) (2005) 127 - 138.

[209] W.R. Liu, L. Robert, M.K. Alexander, Moisture-induced aggregation of lyophilized proteins in the solid state. Biotechnology and Bioengineering 37(2) (1991) 177-184.

[210] H. Sah, A New Strategy To Determine the Actual Protein Content of Poly(lactide-co-glycolide) Microspheres. Journal of Pharmaceutical Sciences 86(11) (1997) 1315 - 1318.

[211] K.N. Jiang C, Yonemitsu Y, Shimazoe T, Watanabe S, Naito M, Tsuruo T, Ohtani H and Y Sawada, In Vivo Delivery of Glial Cell-Derived Neurotrophic Factor Across the Blood-Brain Barrier by Gene Transfer into Brain Capillary Endothelial Cells. Human Gene Theraoy 14 (2003) 1181-1191.

[212] M. Li, O. Rouaud, D. Poncelet, Microencapsulation by Solvent Evaporation: State of the art for process engineering approaches. International Journal of Pharmaceutics 363 (2008) 26-39.

[213] V.M. Tatard, L. Sindji, J. Branton, A. Aubert-Pouëssel, J. Colleau, J.-P. Benoit, C.N. Montero-Menei, Pharmacologically active microcarriers releasing glial cell line - derived neurotrophic factor: Survival and differentiation of embryonic dopaminergic neurons after grafting in hemiparkinsonian rats. Biomaterials 28(11) (2007) 1978-1988.

[214] K. Leach, K. Noh, E. Mathiowitz, Effect of manufacturing conditions on the formation of double-walled polymer microspheres. Journal of Microencapsulation 16(2) (1999) 153-167.

[215] A. Matsumoto, Y. Matsukawa, Y. Horikiri, T. Suzuki, Rupture and drug release characteristics of multi-reservoir type microspheres with poly(dl-lactide-co-glycolide) and poly(dl-lactide). International Journal of Pharmaceutics 327(1-2) (2006) 110-116.

[216] A. Matsumoto, Y. Matsukawa, T. Suzuki, H. Yoshino, Drug release characteristics of multi-reservoir type microspheres with poly(dl-lactide-co-glycolide) and poly(dl-lactide). Journal of Controlled Release 106(1-2) (2005) 172-180.

[217] P.A. Gunatillake, R. Adhikari, Biodegradable Synthetic POlymers for Tissue Engineering. European Cells and Materials 5 (2003) 1 - 16.

[218] F. Kang, G. Jiang, A. Hinderliter, P.P. DeLuca, J. Singh, Lysozyme Stability in Primary Emulsion for PLGA Microsphere Preparation: Effect of Recovery Methods and Stabilizing Excipients. Pharmaceutical Research 19(5) (2002) 629-633.

[219] M. Diwan, T.G. Park, Pegylation enhances protein stability during encapsulation in PLGA microspheres. Journal of Controlled Release 73(2-3) (2001) 233-244.

[220] L. Zhi, Y. Jiang, Y. Wang, M. Hu, S. Li, Y. Ma, Effects of Additives on the Thermostability of Chloroperoxidase. Biotechnology Progress 23(3) (2007) 729-733.

[221] L. Huizhou, Y. Weijing, C. Jiayong, Effects of Surfactants on Emulsification and Secondary Structure of Lysozyme in Aqueous Solutions. Biochemical Engineering Journal 2 (1998) 187-196.

[222] P.B. Ricardo, P. Shona, J.M.C. Gonçalo, E.O. Daniel, M.S.C. Joaquim, P.M. Eduardo, Thermodynamics and mechanism of cutinase stabilization by trehalose. Biopolymers 89(6) (2008) 538-547.

[223] A. Hedoux, J.-F.o. Willart, L. Paccou, Y. Guinet, F.d.r. Affouard, A. Lerbret, M. Descamps, Thermostabilization Mechanism of Bovine Serum Albumin by Trehalose. The Journal of Physical Chemistry B 113(17) (2009) 6119-6126.

[224] N.K. Varde, D.W. Pack, Influence of particle size and antacid on release and stability of plasmid DNA from uniform PLGA microspheres. Journal of Controlled Release 124(3) (2007) 172-180.

[225] K. Fu, D.W. Pack, A.M. Klibanov, R. Langer, Visual Evidence of Acidic Environment Within Degrading Poly(lactic-co-glycolic acid) (PLGA) Microspheres. Pharmaceutical Research 17(1) (2000) 100-106.

[226] S.M. Willerth, S.E. Sakiyama-Elbert, Approaches to neural tissue engineering using scaffolds for drug delivery. Advanced Drug Delivery Reviews 59(4-5) (2007) 325-338.

[227] J.-j. Xu, E.-y. Chen, C.-l. Lu, C. He, Recombinant ciliary neurotrophic factor promotes nerve regeneration and induces gene expression in silicon tube-bridged transected sciatic nerves in adult rats. Journal of Clinical Neuroscience 16(6) (2009) 812-817.

[228] E.G. Fine, I. Decosterd, M. Papaloizos, A.D. Zurn, P. Aebischer, GDNF and NGF released by synthetic guidance channels support sciatic nerve regeneration across a long gap European Journal of Neuroscience 15(4) (2002) 589-601.

[229] M.E. Chávez-Delgado, J. Mora-Galindo, U. Gómez-Pinedo, A. Feria-Velasco, S. Castro-Castañeda, F.A. López-Dellamary Toral, S. Luquin-De Anda, L.M. García-Segura, J. García-Estrada, Facial nerve regeneration through progesterone-loaded chitosan prosthesis. A preliminary report. Journal of Biomedical Materials Research Part B: Applied Biomaterials 67B(2) (2003) 702-711.

[230] X. Xu, W.-C. Yee, P.Y.K. Hwang, H. Yu, A.C.A. Wan, S. Gao, K.-L. Boon, H.-Q. Mao, K.W. Leong, S. Wang, Peripheral nerve regeneration with sustained release of poly(phosphoester) microencapsulated nerve growth factor within nerve guide conduits. Biomaterials 24(13) (2003) 2405-2412.

[231] A. Goraltchouk, V. Scanga, C.M. Morshead, M.S. Shoichet, Incorporation of protein-eluting microspheres into biodegradable nerve guidance channels for controlled release. Journal of Controlled Release 110(2) (2006) 400-407.

[232] M. Singh, C.P. Morris, R.J. Ellis, M.S. Detamore, C. Berkland, Microsphere-Based Seamless Scaffolds Containing Macroscopic Gradients of Encapsulated Factors for Tissue Engineering. Tissue Engineering Part C: Methods 14(4) (2008) 299-309.

[233] M.-H. Chen, P.-R. Chen, M.-H. Chen, S.-T. Hsieh, F.-H. Lin, Gelatin-tricalcium phosphate membranes immobilized with NGF, BDNF, or IGF-1 for peripheral nerve repair: An in vitro and in vivo study. Journal of Biomedical Materials Research Part A 79A(4) (2006) 846-857.

[234] J. Newman, A. Verity, S. Hawatmeh, W.J. Fee, D. Terris, Ciliary neurotrophic factors enhances peripheral nerve regeneration. Archives of Otolaryngology-Head and Neck Surgery 122(4) (1996) 399-403.

[235] S. Lewin, D. Utley, E. Cheng, A. Verity, D. Terris, Simultaneous treatment with BDNF and CNTF after peripheral nerve transection and repair enhances rate of functional recovery compared with BDNF treatment alone. Laryngoscope 107(7) (1997) 992 - 999.

[236] L.E. Kokai, Y.-C. Lin, N.M. Oyster, K.G. Marra, Diffusion of soluble factors through degradable polymer nerve guides: Controlling manufacturing parameters. Acta Biomaterialia 5(7) (2009) 2540-2550.

[237] M. Takahashi, The GDNF/RET signaling pathway and human diseases. Cytokine and Growth Factor Reviews 12(4) (2001) 361-373.

[238] L.F. Paratcha G, GDNF and GFRalpha: a versatile molecular complex for developing neurons. Trends in Neurosciences 31(8) (2008) 384 - 391.

[239] P.H. Henderson CE, Pollock RA, Davies AM, Lemeulle C, Armanini M, Simmons L, Moffet B, Vandlen RA, Simpson LC [corrected to Simmons L, et al., GDNF: a potent survival factor for motoneurons present in peripheral nerve and muscle. Science 266(5187) (1994) 1062-1064.

[240] M.S. Airaksinen, M. Saarma, The GDNF family: Signalling, biological functions and therapeutic value. Nat Rev Neurosci 3(5) (2002) 383-394.

[241] Q.T. Nguyen, A.S. Parsadanian, W.D. Snider, J.W. Lichtman, Hyperinnervation of Neuromuscular Junctions Caused by GDNF Overexpression in Muscle. Science 279(5357) (1998) 1725-1729.

[242] G. Paratcha, F. Ledda, GDNF and GFR[alpha]: a versatile molecular complex for developing neurons. Trends in Neurosciences 31(8) (2008) 384-391.

[243] A. Rupp, W. Schmahl, W. Lederer, K. Matiasek, Strain Differences in the Branching of the Sciatic Nerve in Rats. Anatomia, Histologia, Embryologia: Journal of Veterinary Medicine Series C 36(3) (2007) 202-208.

[244] M.F. Salvatore, Y. Ai, B. Fischer, A.M. Zhang, R.C. Grondin, Z. Zhang, G.A. Gerhardt, D.M. Gash, Point source concentration of GDNF may explain failure of phase II clinical trial. Experimental Neurology 202(2) (2006) 497-505.

[245] ClinicalTrials.gov. U.S. National Institutes of Health, 2009.

[246] P. Brundin, GDNF treatment in Parkinson's disease: time for controlled clinical trials? Brain 125(10) (2002) 2149-2151.

[247] A.S. Varejao, M.F. Meek, A.J. Ferreira, J.A. Patricio, A.M. Cabrita, Functional evaluation of peripheral nerve regeneration in the rat: walking track analysis. J. Neurosci. Methods 108(1) (2001) 1-9.

[248] C.J. Brown, S.E. Mackinnon, P.J. Evans, J.R. Bain, A.P. Makino, D.A. Hunter, G.M.T. Hare, Self-evaluation of walking-track measurement using a sciatic function index. Microsurgery 10(3) (1989) 226-235.

[249] F. Kanaya, J.C. Firrell, W.C. Breidenbach, Sciatic function index, nerve conduction tests, muscle contraction, and axon morphometry as indicators of regeneration. Plast. Reconstr. Surg. 98(7) (1996) 1264-1271.

[250] J.L. Reynolds, M.S. Urbanchek, H. Asato, W.M. Kuzon Jr, Deletion of individual muscles alters rat walking-track parameters. J. Reconstr. Microsurg. 12(7) (1996) 461-466.

[251] F. Di Scipio, S. Raimondo, P. Tos, S. Geuna, A simple protocol for paraffin-embedded myelin sheath staining with osmium tetroxide for light microscope observation. Microscopy Research and Technique 71(7) (2008) 497-502.

[252] D.A. Hunter, A. Moradzadeh, E.L. Whitlock, M.J. Brenner, T.M. Myckatyn, C.H. Wei, T.H.H. Tung, S.E. Mackinnon, Binary imaging analysis for comprehensive quantitative histomorphometry of peripheral nerve. Journal of Neuroscience Methods 166(1) (2007) 116-124.

[253] T. Gordon, The role of neurotrophic factors in nerve regeneration. Neurosurgical FOCUS 26(2) (2009) E3.

[254] A. Hoke, T. Ho, T.O. Crawford, C. LeBel, D. Hilt, J.W. Griffin, Glial Cell Line-Derived Neurotrophic Factor Alters Axon Schwann Cell Units and Promotes Myelination in Unmyelinated Nerve Fibers. J. Neurosci. 23(2) (2003) 561-567.

[255] G. Paratcha, F. Ledda, C.F. Ibáñez, The Neural Cell Adhesion Molecule NCAM Is an Alternative Signaling Receptor for GDNF Family Ligands. Cell 113(7) (2003) 867-879.

[256] T. Iwase, C.G. Jung, H. Bae, M. Zhang, B. Soliven, Glial cell line-derived neurotrophic factor-induced signaling in Schwann cells. Journal of Neurochemistry 94(6) (2005) 1488-1499.

[257] S.Y. Fu, T. Gordan, The Cellular and Molecular Basis of Peripheral Nerve Regeneration. Molecular Neurobiology 14 (1997) 67-115.

[258] M. Brenner, A. Moradzadeh, T. Myckatyn, T. Tung, A. Mendez, D. Hunter, S. Mackinnon, Role of Timing in Assessment of Nerve Regeneration. Microsurgery 28 (2008) 265-272.

[259] M. Carr, T. Best, S. Mackinnon, P. Evans, Strain differences in autotomy in rats undergoing sciatic nerve transection or repair. Annals of Plastic Surgery 28(6) (1992) 538-544.

[260] J.R. Dijkstra, M.F. Meek, P.H. Robinson, A. Gramsbergen, Methods to evaluate functional nerve recovery in adult rats: walking track analysis, video analysis and the withdrawal reflex. Journal of Neuroscience Methods 96(2) (2000) 89-96.

[261] L. Williams, F. Longo, H. Powell, G. Lundborg, S. Varon, Spatial-temporal progress of peripheral nerve regeneration within a silicone chamber: parameters for a bioassay. The Journal of Comparative Neurology 218(4) (1983) 460-470.

[262] L. Williams, N. Danielsen, H. Müller, S. Varon, Exogenous matrix precursors promote functional nerve regeneration across a 15-mm gap within a silicone chamber in the rat. The Journal of Comparative Neurology 264(2) (1987) 284-290.

[263] N. Dubey, P.C. Letourneau, R.T. Tranquillo, Guided Neurite Elongation and Schwann Cell Invasion into Magnetically Aligned Collagen in Simulated Peripheral Nerve Regeneration. Experimental Neurology 158(2) (1999) 338-350.

[264] D. Ceballos, X. Navarro, N. Dubey, G. Wendelschafer-Crabb, W.R. Kennedy, R.T. Tranquillo, Magnetically Aligned Collagen Gel Filling a Collagen Nerve Guide Improves Peripheral Nerve Regeneration. Experimental Neurology 158(2) (1999) 290-300.

[265] M.R. Wells, K. Kraus, D.K. Batter, D.G. Blunt, J. Weremowitz, S.E. Lynch, H.N. Antoniades, H.A. Hansson, Gel Matrix Vehicles for Growth Factor Application in Nerve Gap Injuries Repaired with Tubes: A Comparison of Biomatrix, Collagen, and Methylcellulose. Experimental Neurology 146(2) (1997) 395-402.

[266] X. Yu, G. Dillon, R. Bellamkonda, A laminin and nerve growth factor-laden three-dimensional scaffold for enhanced neurite extension. Tissue Engineering 5(4) (1999) 291-304.

[267] M.C. Dodla, R.V. Bellamkonda, Anisotropic Hydrogels for Peripheral Nerve Regeneration Across Long Nerve Gaps. Biomedical Engineering Society (1996).

[268] K. Matsumoto, K. Ohnishi, T. Kiyotani, T. Sekine, H. Ueda, T. Nakamura, K. Endo, Y. Shimizu, Peripheral nerve regeneration across an 80-mm gap bridged by a polyglycolic acid (PGA)-collagen tube filled with laminin-coated collagen fibers: a histological and electrophysiological evaluation of regenerated nerves. Brain Research 868(2) (2000) 315-328.

[269] P.J. Apel, J.P. Garrett, P. Sierpinski, J. Ma, A. Atala, T.L. Smith, L.A. Koman, M.E. Van Dyke, Peripheral Nerve Regeneration Using a Keratin-Based Scaffold: Long-Term Functional and Histological Outcomes in a Mouse Model. The Journal of Hand Surgery 33(9) (2008) 1541-1547.

[270] P. Sierpinski, J. Garrett, J. Ma, P. Apel, D. Klorig, T. Smith, L.A. Koman, A. Atala, M. Van Dyke, The use of keratin biomaterials derived from human hair for the promotion of rapid regeneration of peripheral nerves. Biomaterials 29(1) (2008) 118-128.

[271] K. Wang, I. Nemeth, B. Seckel, D. Chakalis-Haley, D. Swann, J. Kuo, D. Bryan, C. Cetrulo, Hyaluronic acid enhances peripheral nerve regeneration in vivo. Microsurgery 18(4) (1998) 270-275.

[272] B. Seckel, D. Jones, K. Hekimian, K. Wang, D. Chakalis, P. Costas, Hyaluronic acid through a new injectable nerve guide delivery system enhances peripheral nerve regeneration in the rat. Journal of Neuroscience Research 40(3) (1995) 318-324.

[273] H. Tan, C.M. Ramirez, N.D. Miljkovic, H. Li, J.P. Rubin, K.G. Marra, Thermosensitive injectable hyaluronic acid hydrogel for adipose tissue engineering. Biomaterials In Press (2009).